Curved Steel Bridge Research Report:

I-Girder Bending Component Tests – *Philosophy and Design of the I-girder Bending Component Test*

Publication No. FHWA-HIF-19-064
July 2019

U.S. Department of Transportation
Federal Highway Administration

Sponsored by
Federal Highway Administration
Office of Infrastructure
FHWA-HIF-19-064

Notice

This document is disseminated under the sponsorship of the U.S. Department of Transportation (USDOT) in the interest of information exchange under Task 2 of the FHWA Cooperative Agreement DTFH61-11-H-00027. The U.S. Government assumes no liability for the use of the information contained in this document.

The U.S. Government does not endorse products or manufacturers. Trademarks or manufacturers' names appear in this report only because they are considered essential to the objective of the document. They are included for informational purposes only and are not intended to reflect a preference, approval, or endorsement of any one product or entity.

Quality Assurance Statement

The Federal Highway Administration (FHWA) provides high-quality information to serve Government, industry, and the public in a manner that promotes public understanding. Standards and policies are used to ensure and maximize the quality, objectivity, utility, and integrity of its information. FHWA periodically reviews quality issues and adjusts its programs and processes to ensure continuous quality improvement.

TECHNICAL REPORT DOCUMENTATION PAGE

1. Report No. FHWA-HIF-19-064	2. Government Accession No.	3. Recipient's Catalog No.
4. Title and Subtitle Curved Steel Bridge Research Project: I-Girder Bending Component Test – *Philosophy and Design of the I-Girder Bending Component Tests*		5. Report Date July, 2019 6. Performing Organization Code
7. Author(s) Michael A. Grubb (M.A. Grubb and Associates) and Dann H. Hall (Bridge Software Development International)		8. Performing Organization Report No.
9. Performing Organization Name and Address Bridge Software Development International HDR Engineering		10. Work Unit No. 11. Contract or Grant No.
12. Sponsoring Agency Name and Address Office of Bridges and Structures Federal Highway Administration 200 New Jersey Ave., SE Washington, DC 20590		13. Type of Report and Period Covered Research Report 1992-2000 14. Sponsoring Agency Code

15. Supplementary Notes
Report based on FHWA-sponsored Curved Steel Bridge Research Project (CSBRP) between 1992 and original report date of 2000.

16. Abstract
This report describes the I-girder bending component tests that were conducted as part of the CSBRP. It covers in full detail the philosophy, design, fabrication and set-up of these tests. Appendices A and B of this report were developed based on early work as part of an initial work plan for the project. This initial work plan was later scaled down due to budgetary and time constraints. In this work, detailed elastic analyses were carried out on the preliminary concept for the simple span horizontally curved I-girder bridge that served as the test frame for the component specimen testing. Appendix A presents a comparison of selected analysis results for the bridge obtained using four different commercially available software packages. Appendix B presents the results of BSDI 3D System analyses of variations to the base model. Specifically, variations to the base model were made to determine the effects of cross-frame type, cross-frame spacing, radius, skew and bearing orientation. Of particular interest is the study on the effects of skew contained in Appendix B. This study focused on the effect of skew on vertical bending moments, vertical deflections, lateral flange bending moments and cross-frame forces in the region of the skewed support. The presence of girder end moments at a simple skewed support is illustrated. It is shown that these moments are due to the net longitudinal components of the forces in the skewed end-support cross frame. The effect of cross frame removal in the region of the skewed support is also examined.

17. Key Words curved steel girder, research, experimental testing	18. Distribution Statement No restrictions. This document is available to the public online and through the National Technical Information Service, Springfield, VA 22161.		
9. Security Classif. (of this report) Unclassified	20. Security Classif. (of this page) Unclassified	21. No of Pages 231	22. Price Free

Form DOT F 1700.7 (8-72) Reproduction of completed page authorized

Foreword

This report provides documentation on the philosophy and design of the I-girder component tests for the FHWA Curved Steel Bridge Research Project, which was conducted at the Turner Fairbank Highway Research Center in McLean Virginia beginning in 1992. This research effort provided a theoretical and experimental basis for advancement in the understanding of behavior and design of steel girders for highway bridges, and resulted in many changes to the AASHTO LRFD Bridge Design Specifications and the engineering practices in the U.S.

This report was first authored in 2000 and is now being published electronically. Although it contains references to specifications that have since been superseded, the fundamental principles discussed are the basis for the steel highway bridge design specifications still used today.

Joseph L. Hartmann, Ph.D., P.E.
Director, Office of Bridges and Structures

PREFACE

The FHWA Curved Steel Bridge Research Project (CSBRP) was initiated in the fall of 1992 to study the behavior of horizontally curved steel bridges with the intent of gaining a better theoretical understanding of their behavior, with this improved understanding leading to improved design, construction and performance of these important structures. The planned program represented an experimental program of historical significance. The tests conducted as part of this program represented some of the largest indoor civil-engineering related structural tests ever undertaken. The CSBRP introduced the unique concept of utilizing a full-size three-girder bridge as a test frame to test multiple horizontally curved components. It was envisioned that parts of the full-size bridge could then later be re-used for erection studies and for testing of the bridge as a full-size composite curved-bridge structure. The tests were the first tests known to the researchers that tested full-size components to failure as part of a structure that remained elastic and reusable. Using a full-size curved bridge as a test frame ensured for the first time that realistic boundary conditions would be provided for curved-girder component specimen testing. It also provided assurance that the distortions in the components would be realistic and that material properties would be representative of full-size girders. By using a full-size test, compensatory dead load would also not be required when live load tests were later performed. It was felt that these advancements would provide greater insight into the actual fundamental behavior of horizontally curved girders within a curved-bridge system.

The horizontal curvature of the test frame and components only added to the overall complexity of the planned tests. To address the many unknowns in such an ambitious test program, careful integration of analysis was required throughout the design process. The extent of the analyses that were employed in the design of the various component tests was unprecedented at the time to ensure that the tests could be successfully carried out for the first time, while at the same time providing the desired results without any failures of the test-frame components. The costs of the tests could not have been justified without the confidence gained from the elaborate finite element analyses of the tests prior to fabrication. The interplay between the theoretical (analytical) and physical (experimental) investigations was one of the greatest contributions of this project.

This report describes the I-girder bending component tests that were conducted as part of the CSBRP. It covers in full detail the philosophy, design, fabrication and set-up of these tests. Appendices A and B of this report were developed based on early work as part of an initial work plan for the project. This initial work plan was later scaled down due to budgetary and time constraints. In this work, detailed elastic analyses were carried out on the preliminary concept for the simple span horizontally curved I-girder bridge that served as the test frame for the component specimen testing. Appendix A presents a comparison of selected analysis results for the bridge obtained using four different commercially available software packages. Appendix B presents the results of BSDI 3D System analyses of variations to the base model. Specifically, variations to the base model were made to determine the effects of cross-frame type, cross-frame spacing, radius, skew and bearing orientation. Of particular interest is the study on the effects of skew contained in Appendix B. This study focused on the effect of skew on vertical bending moments, vertical deflections, lateral flange bending moments and cross-frame forces in the region of the skewed support. The presence of girder end moments at a simple skewed support is illustrated. It is shown that these moments are due to the net longitudinal components of the forces in the skewed end-support cross frame. The effect of cross frame removal in the region of the skewed support is also examined.

The reader should note that this report was originally authored in the year 2000. Therefore, it contains numerous references to specifications and specification provisions that have since been superseded. The report should be read with that fact in mind.

TABLE of CONTENTS

LIST OF FIGURES

LIST OF TABLES

PHILOSOPHY AND DESIGN of the I-GIRDER BENDING COMPONENT TESTS

by Michael A. Grubb[1], P.E. and Dann H. Hall[2]

INTRODUCTION

Curved-girder bridges have grown from relative obscurity to comprise up to a third of the steel bridges built in recent years. The earliest curved girders were probably made from rolled shapes that were cold bent about their weak axis. With the acceptance of girder welding, curved girders have steadily grown in popularity. Although horizontally curved girders are used in buildings, such as for balconies, the most widespread use of curved steel girders is in the highway bridge market. Complex roadway alignments that require minimal land usage while permitting acceptable design speeds would not be possible without the advent of horizontally curved steel bridges. Curved girders are fundamentally different than straight girders in that they must resist torsion and a lateral deformation. Torsional loading causes twisting, which complicates the behavior. The lateral distortion occurs at all loads, which is different from tangent girders that remain straight until they buckle. Torsion applied to girders having open sections is resisted through interaction between the members in the bridge. Torsion applied to closed sections, such as box girders, is mostly resisted by torsion within each box section. Torsion due to curvature is always present in curved girders, whereas torsion may or may not be present in tangent girders. Tangent girders are subjected to torsion when loads are applied at locations other than the shear center. Thus, a tangent girder may be thought of as a special case of a curved girder, although the converse is currently the more common perception. In conjunction with the torsion in curved-girder bridges is the transfer of load transversely from each girder to its neighbor toward the outside of the curve, as well as longitudinally along each individual girder to its end supports. Tangent girders having open sections resist torsion primarily through the interaction between adjacent members connected by cross frames. Since the magnitude of this torsion varies from cross frame to cross frame, it is commonly referred to as non-uniform torsion.

The earliest analytical studies of curved girders were based on a strength-of-materials approach, with modifications made to account for the effects of cross-section distortion and amplification of lateral deflections. More recent studies in Japan have employed inelastic finite-element analyses. The earliest laboratory tests of steel curved girders were performed in the U.S. in the late 1960s and early 1970s. The Federal Highway Administration (FHWA) and the Pennsylvania Department of Transportation (PennDOT) financed much of this work. The FHWA sponsored the Consortium of University Research Teams (CURT) Project, which involved a consortium of four different universities. The consortium was composed of researchers from Syracuse University, the University of Rhode Island, the University of Pennsylvania and Carnegie-Mellon University. The research conducted under the CURT Project included both analytical and experimental work that resulted in the development of Tentative Design Specifications for Horizontally Curved Highway Bridges in an allowable stress design format (*1*), which were adopted by AASHTO in 1976. In 1975, the American Iron and Steel Institute initiated Project 190 to develop load factor design criteria for steel curved-girder bridges (*2*). The tentative load factor design criteria were adopted by AASHTO in 1979 and were incorporated with the allowable stress design criteria in the original AASHTO Guide Specifications for Horizontally Curved Highway Bridges, which were printed by AASHTO in 1980 (*3*). Since the completion of the CURT Project, there has been isolated research in the United States on the behavior of horizontally curved girders, but a coordinated and focused effort has been lacking. NCHRP Project 12-38 developed revised guide specifications for horizontally curved steel bridges in a Load Factor Design (LFD) format based on state-of-the-art knowledge (*4*). Experimental studies of curved steel girders,

---

[1] Bridge Software Development International, Ltd. (now with M.A. Grubb & Associates, LLC), Wexford, PA 15090

[2] Bridge Software Development International, Ltd. (now retired), Coopersburg, PA 18036

however, have been extremely limited since the completion of the CURT Project. With the acceptance of probabilistic Load and Resistance Factor Design (LRFD) provisions by AASHTO in 1993 as co-equal alternative bridge-design procedures (*5*), new experimental data on horizontally curved I girders are needed to help generate the necessary statistical data for extension of the LRFD provisions to include horizontally curved girders.

The Japanese have also studied curved-in-plan girders in the laboratory and conducted tests similar to those conducted under the CURT Project. This work culminated in the development of the Hanshin Expressway Corporation of Japan Guidelines for the Design of Horizontally Curved Girder Bridges in 1988 (*6*), which are in an allowable stress format. At the time of this project, the Hanshin Guidelines, along with the AASHTO Guide Specifications, were the only two known design specifications in the world for horizontally curved steel bridges.

These previous experimental studies are discussed in more detail in the next section of this report. Because of the inherent complexity of testing horizontally curved steel girders, each study had its own intrinsic limitations, and therefore, met with varying degrees of success. However, a thorough examination of these studies was instructive in developing an improved philosophy and experiment plan for the FHWA Curved Steel Bridge Research Project (CSBRP), which is focused on the study of horizontally curved I girders. The development of this plan was an enormous challenge fraught with many obstacles. The history of this development is therefore reviewed in some detail below in order to gain a better understanding and appreciation of these challenges and because such a detailed review is considered befitting of the single largest civil-engineering related structural laboratory test ever undertaken.

PREVIOUS EXPERIMENTAL TESTS

Introduction

In previous investigations, tests have been performed on both horizontally curved I-sections and box sections. Most of these tests employed single-girder arrangements. This required artificial torsional restraints at the ends of the torsionally weak I-sections. The box sections were also torsionally restrained at the ends, but this restraint could be supplied with more realistic double bearing arrangements. One exception was the tests by Mozer et al. (*7*), in which two curved I-girders were connected with bracing and tested together.

The tests were performed before finite element modeling had been developed to the level of refinement available in the 1990s. Thus, none of the testing was augmented with finite element analyses in either the experiment-design stage or in the evaluation stage. Simpson at the University of Toronto (*8*) investigated some of these early curved I-girder tests using the ANSYS inelastic finite element code (*9*). His work indicates that the end conditions of the test beams were not critical to the capacity of the beam, but that the girder rotation in the single-girder tests did not adequately represent curved-girder behavior in multi-girder bridges. The reason that the tests were not significantly affected by the end restraints is apparently related to the fact that failure occurred mid-way between brace points. The reason that the beams failed mid-way between brace points is that the lateral moment in the compression flanges is amplified due to the lateral deflection of the flange under load. Strength of materials theory, which does not consider the effect of this amplification, indicates a higher moment at the brace points than at a point mid-way between brace points.

All of the previous I-girder tests were performed on doubly symmetric girder specimens. In this case, the shear center and the center of gravity are coincident.

Culver-Mozer Tests

Both high-bending/low-shear and high-shear tests were performed at Carnegie Mellon University by Mozer, Culver et al. (*7*, *10*, *11*). The girders had web slenderness ratios ranging from approximately 140 to

190.

Report P1 (*10*) presents the results of seven tests of curved I-girders. Each specimen was tested individually. The compression-flange slenderness ratios of Specimens C7, C8, and C9 were such that local buckling was not expected. Specimens D11, D12, D13, and D14 had wider flanges and larger b/t ratios than the C-series tests. Girder depths were between 18 in. (457 mm) and 24 in. (610 mm). Radii of curvature were between 378.0 in. (9600 mm) and 1462.0 in. (37 135 mm). All specimens had a span of 120 in. (3048 mm). The load was applied at the center of the span, but eccentric to the girder to create a specific lateral bending moment (Figure 2.1). The ends of the span were simply supported vertically and pinned torsionally. Rigid-body behavior was ensured at supports and at load points by employing full- depth "stiffeners". Intermediate transverse web stiffeners were also employed. Some specimens were heat curved and some were cut-curved. Tensile properties and residual stresses were recorded. Dimensions of the specimens were measured, including out-of-straightness, which was compared to the allowable AWS out-of-straightness (*12*).

The testing arrangement provided for a variable moment throughout and a reasonably uniform shear throughout the 120-in. (3048-mm) test length. Failures occurred by either web buckling or flange buckling. The failures corresponded well with the predicted mode of failure and with the predicted capacities. Predictions were made using the equations eventually proposed for inclusion in the original AASHTO *Guide Specifications for Horizontally Curved Highway Bridges* (*3*). Numerous strain gages were employed. Girder rotations were measured. The tests are well documented.

Report P2 (*11*) presents results for two curved I-girder specimens, each tested in three arrangements. The girders were supported in a similar fashion to the tests described in Report P1. The span of these girders was 180 in. (4572 mm). Girders were 18-in. (457-mm) deep. The radius was approximately 600 in. (15 240 mm). There were three loading arrangements, "A", "B", and "C". Loading Arrangement "A" tested both girders in pure bending and employed two concentrated loads (Figure 2.2). Loading Arrangements "B" and "C" had 120-in. (3048-mm) spans for both girders. In Loading Arrangement "B", Specimen L1, the left support was moved 5 ft (1.5 m) into the span and a single load was applied 3.25 ft (0.99 m) from the right support. In Loading Arrangement "C", the right reaction was moved 5 ft (1.5 m) into the span and a single load was applied 3.25 ft (0.99 m) from the left support. This permitted two panels in Specimen L1 to be tested with similar loading. This situation created a high-shear/high-moment condition. A similar process was employed for Specimen L2, except that the loads were applied 5 ft (1.5 m) from the supports (Figure 2.2). Loads were applied eccentrically with respect to the shear center so that the lateral moment could be varied. Specimen L1 was subjected to a large eccentricity of load and concomitant lateral flange moments. Specimen L2 was subjected to smaller lateral flange moments. Numerous strain gages were employed. Girder deflection, rotation and web distortion in the test panels were carefully measured with dial gages. Failure modes in bending, shear, and combined shear and bending were observed. Data similar to that described in the first tests were recorded. Results were compared to computed values.

Report P3 (*7*) presents results for tests of a pair of simple-span curved I-girders connected with five intermediate cross frames and with diaphragms at each support (Figure 2.3). The centerline of the two concentric girders had a span of 185 ft (4700 mm) and a radius of 51.5 ft (15.7 m). The girders were spaced 3.0 ft (0.9 m) apart. A clamping mechanism was employed at the ends to provide stability and prevent uplift should it occur. The test girders were not prevented from rotating by these mechanisms, which were described as loose. Loads were applied either over the inside girder or between the girders. Numerous strain gages were utilized and measurements included the measurement of cross-frame strains.

Tests 1 and 2 were high-shear tests. A single concentrated vertical load was applied to the top of the inside girder at the one-sixth point from the support in Test 1 and at the five-sixths point in Test 2. Two different stiffener aspect ratios were tested. One web panel failed in shear in each test. Failed web panels were reinforced by welding a ¼-in. (6.4-mm) thick plate to the web after each test.

Tests 3 and 4 were combined shear and bending tests. A single concentrated load was applied to the top of the inside girder at the one-third point for Test 3 and at the two-thirds point for Test 4. ¼-in. (6.4-mm)

thick plates were added to the failed web panel after each test.

Test 5 was a bending test. Loads were applied at the third-points to the top of the inside girder (Figure 2.3). The center cross frame was removed to provide an unbraced length of approximately 60 in. (1524 mm). This provided an L/b ratio of 15, which was greater than the value of 10 that the researchers had proposed as an upper limit. However, the unbraced length in the adjacent panels was half of that in the center of the span.

Test 7 was similar to Test 5, except that the loads were applied 2.25 ft (0.7 m) from the inside girder instead of directly over the inside girder. The cross frames at the one-sixth point and at the five-sixths point were removed. This arrangement gave an equal unbraced length for the three panels.

Test 6 was similar to Test 4 and thus provided an additional test under combined shear and bending. The load was applied at the one-third point of the span, but 2.25 ft (0.7 m) from the inside girder. This test was not brought to failure in order to preserve the outside girder.

Test 8 was a bending test with loads applied at the one-third and two-third points of the span at a distance of 2.25 ft (0.7 m) from the inside girder. The cross-frame arrangement was the same as for Test 7. The outside girder failed in this test. The cross-frame forces decreased as the outside girder failed and its stiffness decreased. Girder rotations were determined from data measured with dial gages. It was determined that the cross-frame forces were a function of the various deformations in the girders. The top flange deformed as an arch, thus creating a larger force in one cross-frame diagonal than in the other in each cross frame. The theoretical cross-frame forces were not in good agreement with measured values. Significant redistribution of the load near failure indicated the significance of the load transfer between girders in the two-girder system.

Fukomoto Tests

Fukomoto et al. (*13*) performed tests on cold-curved rolled shapes. Six simple-span specimens were tested with a single load applied through a gravity simulator mechanism at the center of the span. The top and bottom of the girders were laterally restrained at the end supports. The end supports were torsionally free. Web slenderness was in the range of 45.

Nakai Tests

Nakai et al. (*14*) tested nine single curved doubly symmetric I-girder specimens. These tests were performed on 2-meter long specimens approximately 800 mm deep. The ends of the specimens were torsionally restrained by rigid cantilever beams (Figure 2.4). The cantilever beams were supported near the ends of the specimen. Downward vertical loads were applied to the cantilever extensions so that the curved beam specimens were tested in near uniform negative bending. There was essentially no shear applied. Web slenderness ratios ranged from 177 to 257. One of the specimens contained a longitudinal web stiffener.

The major shortcoming of these tests is that the brace points are forbidden from any rotation or translation. The test strengths are likely not affected significantly by the end conditions. However, the tests lack a realism that relates to the actual behavior of curved I-girders.

Other Tests

Daniels et al. (*15, 16*) and Nakai and Kotoguchi (*17*) have tested pairs of I-girders. Subsequent tests of curved girders have been performed on rolled beams in Australia since this project was commenced (*18*).

There have been several field tests of bridges. New York DOT performed an early test of a simple-span I-girder bridge (19). The University of Alabama tested a curved I-girder bridge (*20*). The University of Maryland tested a curved box-girder bridge during erection and for live load (*21*). A more recent test

was performed on a curved I-girder bridge in Minnesota by the University of Minnesota (*22*).

DEVELOPMENT OF THE EXPERIMENT DESIGN FOR THE FHWA CSBRP

Introduction

Physical testing of curved-girder specimens is complex and offers significant challenges. This is reflected in the limited number of such tests around the world to date, which have met with varying degrees of success. As discussed briefly in the preceding section, the tests that have been done have generally been conducted on small-scale doubly symmetric specimens composed of very thin plate material; many of which were subject to unrealistic boundary conditions at their ends and relatively large initial distortions associated with the welding of thin plate or sheet.

Typically, stringer highway bridges can be thought of as composed of a series of connected individual elements each possessing their own strength and stability; thus, the individual members can be tested alone as single components. In fact, the entire AASHTO specification is based on designing each individual member to ensure that its component strength is not exceeded. Unlike tangent girders, however, horizontally curved I-girders depend on adjacent members for their stability and must be braced laterally to the adjacent members in order to be statically stable since applied vertical loads produce torsion as well as bending. The adjacent girders and bracing members, combined with the internal vertical bending and lateral flange bending moments, provide equilibrium in curved I-girders.

Therefore, to properly examine the behavior of horizontally curved I-girders, it becomes highly desirable to test them in situ; that is, to conduct the tests on individual components that are part of a complete bridge structure that resists vertical loads and torsion as a system. With the exception of the two-girder tests by Mozer, Culver et al. reported in Report P3 (*7*), previous tests on horizontally curved I-girder component specimens did not adequately represent these conditions. Previous tests were also not conducted on full-scale systems. Full-scale tests eliminate the need for compensatory dead loads and more accurately reflect fabrication influences such as initial web and flange distortions and residual stresses; thus, the results are also considered to be more applicable to real bridges.

Because the testing of components to failure within such a realistic full-size structure had never even been contemplated before, there were a number of obstacles and challenges to overcome to ensure success, not the least of which were budget, schedule and convincing doubters about the viability of this unique concept. As a result, the development of the final experiment design for this project was a slow evolutionary process. The process began with the complete development of the preliminary concept for a full-size three-I-girder test frame representing a complete simple-span composite bridge structure. The frame would initially be used for the testing of several noncomposite I-girder component specimens inserted within the outermost girder of the structure. At the completion of these component tests, a concrete deck would then be cast onto the frame after it was modified. Testing of the completed bridge with a series of concentrated loads would allow for the development of influence surfaces for the actions in various components of the frame and for the eventual testing of the composite curved-bridge structure to failure. Upon completion of this initial investigation of the three-girder test frame, a second detailed investigation was initiated looking into the feasibility of single I-girder component tests as a possible alternative to the test-frame concept. The process then came full circle back the development of a more refined design of the three-girder frame for I-girder component testing only, accompanied by a more realistic and pared down experimental plan to fit the available time and budget.

Adding to the complexity of this unique and historical test was that fact that it was evident from the beginning that this project would have to involve the careful integration of computer analysis, not only to examine and evaluate the test results, but throughout the development of the experimental design. Sophisticated second-order geometric and material non-linear analyses would be required to predict the behavior of the components within the test frame throughout the full range of loading. Such analyses would ensure that potential corruptive secondary effects would be minimized during the tests, and that these tests could be safely and successfully carried out for the first time. The predicted actions would also have to be used to safely design the various test-frame components. A theoretically sound and efficient set of

component specimens would also have developed at the same time. As a result, the coordination of model development and verification, analysis and evaluation of the analytical data, and several iterations of the design of the test-frame components based on that data was a difficult and time-consuming process that extended the time required to develop the final experiment plan. Similar efforts were also required during the investigation of the single-girder tests. The complexities associated with testing a three-girder system were foreseen to some an extent when the project was originally developed. However, the degree of the complexities could not be anticipated and solved until detailed theoretical analyses were undertaken. Although the time required for development of the final plan often led to high levels of frustration, in the end the entire effort was justified in light of the total expenditure of time and resources necessary to carry out such a highly visible and novel test. The eventual successful completion of the component test program, with no major problems experienced, lends further credence to the level of effort expended in the development of the experiment plan.

Following is a description of the complete evolution of the experiment plan from the development of the initial concept for the three-girder test frame, through the investigation of the single-girder component test alternative and finishing with the final design of the test frame and I-girder bending component specimens. This discussion is preceded by a. description of the general overall philosophy guiding the development of the plan. The discussion begins, however, with a brief description of the FHWA Structures Laboratory. The FHWA Structures Laboratory was felt to be singularly appropriate for such a large and complex test because it could rather easily accommodate a reasonable full-size bridge on the laboratory floor.

Description of the FHWA Structures Lab

The FHWA Structures Laboratory, which became fully operational in August 1985, is located at the FHWA Turner-Fairbank Highway Research Laboratory (TFHRC) in McLean, VA outside of Washington, D.C.

The laboratory structural floor system is essentially a 14-ft (4.3 m) deep reinforced concrete box girder with four large cells underneath the working floor level. The entire floor system is instrumented to allow the capability to monitor the response of the floor during testing. The test floor is 50 ft (15.2 m) by 120 ft (36.6 m) in plan, which provided an ideal platform for the design of the planned full-size testing program. The test floor, or top flange of the box, is 2'-6" (0.76 m) thick with a ¾" (19mm) concrete topping. The top flange has 8-in. (0.3 mm) corbels and is heavily reinforced. The floor has 573 tie-down holes approximately 3 in. (76 mm) in diameter spaced in a rectangular grid at 3-ft (0.9 m) centers through which Dywidag threadbar rods can be passed to apply load using a number of possible configurations. Loads can either be applied above or underneath the floor and can be transferred to the specimen using an appropriate configuration of Dywidag rods and reaction beams. Static loads are typically applied using an Enerpac hydraulic system with loading cylinders. Dynamic loading can also be applied using an MTS servo-hydraulic loading system with jacks. Each floor hole is capable of resisting a 100-kip (445 kN) load in either direction, or greater, if a base plate is used to distribute the load. The constraints of the rectangular grid of tie-down holes presented one of several challenges encountered in the design of a safe and workable loading system for the curved I-girder component tests.

The laboratory is equipped with two overhead cranes, each with a capacity of 40,000 lbs (178 kN). Two large doors on the west and north sides of the laboratory provide access for direct delivery of materials. Tests can be monitored from the Test Control Center located next to the laboratory on the south side. A plan view of the laboratory is shown in Figure 2.5.

Three-Girder Test Frame - Preliminary Concept

***Introduction*:** Since it was felt early on in the project that the testing of a single curved I-girder that derives part of its strength from an entire system would be too complex, it was decided to initially investigate the concept of testing individual I-girder component specimens within a full-scale simple span curved bridge. By using a bridge as a test frame for component testing, ideal boundary conditions

representing more realistic torsional restraints could be obtained. The components could be subjected to nearly pure vertical bending or a combination of vertical bending and shear within the frame under more realistic loading conditions. The distribution of lateral flange bending would be more representative of actual conditions. In addition, for economy, parts of the test frame could possibly be reused later on should it be desired to cast a concrete deck on the frame and test the structure as a full-scale prototype bridge under controlled laboratory conditions.

Such a test would represent a historic advancement since it would represent the first time that multiple component specimens would be tested to failure within a complete structure that serves as a reusable test frame, and also it would represent the first time that a structural test would be analyzed so completely prior to the construction of the frame or test components.

Philosophy: There are numerous complexities introduced by testing components within an entire curved-bridge structure. For one, it becomes more difficult to predict the behavior of an individual component specimen within the system. Curved members in a bridge system receive load directly, as well as from the other girders in the system, through the cross-bracing members. As one girder yields, typically the outermost girder first, its stiffness is reduced significantly so as to affect the load distribution in the girders. Under this condition, all the cross-frame forces do not necessarily increase in the same sense with increasing load. Instead of adding load to the outermost girder, the sense of the load in some of the cross-frame members will tend to reverse with increasing load and the girders that have remained elastic will begin to carry a disproportionate amount of the increased load. The load transferred to the innermost girder may begin to drop off due to the tendency of this girder to want to uplift as the outermost girder softens. At a point when the outermost girder will no longer accept any load, the system will continue to accept load as long as the structure has not reached its maximum capacity or become unstable. That is, the structure will continue to resist load along a different increasing load-deflection path as long as one or more of the other girders can adequately sustain the load. This behavior is contradictory to the classical load-deflection behavior that is often observed in individual member tests where the load drops off to a plateau after the member reaches its ultimate capacity. As a result, the definition of the ultimate (or failure) load of a component specimen located, for example, within the outermost girder of a curved structure, becomes more subjective. The ultimate load might be defined by the point where one or more of the interior girders are resisting nearly all the additional applied load, or else deflection, rather than load, might be the limiting condition that defines the ultimate load for the specimen.

In an actual curved bridge with moving loads, the situation is quite complex. The position of the live loads producing the maximum load in the outermost girder may not also produce the maximum load in the adjacent girder. In this situation, the next girder would have additional capacity. If the next girder is loaded to its maximum load by the live load position that produces the maximum load in the outermost girder, the bridge may not have much additional capacity after the outermost girder reaches its ultimate load. This behavior is quite different from tangent girder bridges that typically have significant additional capacity when any girder is loaded to ultimate by live load.

The physical loading of such a system is also complicated by the fact that each curved girder in the frame will begin to twist and deflect immediately upon loading. The measurement of end reactions and cross-frame forces, which is critical to the accurate determination of the actions in the component, also offers unique challenges. In addition to vertical reactions, the bearings are subjected to lateral and radial forces. Resistance to these forces introduces forces not only into the bearings, but also into the girders, which affect the girder moments, shears and torques. In order to minimize these lateral reactions in the test frame, minimum lateral restraints were used.

Such an ambitious undertaking could not even be contemplated without first being able to predict the behavior of the test frame analytically prior to testing. In previous curved-girder tests in the late 1960s, the technology was not yet available to practically perform the geometric and material non-linear analyses that are required to predict the behavior of component specimens located within a full-size multi-girder test frame up to their ultimate capacities. For the planning of this test program, the necessary analysis tools were indeed available, which made it possible to better predict the movements, reactions and internal actions in all members of the test frame so that such an ambitious test program could be carried out safely

for the first time. As described later on, these analysis results were an integral part of the successful design of the experimental program for this project and clearly illustrate the necessity of incorporating rigorous preliminary analyses into the development and design of large-scale experimental tests.

This undertaking would also not have been practical without the advent of modern data-acquisition systems. These systems allow for the automatic collection and reduction of the enormous amounts of data that must be generated in a test of this magnitude to properly examine the behavior of the test frame and component specimens.

One of the important initial decisions that had to be made during the preliminary design of the test frame was the selection of the number of girders in the cross section. Initial consideration was given to a two-girder system consisting of two curved girders connected by cross frames and supported by bearings at their ends, as tested by Mozer, Culver et al. (*7*). This structural system is stable when the bearings and cross frames between the girders are capable of ensuring equilibrium. In a two-girder setup, however, the loads must be applied at a location in-between each girder to ensure stability and prevent uplift at the ends of the inside girder, which complicates the required loading mechanism. A two-girder system is definitely much more susceptible to uplift than a multiple-girder system when one of the girders, or when a significant portion of one of the girders, fails. Mozer, Culver et al. experienced these problems in Test 6 of Report P3. With a two-girder system, stability is achieved from the interaction between girders since neither girder alone would be stable. Failure of one of the girders would cause a significant reduction in the stability of the system and would probably lead to collapse. Therefore, practically speaking, it would be risky to fail one girder, or a portion of one girder containing an individual component specimen, while attempting to keep the other girder and the cross frames elastic and the entire system stable. A three-girder system would offer greater stability and redundancy and would be less susceptible to uplift. By ensuring greater stability throughout the entire range of loading, it should then be easier to fail an individual component specimen, located within the outermost girder, while keeping the remaining two girders and the cross frames elastic. The possibility of using four girders was considered but was rejected because of space limitations in the laboratory and the desire to eliminate scaling down the experiment to less than full size. Therefore, a three-girder system was chosen for the test frame.

The decision was next made to utilize a simple span for the test frame, again because of space limitations in the laboratory and the desire to eliminate the need for any scaling. It was thought that a simple-span arrangement would be adequate to test pure bending and high shear. The frame would be supported on abutments at each end and would be approximately 6.5 ft (2.0 m) off the laboratory floor for ease of access. If necessary, one of the abutments could be moved inward and the test frame appropriately loaded to induce negative bending and simulate the conditions over the interior pier of a continuous span. A plan view of the initial concept for the three-girder test frame is shown in Figures 2.6 and 2.7. The basic framing plan utilized radial supports. In the beginning, the arc span along the longitudinal centerline of the outermost girder (Girder 3 or G3) was set at 114'-0" (34.7 m). Cross frames were equally spaced at 19'-0" (5.8 m) along the centerline of G3. The girder spacing was set at 10'-0" (3.05 m) and the centerline radius for G3 was set at 250'-0" (76.2 m). Because of the concern of laboratory personnel over space limitations and the desire to keep some of the floor space clear for other projects, it was decided to reduce the arc span to 90'-0" (27.4 m) along the centerline of the center girder (Girder 2 or G2), reduce the basic cross frame spacing to 10'-0" (3.05 m) along the centerline of G2, reduce the girder spacing to 8'-9" (2.7 m), and set the centerline radius for G2 to 200'-0" (61.0 m), as shown in Figure 2.8.

Skewed supports are frequently encountered in practice and are particularly troublesome. Skewed supports introduce torsion into the girders whether the girders are tangent or curved. Torsion in curved girders introduced by skew is generally additive to torsion due to curvature. Torsion due to effects other than curvature can be more severe than torsion due to curvature. However, torsion in tangent girders does not create the level of lateral bending amplification experienced in curved girders. To examine the combined effect of torsion due to curvature and due to skew, a series of bolted field splices was proposed near the ends of the girders in each scheme to allow different skews to be introduced into the basic framing. The skew would be introduced by removing or adding girder sections at the bolted splices and relocating the abutments and bearings as necessary. Allowances were also made to permit modifications to the cross-frame members and cross-frame spacing, the addition of bottom flange bracing, and the changing of

bearing type, orientation and degree of lateral restraint at each bearing. It was envisioned that two different types of bearings would be investigated: 1) pot bearings, and 2) steel-reinforced elastomeric bearings.

A rather ambitious three-phase test program was initially envisioned utilizing the test frame. The first phase would involve studies during the construction of the test frame in the laboratory. These studies would examine the sequence of girder and cross-frame erection, the use of temporary supports during the erection, the stability of a single girder with various end restraints, the effect of skewed supports and girder out-of-plumb, the effect of different bearing types and arrangements, the effect of different relative girder stiffness values, the effect of bottom flange bracing, the effect of cross frame location, type and spacing, and the effect of cross frame detailing assumptions. Fabrication of the test frame would be performed in a commercial bridge-fabrication shop. The frame would be pre-assembled in the shop to ensure fit-up and then disassembled and shipped to the laboratory for erection. Steel material to be used in the fabrication would be tested to determine the static yield stress and ultimate tensile strength for comparison to mill test results. Bearings would also be tested. For each planned erection sequence and framing plan, it was envisioned that the test-frame girders would be erected on temporary supports in the laboratory until the cross frames were bolted. Load cells would be placed to measure the reactions. The temporary supports would then be removed. Tests to simulate the effect of deck weight on different framing and bearing arrangements would then be conducted by pulling down on the girders from the top with a series of concentrated loads. These loads, determined from a finite-element analysis of the test frame, would be designed to reproduce the correct weight on each girder, along with the correct end shear and vertical bending moment. Since the lateral flange bending moments are directly related to the vertical bending moments, the correct lateral flange bending moments would also be reproduced. Detailing would be such that the girders would be plumb and have a level profile after each simulated deck pour, which is difficult when different skews are considered. As a result, different cross frames would likely be required for each framing arrangement. Prior to the third and final phase of the test program (see below), a concrete deck would be cast onto a single selected framing plan in a single pour.

The second phase would involve component specimen testing within the noncomposite frame utilizing the original radial support arrangement. Noncomposite component test specimens, with varying web and compression-flange slenderness ratios and transverse stiffener spacings, would initially be inserted in the center of the outermost girder. Each specimen would be inserted and removed using bolted field splices at each end of the specimen. A series of concentrated loads would then be applied to subject the specimens to nearly pure bending. The loads would be applied so as to minimize the potential for uplift and to maximize the load effects in each component specimen while limiting the stresses in the remaining portions of the frame to the elastic range. By keeping all remaining portions of the test frame elastic throughout the test, it should be possible to deduce the moment in the yielded component specimen at the point of failure from statics, as described below. Such computations would require the accurate measurement of elastic girder strains, vertical and horizontal end reactions and cross frame forces. Deflection measurements of the test frame in three-dimensional space would also be desirable. Test results for each component would then be compared to various equations used to predict curved girder component bending strengths and to the results from analytical models of the test frame. It was anticipated that the configuration of the test frame would then be changed appropriately (e.g., one abutment moved to the center of the bridge) to subject a separate set of component specimens to different combinations of vertical bending moment and shear.

As mentioned above, all component specimens would be noncomposite. Because of the paucity of tests on curved I-girders and the inherent complexities in testing curved girders, it was felt that the component tests should initially be done on noncomposite specimens. While it is recognized that the majority of sections are composite when checking their strength (particularly in positive bending), adding a composite deck to a curved bridge structure causes the shear center of the combined bridge section to lie above the deck, while the shear center of an individual composite section lies within the cross-section. Thus, although the design of both curved- and straight-girder bridge members is currently based on member or component strength, the extrapolation of the results from a composite component test (in a noncomposite frame) to a girder in a composite curved-bridge system might be called into question. The deviation in component and system behavior for the noncomposite structure is not expected to be as large. The effects of lateral flange bending are also less on curved composite I girders in positive flexure because of the support offered to the top (compression) flange by the hardened concrete deck.

Complicating the design of the component specimens further is the fact that there are almost an infinite number of variables that may affect the bending and shear resistance of curved I-girders. These variables include the span length, radius, unbraced length, flange width, web slenderness, web stiffening and whether the girder is singly or doubly symmetric. It would certainly not be possible to independently study the effect of each of these variables in this experimental program. For example, the costs and complexities that would result from testing components with a different radius either within this single frame, or using a second separate frame, would be prohibitive. However, successful testing of even a limited number of specimens, containing variations of as many of the important variables as possible, would represent a significant stepwise advancement and serve as a model for additional testing in the future. Also, reasonable simulation of these tests through non-linear finite-element analyses may lead to future analytical parametric studies by others to generate additional data in lieu of more costly experimental tests.

The third and final phase of the planned test program would involve testing the completed frame, with a concrete deck, for simulated placement of live load and for thermal changes. The composite test frame would then be loaded to failure, with the specific indicator of failure to be determined. First, concentrated unit loads would be applied to the deck to establish elastic influence surfaces for numerous load effects such as reactions, moment, shear and cross frame forces. These influence surfaces would then be compared to analytically determined influence surfaces. ·From the influence surfaces, positions would then be determined for placement of concentrated loads to simulate the design live load. H20 truck loads would be simulated by placing sets of concentrated loads on the deck utilizing Dywidag bars running through holes in the deck to jacks underneath the laboratory floor. The concentrated loads would simulate the wheel loads. Although lane loads governed the design, it was not felt to be necessary to simulate these loads in the test. Lane loads controlled on this rather short bridge because H20 was assumed for the design live load and H20 lane loading is specified by AASHTO to be the same as HS20 lane loading. It was further envisioned that by wrapping components of the bridge in plastic, or by embedding pipes in the deck, heat could be applied locally or globally to study the effect of thermally induced movements on the frame when configured with various bearing types, orientations and restraint conditions. Finally, a single set of concentrated loads would be used to simulate a single live load that would fail the bridge, with failure most likely defined by some maximum deflection limit. The live load would be positioned over the girder anticipated to be the critical girder for failure, with the position determined to maximize the selected girder response assuming the structure remains elastic.

Although this initial test plan was eventually modified and pared down considerably due to scheduling and budgetary constraints, it still served as an important underlying basis for guiding all the work that was eventually done in this project. As such, the work and thought that went into this plan in the beginning of the project was extremely critical in establishing the overall philosophy of the experimental program and in helping to get the project started. As time and budget permitted, many of the important concepts and ideas that were conceived in this early plan were eventually implemented in some form in the actual experimental program that was carried out. Hence, it was felt to be important to review this plan in some detail at this stage of the report.

To ensure that the overall philosophy of testing component specimens to failure within a full-size three-girder test frame would be successful, a reasonable strategy had to be developed for deducing the actions in the component through the entire range of loading (including through the inelastic range). To provide a measure of redundancy and confirmation, a three-pronged strategy utilizing three independent approaches was developed for experimentally and analytically deducing the actions in the component specimens. All three approaches are fundamentally grounded in the principles of statics. The first approach is termed the indirect statical-moment method, the second approach is termed the free-body diagram method, and the third approach is termed the G3 moment method. A requirement of these approaches is that the portions of the test frame outside the test component must remain elastic and stable until the component has reached its maximum moment capacity. When the component specimen starts to fail, the stiffness of the specimen decreases resulting in a decrease in the overall stiffness of the frame. This causes the load-deflection path for the structure to change slope, but not to become horizontal. The load-deflection path for the structure will reach a maximum only when the entire structure has reached its maximum capacity or has become unstable. At some point, the test component will not be able to resist any additional load. At this point, the center girder in the frame will be resisting nearly all the additional applied load. The

determination of this point and the maximum vertical bending moment in the component specimen at this point is critical to the success of the test-frame concept. The three proposed approaches for deducing the vertical bending moment in the component specimens within the test frame are discussed in more detail below:

Indirect Statical-Moment Method. In the indirect statical-moment method, the total vertical bending moment in the three girders at any section, or the statical moment, can be determined from the measured applied loads and reactions. At a given section, the vertical bending moment in any one girder is then taken equal to the statical moment at that section, as described above, minus the vertical bending moment in the other two girders. The vertical bending moment in the other girders can be determined from the integration of stresses predicted from strain measurements on the other two girders, as long as those girders remain elastic. In the planned tests, only the outermost girder containing the component specimen is expected to experience yielding. Thus, it must be ensured in the design of the test frame that the other two girders remain elastic so that the measured strains will be reliable predictors of the elastic stresses, and hence, the elastic moments in those girders. While the component specimen is elastic, the vertical bending moment in the component can be computed directly from the strain readings and compared to the moment determined by the indirect method. When the strain readings in the component are no longer reliable predictors of stress, the indirect statical-moment method can be used to determine the vertical bending moment in the component.

Free-Body Diagram Method. Since the statical-moment method is an indirect method of measuring the vertical bending moment, it was felt that a second method was needed to confirm the results. By assuming a cut through the cross frames between the outermost girder containing the component and the center girder, a free body is obtained. The loads applied to the free body are the reactions, applied loads and cross-frame forces. The vertical bending moment in the component can then be determined by applying the external actions to the girder. In addition to the reactions and applied loads, this method requires the determination of the axial forces and moments in the cross-frame members attached to the outermost girder containing the component.

G3 Moment Method: Since the component fails in the section at midspan, the vertical bending moment at other points in G3 is likely to remain elastic at failure and can be determined from the strain gage readings at those points. For example, this method can be used at sections near the brace points in the test components where strain gages are located. The vertical bending moment at these sections can also be checked by the first method given above. The vertical bending moment determined from the strain gage readings at these sections should also give a rather close estimate of the vertical bending moment at the midspan section since the vertical bending moment is nearly constant within this region.

Analysis and Design: Having agreed upon the initial overall philosophy and a suitable framing plan for this initial configuration of the three-girder test frame (Figure 2.8), work then proceeded to perform an analysis of the frame and an accompanying design of its components. At this stage, the decision was made to initially analyze and design the test frame as a conventional horizontally curved I-girder bridge.

The test frame (prototype bridge) was designed according to the Load Factor Design procedures given in the 1993 AASHTO Guide Specifications for Horizontally Curved Highway Bridges (23) and the 15th Edition of the AASHTO Standard Specifications for Highway Bridges (1992), including the 1993 Interim Specifications (24). A cross section of the bridge is shown in Figure 2.9. The girder spacing is set at 8'-9" (2.7 m), with deck overhangs set at 2'-9" (0.84 m), for a total out-to-out width of 23'-0" (7.0 m). AASHTO M270 Grade 50 (M270M Grade 345) steel is used for the design of the girder web and flanges and AASHTO M270 Grade 36 (M270M Grade 250) steel is used for the design of all other components.

The specified 28-day compressive strength of the deck concrete, f'_c, is taken equal to 4,500 psi (31.0 MPa). Composite design is assumed using three 7/8" x 6" (22.1 mm x 152.4 mm) stud shear connectors per row on the top flange. An 8-inch (200 mm) cast-in-place concrete deck (with no integral wearing surface) is designed to span the 8'-9" (2.7 m) girder spacing. The deck is assumed flared from the edge of the deck haunch over the outermost and innermost girders to a thickness of 9.5 inches (240 mm) at the edge of the deck overhangs. The deck haunch is assumed to be 14-inches (355 mm) wide by 3-inches (76 mm) thick over each girder. The thickness of the haunch is measured from the top of the web to the bottom of the deck. Five percent of the total steel weight is added as an additional noncomposite dead load to approximately account for detail weight. Superimposed dead loads include two 1'-6" (0.46 m) wide parapets, each with a unit weight of 505 lbs/ft (752 kg/m), applied at the extreme edges of the deck, which results in a roadway width of 20'-0" (6.1 m). A future wearing surface of 25 psf (122 kg/m2) is also assumed in the design. The parapets and future wearing surface are applied to the long-term 3n composite section. An AASHTO Case II roadway is assumed for the fatigue design. Constructibility is checked according to both AASHTO and PennDOT DM-4 (25) criteria. Field splices and cross frame connections are designed using black 7/8" (22 mm) diameter ASTM A325 (A325M) Type 1 high-strength bolts.

H20-44 is specified as the design live loading. The H20-44 truck loading has two axles, with a front axle weight of 8.0 kips (35.6 kN) and a rear axle weight of 32.0 kips (142.3 kN). The spacing between the two axles is fixed at 14'-0" (4.3 m). Lane loading is a 640 lb/ft (952 kg/m) uniform load in conjunction with an 18.0 kip (80 kN) concentrated load for moment and a 26.0 kip (116 kN) concentrated load for shear. All live loads are assumed placed in 10-ft (3.05 m) design lanes. Impact is applied according to Article 3.8 of the Standard Specifications. H20 was selected instead of HS20 as the design live loading to reduce the overall capacity of the test frame to better fit the available jack capacity at the laboratory. It was also felt that the smaller number of wheels (four versus six for HS20) would be easier to simulate in the composite bridge test.

The analysis and design were completed using the commercially available Bridge Software Development International (BSDI), Ltd. BRIDGE SYSTEM 3D finite-element software (*26*). Using the 3D System, a full three-dimensional elastic finite element analysis of the bridge was conducted. The basic model was developed in accordance with Figure 2.8, except that the bottom lateral bracing in the end bays was not initially included in the model. Referring to Figure 2.8, the model was developed with the following boundary conditions at the end bearings:

Girder 1: Girder 1 was fixed against vertical, tangential and radial translation at Line 1L. In addition, Girder 1 was restrained against rotation about the vertical axis at Line 1L. At Line 1R, Girder 1 was fixed against vertical translation, but was free to translate in the tangential and radial directions.

Girder 2: Girder 2 was fixed against vertical translation and was free to translate in the tangential and radial directions at Lines 1L and 1R.

Girder 3: Girder 3 was fixed against vertical translation and was free to translate in the tangential and radial directions at Lines 1L and 1R.

All restraints were applied in the local or element coordinate system. With the exception of the rotation about the vertical axis at Girder 1 Line 1L, all girders were free to rotate about their local X, Y and Z axes at Lines 1L and 1R.

The concrete deck was modeled using 8-node solid elements consisting of nodes located at each of the four corners in two overlying X-Y planes separated by a distance Z. By using 8-node elements, the actual deck thickness was represented. Each of the 8 nodes has three degrees of freedom corresponding to displacements along the global X, Y and Z-axes. The deck was connected to the girders with beam elements representing shear connectors. These beam elements are very stiff in bending, thus restraining the deck from rotating with respect to the girders.

The girder flanges were modeled using straight beam elements between nodes. Each of the nodes has

six degrees of freedom corresponding to displacements along, and rotations about, the global X, Y and Z axes. As a result, both the axial force and lateral bending moments in each flange can be determined. The model included 18 top- and bottom-flange elements along the length. The girder web was modeled using a single straight plate element through the depth and between nodes. The degrees of freedom in each web element are compatible with those in the flanges. The model included 18 web elements along the length.

The cross frames (Figure 2.9) were modeled with truss elements that represented the individual members. The end connections of all the cross-frame members were assumed to be pinned in the analysis; thus, each element has a single degree of freedom representing axial translation. The cross-frame connection plates were not included in the model. The cross frames were connected directly to the top and bottom web nodes in the model.

The self-weight of the structural steel members was applied as vertical body forces. The weight of the concrete deck was applied to the top-flange nodes as equivalent concentrated loads. The weight of the parapets was applied as equivalent concentrated loads to the nodes along the edges of the deck overhangs. The future wearing surface load was applied as a vertical body force. Influence surfaces were generated for live-load vertical bending moment, shear and bottom flange lateral bending. The live load effects were then determined by loading the appropriate influence surface.

The analysis results are summarized in Appendix A. Similar elastic analysis results for this bridge, computed using the general-purpose finite-element analysis software GTSTRUDL (*27*), the commercially available two-dimensional grid-analysis software MDX (*28*), and the approximate V-Load analysis software VANCK (*29*), are also summarized in Appendix A. In addition to the results for the base configuration of the model, a number of parametric variations to the base configuration were made and analyzed with the BSDI 3D System software. The specific variations that were made and the results of those analyses are discussed in detail in Appendix B.

After two or three iterations, the girder sizes shown in Figures 2.10 through 2.12 were selected. The web depth of 48 inches (1219 mm) provided a span-to-depth ratio for the steel girder ranging from 21.5 for Girder 1 to 23.5 for Girder 3. The girders were each checked against the aforementioned specification provisions. The maximum performance ratios were 0.98 for Girder 3, 0.81 for Girder 2, and 0.48 for Girder 1. The factored tip stress for strength in the bottom flange at midspan governed in each case. Although the l" x 14" (25 x 355 mm) top flange of each girder qualified as compact, the tip stress was conservatively checked for both flanges. Uplift was not detected at the ends of Girder 1.

Cross frames were spaced at 10'-0" (3.05 m) along the centerline of Girder 2 in the model. The maximum cross-frame forces from the model were used to arrive at the cross-frame sizes shown in Figure 2.9, and to design the cross-frame connections. The finite-element analysis results were also used to design stud shear connectors, transverse stiffeners (on one side of the web only), bearing stiffeners, cross-frame connection plates, the bolted field splices and the flange-to-web fillet welds. Since a decision had not yet been made on the final configuration of the abutments, designs for the abutments were not yet completed at this stage.

After arriving at a satisfactory preliminary design for the girders and cross frames, modifications to the basic model were then made in an attempt to achieve an improved understanding of the behavior of the bridge acting as a test frame during component testing prior to conducting more complex inelastic analyses. First, the diagonal bottom flange lateral bracing members shown in Figure 2.8 were added to the model at each end of the bridge. Structural tees were used for these members. During component testing, these members are necessary to provide overall stability to the noncomposite frame and to resist relative longitudinal movement or racking of the noncomposite girders. A series of elastic analyses were then conducted with a preliminary set of component specimens inserted one at a time into the center of the outermost girder and subjected to the design dead and live loads. To roughly simulate the conditions that might exist in the test frame once a component specimen has yielded, the analyses were then conducted under the following conditions for one of the component specimens: 1) using a reduced Young's modulus equal to 0.5E in the flanges and web of the component specimen, 2) using a reduced Young's modulus equal to 0.75E in the flanges of the component specimen, 3) using a reduced Young's modulus equal to

0.75E in the flanges of the component specimen with the diagonals in the cross frames in the outer bay at Lines 5L and 5R removed, and 4) the preceding condition with the diagonals in the cross frames in the outer bay at Lines 4L and 4R also removed.

From the results of these analyses, it became clear that significant additional modifications to the prototype bridge would be necessary to ensure elastic behavior outside the component specimen when the bridge is acting as a test frame. At the same time, work was progressing on the development of an ABAQUS *(30)* model of the prototype bridge in order to conduct more sophisticated second-order inelastic analyses of the bending tests, but the results were not yet available to allow more informed critical decisions to be made. Configurations of the bridge for testing of component specimens under various combinations of bending and shear had also not yet been studied, nor had the behavior of the composite bridge in the inelastic range. Therefore, because of the numerous details that still had to be worked out on the test frame at this stage (including the design of the loading mechanism and support structures), and the desire of the FHWA to begin testing in the laboratory as soon as possible, the decision was made to begin a simultaneous investigation of a possible alternative scheme for testing of the component specimens. This scheme would involve testing of the component specimens within an isolated single girder. It was felt that the single-girder arrangement would allow more specimens to be tested in a quicker time frame. Also, the data analysis of a single-girder test would not be complicated by the load sharing that occurs through the cross frames in the three-girder test frame.

Single-Girder Test

***Introduction*:** While work continued on the development of a detailed ABAQUS model of the three-girder test frame, a separate investigation was simultaneously initiated to investigate in detail the feasibility of an alternate scheme for the component testing. In this alternate scheme, the component specimens would instead be inserted at various locations within a single simple-span horizontally curved I girder representing the outermost girder (Girder 3) of the prototype bridge. As such, the girder would be 93.9375 ft (28.6 m) long (measured along the arc) and would have a radius of 208.75 ft (63.6 m). The girder would be supported such that the bottom of the girder web would be located approximately 6'-6" (2.0 m) off the laboratory floor. A detailed investigation of this single-girder test configuration lasted approximately six months.

***Philosophy*:** The overall philosophy for the design of the single girder test was to support the girder in such a way that the deformations of the component specimen and the lateral flange bending moments within the specimen would be compatible with those experienced by the specimen within the three-girder frame. The investigation concentrated primarily on bending tests in which the component specimens would be inserted in the center of the single girder (Figures 2.13 and 2.14), which would then be loaded with equal concentrated loads at approximately the third-points of the span in order to subject the specimens to nearly pure vertical bending. As in the three-girder test, the portions of the singly symmetric girder outside the component specimen would be proportioned to limit the possibility of yielding or local and lateral distortions of the web or compression flange of the supporting portions of the girder during component testing. For this study, the proportions of Girder 3 from the prototype bridge (Figure 2.12) were initially used for the supporting portions of the single girder. As the investigation progressed, however, it became evident that to ensure that the supporting girder remained elastic and stable throughout the test, the yield stress of the supporting portions of the girder would have to be increased from 50 ksi (345 MPa) to 70 ksi (485 MPa). Also, it was decided to conservatively increase the web thickness of the outer (supporting) portions of the girder from 3/8" (9.5 mm) to 9/16" (14 mm).

Further component tests were also originally envisioned under different combinations of vertical bending moment and shear. To test specimens under high vertical bending moment and low shear, it was envisioned that the applied loads would be moved closer to the end supports. The specimens would then be inserted in the girder near each support, which would allow for the testing of two specimens at the same time. To test specimens under a combination of high vertical bending moment and shear, it was envisioned that the specimens would be inserted at the center of the girder and loaded by a single concentrated load applied at midspan. To subject specimens to even steeper moment gradients, consideration would then be

given to moving the end supports closer together. Testing of the component specimens with a composite slab was not originally contemplated using this single-girder arrangement. Instead, the conceived plan still called for casting a deck slab on the three-girder system at the completion of component testing.

***Analysis and Design*:** Preliminary linear elastic analyses of the single girder test set-up for the bending component tests were run using ABAQUS to obtain an initial feel for the predicted maximum deflections of the girder and the associated reactions at each support for various assumed boundary conditions. Each of the nine preliminary component specimens was inserted one at a time at the center of the girder for the analyses. In the model, 8 shell elements were used through the depth of the web and 120 elements were used along the length. The flanges consisted of 2 elements across the width and 120 elements along the length. Since the actual physical boundary conditions were unknown at this stage, a sensitivity study was conducted to investigate the effect of varying degrees of restraint on the results.

To obtain preliminary sizes for the test fixtures, numerous linear elastic analyses of the proposed single girder test set-up were then run on coarser models using both GTSTRUDL and the BSDI 3D System. The configuration of the test frame and bracing necessary to support the single girder was determined by comparing these analysis results to the results from a linear elastic analysis of the three-girder test frame. In the initial scheme, it was envisioned that the girder would be braced on both sides at set intervals along its length by approximately 7-ft (2.1 m) long threaded rods (Dywidag bars) attached to W24x76 (W610x113) stub columns spaced 18-ft (5.5 m) apart in the radial direction. The columns, in turn, would be braced by struts extending diagonally to the laboratory floor on the outside of each column. The analyses showed, however, that extremely large bending moments would be generated if the columns were free to deflect as cantilevers as the full-size horizontally curved girder deflects and twists. Therefore, the columns were extended in height and a W27x94 (W690x140) cap beam was added to create a complete support frame at each bracing line, which significantly reduced the column base moments in the analysis. As shown in Figure 2.15, the bottom of the cap beam was assumed to be located 1'-0" (0.3 m) above the top of the girder web. Each column was assumed rigidly connected to a 2-in. (51 mm) thick base plate that would be bolted down to the laboratory floor. Because the flange of each column to which the bracing would be attached had to be oriented so that the bracing would be radial to the girder and because the hole pattern on the laboratory floor was orthogonal, this necessitated a different size and shape for each column base plate, as shown in Figure 2.16.

To allow the girder to deflect vertically and also twist in a manner similar to the outermost girder in the three-girder test frame, the threaded rods supporting the girder on the outside of the curve would need to run from the bottom of the girder to the supporting frames. On the inside of the curve, the rods would need to run from the top of the girder to the supporting frames. In an attempt to match the maximum vertical, radial and tangential displacements of the girder in the three-girder frame from a linear elastic analysis of the frame, it was further determined that the supporting rods on the inside of the curve would need to be inclined downward approximately 1'-6" (457 mm), as shown in Figure 2.15. The supporting rods on the outside of the curve would also need to be inclined upward approximately 3" (76.mm). This support arrangement would essentially force the girder to follow a predetermined deformation pattern along two circular arcs corresponding in an approximate fashion to the elastic deformation pattern of the outermost girder in the three-girder frame. It was also felt that supporting the girder in this manner would result in a reasonable match of the first-order lateral flange bending moment distribution within the component specimen determined from the system analysis. The braces would be attached to connection plates on the girder at points 6 in. (152 mm) below the top flange on the inside of the curve and 6 in. (152 mm) above the bottom flange on the outside of the curve.

In the initial analyses, 2.25-in. (57 mm) diameter threaded rods were assumed for the bracing members. Based on the analysis results, the diameter of the rods was later reduced to 1.375" (35 mm). To allow near free rotation in any direction at each end of the threaded rods, it was proposed that a series of shackles and clevises be used at each end of each rod. A #8 clevis with a safe working load of 135 kips (601 kN) and a maximum capacity of 270 kips (1201 kN) would be attached to each end of the rod. Each clevis would then be attached to two 2.5-in. (64 mm) anchor shackles connected in

series and configured to allow near free rotation of each end of the rod. Each anchor shackle would have a safe working load of 110 kips (489 kN) and a maximum capacity of 242 kips (1076 kN).

In the analyses, rigid supports were assumed in the vertical direction at each end of the girder. Restraint in the tangential direction was provided at one end of the girder at the neutral axis of the end section. Restraint was provided at the neutral axis in order to minimize the magnitude of the tangential restraint force that could potentially develop at the actual location of the bearing (immediately below the bottom flange). No radial restraint was assumed at either end, although some degree of radial restraint would be provided by load cells that would be used to measure the reactions at each bearing. Each support was also assumed to be free to rotate about all three axes. Loads were applied in the analysis by pulling down on the bottom flange at approximately the third points of the girder. It was assumed that loads would be applied in the test utilizing deflection control to ensure stability of the girder beyond the ultimate load of the specimen as the girder unloads.

Providing the actual physical restraints and loading mechanisms in the test to duplicate the preceding modeling assumptions is a significant challenge. Adding to the challenge is the fact that instrumentation (load cells, etc.) must be incorporated within the design for measurement of the reactions. Several schemes were investigated for the design of the end supports and the loading fixtures. At the end supports, the bearing scheme shown in Figure 2.15 consisting of two stacked orthogonal pivot bars resting on a pedestal was eventually discarded as being too unwieldy. An alternate scheme was investigated in which the girder would rest on Hillman rollers, which in turn would sit atop a spherical bearing resting on a 300-kip (1334 N) load cell. The possibility of suspending the girders at each end was even considered. It was proposed that tangential support be provided by a rigid K-frame attached to the floor that would be pinned to one end of the girder at its neutral axis (a similar concept was eventually used for the three-girder test frame). For the load fixtures, it was proposed that a frame be placed around the girder at each of the load points that would be attached to a Dywidag threadbar running vertically down through the floor to a center-hole jack, which would react against the floor. The threadbar would be attached to the bottom of the load frame underneath the centerline of the girder web using a clevis and two anchor shackles, again connected in series. One concern with this arrangement was how to maintain the load in a near vertical position as the girder deflects and twists. Another concern was whether or not the threadbar (which is relatively weak in bending) would butt up against the side of the approximately 3-in. (76 mm) diameter hole in the laboratory floor at some point during the test, which could possibly result in failure of the bar.

Although these problems and concerns were not considered insurmountable, further investigations leading to final designs for the bearings, support structures and loading fixtures for the single-girder test were never initiated. For as this work was proceeding, work was also ongoing on a material and geometric non-linear ABAQUS analysis of the proposed single-girder test set-up (Figure 2.17). The component specimen with the largest predicted bending capacity was inserted into the model for the analysis. The analysis also included the effect of residual stresses. This analysis was initiated in order to more accurately assess the behavior of the girder, component specimens, and test fixtures throughout the entire range of loading. As the component specimens undergo yielding and increasingly large displacements at their ultimate load and beyond, the behavior of the girder is highly non-linear. As a result, the predicted actions from a linear elastic analysis become much less reliable.

Figure 2.18 shows a deformed plot of the ABAQUS model at an applied load of 140 kips (623 kN) at each load point. At this load, it was predicted that the component specimen would be just beyond its ultimate capacity. The maximum vertical deflection of the specimen at this load was predicted to be 17.5 in. (445 mm) versus a predicted maximum deflection of 13.8 in. (351 mm) from the linear elastic analysis. In the linear elastic analysis, the sum of the vertical end reactions was greater than the sum of the applied loads as a result of the additional vertical components of force in each of the inclined braces supporting the girder laterally. In the non-linear analysis, the opposite effect was noted; the sum of the vertical end reactions was less than the sum of the applied loads. As the struts deflected in the non-linear large-displacement analysis, the vertical force components in each of the inclined struts changed affecting the net sum of these forces so as to result in a smaller ratio of the end reactions to the applied loads. This effect could obviously not be discerned in the

small-displacement linear elastic analysis. Figure 2.19 shows that an axial tensile force F of 14.3 kips (63.6 kN) was predicted in the bracing member on the inside of the curve near one load point under the 140-kip (623 kN) loads. A close-up of the component specimen under these loads is shown in Figure 2.20. The distortion (or kink) near the center of the specimen is caused by the presence of a transverse stiffener on the inside of the web that was included in the model.

On the descending branch of the load-deflection curve at an applied load of 130 kips (578 kN) at each load point, the predicted vertical deflection of the specimen was 24.0 in. (610 mm). However, under these loads, it was also noted that an axial compressive force of -7.5 kips (-33.4 kN) now existed in the critical bracing member, or the member that had previously experienced a maximum tensile force of 14.3 kips (63.6 kN) under the 140-kip (623 N) loads (Figure 2.19). An independent non-linear analysis of the single-girder test set-up using the finite-element software MSC/NASTRAN (*31*) confirmed this force reversal or "snap-through" behavior observed in the ABAQUS analysis. The bracing members, or threaded Dywidag rods, were not designed to resist compression raising obvious safety concerns since the actual peak load and load-deflection curve were not known with certainty. The clevis and anchor shackle connection details at the ends of each bracing member were also not designed to resist compression. The development of an alternate detail that would allow the bracing members to also resist compression and still permit free rotation at each end of the member did not appear to be feasible at the time.

This predicted reversal of force in a critical bracing member, which again could not be discerned in the linear elastic analysis, raised significant concerns about the viability of the single-girder scheme for the bending component tests. In addition, preliminary cost estimates indicated that the total cost of the support fixtures, as developed to this point for the single-girder test (without even considering a re-design of the bracing members and their connections to accommodate a possible force reversal), would exceed the total cost of the three-girder prototype bridge, including the concrete deck. Since the testing of a curved I-girder bridge was also required at some point during the experimental program under the contract in force at the time, the decision was made to abandon the single-girder set-up for the bending component tests at this stage and revisit the idea of using the three-girder prototype bridge as a test frame for component testing.

Three-Girder Test Frame - Final Design

***Introduction*:** After conducting a detailed investigation of the feasibility of using a single-girder set-up for the bending component tests, a rational and informed decision was made to return to the original concept of using a simple-span three-girder test frame for the bending tests. It was decided that utilizing a three-girder test frame for the bending component tests would be safer, more cost-effective and more efficient. To recap some of the inherent advantages of this strategy of using a test frame that looks and functions like a real bridge: 1) it provides more realistic boundary conditions for the component specimen testing, 2) it presents fewer safety concerns because the structure is more stable, 3) it allows for possible reuse of parts of the test frame for future testing of a prototype curved bridge with a concrete deck, and 4) it allows for more realistic and representative erection studies to be conducted. One disadvantage of this approach is the increased number of possible load paths, which complicates the instrumentation, data reduction and data analysis.

Because of time constraints and the desire to get the frame into the laboratory as soon as possible, the decision was also made to focus the design of the frame at this stage on the bending component tests only. Although the final design of the frame concentrated primarily on accommodating the bending component tests, the idea of utilizing the frame for other possible tests in the future still had an influence on some of the design decisions. Possible future tests under consideration included additional component tests under different combinations of vertical bending moment and shear and testing of the frame as a full-size composite curved I-girder bridge.

Upon arriving at the decision to again utilize a three-girder system as a test frame, it was decided to first make some adjustments to the cross-frame arrangement from the arrangement used in the original prototype bridge design shown in Figure 2.8. As shown in Figure 2.21, the cross-frame spacing measured along the centerline of G2 was reduced from 10'-0" (3.0 m) to 7'-6" (2.3 m). This reduced spacing allowed for removal of every other cross frame in-between the center girder G2 and the outermost girder G3 for the

component testing (Figures 2.22 and 2.23) in order to provide an unbraced length for each bending specimen (inserted in the center of G3) of 15.65625 ft (4.8 m). At this unbraced length, L, and radius, R, of 208.75 ft (63.6 m), the R/L ratio for each specimen was 13.33. Most practical curved-girder designs have R/L ratios ranging from 13.33 to 20. Thus, the component tests were conducted near the lower range of the practical limits. A uniform cross-frame spacing was used to ensure a more uniform distribution of lateral flange bending moments along each component specimen. The reduced cross-frame spacing also provided extra lines of cross frames between the center girder G2 and the innermost girder G1 (Figure 2.23). These extra cross-frame lines provided additional stability to G2 and G1, reduced the lateral flange bending stresses in those girders, ensured additional load distribution to the outermost girder G3 supporting the component specimen, and helped ensure that G2 and G1 remained elastic throughout the entire range of test loads. As indicated in Figures 2.22 and 2.23, the bottom flange lateral bracing between girders was retained at the ends of the test frame to provide overall stability to the noncomposite frame and to resist relative longitudinal movement, or racking, of the noncomposite girders.

The arc span (between the centerline of bearings) along the centerline of G2 was retained at 90'-0" (27.4 m) and the centerline radius for G2 was retained at 200'-0" (61.0 m). The girder spacing of 8'-9" (2.7 m) was also retained from the original prototype design. As a result, the arc span of G3 was equal to 93.9375 ft (28.6 m) and its centerline radius was equal to 208.75 ft (63.6 m). The arc span of G1 was equal to 86.0625 ft (26.2 m) and its centerline radius was equal to 191.25 ft (58.3 m). G1 and G3 were also each extended 1'-0" (0.3 m) beyond the centerline of the end bearings. G2 was extended 1'-0" (0.3 m) beyond the centerline of the east end bearing and 1'-8" (0.5 m) beyond the centerline of the west end bearing to allow G2 to be connected to a tangential support frame (described below) at the west end. As shown in Figure 2.24, the arc length of each component specimen in G3 between the centerline of the bolted field splices was set at approximately 25.4 ft (7.7 m). In the original prototype design, a series of additional bolted field splices had been proposed near the ends of the girders to allow different skews to be introduced into the basic framing. This would be accomplished by removing or adding girder sections at the bolted splices and relocating the abutments and bearings as necessary. However, since the primary focus of the design at this stage was on the bending component specimen testing only, the decision was made to eliminate these extra field splices from the test-frame design and make both supports radial in order to save valuable time and resources. As a result, the only bolted field splices shown in Figure 2.23 are the two required to splice each component specimen into the center of G3.

Following is a description of the steps that were taken to arrive at a final design for the various components of the three-girder test frame. As work resumed on the development of a refined ABAQUS model to perform a non-linear analysis of each bending component within the revised test-frame configuration, initial design decisions had to be made based on linear elastic analysis results from BSDI 3D System and GTSTRUDL models of the frame. As results from the non-linear ABAQUS model were eventually obtained, modifications to the design were then made, as necessary, to reflect the increased knowledge about the overall behavior of the frame as each component was loaded (analytically) to its ultimate load and beyond. The design modifications then had to be reflected in the non-linear computer model and the analyses re-run to ensure satisfactory performance. This iterative design process was slower than the normal bridge-design process because of the complexities of the non-standard design details and the non-linear model. Extra care was also taken at each step to ensure safety and the desired performance of the test-frame components at the high loads and stress levels that would most definitely be experienced in the tests. In fact, a completely independent non-linear analysis of the test frame using MSC/NASTRAN was initiated as a check on the veracity of the ABAQUS results. In addition to the design revisions to the test-frame components and test fixtures, the original nine component specimens were replaced during this period with a more cost-efficient set of six component specimens with different proportions, which further complicated the process (note: two additional component specimens were later added after the initial six were tested).

To keep the project moving forward, however, contract plans and bid documents for fabrication of the frame, test fixtures and component specimens were prepared and issued based on the initial design formulated from the linear elastic analysis results. As the design was then modified and refined based on the non-linear analysis results, addenda had to be issued to the bid documents and eventually to the final contract documents in order to reflect these revisions. Although this certainly complicated the procurement

and fabrication processes, it was a necessary step in order to ensure the fastest possible delivery of the test frame and its components given the fact that it was not physically possible to accelerate this non-conventional iterative design process.

Girder Design: As discussed earlier, three unique approaches founded on the basic principles of statics are used to deduce the actions in the component specimens within the three-dimensional system. A fundamental requirement of these approaches is that the portions of the test frame outside the test component must remain elastic and stable until the component has reached its maximum moment capacity. Earlier linear and non-linear analyses had raised some concerns about the potential of the original singly symmetric prototype girders to remain elastic and stable throughout the entire test. Therefore, the decision was made to strengthen each of the test-frame girders. Furthermore, because the test frame is noncomposite for the component specimen testing, it was decided to also make each of the girders doubly symmetric. Up to this point, there had been no known tests of full-size singly symmetric horizontally curved I girders, especially in the inelastic range. Thus, it was not possible to accurately predict the stability of the original singly symmetric prototype girders under the high loads anticipated during the component testing.

In the re-design, the web depth of each of the girders was retained at 48 inches (1219 mm). The web thickness of G1 was increased from 3/8" (9.5 mm) to 7/16" (11 mm). The web thickness of G2 and G3 was increased from 3/8" (9.5 mm) to ½" (12.7 m). After several design iterations, the top and bottom flange plates on G3 were increased to 2-1/4" x 24" (55 mm x 600 mm). The top and bottom flange plates on G2 were increased to 1-1/4" x 20" (32 mm x 500 mm). The top and bottom flange plates on G1 were increased to 1" x 16" (25 mm x 400 mm). AASHTO M270 Grade 50 (M270M Grade 345) steel was originally assumed for all the web and flange plates. Since low temperatures were not a concern in the controlled laboratory environment, all steel for the main components of the test frame (girders, component specimens, stiffeners, cross frames, field splices, bearing plates and lateral bracing) was ordered to satisfy the non-fracture critical toughness requirements specified for AASHTO Temperature Zone 1.

The revised girder sizes were input into the original BSDI 3D System model for the prototype bridge and checked for the design live load of H20 (concrete deck, haunch, parapet and cross frame sizes were retained from the previous runs) against the 1993 Guide Specification LFD provisions. The maximum performance ratios were 0.85 for Girder 3, 0.80 for Girder 2, and 0.60 for Girder 1. The factored tip stress for strength in the bottom flange at midspan again governed in each case. For greater efficiency and to simplify the ordering of plate material, slight adjustments were then made to the top and bottom flange plates of G1 and G2 in order to utilize the same plate thicknesses that would be used in the fabrication of two of the nine original component specimens. The top and bottom flange plates of G1 were increased from 1" (25 mm) to 1-1/16" (27 mm) and the top and bottom flange plates of G2 were decreased from 1-1/4" (32 mm) to 1-3/16" (30 mm). Although the original intentions were good, this intended efficiency was lost after the component specimens were later re-designed and the yield stress of G2 was changed, as discussed below.

As each component specimen yields and approaches its ultimate load, the overall stiffness of G3 is reduced significantly so as to affect the load distribution in the girders. Therefore, instead of adding load to G3, the sense of the load in some of the cross-frame members adjacent to the component specimen will reverse and load will begin to be transferred to G2. The load transferred to G1 will also begin to drop off gradually due to the tendency of G1 to want to uplift as G3 softens. At a point when G3 and G1 will no longer accept any load, the system will continue to resist load along a different increasing load-deflection path as long as G2 can adequately sustain the load. Since this behavior was confirmed in the early non-linear analysis results, the decision was made to use AASHTO M270 Grade 70W (M270M Grade 490W) steel for the flanges and web of G2 in order to ensure that G2 remained elastic and could sustain the additional load throughout the component tests. It should be noted that AASHTO M270 Grade HPS70W (M270M Grade HPS490W) high performance steel was not readily available at the time the test frame was fabricated. Therefore, the original quenched and tempered M270 Grade 70W (M270M Grade 490W) steel was used. Because quenched and tempered Grade 70W (Grade 490W) steel is only available in plate lengths up to 50 ft (15.2 m), welded shop splices were required in the web and flanges of G2 approximately 25 ft (7.6 m) from each end of the girder. It was further specified that the

complete joint penetration welds for these web and flange splices be offset longitudinally by approximately 1'-0" (0.3 m) during the fabrication of G2.

Plan and elevation views of the final girder designs for G1, G2 and G3 are given in Figures 2.25 through 2.27. All flange-to-web welds were designed as 5/16" (8 mm) fillet welds. Calculations indicated that undermatched fillet welds could safely be used for the Grade 70W G2. The design of the bolted field splices for G3 and the stiffeners on all three girders is discussed in more detail below. The center section of G3 in-between the bolted field splices (Figure 2.27) was set aside during the component testing. This section was fabricated for use during erection studies on the three-girder frame and for possible later use should the frame eventually be tested as a composite bridge. Although bolted field splices are not shown in G1 and G2, the incorporation of these splices would have been permitted had the fabricator determined that these girders were indeed too long for shipping. Note that in the first end panel of each girder at a distance of 2'-0" (0.6 m) from the centerline of each bearing, 1-1/2" (38 mm) diameter holes were provided at mid-depth to allow for the installation of tie-downs in the laboratory, if desired for additional safety.

The girder cambers were determined to accommodate the possible future casting of a concrete deck onto the frame. To obtain a reasonable estimate of the girder cambers, a new BSDI 3D System model was built with the cross frames equally spaced at 15'-0" (4.6 m) along the centerline of G2. This cross-frame arrangement was felt to be more representative of the arrangement in a real bridge of this type. The design live load was again taken to be H20. The concrete deck, haunch, parapet and cross-frame sizes were retained from the previous runs for the original prototype bridge. AASHTO M270 Grade 50 (M270M Grade 345) steel was assumed for all the girders. Based on the analysis results, the girders were then designed to satisfy the 1993 AASHTO Guide Specification LFD criteria. Ratios of n-composite girder stiffnesses were then computed; that is, the ratio of the n-composite girder stiffness for G3 to the n-composite girder stiffness for G2, and similar ratios for the stiffness of G3 to the stiffness of G1 and the stiffness of G2 to the stiffness of G1. To provide similar ratios after casting the same deck onto the actual test-frame girders, it was determined that it would be necessary to flame cut the top and bottom flanges of G2 and G3 to reduce their width slightly prior to casting the deck. Based on these revised proportions of G2 and G3, a second 3D System analysis was run for the same bridge geometry, only with the parapets removed (since there would most likely be no parapets on the composite bridge in the laboratory). From the results of this analysis, the girder cambers shown in Figure 2.28 were computed based on the sum of the elastic vertical girder deflections due to the self-weight of the steel plus the weight of the concrete deck and deck haunch.

***Cross-Frame Design*:** Cross frames transfer significant loads in horizontally curved I-girder bridges and provide stability to the curved-girder system and are therefore considered to be primary members. In a horizontally curved I-girder subject to a near constant vertical bending moment, the vertical bending moment creates non-collinear axial forces in the flanges. To satisfy equilibrium, torsion is created along the girder, which in turn causes restoring forces in the cross frames. Vertical and lateral loads result in the cross-frame members. The sum of the vertical components of the cross-frame forces represents the load transferred between girders through the cross frames to establish equilibrium of the system.

During the component testing, the cross-frame members in the test frame ensure stability of the frame as the component specimen yields by limiting lateral flange bending stresses in the girders, and by transferring load to G2 as G3 softens, and also as G1 tends to want to uplift. In particular, the cross frames between G2 and G3 adjacent to the component specimen are subject to very large forces during the tests. Accurate measurement of the actions in all the cross-frame members is essential in order to properly deduce the actions in the yielded component specimens.

To evaluate various possible configurations of cross-frame members for the re-designed test frame, an initial study was conducted utilizing the results from a linear elastic GTSTRUDL model of the frame. The model was loaded with 100 kip (445 N) concentrated loads at approximately the third points of each girder (six loads total) plus self-weight. The six 100-kip (445 N) loads were considered to be a conservative estimate of the total applied load necessary to reach the maximum capacity of the largest component specimen. One configuration that was studied used cross frames made up primarily of structural tee

sections (the basic cross-frame design from the original prototype bridge was used), a second configuration used cross frames made up of structural steel pipe sections, and a third configuration used pipe sections for the cross frames in-between G2 and G3 and tee sections for the cross frames in-between G1 and G2. For efficiency, larger pipe sections or back-to-back tee sections, as applicable, were used for the more heavily loaded cross frames, and smaller pipe sections or single tee sections were used for the more lightly loaded cross frames. A K-type configuration with the diagonal members intersecting at the center of the bottom chord was selected. This configuration was selected because it was anticipated that the bottom chord would have the largest axial compressive forces and would require additional support. All end connections of the cross-frame members were assumed to be pinned in the analysis. The bottom chord was assumed to be continuous at the intersection with the diagonals. Comparisons of the maximum vertical displacement of each girder at midspan, the cross frame axial forces at Lines 4L and 6L (Figure 2.23), and the vertical end reactions for each case did not show any significant differences.

Tee sections are often used for cross-frame members in curved bridges and allow for the use of simple connection details. However, instrumenting and deducing the axial force in structural tees is not simple or reliable due to built-in eccentricities of the connections and the presence of significant torsional warping stresses in the open section. Similar problems would also exist should angles be used. Although the use of pipe sections for the cross-frame members complicated the design of the connection details, it was felt that the advantages offered by using pipes far outweighed the complexities of the connection design. Pipes are excellent compression members with equal buckling strength about either principal axis and are therefore less susceptible to buckling than open sections. When the connection design is done properly, pipes are also subject to fewer eccentricities. The St. Venant shear stiffness is so great compared to the warping torsional stiffness of a pipe that warping may be ignored. Thus, torsion introduces no longitudinal stress in the pipe cross-frame members. Therefore, for this experiment, measurement of the axial force and bending actions could be deduced with a minimum of strain gages using pipes. Therefore, the decision was made to use steel pipes for the cross-frame members in the test frame. The design of these pipe sections and their connections is discussed in more detail below. The process used to determine an appropriate instrumentation scheme and then calibrate the pipe sections to determine the member actions during the component tests is discussed in more detail elsewhere[3].

Initially, it was decided to use two sets of cross-frame sizes in order to minimize the weight of the frame. Type A cross frames would consist of smaller pipe sections and would be used for more lightly loaded cross frames. Type B cross frames would utilize larger pipe sections and would be used for the more heavily loaded cross frames. It was proposed that Type B cross frames be used at the abutments, at cross-frame lines 6L and 6R in-between G2 and G3 and in-between G1 and G2, and at cross-frame lines 4L and 4R in-between G2 and G3 only. All other cross frames would be Type A cross frames. From the GTSTRUDL analyses, the following maximum design actions were determined:

	Type A	Type B
Top Chord:	$P_u = \pm 54.0$ kips (240.2 kN)	$P_u = \pm 107.0$ kips (476.0 kN)
Diagonals:	$P_u = \pm 46.0$ kips (204.6 kN)	$P_u = \pm 92.0$ kips (409.2 kN)
Bottom Chord:	$P_u = \pm 79.0$ kips (351.4 kN)	$P_u = \pm 157.0$ kips (698.4 kN)
	$M_{ux} = \pm 14.0$ kip-ft (19.0 kN-m)	$M_{ux} = \pm 27.0$ kip-ft (36.6 kN-m)

The bending moment in the bottom chord about a horizontal axis (x-axis) through the pipe cross section was caused by the net vertical component of the unequal diagonal forces coming into the bottom chord.

The pipe members were designed according to the provisions of the 2nd Edition of the AISC *Load and Resistance Factor Design (LRFD) Specification for Structural Steel Buildings* (*32*). The top chord and

---

[3] Linzell, D.G., "Studies of a Full-Scale Horizontally Curved Steel I-Girder Bridge System under Self-Weight, Ph.D. Dissertation, The Georgia Institute of Technology, Atlanta, GA, August 1999.

diagonals were designed as compression members according to Section E2 of the AISC LRFD Specification. Although the actual pipe length was much less because of the gusset plates, a length of 8.75 ft (2.7 m) was conservatively assumed for the top chord and a length of 5.92 ft (1.8 m) was conservatively assumed for the diagonals. The effective length factors K_x and K_y were both assumed to be 1.0. The specified minimum yield stress of the steel was assumed to be 60 ksi (414 MPa). It was felt that high-strength pipe with a specified minimum yield stress greater than or equal to 50 ksi (345 MPa) should be used to ensure that the cross-frame members remain elastic throughout the component testing. The ratio of the diameter, D, of the pipe to the thickness, t, was limited to 3,300/Fy or 55.0 according to LRFD Table B5.1. The specified resistance factor for compression equal to 0.85 was applied. The bottom chord was designed as a beam column subject to axial compression and flexure according to Section H1.2 of the AISC LRFD Specification. A member length of 8.75 ft (2.7 m) was conservatively assumed. The flexural capacity was determined according to Section F1 of the specification using a resistance factor for flexure equal to 0.90. In this case, D/t was limited to $2{,}070/F_y$ or 34.5, which is the specified limit for a compact tubular section in flexure. From the results of these calculations, it was proposed that Type A cross frames consist of 3" (76 mm) OD pipes with a ½" (12.7 mm) thick wall for the top chord, 2-7/8" (73 mm) OD pipes with a¼" (6.4 mm) thick wall for the diagonals, and 4" (101.6 mm) OD pipes with a ½" (12.7 mm) thick wall for the bottom chord. Type B cross frames would consist of 3-1/2" (89 mm) OD pipes with a 5/8" (15.9 mm) thick wall for the top chord, 3" (73 mm) OD pipes with a ¼" (6.4 mm) thick wall for the diagonals, and 4" (101.6 mm) OD pipes with a ½" (12.7 mm) thick wall for the bottom chord. It was further proposed that high-strength alloy mechanical tubing made from ASTM A519, Grade 4140 steel be used.

Once the design actions had been determined and the members were sized, preliminary designs of the cross-frame connections to the girder and to the K-joint center gusset plate were prepared. To connect the cross-frame members to the girders and to the center gusset, it was decided to weld the ends of the pipes to 1-in. (25 mm) thick end plates using full-penetration groove welds. Two 7/8-in. (22 mm) thick gusset plates, full-penetration groove welded to the other side of each end plate, would then be used to attach each member to the girder connection plates and center gusset plates using high-strength bolts. The gap between the two gusset plates was specified to be no more than 1/16" (1.6 mm) ± 1/32" (0.8 mm) larger than the thickness of the plate to which it would be attached. By using two gusset plates to attach the member, any force eccentricities at the member ends would be minimized. Also, the bolted gusset-plate connections would resist the member loads in double shear. This helped to reduce the size of the connections, which had to be designed for rather large forces. Nevertheless, because of the size of the required connections, the centerline of the top chord was located 6 in. (152.4 mm) below the bottom of the top flange and the centerline of the bottom chord was located 8 in. (203.2 mm) above the top of the bottom flange.

A disadvantage of the dual gusset-plate arrangement is that it makes it much more difficult to install (and remove) the cross frames. In essence, the pre-assembled cross frames must first be brought into position in-between the girders at an angle and then be rotated into place by wedging the dual gusset plates onto the girder connection plates. After further study, it became clear that this would not be possible without splitting the bottom chord member into two pieces. Therefore, the bottom chord was split into two shorter members at the large K-joint center gusset plate. This would allow each pre- assembled top chord and diagonal unit (including the center gusset plate) to first be rotated into position. This operation would then be followed by the simple installation of the two bottom chord members.

A 7/8-in. (22 mm) thick plate was used for the center gusset plate. A 5/8" x 4" (16 mm x 102 mm) plate was fillet welded to the top of the gusset plate to stiffen the plate against buckling. AASHTO M270 Grade 50 (M270M Grade 345) steel was specified for all end plates and gusset plates.

It soon became evident that the assumption of pinned end connections in the analysis would not adequately represent the rotational stiffness of the actual end connections; the dual gusset-plate arrangement and the center gusset plate at the K-joint had to provide some degree of end fixity. Therefore, the GTSTRUDL analysis was re-run conservatively assuming full fixity of the cross-frame member end connections against rotation in the plane of the cross frame. At the same time, preliminary analysis results from the non-linear ABAQUS model of the test frame became available for three of the original nine component specimens. Similar assumptions were made regarding the fixity of the end connections in the

ABAQUS analysis. A set of revised design actions, which enveloped the maximum values from the GTSTRUDL and ABAQUS analyses and also the previous GTSTRUDL analysis results assuming pinned connections, were developed as follows:

Top Chord:	P_u =	± 130.0 kips (578.3 kN)
	M_{ux} =	± 5.0 kip-ft (6.8 kN-m)
Diagonals:	P_u =	± 180.0 kips (800.7 kN)
	M_{ux} =	± 8.0 kip-ft (10.8 kN-m)
Bottom Chord:	P_u =	± 157.0 kips (698.4 kN)
	M_{ux} =	± 15.0 kip-ft (20.3 kN-m)

The cross-frame members were then re-designed for the revised design actions using the same design assumptions as before. K_x and K_y were again conservatively taken equal to 1.0. To simplify detailing and fabrication, the decision was also made at this stage to use the same member sizes for each cross frame. In addition, preliminary investigations had begun to raise questions about the availability of a number of different pipe sections, especially smaller diameter sections made from higher strength steels. Some higher strength material cannot easily be formed into smaller diameter sections. Based on the revised design actions, it was proposed that 4-in. (101.6 mm) OD pipes with a ¾-in. (19 mm) thick wall be used for the top chord and diagonal members and 5-in. (127 mm) OD pipes with a ¾-in. (19 mm) thick wall be used for the bottom chord members of each cross frame. Upon further review, it was felt that pipes with ¾-in. (19 mm) thick walls would be too stiff and would be difficult to effectively instrument and calibrate in order to accurately determine the member actions experimentally. It was discovered too that there is very limited availability of higher strength 5-in. (12.7 mm) OD pipe with a ¾-in. (19 mm) thick wall. Since the design actions given above were also felt to be quite conservative, it was therefore decided to reduce the pipe wall thickness of all members to ½ in. (12.7 mm). The design was then re-checked using a reduced effective length equal to the distance between the centerline of the bolt groups in the end connections. The assumed lengths were 7.5 ft (2.3 m) for the top chord, 2.67 ft (0.8 m) for the diagonals, and 7.5 ft (2.3 m) for the bottom chord.

The design actions given above were also used for the final design of the cross-frame connections. The end plate welds and dual gusset plate welds were designed to resist combined axial load and flexure. As mentioned previously, complete joint penetration welds were required. The end plate welds were designed to develop the strength of the ¾-in. (19 mm) thick pipes.

The high-strength bolted connections were designed to resist combined axial load and flexure according to conventional elastic-design procedures for eccentrically loaded bolted connections. The connection of the dual gusset plates to the girder connection plates at the intersection of the top chord and diagonal was designed for the top chord axial force plus the horizontal component of the axial force in the diagonal, the vertical component of the axial force in the diagonal and the net bending moment at the connection. All other connections were simply designed for the axial force plus the bending moment in the member under consideration. The resultant force was computed for each bolt in the group. The x and y component of force due to the bending moment was determined using the polar moment of inertia of the bolt group. The center-to-center spacing between bolts was set at 3 in. (76 mm). At the gusset plate/girder connection plate connections, a minimum edge distance of 1.5 in. (38 mm) was required for the first bolt line on the girder connection plates to prevent interference of the cross-frame members with the girder flanges when rotating the cross-frame components in/out. All bolts were assumed to be black 7/8"-in. (22-mm) diameter ASTM A325 (A325M) high-strength bolts in standard holes.

All bolted connections were conservatively designed to prevent slip under the maximum resultant design force. Prevention of connection slip during the component tests was considered to be extremely important since a sudden displacement of the three-girder system due to bolt slip would contaminate the strain and displacement readings and the resulting non-linear behavior of the frame would be nearly impossible to replicate analytically. The slip resistance of the bolts in double shear was computed according to the provisions of the AISC LRFD Specification assuming a Class B faying surface condition. A Class B surface condition provides a higher slip resistance than clean mill scale (Class A) and requires blast cleaning and coating of the faying surface with a Class B coating. As a result of the design, 10 bolts

were required at each top chord/diagonal connection, 6 bolts were required at the connection of each diagonal to the center gusset plate, 6 bolts were required at each bottom chord connection to the girder connection plate, and 8 bolts were required to connect each bottom chord to the center gusset plate.

Adequate slip resistance also assumes that the faying surfaces are brought into direct contact with no gaps, which was a concern with the 7/8″-in. (22-mm) dual gusset plates. It was anticipated that a significant amount of force would be required to close the initial gap that was provided between the dual gusset plates and the girder connection plates to help ensure fit-up. As it turned out, a special procedure had to eventually be developed in the laboratory to over-tighten the bolts in order to eliminate gaps in the gusset plate/connection plate connections that were observed after the initial installation of the cross frames. A load-displacement curve for the A325 (A325M) bolts was first developed in a Skidmore test frame, which indicated that the bolts could be tightened a full turn past snug tight without a drop-off in the clamping force. An over-tightening procedure was then developed in which the threads of each nut were greased and then a snug condition for the connection was established by repeatedly going through each bolt pattern until all elastic unloading was eliminated. At this point, the bolts were then tightened to 2/3 of a turn. On connections with more significant gaps, shims were first installed to fill the gaps between the connection and gusset plates.

In the meantime, work was progressing on refinement of the ABAQUS non-linear analysis model of the test frame. With the cross-frame member and connection designs completed, detailed modeling of the cross-frame members and their connections (including all gusset plates) was underway. As such, the model now reflected the actual location of the cross-frame members, or the vertical offset of the members from the girder flanges. To the extent possible given the modeling assumptions, the model also better reflected the actual rotational stiffness provided by the member end connections. It was also felt that more reliable predictions of the in-plane and out-of-plane bending moments and torsional moments in each cross-frame member could be obtained by detailed modeling of the cross-frame connections. In addition, during this time period, the original nine component specimens had been re-designed and pared down to a more cost-efficient set of six specimens, which had different proportions than the original nine specimens. A re-analysis of the frame, using the more detailed non-linear model, was conducted with each of the six new component specimens inserted one at a time in the center of G3. From an early examination of the analysis results, the design actions that had previously been used to design the cross-frame members and their connections now appeared to be quite conservative. There were also some concerns that the ½-in. (12.7 mm) thick pipes were still too stiff and were adversely affecting the behavior of the frame. Therefore, the decision was made to again reduce the thickness of the pipe walls from ½ in. (12.7 mm) to 1/8 in. (3.2 mm). To further simplify the detailing and ordering of the material for the cross frames, it was also decided at this time to specify 5-in. (127 mm) OD pipes for all the cross-frame members. Since alloy mechanical tubing was quite expensive and not readily available in the desired size, it was further decided based on the recommendation of a large supplier of tubular material to specify the pipe material as ASTM A513 Type 5 DOM (Drawn Over Mandrel). A specified minimum yield stress of 65 ksi (448 MPa) was conservatively assumed for this material. The non-linear analyses were then re-run using the revised size and yield stress for the cross-frame members. As a result of these analyses, the following new set of ″worst-case″ design actions were developed for each cross-frame member:

Top Chord:	P_u	=	-49.5 kips (-220.2 kN); +74.5 kips (+331.4 kN)
	M_{ux}	=	-0.8 kip-ft (-1.1 kN-m); +0.4 kip-ft (+0.5 kN-m)
	M_{uy}	=	-3.6 kip-ft (-4.9 kN-m); +3.7 kip-ft (+5.0 kN-m)
	M_{uz}	=	-3.0 kip-ft (-4.1 kN-m); +3.1 kip-ft (+4.2 kN-m)
Diagonals:	P_u	=	-69.5 kips (-309.1 kN); +62.0 kips (+275.8 kN)
	M_{ux}	=	-1.7 kip-ft (-2.3 kN-m); +1.7 kip-ft (+2.3 kN-m)
	M_{uy}	=	-2.9 kip-ft (-3.9 kN-m); +2.7 kip-ft (+3.7 kN-m)
	M_{uz}	=	-2.3 kip-ft (-3.1 kN-m); +2.8 kip-ft (+3.8 kN-m)
Bottom Chord:	P_u	=	-99.0 kips (-440.4 kN); +53.5 kips (+238.0 kN)
	M_{ux}	=	-1.9 kip-ft (-2.6 kN-m); +1.6 kip-ft (+2.2 kN-m)
	M_{uy}	=	-2.8 kip-ft (-3.8 kN-m); +2.5 kip-ft (+3.4 kN-m)
	M_{uz}	=	-1.9 kip-ft (-2.6 kN-m); +1.9 kip-ft (+2.6 kN-m)

To determine the most efficient and economical means of instrumenting and calibrating the pipe members to accurately determine the member actions during component testing, it was decided to perform a series of laboratory tests on individual pipe members. Also, since the behavior of pipe sections under both concentric and eccentric compressive and tensile loads is not well-known, it was felt that these tests could also be used to check the capacity of the members under these conditions. Initial tests were conducted on five 5-in. (127 mm) OD x 1/8-in. (3.2-mm) thick pipe members with 1-in. (25- mm) thick end plates groove welded onto each end of each member. The pipes were each approximately 6'-2" (1.9 m) in length, which is equal to the length of the top chord in the cross frame. Each of these specimens was tested in compression; three were tested under concentric loading and the other two were tested with a 2-in. (50-mm) eccentricity imposed at each end. Each specimen was instrumented with both single-arm strain gages and with rosettes located at mid-length of the pipe. End rotations and lateral and axial deflections were also measured. A detailed description of the test set-up and the test results for these tests and several additional tests of similar nature is given elsewhere[4].

The tests demonstrated that four single-arm gages, located at mid-length of the member and at alternating 0° and 45° angles with respect to the longitudinal axis of the member, would allow for sufficiently accurate measurement of the forces and moments in the members in the elastic range. However, the tests also indicated that 1/8-in. (3.2 mm) thick pipes would not have the necessary capacity to remain elastic under the predicted combination of axial load and bending moment in the most highly loaded cross-frame member during component testing. Therefore, based on these tests, the decision was made to revise the wall thickness of the pipes one final time up to ¼" (6.4 mm) in order to provide additional capacity and a larger margin of safety against yielding of the members under the combined actions. Subsequent tests, similar to those described above, indicated that ¼-in. (6.4 mm) thick pipes should provide the necessary capacity to keep the cross-frame members elastic during component testing. From this point on, all analyses were run using the 5-in. (127 mm) OD x ¼-in. (6.4-mm) thick pipes for all cross-members.

The elastic section properties of a 5-in. (127 mm) OD x ¼-in. (6.4-mm) thick pipe are compared below to the elastic section properties of a 5 x 5 x 7/16 (127 x 127 x 11.1) single angle:

	5 in. OD x ¼-in. pipe
Area	3.73 in.^{2} (2406.4 mm^2)
Moment of Inertia	10.55 in.^{4} (4.4 x 106 mm^4)
Radius of Gyration	1.68 in. (42.7 mm)
Torsion Constant J	J = 21.10 in.^{4} (8.8 x 106 mm^4)
	5 x 5 x 7/16 single angle
Area	4.18 in.^{2} (2696.8 mm^2)
Moment of Inertia	$I_x = I_y$ = 10.00 in.^{4} (4.2 x 10^6 mm^4)
	I_z = 4.06 in.^{4} (1.7 x 10^6 mm^4)
Radius of Gyration	$r_x = r_y$ = 1.55 in. (39.4 mm)
	r_z = 0.986 in. (25.0 mm)
Torsion Constant J	J = 0.27 in.^{4} (112.4 x 10^3 mm^4)

The axial and flexural stiffnesses of the pipes are approximately equivalent to the axial and flexural stiffnesses (about the geometric axes) of the single angle member, which is a typical member used for cross frames in bridges. However, by eliminating the eccentricity of the connections, the pipes are capable of carrying a much larger axial load than the angle with a slightly larger area. An angle capable of carrying the same axial load as the pipe would be much stiffer than the pipe. The pipe has a significantly larger St. Venant torsional stiffness, J, than the open angle section. Separate non-linear analyses were run with the St. Venant torsional stiffness of all the pipes set equal to zero. The results indicated that the additional torsional stiffness offered by the pipes had a negligible effect on the overall behavior of the frame.

---

[4]Linzell, D.G., "Elastic Experimental and Analytical Studies of Curved Steel Bridge Behavior Under Self-Weight," *3rd Structural Specialty Conference of the Canadian Society of Civil Engineering*, London, Ontario, June 7-10, 2000.

The final detail to be worked out in the cross-frame design involved the design of the large gusset connection at the center of the bottom chord. In checking the compressive resistance of the bottom chord, the entire length of the chord (in-between the connections to the girders) was used. Therefore, it had to be ensured that the center gusset plate connection provided a stiffness at least equivalent to the stiffness of the pipe section in order to prevent a weak spot that could potentially be subject to lateral buckling. Several different configurations were considered for making the splice at the center gusset. The final configuration that was chosen is shown in Figure 2.29. The end plate of each bottom chord piece facing the center gusset plate is complete penetration groove welded to dual 7/8" (22 mm) x 8" (203.2 mm) gusset plates that are each 1'-2" (0.36 m) long. To provide additional lateral stiffness, a 7/8" (22 mm) x 2-1/2" (63.5 mm) plate is fillet welded to the outside of each gusset plate. To connect the bottom chord members, the dual gusset plates on each chord member are then placed over the 7/8-in. (22-mm) thick center gusset plate and the plates are all bolted together using two 7/8" (22 mm) x 4" (101.6 mm) x 2'-1/2" (0.62 mm) plates on each side of the connection (refer to Section B-B in Figure 2.29). AASHTO M270 Grade 50 (M270M Grade 345) steel was specified for all the plates. Once a final configuration for this detail had been decided upon, the elastic section properties -- as well as the axial compressive and flexural resistances at Sections B-B and C-C (refer to Figure 2.29) -- were computed to check that the values equaled or exceeded the corresponding values for the 5-in. (127 mm) OD x ¼"-in. (6.4-mm) thick pipe section. The tensile resistance at these two sections was also checked. The calculations indicated that the proposed detail was more than sufficient.

The final details for the cross frames are shown in Figure 2.29. The extra cross frames between G2 and G3 that were not used for the bending component tests (at Lines 3L, 3R, 5L, 5R, and 7 in Figure 2.23) were fabricated anyway and set aside for possible use during future component tests and/or the composite bridge test.

Lateral-Bracing Design: As mentioned previously, bottom lateral braces are provided between the girders at each end of the test frame in-between the first two cross-frame lines (Figure 2.23) to provide overall stability to the noncomposite frame and to resist relative longitudinal movement or racking of the noncomposite girders during the component testing. This movement is possible since the bearings under G1 and G3 have no lateral or tangential restraint. When the tangential forces in adjacent girders differ, forces must be generated to maintain equilibrium. In this case, without the lateral bracing, these stabilizing forces would induce out-of-plane bending in the cross-frame connection plates and prying on the bolted cross-frame connections. These forces are also of consequence in actual bridges when no lateral bracing exists and there is not at least one tangential bearing restraint on each girder. Once any portion of the deck has hardened, the necessary shear restraint exists. Therefore, in these cases, some type of temporary constraint would be necessary, but only until some portion of the deck has hardened.

The results from the non-linear ABAQUS analyses were used to design the lateral bracing members and their connections. Separate analyses were run for the following lateral bracing members: 1) using back-to-back WT6 x 29 (WT155 x 43) structural tees for each lateral bracing member, 2) using single WT6 x 29 (WT155 x 43) structural tees for each lateral bracing member, 3) the preceding case with the lateral bracing members removed from the right (east) end of the frame, and 4) all lateral bracing members completely removed. For the first two cases, with horizontal restraint at the G1 and G3 bearings equal to zero, it was observed that the lateral bracing members experienced compressive axial loads no greater than 8.0 kips (35.6 kN) up to a vertical load of 75.0 kips (333.6 kN) at each of the six load points (located at approximately the third points of each girder). As the loads increased beyond 75.0 kips (333.6 N) up to approximately 95.0 kips (422.6 kN), however, the compressive loads in the lateral bracing members increased quite rapidly in a non-linear fashion. The maximum predicted compressive loads in the members were 25.0 kips (111.2 kN) for the case of the back-to-back tees and 20.0 kips (89.0 kN) for the case of the single tees under the 95.0-kip (422.6 kN) loads. The effect of single versus double tees on the reactions, displacements and cross-frame forces was negligible. Removal of the bracing at the right (east) end, or in its entirety, had a negligible effect on the reactions and displacements of the test frame, but it did have a noticeable effect on the distribution and the sign of some of the forces in the cross-frame members nearest the ends of the frame.

From the results of the preceding study, it was decided that single WT6 x 29 (WT155 x 43) structural

tees would be sufficient for these members. A load factor of 1.4 was applied to the maximum load from the analysis. Since the flange of the tee would be bolted directly to the top of the bottom flanges of the girders at each end, a slight moment about the strong axis of the tee is induced at each end. The moment is caused by the eccentricity between the applied load at the connection and the centroid of the tee. The tee was checked for combined axial compression and flexure according to Section H1.2 of the AISC LRFD Specification. AASHTO M270 Grade 50 (M270M Grade 345) steel was assumed. The member length was taken as $\sqrt{(8.75)^2 + (7.5)^2} = 11.52$ ft (3.5 m). The compressive resistance was determined according to Section E2 of the AISC LRFD Specification with the effective length factor, K, taken equal to 1.0. The specified resistance factor for compression equal to 0.85 was applied. The flexural resistance was determined according to Section Fl (Article 2c) of the AISC LRFD Specification for the case where the stem of the tee is in tension. The resistance factor for flexure equal to 0.90 was applied.

The high-strength bolted connections of the tees to the girder flanges were designed as axially loaded connections to prevent slip under the design load. A Class B surface condition was assumed in computing the slip resistance. Four 7/8" (22 mm) diameter ASTM A325 (A325M) high-strength bolts were required at each end of each tee. To allow for fit-up, oversize 1-1/16-in. (27 mm) diameter holes were specified for the bolt holes in the structural tees. Hardened steel washers were installed over the holes in the tees in the outer ply; as required by AASHTO whenever oversize holes are used in an outer ply. Standard-size 15/16-in. (24 mm) holes were specified for the bolt holes in the girder flanges at each connection. Final details for the bottom lateral bracing are shown in Figure 2.30.

Field Splice Design: Bolted field splices are provided in the outermost girder G3 of the test frame to allow the different bending component specimens to be installed and removed (Figure 2.24). The splices are located 34'-3-1/4" (10.5 m) from the centerline of each end bearing. The location of the splices was selected to ensure that the splices would clear the cross-frame connection plates located on G3 at Lines 5L and 5R.

The design of the field splices presented a significant challenge because of the different proportions of the component specimens. The splices also had to accommodate the center section of G3. An efficient scheme was developed that allowed a minimum number of splice plates to be used. Such a scheme allowed the splice plates to be re-used during the component testing, which resulted in fewer pieces to keep track of along with a significant cost savings. For reasons discussed previously, it was also desired to prevent slip at all bolted connections in the test frame. The decision was then made to conservatively design the bolted splice connections to prevent slip at the full plastic moment capacity of each specimen. A Class B surface condition was again assumed in computing the slip resistance of the bolts. To accommodate each specimen using the same set of splice plates, different numbers of bolts were installed in the flange splice plates for each specimen (refer to Figure 2.31 -- an open circle in the flange splice represents an open bolt hole and a black circle represents a filled bolt hole). All bolts were 7/8" (22 mm) diameter ASTM A325 (A325M) high-strength bolts placed in standard holes. AASHTO M270 Grade 50 (M270M Grade 345) material was specified for the splice plates and ASTM A36 (A36M) material was specified for all fill plates. Although the splice plates were to be re-used, new bolts were used when splicing each specimen into G3. To ensure that testing would not be unduly held up by possible damage to the splice plates, it was also specified that a complete duplicate set of all flange and web splice plates be fabricated as a precaution.

Flange Splices: The flange splices were designed to develop the full capacity of the component specimen flanges. As discussed in a later section of this report, the component specimen flanges were originally proportioned assuming the static yield stress of the flange material to be 55 ksi (379 MPa). The nominal proportions of the compression flange of each specimen were determined to provide a desired theoretical local buckling capacity for the assumed 55-ksi (379 MPa) material equivalent to the capacity of a 50-ksi (345 MPa) compression flange (at a stress level equal to the yield stress). As a result, for a given thickness, slightly narrower flanges were necessary in order to provide an equivalent local buckling capacity at the higher stress. The plan was to then later adjust the original nominal flange widths of the specimens prior to fabrication based on the actual static yield stress of the material (determined from tension tests conducted on the actual flange plate material) and on measurements of actual flange-plate thicknesses. The intent was to ensure that the desired effective compression-flange slenderness ratios would

be provided. In the meantime, to assist the fabricator in ordering the plate material, a table of maximum possible flange-plate widths for the component specimens (Figures 2.53 and 2.54) was prepared assuming the static yield stress of the material to be exactly 50 ksi (345 MPa) and using the assumed flange thicknesses discussed below.

Actual flange thicknesses are typically slightly greater than the nominal flange thicknesses. Therefore, for the computation of the flange design force for the splice design, the top- and bottom-flange thickness of Specimens B1, B2 and B3 and the top-flange thickness of B4 were arbitrarily adjusted upward from 0.75 in. (19 mm) to 0.80 in. (20.3 mm). The bottom-flange thickness of Specimen B4 was arbitrarily adjusted upward from 1.25 in. (31.8 mm) to 1.31 in. (33.3 mm). The top- and bottom-flange thickness of Specimen B5 was arbitrarily adjusted upward from 0.9375 in. (23.8 mm) to 0.9675 in. (24.6 mm). Finally, the top- and bottom-flange thickness of Specimen B6 was arbitrarily adjusted upward from 1.1875 in. (29.1 mm) to 1.2475 in. (31.7 mm). The corresponding flange widths were then also adjusted upward slightly to provide the same b/t ratio that would be calculated using the nominal dimensions. (Note: see the later section of this report on the bending component specimen design for a more detailed description of the component Specimens B1 through B6).

The flange design force was then computed to be the larger of the following: 1) the factored-up thickness of the flange times the adjusted width of the flange times 55 ksi (379 MPa), or 2) the maximum possible flange width times the factored-up flange thickness times 50 ksi (345 MPa).

Since fill plates were required for all the specimens, the resulting eccentricity in the connection was considered in distributing the flange design force to the inner and outer splice plates. The number of bolts was then determined by dividing the maximum splice plate force (assumed to act on a single shear plane) by the calculated slip resistance of a 7/8" (22 mm) bolt in single shear. For the top- and bottom flange splices of Specimens Bl, B2, B3 and B5 and the top-flange splice of Specimen B4, a total of 32 bolts were required. For the top- and bottom-flange splices of Specimen B6, 38 bolts were required. For the bottom-flange splice of Specimen B4, 50 bolts were required. For the center section of G3, it was decided to specify 38 bolts for the top-flange splice and 50 bolts for the bottom-flange splice (the largest numbers for each from above) so that the same splice plates could be used.

To accommodate the largest number of bolts and also allow for the same splice plates to be used for different specimens, it was necessary to stagger the bolts. The splice plates were designed to prevent yielding on the effective area of the plates and fracture on the net area of the plates under the maximum splice plate force. In the calculations, the yield stress of the plates was assumed to be 50 ksi (345 MPa) and the ultimate tensile strength of the plates was assumed t be 65 ksi (448 MPa). The critical section for the splice plates was determined to be the staggered line running through the first two rows of bolts adjacent to the centerline of the splice. The conventional "$s^2/4g$" correction was applied in determining the net width along the stagger. For the bottom-flange splice for Specimen B4 and the center section of G3, a 7/8" (22 mm) x 20" (508 mm) plate was selected for the outside splice plate and two 1-1/4" (31.8 mm) x 9-1/4" (235 mm) plates were selected for the inside splice plates. For all other splices, a ¾" (19 mm) x 16-1/2" (419 mm) plate was selected for the outside splice plate and two 1-1/8" (28.6 mm) x 7- 1/2" (190.5 mm) plates were selected for the inside splice plates.

Since a relatively large number of bolts were required in relatively narrow flanges, it was decided to taper the splice plates at their ends in order to reduce the number of holes in the flange until the flange could be sufficiently unloaded to accommodate four holes across the width (refer to Figure 2.31). At the first row, with only two holes allowed in the splice plates because of the taper, the flange was checked for yielding on the effective area of the flange and fracture on the net area of the flange under the full maximum flange design force. At the second row, there are again only two holes, but the flange design force at this section has been reduced by the ratio of (2/total # of bolts) times the force, so that this section does not govern. The next critical section is a staggered line running through the third and fourth rows from the end of the splice plates. At this section, the flange design force has been reduced by (4/total # of bolts) times the force. In each case, the proportions of the flange at this critical section are satisfactory to prevent yielding and fracture of the flange under the governing design force. Final details of the flange splices are

shown in Figure 2.31.

Web Splices: The web splices are designed for the following: 1) a design shear conservatively assumed to equal 100 kips (444.8 kN), 2) a moment due to the eccentricity of the design shear, and 3) the plastic-moment capacity of the web. The plastic-moment capacity of the web is computed assuming a 3/8-in. (9.5-mm) thick web, which is the thickest of the component specimen webs (for Specimens B2 and B3), and assuming a static yield stress of 55 ksi (379 MPa). It should be noted that these assumptions are extremely conservative since the actual shear is very low and the curved components fail by lateral bending rather than vertical bending.

Using the conventional elastic-design approach for eccentrically loaded bolted connections, three rows of bolts are required to prevent slip in the critical bolt under the combined design actions (42 bolts total). The bolts are spaced at 3 in. (76.2 mm) in the horizontal and vertical direction. The row closest to the web gap is 2 in. (50.8 mm) from the centerline of the splice resulting in an eccentricity of the design shear equal to 5 in. (127 mm). A maximum web gap of ¼" (6.4 mm) is specified.

The web splice plates are designed to limit the vertical bending stress in the plates under the total moment to prevent yielding on the effective area of the plates and fracture on the net area of the plates. In the calculations, the yield stress of the plates is assumed to be 50 ksi (345 MPa) and the ultimate tensile strength of the plates is assumed to be 65 ksi (448 MPa). Two 9/16" (14.3 mm) x 42" (1067 mm) plates are specified. Filler plates are also specified as required. Final details of the web splices are shown in Figure 2.31.

Bearing Design: The ideal boundary conditions at each of the six bearings at the end supports of the test frame are shown schematically in Figure 2.32. Since accurate measurement of horizontal reactions, or tangential and radial reactions, in the laboratory is extremely difficult, these boundary conditions are intended to provide the minimum amount of horizontal restraint to the test frame while still maintaining static equilibrium. This set of boundary conditions was selected based on an examination of several different possible sets of boundary conditions using the GTSTRUDL linear elastic model of the test frame.

At the ends of G1 and G3, the bearings are to provide vertical support only. These non-guided bearings are intended to theoretically allow free translation of the girders (except for friction) in the tangential and radial directions, as well as free rotation of the girder about all three axes, at both ends. At both ends of G2, the bearings are to be guided tangentially. As such, the bearings under G2 are to provide radial restraint to the girder. Free rotation of all girders, including G2, about all three axes is to be permitted. Since the bearings provide no tangential restraint, a tangential support frame (discussed in more detail in the next section) is to be provided at the left (west) end of G2 to supply the necessary tangential restraint to the frame. To minimize the tangential reaction, the tangential support frame is to be connected to the neutral axis of the web.

Because large loads and significant rotations were expected in the planned test program, it was decided to specify spherical expansion bearing assemblies for the test-frame girders. Spherical bearings typically consist of woven PTFE (Teflon) either bonded or mechanically fastened to a steel plate with a concave spherical surface. This plate then mates with a solid stainless-steel plate with a convex spherical surface. The PTFE provides a low friction interface and the mating spherical surfaces allow for rotation about any axis. To provide freedom of translation, a 16-gage stainless steel sheet is seal welded around its entire periphery to the sole plate that is placed on top of each bearing. The stainless steel mates with PTFE bonded to the flat top of the steel concave plate to allow the bearing to translate freely. Guides to prevent translation in the radial or tangential direction are usually integral with the sole plate; that is, the sole plate is recessed directly above the bearing to allow translation of the bearing in the desired direction and prevent translation of the bearing in the orthogonal direction.

The size of the bearing is determined based on a specified unit load (or unit stress). Spherical bearings with woven PTFE surfaces are typically designed for a maximum unit stress of either 3.5 ksi (24.1 MPa) or 6.0 ksi (41.4 MPa). Since the coefficient of static friction, μ, generally decreases with increasing unit load (a more expensive Kevlar reinforced PTFE is typically used), it was decided to specify a unit stress of 6.0

ksi (41.4 MPa) for the design of the test-frame bearings. The lubricant area (*LA*), or projected plan area of the sliding surface (not the total spherical area), is then calculated as the maximum predicted vertical load acting on the bearing divided by the unit stress. The lubricant chord (*LC*) is then calculated from simple geometry as the diameter of a circle with an area equal to the lubricant area, or $LC = \sqrt{LA/0.7854}$. The limited expected life of the bearings seemed to justify the use of a higher design stress, which also resulted in smaller and less expensive bearings.

The maximum radius of the spherical surface is designed to accommodate the maximum predicted rotation, β, of the bearing. In addition, the radius is designed to prevent uplift when the bearing is subject to the minimum vertical load in combination with the maximum horizontal load. That is, the radius is designed so that the resultant of the minimum vertical dead load (self-weight reaction) and the maximum horizontal load acting on the bearing is normal to the spherical surface at the maximum design rotation of the bearing (i.e., at the edge of the spherical surface). In a real bridge, it is indeed possible for the maximum horizontal load (due to wind, seismic or thermal loading) to be acting in combination with the minimum vertical dead load. In this controlled laboratory experiment, however, it is known that the maximum predicted horizontal load on the bearings will only occur in conjunction with a significant applied vertical load. Therefore, to minimize the radius of the spherical bearings for this test, it was specified that the *average* of the maximum and minimum vertical loads acting on the bearing be used to determine the radius. The angle, α, of the resultant force is therefore determined as follows:

$$\tan\alpha = \frac{Maximum\ horizontal\ load}{Average\ vertical\ load} \tag{1}$$

The total design angle, θ, for the bearing is equal to the angle α plus the angle β. The maximum radius, *R*, is then simply determined as $R = LC/2\sin\theta$.

The parameters specified for the design of the bearings· are summarized below in Table 2.1. These parameters were determined using the various finite-element models of the frame. The maximum vertical design loads specified for each bearing were estimated using the BSDI 3D System linear elastic model of the composite bridge discussed earlier. It was decided to design the bearings to try to accommodate the possibility for such a test in the future so that new bearings would not be required. In this particular analysis (which was done prior to the analysis used to determine the girder cambers discussed previously), it was assumed that a component specimen with a 1-1/8" (28.6 mm) x 19" (483 mm) top flange, a 5/16" (8 mm) x 48" (1219 mm) web, and a l" (25 mm) x 22" (559 mm) bottom flange would be inserted in the center of G3 prior to casting the deck. The static yield stress of the steel for the component specimen was assumed to be 42 ksi (289.6 MPa).

Table 2.1. Bearing Design Parameters

BEARING DESIGN PARAMETERS							
Girder	**Maximum Vertical Load**	**Minimum Dead Load**	**Maximum Horizontal Load**	**Maximum Rotations**		**Maximum Movements**	
				About Radial Axis	**About Tangential Axis**	**Radial**	**Tangential**
Gl	100 kips	3 kips	10 kips	2.1°	1.5°	0.8"	1.8"
G2	275 kips	14 kips	38 kips	4.5°	1.5°	Fixed	2.3"
G3	375 kips	29 kips	38 kips	6.0°	1.5°	0.8"	1.8"

1 kip = 4.4482 kN

An 8-in. (203 mm) thick concrete deck was assumed with an f'_c of 3.0 ksi (20.7 MPa). Lower steel and concrete strengths were assumed to try and minimize the total load required to fail the composite specimen. From the analysis results, it was estimated that two simulated H20 trucks side-by-side (with impact included) times 3.5 would be required to reach the theoretical moment capacity of the assumed composite specimen. The moment capacity was controlled by crushing of the concrete deck. Adding the calculated vertical reactions for the steel and the concrete deck to the vertical reactions due to the required simulated live load, the total vertical reactions at each end were approximately 325 kips (1445.6 kN) for G3, 222 kips (987.5 kN) for G2, and 140 kips (622.7.7 kN) for Gl.

The test frame behaves differently than the composite bridge. In recognition of the non-linear behavior of the system as the component specimen in G3 yields and much of the load is gradually transferred to G2, the vertical reaction for G2 was arbitrarily adjusted upward to 275 kips (1223.3 kN). A second arbitrary adjustment was later made to the reactions for G1 and G3 resulting in the final design values of 375 kips (1668 kN) for G3, 275 kips for G2 (1223.3 kN), and 100 kips for G1 (444.8 kN). The vertical reaction for G3 was increased to account for the anticipated non-linear behavior of this girder and to allow for the possibility of future component tests under combined shear and bending where specimens could potentially be inserted in G3 immediately adjacent to a bearing. The vertical reaction for G1 was reduced because of the predicted tendency of G1 to want to uplift as the component specimen yields. The live-load simulation would be accomplished by placing the loads so as to produce the maximum load on G3, which is different from the position of the live load to produce the maximum load on G1.

It should be emphasized that the preceding analysis was done only to obtain a reasonable and rational estimate of the maximum vertical design reactions for the bearings and does not necessarily represent how the composite bridge test may eventually be done.

The specified minimum vertical dead loads are simply the predicted vertical end reactions in the test-frame girders due to the steel weight. These reactions were obtained from the linear elastic GTSTRUDL model of the frame.

Horizontal reactions can develop at the test-frame bearings that have no lateral restraints due to friction, artificial or unintentional restraints at the bearings, and corruptive lateral forces on the system resulting from slight unintentional inclinations of the applied vertical loads as the test-frame girders twist and deflect. It was desired to minimize these reactions during the component tests because of the difficulty in accurately measuring their magnitudes experimentally, concerns about their potential corruptive effect on the data, and concerns about the ability of load cells (used to measure the vertical reactions at the bearings) to resist significant horizontal forces.

Friction was a concern because if a sudden movement of the bearings occurs as the frictional resistance in the bearings is overcome (with an increase in the vertical loads), it might potentially contaminate the strain and displacement readings with sudden adjustments. To try and minimize the effects of friction, a maximum coefficient of static friction of 0.045 (4.5 percent) was specified for the bearing design. In addition, the highest unit stress was specified and a procedure was proposed for minimizing the radius of each bearing, as described earlier. It was also required that the bearings be tested by the manufacturer to measure the actual sliding coefficient of friction at the design capacity of the bearing according to the requirements of the AASHTO Standard Specifications Article 18.3.5.3.2 in Division II (prior to the 1997 Interim Specifications). In this test, the bearing is loaded up to its rated vertical capacity for at least 12 hours. The bearing is then subjected to an initial movement at a sliding speed of less than 1 in./min. followed by 100 movements at a speed of less than 1 ft/min. The static and dynamic coefficients of friction are measured and reported during the first and last movement. Working the bearing in this manner helps to reduce the initial coefficient of friction slightly. In larger bearings designed for higher vertical loads, there is a slight increase in the coefficient of friction at lower loads, but the increase is typically limited to 1 or 2 percent according to the bearing manufacturers. It should be noted that it was also required that the bearings be proof load tested, as specified in the AASHTO Standard Specifications Article 18.3.5.3.1 in Division II (prior to the 1997 Interim Specifications). In the proof load test, the bearing is loaded up to 150% of its rated capacity under a specified rotation for a period of one hour and is then examined for deformation of the PTFE or other defects. The results of the friction test for the non-guided G3 bearing are

given below:

	Static Coefficient of Friction	Dynamic Coefficient of Friction
1st Movement	0.016	0.014
101st Movement	0.014	0.013

A horizontal design reaction of 10 percent of the maximum vertical reaction was assumed at all the bearings, including the non-guided bearings, to conservatively account for the effect of friction and other possible corruptive effects. For the bearings under G2, an additional 10 kips (44.5 kN) was added. This load was a conservative estimate of the largest radial or tangential reaction that these particular bearings would be expected to experience based on an examination of the results from the various analyses of the test frame. The resulting maximum horizontal design loads for each bearing are shown in Table 2.1. The maximum expected rotations and movements at each bearing shown in the same table envelope the largest values determined from the ABAQUS non-linear analysis of the frame.

Based on these design parameters, the maximum design radius for each bearing is determined as follows (Table 2.2) according to the procedure given above:

Table 2.2. Maximum Design Radius for Bearings

Girder	α	β	θ	**LC**	**Maximum Design R**
G1	10.99°	2.1°	13.09°	4.61"	10.18"
G2	14.73°	4.5°	19.23°	7.64"	11.60"
G3	10.65°	6.0°	16.65°	8.92"	15.57"

1 in. = 25.4 mm

Final details for the bearings are shown in Figure 2.33. The detailed design and fabrication of the bearings was performed by the selected manufacturer COSMEC, Inc. Therefore, the actual final size of each bearing is not shown in the figure. In addition to the bearings, the manufacturer also provided the indicated sole plates, shim packs and masonry plates. The plates were all fabricated from ASTM A709 Grade 50 (A709M Grade 345) steel. Note the integral guide built-in to the sole plate for G2 to prevent radial translation. A 1-in. (25-mm) shim pack was specified to allow for slight elevation adjustments of each bearing in the laboratory. Shims ¼"-in. (6.4-mm) thick or greater were specified to be ASTM A36 (A36M) plate material. Shims less than ¼"-in. (6.4-mm) thick are sheet material and were therefore designated as ASTM A570 Grade 36 (A570M Grade 250) material. At the time the bearings were to be manufactured, a final design of the support structures for the test frame had not yet been completed. Therefore, masonry plates were specified and supplied in case concrete abutments were eventually used. Each plate had 2-1/4" (57 mm) holes provided in each comer to allow for the installation of 1-1/4" (32 mm) diameter anchor bolts. Since the decision was finally made not to use concrete abutments for the support structures (see below), the masonry plates were not needed in the laboratory and were set aside. For shipment to the fabricator (and later to the laboratory), the manufacturer tack welded the sole plate to the base plate to keep each bearing level and also to allow for removal of the shim packs and masonry plates prior to installation at the laboratory. The tack welds were removed at the laboratory and the sole plates were then fillet welded to the bottom flanges of the girders.

The instrumentation scheme used to measure the vertical and horizontal reactions at each bearing in the laboratory is discussed in more detail elsewhere in other project reports.

Support Structure Design: The support structures necessary for this test included abutments or pedestals to support the test-frame girders at their ends and a support frame to provide tangential support to the test frame at the west end of G2.

End-Support Structures: Several different schemes were considered for the design of the end-support structures. It was decided initially that the bottom of the girder webs should be located approximately 6'-6" (2.0 m) off the laboratory floor. This would allow room for relatively unobstructed access underneath the test frame and also allow for the installation of instrumentation and for the possible application of loading underneath the frame.

Initially, it was proposed that a pair of concrete abutments be used (Figure 2.34). The abutments would be 22'-6" (6.9 m) long, 6'-6" (2.0 m) wide and approximately 6'-0" (1.8 m) high with provision for tie-down to the laboratory floor using six Dywidag rods each. The abutments were designed for a maximum vertical reaction of 300 kips (1334 kN) and a maximum horizontal reaction of 45 kips (219.7 kN). It soon became evident, however, that these abutments would be too bulky and heavy for use in the laboratory and would not be re-useable in all likelihood.

Therefore, a complete design of a set of six individual concrete piers was prepared. It was proposed that each test-frame girder be supported at each end by one of the piers. Each pier would consist of a square 2'-6" x 2'-6" (0.76 m x 0.76 m) concrete column centered on an integral square 8'-0" x 8'-0" (2.4 m x 2.4 m) concrete footing. Girder bearings would then rest on masonry plates placed on top of each pier. Each pier was designed for a maximum vertical reaction of 300 kips (1334.4 kN) and a maximum horizontal reaction of 60 kips (266.9 kN). The piers were checked for overturning and for shear and bending in the various individual components. The main reinforcing in the columns was specified to be #9 bars at 9-in. (229-mm) spacing. The reinforcing in the footing was specified to be #8 bars at 9-in. (229-mm) spacing. #4 stirrups and hoop bars would also be required. Although it was determined that overturning would not be a problem, provision was still made in the design for pipe sleeves to be provided in the footing. These sleeves could be lined up with several holes in the laboratory floor so that Dywidag anchor rods could be used, if necessary, to anchor cross beams across the footings to prevent uplift. The total weight of each pier of 26.8 kips (119.2 kN) was well within the laboratory crane capacity of 40 kips (178 kN) so that the piers could easily be moved around and set into position.

In the meantime, concerns began to be raised about utilizing such stiff supports. It was planned to use conventional load cells underneath each bearing to measure the vertical end reactions, and there was concern about whether or not these load cells would be capable of resisting large horizontal forces that might be generated at the bearings, particularly with such large unyielding vertical supports. Also, a reasonable cost-efficient scheme for accurately measuring horizontal reactions at the bearings had not yet been developed. Therefore, it was proposed that large-diameter pipe sections be considered for use as pedestal supports. Pipe sections would be more flexible and could also potentially be gauged and calibrated to function as load cells to provide vertical and horizontal loads (reactions). It was proposed that each pipe be attached with a moment connection to a steel base plate bolted to the laboratory floor. There would be no bracing between the adjacent pipe pedestals so that each pipe would act as a free-standing cantilever. The moment connection would be achieved by fillet welding the pipe all-around to a 2-1/2" (63.5 mm) base plate and stiffening the pipe at the base using four ¾" (19 mm) vertical gusset plates. All strain gages would be placed at mid-height of the pipe to ensure sufficient clearance from the gusset plates.

Each pipe was designed as a beam-column subject to axial load and biaxial bending according to Section H1.2 of the AISC LRFD Specification. The axial load was taken as the maximum vertical reaction at each bearing determined based on an earlier BSDI 3D System analysis of the composite test frame (discussed in the preceding section of this report on Bearing Design). These reactions were 325 kips (1445.7 kN) for G3, 275 kips (1223.3 kN) for G2, and 140 kips (622.7 N) for G1. The maximum horizontal reaction in both directions at all the non-guided bearings (on G1 and G3) and in the tangential direction at the guided bearings on G2 was taken as the corresponding maximum vertical reaction times an assumed friction coefficient (for the bearings) of 5.0 percent. The maximum horizontal reaction in the radial direction on the bearings at G2 was conservatively estimated to be 16.0 kips (71.2 kN). The moments about

the tangential and radial axes at the top of each pedestal were then calculated as the assumed horizontal reaction times the height from the base of the bearing to the base of the pedestal, assumed to be 6.5 ft (2.0 m). An additional moment equal to the maximum vertical reaction times an assumed eccentricity of 2" (51 mm) was also added to the moment about each axis. This resulted in total moments of 69.0 kip-ft (93.6 kN-m) about both axes of the G1 pedestal, 135.0 kip-ft (183.0 kN-m) about the radial axis and 150 kip-ft (203.4 kN-m) about the tangential axis of the G2 pedestal, and 160 kip-ft (216.9 kN-m) about both axes of the G3 pedestal.

The compressive resistance of each pipe was determined according to Section E2 of the AISC LRFD Specification. A length of 6.5 ft (2.0 m) was conservatively assumed. The effective length factors, K_x and K_y, were both assumed to be 2.1. The specified minimum yield stress of the steel was assumed to be 50 ksi (345 MPa). The ratio of the diameter, D, of the pipe to the thickness, t, was limited to $3{,}300/F_y$ or 66.0 according to LRFD Table B5.1. The specified resistance factor for compression equal to 0.85 was applied. The flexural capacity was determined according to Section Fl of the specification using a resistance factor for flexure equal to 0.90 and an assumed unbraced length of 6.0 ft (1.8 m). In this case, D/t was limited to $2{,}070/F_y$ or 41.4, which is the specified limit for a compact tubular section in flexure. The intent was to select pipes with a wall thickness less than ½" (12.7 mm) to ensure greater accuracy in the measurement of the axial and lateral loads in each pipe. Initial preliminary designs that had been done resulted in pipes that were deemed to be too thick. The initial sizes that had been selected were as follows: a 12-3/4" (324 mm) OD pipe with a ½" (12.7 mm) thick wall for the G1 and G3 pedestals and a 20" (508 mm) OD pipe with a ½" (12.7 mm) thick wall for the G2 pedestal (Figure 2.35). The original intent was to try and "tune" the response of the pedestals to the horizontal loading from the girders by selecting a pipe with a much higher moment of inertia for the G2 pedestal, since it was anticipated that it would be subject to much larger horizontal reactions. In the re-design, the following pipe sizes (with thinner walls) were selected based on the predicted actions given above: a 12-3/4" (324 mm) OD pipe with a 3/8" (9.5 mm) thick wall for the G1 pedestal, and an 18" (457.2 mm) OD pipe with a 7/16" (11 mm) thick wall for the G2 and G3 pedestals.

Before these pedestals could be fabricated and calibrated, however, the development of a simpler and more cost-effective scheme for measurement of the horizontal reactions was initiated. Several different schemes were investigated. The scheme that was finally chosen for use involved supporting each bearing and load cell combination on top of a bed of confined pressurized grease in order to isolate the load cell. The grease is confined within an O-ring gasket placed within a ring plate (or puck). Four instrumented studs spaced 90 degrees apart are placed within the wall of the ring plate and are calibrated to provide the horizontal reactions based on the measured loads in the studs. A more detailed description of the development and calibration of this system is given elsewhere. The use of this system negated the need for the more costly instrumented pipe pedestals.

With the development of the system described in the preceding paragraph, consideration could again be given to the use of concrete piers or possibly steel abutments. In deciding between steel and concrete supports, FHWA laboratory personnel reiterated their desire for a light and flexible system of abutment supports that could be easily re-configured and re-used and that would be compatible with existing laboratory fixtures. As a result, they proceeded with the development of the I-beam abutments shown in Figure 2.36 that were eventually selected for use. As shown in the figure, each abutment is prestressed to the laboratory floor using double channel spreader beams and Dywidag rods. Additional bracing can be added to each abutment as necessary. The abutments were designed for this particular test to maintain the bottom of each girder web the desired distance of 6'-6" (2.0 m) off the laboratory floor.

Tangential Support Frame: To provide tangential support to the test frame, a separate support frame was designed for attachment to the left (west) end of G2. A plan view of this support frame is shown in Figure 2.37. Note that the frame is oriented to be tangent to the centerline of G2 at the left end of G2. Therefore, the frame is rotated 12.9° in a counterclockwise direction from the vertical (east-west) plane.

An elevation view of the tangential support frame is shown in Figure 2.38. This simple frame consists of a W12 x 40 (W310 x 60) column supported by an inclined W12 x 40 (W310 x 60) strut. Both the column and strut are fillet welded to a 2-1/4" (57 mm) thick rectangular base plate. The base plate is 4'-6" *x* 5'-6" (1.4 m *x* 1.7 m) in plan. The base plate is anchored to the laboratory floor with

four Dywidag rods placed in 3-in. (76 mm) diameter holes. A W12 x 40 (W310 x 60) arm stretching out horizontally from the support-frame column is provided to attach onto G2 at mid-height of its web, or at a vertical distance of 8'-6" (2.6 m) off the laboratory floor. The frame is attached at mid-height (i.e. at the neutral axis) of the noncomposite G2 to minimize the magnitude of the tangential support reaction at the G2 bearing. The distance from the attachment point on the G2 web to the centerline of the support-frame column is 5'-7" (1.7 m) in order to provide sufficient clearance for installation of the end-support structure. The support-frame column is stiffened at the connection with the horizontal arm using three pairs of horizontal ½-in. (12.7-mm) thick stiffener plates spaced 6-in. (152.4-mm) apart in the vertical direction. A 1-1/2" (38 mm) diameter lift hole is provided near the top of the support-frame column to allow the frame to be lifted and placed using the laboratory crane. All material for the main components of the support frame is specified to be ASTM A572 Grade 50 (A572 M Grade 345) material.

The main components of the support frame are conservatively designed for an assumed tangential force of 100 kips (444.8 kN) applied at the top of the frame. This force results in equal and opposite reactions of 213 kips (947.5 kN) at the base of the column and the inclined strut, and a maximum axial force in the strut of 235 kips (1045.3 kN). The effective length factor, K, for the strut is assumed to be 1.2. The base plate is allowed to achieve its full plastic moment capacity under the opposing 213-kip (947.5 kN) reactions, which is considered acceptable since the assumed 100-kip (444.8 kN) design force is quite conservative.

The horizontal arm of the support frame is attached to G2 using a pair of 1-in. (25-mm) thick splice plates and a 2-in. (51 mm) diameter pin. The flanges of the horizontal arm are trimmed back and six standard 15/16" (24 mm) diameter holes for 7/8" (22 mm) diameter high-strength bolts are provided in the remaining web to accommodate the splice plates (refer to Figure 2.39). The bolts are designed to prevent slip in double shear under the 100-kip (444.8 kN) design force assuming a Class A surface condition. The matching holes in the splice plates are long slotted holes to allow for some vertical adjustment during installation. Structural plate washers 5/16" (7.9 mm) in thickness with standard 15/16" (24 mm) diameter holes are placed over the long-slotted holes in the outer plies. Hardened washers are then placed over the holes in the plate washers when making the connection. A shim pack is also specified to compensate for possible irregularities in the fit-up.

The pin is placed in a 2-1/8" (54 mm) diameter hole located 6 in. (152.4 mm) from the left (west) edge of G2 (refer to Figure 2.26). Two 3/8-in. (9.5 mm) cotter pins are specified to hold the pin in place. The pin conforms to the specifications for ASTM A108 material. Bearing of the pin against the side of the hole is checked for a maximum expected force of 10 kips (44.5 kN), estimated from the GTSTRUDL linear elastic analysis of the frame, and found to be satisfactory. During installation, the pin is centered within a bean-shaped hole fabricated into the splice plates. The dimensions of this hole, shown in Figure 2.39, are determined to accommodate the predicted maximum end rotation of G2 during the component tests. This hole is provided to prevent binding of the pin as the girder rotates since the maximum vertical load that can be accommodated by the support frame at the connection to G2 is computed to be 15 kips (66.7 kN). This limiting vertical load is calculated to prevent overstressing of the welded connection of the arm to the support-frame column under combined bending (due to the vertical load) plus the assumed axial design force of 100 kips (444.8 kN).

***Loading Fixture Design*:** For the bending component tests, it was decided to apply six equal vertical loads at the same time to the flanges of all three girders in the frame at approximately the third points of each girder arc span. This loading nearly represents the application of a multiple of the deck weight to the noncomposite steel girders. As a result, the component specimen in the center of the span of G3 is subjected to a nearly constant vertical bending moment (the vertical bending moment due to the self-weight of the steel is not constant). The loads applied to the outermost girder G3 are applied just outside the component specimen (refer to Figure 2.27). Due to the inherent stability requirements of curved-girder bridges discussed above, the outermost girder G3 will resist the largest portion of the total load. Thus, the component specimen, located within G3, can be loaded to its ultimate load without yielding any remaining portions of the test frame. Loading the test-frame girders equally also prevents uplift of the innermost girder G1.

Loading of the test frame is complicated by the fact that each curved girder will begin to twist and deflect laterally immediately upon loading, which makes it difficult to maintain the applied loads in a

vertical position. Inclination of the applied loads would result in corruptive horizontal forces. In the linear elastic GTSTRUDL models, small radial and tangential loads were applied at each of the load points to study their effects. The observed potential significance of these non-vertical loads led to an evolutionary design of the load fixtures. Two objectives in this process were: 1) minimize the corruptive effects of any horizontal components of the loads generated by inclination of the applied loads, and 2) prevent any Dywidag rods from contacting the approximately 3-in. (76 mm) diameter holes in the laboratory floor that they passed through since the rods are not designed to resist any bending.

Several different schemes for loading of the test frame were considered. These schemes included the use of different reaction and spreader beam arrangements above and/or underneath the frame in combination with spherical bearings to accommodate the rotations, the use of low-friction pulley arrangements, and the use of gravity-load simulators as employed by Lehigh University in testing a frame in the 1960s. A type of spreader-beam arrangement was chosen for reasons of economy and simplicity.

The first scheme to be investigated in some detail entailed a plan to apply the loads through a spreader-beam arrangement underneath the test frame so that each girder in the frame would be loaded approximately equally. Because the bottom flanges of the girders were predicted to experience less radial movement than the top flanges during twisting of the girders, it was felt that applying the loads underneath the frame to the bottom flanges would help to minimize the inclination of the applied loads. Preliminary non-linear analyses of the test frame using ABAQUS with one of the initial component specimens inserted in G3 indicated that the predicted ultimate capacity of the specimen changed less than 5 percent when the loads were applied to the bottom flanges (versus the top flanges) of the test-frame girders.

Several design iterations were required to arrive at the final configuration for this planned loading scheme. Two spreader beams were to be used; one running between G1 and G2 and the other running between G2 and G3. As shown in the plan view given in Figure 2.40, the spreader beams would be slightly offset from each other. Load would be applied to each spreader beam (made up of back-to-back channels) through a single Dywidag rod running through an appropriate hole in the laboratory floor to a center-hole jack located underneath the floor (Figure 2.41). As shown in Figure 2.41, each rod would be anchored to a spherical bearing on top of each spreader beam in order to accommodate the rotations of each beam. At the end of each spreader beam, connections to the test-frame girders were to be made utilizing three anchor shackles connected in series with a load sensing tension link. Details of this connection are shown in Figure 2.42. The tension links were to be used to measure the applied loads. The anchor shackles were inserted to accommodate the movement and twisting of the test-frame girders in any direction.

Because of concerns about the Dywidag rods bearing against the holes in the floor, it was decided to limit the tangential and radial movements of the spreader beams. Therefore, heavy-duty wheel casters were specified on the ends (tips) of each spreader beam and heavy-duty ball casters were specified on the sides of the spreader beams near each end (Figures 2.43 and 2.44). These casters were intended to roll vertically along spreader-beam guides, or small cantilever stub columns anchored to the laboratory floor, to allow movement of the spreader beams primarily in a vertical plane (Figure 2.45). At the extreme ends of each spreader beam adjacent to G1 and G3, channels were to be used for the spreader-beam guides. Adjacent to G2, wide-flange beams were to be used for the guides (Figure 2.40). As illustrated in Figure 2.40, wide-flange spreader-beam guides to restrict movement in the tangential direction could only be provided on one side of each spreader-beam end at G2. Therefore, to restrict tangential movement in the opposite direction, matching 1-in. (25-mm) thick stainless-steel plates were attached to the inside of each beam (refer to Section B-B in Figures 2.43 and 2.44) near the beam ends adjacent to G2. A PTFE (Teflon) pad, provided on one of the mating plate surfaces, was intended to allow vertical movement at that location.

To investigate the feasibility of this loading scheme, the spreader-beam arrangement was incorporated in the ABAQUS model of the test frame. One analysis was run assuming that the spreader-beam guides acted as fully rigid supports in the radial and tangential directions. A second analysis was run with the spreader-beam guides represented by grounded springs in the radial and tangential directions, each with an assumed stiffness of 129 kips/in (22.6 kN/mm). A third analysis was run assuming no restraints applied to the spreader beams. The first two analyses indicated that relatively large tangential forces are developed at the spreader-beam guides. These forces indicate that the loading system would experience out-of-plane

motions that would undoubtedly cause the system to bind during the tests. Binding within the loading system would reduce the effect of the applied loads on the component specimen and would likely result in unsymmetric behavior of the test frame. As a result, the component specimen would not be subject to a nearly constant vertical bending moment as intended. From the predicted tangential displacements of the loading system -- determined from the analysis assuming the support guides were removed -- it was not clear whether or not the Dywidag rods would come into contact with the holes in the laboratory floor.

The ABAQUS analyses described above are an example of the value of finite-element investigations of a test at the time of design. Based on the results of these analyses, it was decided to abandon the complex spreader-beam scheme in favor of a simpler and less costly scheme in which the loads are applied directly to the top flanges of each girder. As shown in Figure 2.46, the loads are applied at approximately the third points of each girder using a simple orthogonal frame that supports the jack in a conventional vertical orientation. Each orthogonal loading frame is supported near each corner of the frame by a Dywidag rod, approximately 14 ft (4.3 m) in length, that runs vertically from the frame through a hole in the laboratory floor where it is anchored by a "chair" against the underside of the floor. The four rods for each loading frame must be orthogonally spaced at 6'-0" (1.8 m) to correspond with the holes in the floor. Thus, the jack load is resisted roughly equally by the four tension rods (it should be noted that as a result of the location of the holes in the floor with respect to the curved girders, the jacks were not located at the geometric centers of the loading frames. Thus, the tension in the rods was not exactly equal). Each jack is mounted to a cross beam attached to the orthogonal frame (Figure 2.47). A greased ball-and-socket type bearing arrangement below each jack maintains the load in the vertical position as the loading frame moves laterally. The ball is installed at the end of the jack and the socket is placed on top of a load cell that is used to measure the magnitude of the applied load. The load cell is in turn mounted on a plate attached to the girder top flange. The flexibility of the 14-ft (4.3-m) long Dywidag bars allows the loading frame to follow the test frame as it moves laterally. Although a gravity-load simulator would further reduce lateral effects, the magnitude of any corruptive lateral forces that resulted due to inclinations of the applied loads was determined to be minimal. The length of the Dywidag rods reduces the angle caused by the lateral movement, thus making it less likely that the rods will contact the edges of the holes during testing.

The cross beam consists of back-to-back MC 12 x 45 (MC 310 x 67) channels (Figure 2.48). Each cross beam is 8'-0" (2.4 m) long. The channels are bolted together through their webs using 7/8" (22 mm) diameter A325 (A325M) high-strength bolts passing through 3-in. (76-mm) long ASTM A53 Schedule 40 pipe spacers and standard holes in the web of each channel. As shown in Figure 2.47, the cross beam is supported on top of two end beams, running perpendicular to the cross beam, which are identical in size to the cross beam. The end beams are attached to the cross beam using short Dywidag rods. Each jack pushes down on the girder and up on the cross beam, which in turn pushes up on the end beams. The Dywidag rods at the ends of the end beams provide the reaction points. The cross beam was designed for a maximum vertical load in the jack of 177 kips (787.3 kN). This load was computed as the maximum anticipated load in a possible future shear component test of 126.5 kips (560.5 kN) times a load factor of 1.4. The end beams were designed for the maximum computed end reaction from the cross beam of the G3 loading fixture equal to 108 kips (480.4 kN). This load was then conservatively applied at mid-span of the end beam. Each channel was assumed to carry half of the jack load. Twist was neglected since the channels are bolted together and the load is applied through the shear center of the channel pair. The flexural capacity of the members was checked according to the provisions of Appendix F of the AISC LRFD Specifications. All material was assumed to be ASTM A572 Grade 50 (A572M Grade 345) material. The specified resistance factor for flexure equal to 0.90 was applied. The moment-gradient correction factor C_b was taken equal to 1.0. Yielding of the beams under the unfactored load was also checked. The calculations indicated that MC 12 x 31 (MC 310 x 46) channels would have been satisfactory for the cross beam and that MC 10 x 25 (MC 250 x 37) channels would have been satisfactory for the end beams. However, for simplicity, MC 12 x 45 (MC 310 x 67) channels were conservatively used for both the cross and end beams.

As an extra precaution to ensure in-plane stability of the loading frames, lateral braces are provided to connect the ends of the end beams (Figure 2.49). Since these braces were not anticipated to carry any significant loads during testing, no analysis of these members was performed. A single standard C 10 x 15.3 (C 250 x 23) channel was selected for these members. As illustrated in Figure 2.49, each bracing member is connected to the end beams using 7-in. (178 mm) long L 6 x 3-1/2" x 3/8" (L 152 x 89 x 9.5)

single angles. Long-slotted holes are provided in the connection angles to allow for adjustments during fit-up. As required by AASHTO, plate washers are specified to completely cover the long-slotted holes in the outer plies. Note in Figure 2.49 that ¼" (6.4 mm) thick plain neoprene pads (50 ± 5 Durometer Grade 0) were also specified to provide a seating for the load-cell mounting plate on each flange, if desired.

It should be noted that the loading fixtures described above that were eventually used in the tests were never modeled in the finite-element investigations. Instead, the applied loads were applied vertically at all times. In the non-linear ABAQUS analyses, the loads followed the lateral deflection of the structure to which they were attached. In the BSDI 3D System and GTSTRUDL linear elastic analyses, the deformation of the structure is not recognized with respect to application of the loads.

***Miscellaneous Items*:** This section covers the design of miscellaneous items for the test-frame girders, such as the design of the intermediate transverse stiffeners, cross-frame connection plates, bearing stiffeners and loading fixture stiffeners. AASHTO M270 Grade 50 (M270M Grade 345) material was specified for all stiffeners and connection plates, including the stiffeners and connection plates on the Grade 70W (Grade 490W) G2.

Intermediate Transverse Stiffeners: The intermediate transverse stiffeners (i.e. intermediate stiffeners not serving as cross-frame connection plates or loading fixture stiffeners) for the test-frame girders were designed to satisfy the provisions of both the 1993 AASHTO Guide Specifications and the Japanese Hanshin Guidelines. Although these stiffeners were not theoretically required on the test-frame girders, they were provided to ensure the integrity of these girders throughout the component testing.

The stiffeners were sized to provide the minimum rigidity required by both specifications and also to satisfy the width-to-thickness requirement for transverse stiffeners given in the AASHTO Guide Specification. As shown in Figures 2.25 through 2.27, between cross frame lines 1L and 5L and 1R and 5R, these stiffeners were placed halfway between the cross-frame connection plates on each of the test-frame girders resulting in stiffener spacings of 0.98D, 0.94D and 0.90D on G3, G2 and G1, respectively. In-between cross frame lines 6L and 6R on G1 and G2, the spacings were reduced in half due to the installation of extra cross-frame connection plates at Lines 6aL and 6aR (discussed in more detail below) to accommodate possible future tests. The stiffener spacings were also adjusted slightly on the center section of G3 between Lines 6L and 6R since only one cross-frame connection plate was provided on this section of G3 at Line 7. For G1 and G2, 7/16" x 5" (11 mm x 127 mm) plates were selected for these stiffeners. For G3, 5/8" x 7" (16 mm x 178 mm) plates were selected.

On each girder, these stiffeners were placed on one side of the web only; the side of the web facing the inside of the curve. Since the stiffeners were one-sided, the decision was made to extend and connect the stiffeners to both the top and bottom flanges (refer to Section E-E in Figure 2.50). The stiffeners were connected to the flanges and web using minimum-size 5/16" (8 mm) fillet welds. Snipes were provided at the top and bottom of the stiffener to clear the flange-to-web fillet welds (refer to Detail 1 in Figure 2.50 for the dimensions of the snipes). All welds were stopped short of the snipes by a specified distance.

Cross-Frame Connection Plates: Transverse stiffeners serving as cross-frame connection plates were increased in size since these plates would be subject to significant cross-frame forces. The connection plates also had to accommodate the bolted connections for the cross frames. For G1, 5/8" x 7" (16 mm x 178 mm) plates were selected for these stiffeners. For G2 and G3, 13/16" x 9" (21 mm x 229 mm) plates were selected. Both plate sizes satisfied the width-to-thickness requirement for transverse stiffeners given in the AASHTO Guide Specification.

As required by AASHTO, the connection plates must be rigidly connected to the top and bottom flanges. The welds to the flanges must be designed to transmit to the flanges the maximum resultant of the net horizontal forces *and* moments seen by the connection plate at the intersections with the top and bottom chords of the cross frames. The resultant force on the welds can be estimated assuming the connection plate acts as a simply supported beam between the flanges. Based on the initial estimates of the maximum cross-frame forces and end moments, it was felt that connection plates would be required on both sides of the web of the two fascia girders G1 and G3. By using two connection plates, it was felt that the large net

resultant force on the welds could be equally distributed to the welds on both sides of the web. This distribution was assumed to occur through tension in the connection-plate to web welds. As more refined estimates of the cross-frame forces and moments were developed indicating smaller magnitudes of these actions, it was decided to eliminate the connection plates on the fascia sides of G1 and G3, especially since these plates are not normally seen on typical bridges.

The final welds were designed using maximum predicted shear stresses at the connection plate-to-flange joints from the ABAQUS non-linear model of the test frame with the connection plates on the fascia sides of G1 and G3 removed. Multiplying the maximum predicted shear stress of 32.0 ksi (220.6 MPa) at Lines 6L and 6R on the largest component specimen by the cross-sectional area of the connection plate on G3 resulted in a design force of 234 kips (1040.9 kN). Complete joint penetration (CJP) welds would be required for the connection plate-to-flange welds to resist this force. Therefore, these welds were conservatively specified for use on the G3 connection plate at Lines 5L and 5R adjacent to the component specimen (refer to Section K-K in Figure 2.51). Since the center section of G3 could potentially be used in future component tests, CJP welds were also specified for connecting the single cross-frame connection plate on this girder section to the flanges at cross frame Line 7. The design force for all remaining connection plate-to-flange welds on G3 was determined to be 109.7 kips (488 kN) based on a maximum predicted shear stress of 15.0 ksi (103.4 MPa). 3/8" (9.5 mm) fillet welds were satisfactory at these locations (refer to Section J-J in Figure 2.51). On G2, connection plates were required on both sides of the web. All connection plate-to-flange welds on G2 were also specified to be 3/8" (9.5 mm) fillet welds based on the 109.7-kip (488 kN) design force (refer to Section H-H in Figure 2.50). The design force for the connection plate-to-flange welds on G1 was determined to be 43.8 kips (195 kN) based on a maximum predicted shear stress of 10 ksi (69 MPa). 5/16" (8 mm) fillet welds were satisfactory for these welds on G1 (refer to Section B-B in Figure 2.51). As alluded to earlier, it was decided to go ahead and provide extra connection plates on G1 and G2 at Lines 6aL and 6aR to allow for a different cross-frame spacing to be used along the component specimen in possible future component tests. Details of these connection plates are shown for G2 in Section V-V of Figure 2.51, and for G1 in Section F-F of Figure 2.51. Note that holes were not to be drilled in these connection plates until they would be needed.

The connection plate-to-web welds were designed for the net vertical component of the force in the cross-frame diagonal(s). 5/16" (8 mm) fillet welds were determined to be satisfactory for these welds on all connection plates.

Bearing Stiffeners: Bearing stiffeners for each girder were designed according to AASHTO Working Stress Design procedures given in Article 10.34.6. The stiffeners were checked as equivalent axially loaded columns assuming an effective length factor, K, equal to 1.0. A centrally located strip of web equal to 18 times the web thickness was included in determining the properties of the equivalent column, as permitted by AASHTO. Bearing was checked against the allowable bearing stress of $0.80F_y$. The stiffeners were checked for the maximum vertical reaction at each bearing determined based on an earlier BSDI 3D System analysis of the composite test frame (discussed in the preceding section of this report on Bearing Design). These reactions were 325 kips (1445.7 kN) for G3, 275 kips (1223.3 kN) for G2, and 140 kips (622.7 N) for G1. Since the web thickness of G2 is the same as for G3, the same size bearing stiffeners, 1" x 9" (25 mm x 229 mm) plates, were specified for both G2 and G3. Two ¾" x 7" (19 mm x 178 mm) plates were specified for G1. As shown in Figure 2.27, two extra lines of bearing stiffeners were conservatively provided at both ends of G3 since G3 was expected to experience the largest translations in the tangential direction. Each additional stiffener pair was placed 7 in. (178 mm) on either side of the stiffener pair at the centerline of bearing (refer to Section T-T in Figure 2.50). These extra stiffeners were not considered in the design of the primary bearing stiffeners for G3 (initially placed over the centerline of the bearings).

The bearing stiffeners were specified to be mill-to-bear on the bottom flange and were to be connected to both flanges with fillet welds. At the centerline of bearing, 3/8" (9.5 mm) fillet welds were specified for G3 (refer to Section M-M in Figure 2.51) and for G2 (refer to Section L-L in Figure 2.51). At the centerline of bearing for G1 (refer to Section C-C in Figure 2.50) and for the additional bearing stiffeners on G3 (refer to Section S-S in Figure 2.50), 5/16" (8 mm) fillet welds were specified. All stiffener-to-web welds were specified to be 5/16" (8 mm) fillet welds.

Loading Fixture Stiffeners: Similar procedures were used to design the loading fixture stiffeners. These stiffeners, centered directly under the loading fixtures, are located 16'-3" (4.95 m) on either side of the centerline of G1, 16'-5-3/4" (5.02 m) on either side of the centerline of G2, and 16'-8-7/16" (5.09 m) on either side of the centerline of G1. The same size stiffeners, 13/16" x 9" (21 mm x 229 mm) plates, were specified for both G2 and G3. Two 5/8" x 7" (16 mm x 178 mm) plates were specified for G1. These stiffener sizes were more than satisfactory for the maximum expected load at each loading fixture during the component testing. The loading fixture stiffeners were specified to be mill-to-bear on the top flange and were to be connected to both flanges with 5/16" (8 mm) fillet welds. All stiffener-to- web welds were again specified to be 5/16" (8 mm) fillet welds (refer to Section G-G in Figure 2.50).

Bending Component Specimen Design

Introduction: As mentioned previously, the design of the bending component specimens was complicated by the number of variables that affect the bending resistance of curved I-girders. Among these variables are the span length, radius, unbraced length, flange width, web slenderness, web stiffening and the cross-sectional symmetry of the girder. It was evident early on that it would not be possible, due to budgetary constraints, to independently study the effect of each of these variables in this experimental program. For example, one variable assumed to have a reasonably significant effect on the bending resistance of a curved I-girder is the radius of the girder. However, after further study, it was clear that the costs and complexities that would result from testing components with a different radius either within this single test frame, or using a second separate test frame, would be prohibitive. As a result, the strategy that evolved was to develop a small, but efficient, set of component specimens with a single radius of 208.75 feet (63.6 m) (corresponding to the relatively sharp radius of G3) that would contain rational variations of as many of the other important variables as possible. It was felt that these tests would then pave the way for future analytical parametric studies by others to generate additional data for specimens with different radii, proportions, etc. The parametric data, in conjunction with the experimental data, could then be used for the statistical calibration of future AASHTO LRFD provisions for horizontally curved girders.

Specimen Design: As for the design of many of the test-frame components, the design of the final set of bending component specimens evolved through several iterations. In all iterations, the specimens were designed to be full-size specimens with a web depth of 48 inches (1219 mm). In order to simplify the detailing, the web depth of the specimens was selected to match the web depth that was selected for the test-frame girders in the design of the original prototype bridge. The web thickness of each specimen was then selected to achieve a desired web slenderness ratio. Compression-flange proportions for each specimen were also selected to achieve a desired slenderness ratio and to achieve a desired ratio of lateral flange bending stress, f_w, to vertical bending stress, f_b. For reasons discussed previously, all component specimens were assumed to be noncomposite.

At the beginning of the project, a preliminary set of nine bending component specimens, labeled Tl through T9, was developed (Table 2.3 -- the computation of the predicted capacities of these specimens shown in the table is discussed in the next section). This set of specimens was designed to be inserted into the original test-frame shown in Figure 2.8. Based on the cross-frame spacing, L, along the specimen of 10.4375 ft (3.2 m) measured along the arc and the radius, R, of G3 equal to 208.75 ft (63.6 m), the L/R ratio for each specimen was 0.05. The maximum permitted L/R ratio according to the 1993 AASHTO Guide Specification is 0.1. The specified minimum yield stress of each specimen was 36 ksi (250 MPa). The lateral flange bending moment due to the effects of curvature, M_w, shown in the table was computed from the following approximately formula derived based on V-load analysis theory (*33*):

$$M_w = \frac{Md^2}{10\ hR} \tag{2}$$

where: M = vertical bending moment in the curved girder (taken equal to the theoretical yield moment

M_y in this case)

d = cross-frame spacing
R = girder radius
h = vertical distance between flange centerlines

The lateral flange bending stress, f_w, used to compute the f_w/f_b ratio shown in the table, was then computed as M_w divided by the section modulus of the compression flange about a vertical axis through the web.

Upon further evaluation of this preliminary series of specimens, it was felt that the flange thickness of ½" (12.7 mm) chosen for several of the specimens was too thin and might result in significant distortions of the flange during welding. It was also decided that it would be preferable to test a majority of specimens with a specified minimum yield stress of 50 ksi (345 MPa) since 50-ksi (345-MPa) steel is more commonly used. Also, the web slenderness ratios that were chosen for the specimens would be closer to the slenderness limits in the AASHTO specifications that are based on 50-ksi (345-MPa) steel.

As a result, the nine initial component specimens were re-designed resulting in a new set of specimens, labeled Bl through B9, shown in Table 2.4. These specimens were designed to be inserted into the re-designed test frame (Figure 2.23). Based on the increased cross-frame spacing, L, along the specimen of 15.65625 ft (4.8 m) in the re-designed frame (measured along the arc), the L/R ratio for each specimen was increased to 0.075. This was felt to be near the maximum practical value of the L/R ratio. The panels between G2 and G3 were arranged such that there were three 15-ft (4.6-m) panels in the center of the span and one approximately 7.5-ft (2.3-m) panel at each end (measured along G2). Thus, the centrally located test component would be centered within panels of equal unbraced length. This equality is important to ensure proper end conditions. To strengthen G2, the unbraced length of the panels between G1 and G2 was kept at about 7.5 ft (2.3 m) over the entire span. Thus, the lateral bending in G1 and G2 was greatly reduced from that in G3. The critical girder G2 was thereby strengthened by reducing its unbraced length to 7.5 ft (2.3 m) and by using 70-ksi (490-MPa) steel rather than by using larger plates, which would have increased its bending stiffness. It was important to provide a minimum practical bending stiffness for G2 to ensure that it attracted as little load as possible. In that way, the component in G3 could be failed with the minimal total applied load.

Typically, a curved-girder bridge is designed for the maximum factored load it is expected to receive. In the case of the test frame, G2 was designed for the load that it was expected to see after G3 had failed. Failure of G3 leads to G2 resisting a greater portion of the moment than it would have had G3 not experienced a reduction in stiffness.

At the time, it was proposed that the arc length of each specimen would be approximately 27.4 ft (8.4 m). The specified minimum yield stress of eight of the specimens was 50 ksi (345 MPa). The specified minimum yield stress of Specimen B8, with a compact web and compression flange, was 36 ksi (250 MPa) in order to keep the loads required to reach the predicted maximum capacity of this specimen at a reasonable value.

In addition to providing a desired slenderness ratio, the compression flanges on eight of the specimens were proportioned to provide a ratio of the computed f_w/f_b at the brace points slightly above the maximum limit of 0.5 given in the 1993 AASHTO Guide Specification (with f_w computed according to the approximate Equation 2 given above). Lower f_w/f_b ratios would be possible, but at the expense of larger specimens with greater capacities in order to maintain the same slenderness ratios. At these f_w/f_b and L/R ratios, it was felt that the capacities of the component specimens would represent lower-bound values; that is, greater flexural capacities would be expected at lower and more typical f_w/f_b and L/R ratios. The compression flange on Specimen B3 was proportioned to provide an f_w/f_b ratio closer to 1.0. The resulting L/b ratio (where b is the compression-flange width) for eight of the specimens was approximately 11.0. The L/b ratio for Specimen B3 was approximately 16.0. The upper limit on the L/b ratio in the 1993 Guide Specification is 25.0. The ratio of area of the top (compression) flange to the area of the web ranged from approximately 0.49 to 1.31.

Table 2.3. Preliminary Bending Component Specimens T1 through T9

COMPONENT						M_u (k-ft)						ELASTIC		
ID	TOP FLG.	WEB	BOT. FLG.	L/R	F_y (ksi)	AASHTO	YOO	HANSHIN	FUKO.	NAKAI	M_p (k-ft)	M_y (k-ft.)	M_w (k-ft)	f_w/f_b
T1	12" x 1/2"	48" x 5/16"	12" x 1/2"	0.05	36	704	1216	829	1194	1156	1413	1217	15.7	0.436
T2	12" x 1/2"	48" x 1/2"	12" x 1/2"	0.05	36	798	1428	924	1450	1327	1737	1428	18.4	0.511
T3	12" x 3/4"	48" x 5/16"	12" x 3/4"	0.05	36	1578	1645	1157	1579	1584	1856	1645	21.1	0.392
T4	12" x 3/4"	48" x 1/2"	12" x 3/4"	0.05	36	1779	1854	1259	1843	1758	2180	1855	23.8	0.442
TS	12" x 1/2"	48" x 5/16"	17" x 1"	0.05	36	775	1240	911	1676	1323	1936	1392	17.9	0.497
T6	12" x 1/2"	48" x 1/2"	17" x 1"	0.05	36	886	1662	1022	2051	1546	2369	1663	21.4	0.595
T7	12" x 3/4"	48" x 5/16"	20" x 1 1/4"	0.05	36	1750	1692	1256	2117	1TT5	2431	1844	23.6	0.436
T8	12" x 3/4"	48" x 1/2"	20" x 1 1/4"	0.05	36	2021	2128	1386	2600	2017	2985	2129	27.2	0.503
T9	14" x 1"	48" x 3/8"	14" x 1"	0.05	36	2358	2431	1807	2378	2484	2706	2432	31.1	0.317

1 in. = 25.4 mm

1 ksi = 6.8948 MPa

1 K-ff = 1.35582 kN-m

Notes: 1) M_w is the lateral flange bending moment computed from Equation 2.
2) M_y is computed as the expected yield stress multiplied by the section modulus to the top flange, assuming a uniform stress in the flange. However, yielding is expected to occur first at the flange tips due to lateral flange bending.
3) M_p is the plastic moment capacity for vertical bending only.

Table 2.4. Preliminary Bending Component Specimens B1 through B9

ID	Cross Sectional Dimensions						Girder Geometry and Geometric Properties								Material		M_u by various predictor equations				Section Capacities			
	Top Flange (Comp.)		Web		Bottom Flange (Tens)																			
	b_{cf} (in)	t_{cf} (in)	d_w (in)	t_w (in)	b_{tf} (in)	t_{tf} (in)	L (ft)	L/b_{cf}	R (ft)	D_c/D	L/R	$(2*D_c/t_w)*(F_{yf}/F_{yn})^{0.5}$	$(b_{cf}/t_{cf})*(F_{yf}/F_{yn})^{0.5}$	$A_{top\ flg}/A_{web}$	$F_{y\text{-}Nom}$ (ksi)	$F_{y\text{-}Expct}$ (ksi)	AASHTO (K-ft)	YOO (K-ft)	HANSHIN (K-ft)	FUKOMOTO (K-ft)	M_p ($F_{y\text{-}E}$) (K-ft)	M_y ($F_{y\text{-}E}$) (K-ft)	f_w/f_b	M_p ($F_{y\text{-}N}$) (K-ft)
Main Girders																								
G3	24	2 ¼	48	½	24	2 ¼	15.66	7.83	208.75	0.500	0.075	100.69	11.19	2.250	50	55	12053	12699	9025	11626	13758	12716	0.360	12507
G2	20	1 ¼	48	½	20	1 ¼	7.50	4.50	200.00	0.500	0.038	100.69	16.78	1.042	50	55	5129	6336	5612	6678	6963	6341	0.114	6330
G1	16	1	48	7/16	16	1	7.17	5.38	191.25	0.500	0.038	115.07	16.78	0.762	50	55	3326	4260	3671	4502	4749	4261	0.144	4317
Specimens: Bending Series																								
B1	16 ½	7/8	48	5/16	16 ½	7/8	15.66	11.39	208.75	0.500	0.075	161.10	19.78	0.963	50	55	1745	3661	2253	3032	4059	3708	0.587	3690
B2	17 ½	11/16	48	5/16	17 ½	11/16	15.66	10.74	208.75	0.500	0.075	161.10	26.70	0.802	50	55	1539	3134	1952	2678	3510	3182	0.573	3191
B3	11 13/16	5/8	48	5/16	11 13/16	5/8	15.66	15.90	208.75	0.500	0.075	161.10	19.82	0.492	50	55	756	1814	1072	1416	2471	2161	0.940	2246
B4	16 ½	7/8	48	3/8	18 ½	1 3/8	15.66	11.39	208.75	0.599	0.075	160.84	19.78	0.802	50	55	1833	3919	2389	3904	5116	4065	0.641	4651
B5	Same as B4; w/intermediate transverse stiffeners tight fit at tension flange.																							
B6	Same as B4; w/intermediate transverse stiffeners at 1.96D.																							
B7	Same as B4; no intermediate transverse stiffeners.																							
B8	16 ¾	1 1/16	48	5/8	20	1 ¼	15.66	11.22	208.75	0.551	0.075	91.45	17.03	0.593	36	42	3686	3964	2318	3788	4870	3967	0.654	4174
B9	16 ½	1 3/16	48	5/16	16 ½	1 3/16	15.66	11.39	208.75	0.500	0.075	161.10	14.57	1.306	50	55	4358	4792	2988	3943	5243	4838	0.561	4766

Notes: 1) Transverse stiffeners will be on the inside of girder web only.

2) Specimens B1 through B5 and B9 will have intermediate transverse stiffeners spaced at 0.98D.

3) Specimens B1 through B4, B6 and B9 will have the intermediate transverse stiffeners welded to the top and bottom flanges

4) Specimens B7 and B8 will have no intermediate transverse stiffeners.

5) Specimens will be inserted at the center of girder G3 and will be subject to a near constant vertical moment along their length.

6) Specimen length is approximately 27.4 feet.

7) Vertical loads will be applied to the bottom flange of each girder, approximately 26.8 feet (G1), 28.5 feet (G2), and 30.3 feet (G3) from each abutment.

8) M_y is computed as the expected yield stress multiplied by the section modulus to the top flange, assuming a uniform stress in the flange.

However, yielding is expected to occur first at the flange tips due to lateral flange bending. M_p is the plastic moment capacity for vertical bending only.

Specimens B4 through B8 were designed to be singly symmetric. To the knowledge of the authors, a singly symmetric horizontally curved I-girder specimen has never been tested prior to this research program. For the singly symmetric specimens, the tension flanges were proportioned to ensure that the effective web slenderness ratio based on the elastic depth of the web in compression D_c (for Specimens B4 through B7), or the depth of the web in compression at the plastic moment D_{cp} (for Specimen B8), was near the desired value. The ratio of D_c to the total web depth D was between 0.55 and 0.60 for these five specimens.

Each specimen was proportioned assuming the static yield stress of the steel to be 55 ksi (379 MPa). Because static loads are to be applied to the test frame in a controlled laboratory environment, all data must be correlated with the static yield stress. The static yield stress is determined by periodically imposing a zero-strain rate in a strain-controlled tension test until the load at a given strain has stabilized (*34*). The tensile specimen is loaded slightly beyond the elastic range and then the test is periodically stopped at three to five arbitrarily chosen strains or deflections. The static yield stress is then determined by drawing a line between the points where the load has stabilized (discounting any leakage). If the line deviates much from the horizontal, the static yield stress should be determined by the offset method or extension-under-load method. The static yield stress typically falls somewhere above the specified minimum yield stress and below the yield stress given in the mill report (which is determined based on tensile tests conducted at a specified ASTM strain rate). In order to provide a desired theoretical local buckling capacity for the compression flange and web based on the assumed 55-ksi (379 MPa) material equivalent to the capacity based on 50-ksi (345 MPa) material (at a stress level equal to the yield stress), adjustments to the slenderness ratios are necessary. To provide equivalent capacities, the actual slenderness ratios are multiplied by $\sqrt{F_{ys}/F_y}$ to yield the effective slenderness ratios, where F_{ys} is the expected static yield stress and F_y is the specified minimum yield stress. As a result, for a given thickness, slightly narrower flanges and shallower webs are necessary in order to provide equivalent local buckling capacities at the higher stress.

After initially proportioning the specimens based on an assumed static yield stress of 55 ksi (379 MPa), the plan was to then later make slight adjustments to the flange widths prior to fabrication based on the actual static yield stress of the material determined from tension tests conducted on the actual flange plate material. Actual measured flange-plate thicknesses would also be used in calculating the necessary adjustments. These adjustments would be made to ensure that the desired effective compression-flange slenderness ratios would be achieved. To assist the fabricator in ordering the plate material for the flanges, a table of maximum possible flange-plate widths for the component specimens was prepared assuming a lower bound value of 50 ksi (345 MPa) for the static yield stress and using a set of assumed actual flange-plate thicknesses. It was decided that similar adjustments to the specimen web depths would not be practical and would severely impact the fabrication schedule. To help ensure that the actual static yield strengths of the plate material for the flanges and webs of the component specimens would not deviate too greatly from the assumed value of 55 ksi (379 MPa), it was specified that this material be normalized. In addition, it was specified that this material be ordered to require plate tensile testing (i.e., one tension test to be conducted on specimens taken from each as-rolled or as-heat treated plate), as allowed in the supplementary requirements of AASHTO M270 (M270M).

A brief description of each of the Specimens B1 through B9 is given below. All transverse stiffeners are placed on the side of the web facing the inside of the curve and are welded to the top (compression) flange. Unless otherwise specified, the stiffeners are also welded to the bottom (tension) flange. It has been suggested by Mozer, Culver et al. (*7*, *10*, *11*) and Nakai et al. *(14*, *35*, *36)* that the configuration of the transverse stiffeners (both sides of the web versus one side of the web, welded versus tight fit versus cut back from the flanges) might affect the bending strength of horizontally curved I-girders. The transverse stiffeners are spaced at a distance approximately equal to the web depth D, unless otherwise noted. D is the maximum permitted transverse-stiffener spacing on horizontally curved girders according to the 1993 AASHTO Guide Specification and new Recommended Specifications for curved-girder bridges that were developed under NCHRP Project 12-38 *(37)* and adopted by AASHTO in 1999 to replace the 1993 Guide Specification.

Specimen B1: This doubly symmetric specimen has effective web and compression-flange slenderness ratios that are approximately at the upper limits specified for sections with non-compact compression flanges and webs fabricated from 50-ksi (345-MPa) steel in the Load Factor Design portion of the 1993 AASHTO Guide Specification. These limits are as follows:

Compression flange: $\frac{b}{t} = \frac{4{,}400}{\sqrt{F_y}} = \frac{4{,}400}{\sqrt{50{,}000}} = 19.7$ $\left(\frac{b}{t} = \frac{365}{\sqrt{F_y}} = \frac{365}{\sqrt{345}} = 19.7\right)$

Web: $\frac{D}{t_w} = \frac{36{,}500}{\sqrt{F_y}} = \frac{36{,}500}{\sqrt{50{,}000}} = 163.2$ $\left(\frac{D}{t_w} = \frac{3{,}030}{\sqrt{F_y}} = \frac{3{,}030}{\sqrt{345}} = 163.1\right)$

The reduction factor $[1-8.6(d_o/R)+34(d_o/R)^2]$, where d_o is the transverse stiffener spacing and R is the girder radius, that is applied to the above web-slenderness limit in the 1993 Guide Specification was ignored in the design of this specimen and all subsequent specimens. This factor was developed in the CURT studies and was intended to prevent fatigue problems from developing due to through-thickness bending stresses in the curved web. It is felt that these stresses should be controlled in some other fashion (e.g., by limiting bend buckling in the web at all limit states) rather than by instituting such a relatively severe limit on the web slenderness ratio. The NCHRP 12-38 Recommended Specifications for curved-girder bridges limit the web slenderness of transversely stiffened girders to 150 and limit the flexural stresses in the web at all limit states to the theoretical elastic web bend-buckling stress.

Specimen B2: This doubly symmetric specimen has the same effective web slenderness ratio as Specimen B1. The effective compression-flange slenderness ratio is approximately at the upper limit given in the First Edition of the AISC LRFD Specifications (*38*) for flanges of I-shaped sections under uniform compression fabricated from 50-ksi (345-MPa) steel to reach the yield stress prior to elastic local flange buckling. This limit can be written as follows:

Compression flange: $\frac{b}{t} = \frac{6{,}008}{\sqrt{F_y}} = \frac{6{,}008}{\sqrt{50{,}000}} = 26.9$ $\left(\frac{b}{t} = \frac{498.4}{\sqrt{F_y}} = \frac{498.4}{\sqrt{345}} = 26.8\right)$

Specimen B3: This doubly symmetric specimen has the same effective web and compression-flange slenderness ratios as Specimen B1. However, the flanges have been proportioned to provide an f_w/f_b ratio approximately equal to 1.0 (assuming f_w is computed according to Equation 2). The resulting L/b ratio of the specimen is approximately 16.0.

Specimen B4: This specimen has approximately the same effective web and compression-flange slenderness ratios as Specimen B1 but is singly symmetric.

Specimen B5: This singly symmetric specimen has the same proportions as Specimen B4, only the intermediate transverse stiffeners (not serving as cross-frame connection plates) are specified to be tight fit rather than welded at the tension flange.

Specimen B6: This singly symmetric specimen has the same proportions as Specimen B4, only the intermediate transverse stiffeners are spaced at approximately 2D rather than D.

Specimen B7: This singly symmetric specimen has the same proportions as Specimen B4, only with

no intermediate transverse stiffeners between the cross-frame connection plates.

Specimen B8: This singly symmetric specimen is proportioned to have an effective compression-flange slenderness ratio approximately at the upper limit specified for sections with compact compression flanges fabricated from 36-ksi (250-MPa) steel in the Load Factor Design portion of the 1993 AASHTO Guide Specification. The effective web slenderness ratio (based on the depth of the web in compression at the plastic moment D_{cp}) is approximately at the upper limit specified for compact sections in tangent girders fabricated from 36-ksi (250-MPa) steel in the Load Factor Design portion of the AASHTO Standard Specifications. These limits are as follows:

Compression flange: $\frac{b}{t} = \frac{3,200}{\sqrt{F_y}} = \frac{3,200}{\sqrt{36,000}} = 16.9 \quad \left(\frac{b}{t} = \frac{265.5}{\sqrt{F_y}} = \frac{265.5}{\sqrt{250}} = 16.8 \right)$

Web: $\frac{2D_{cp}}{t_w} = \frac{19,230}{\sqrt{F_y}} = \frac{19,230}{\sqrt{36,000}} = 101.4 \quad \left(\frac{2D_{cp}}{t_w} = \frac{1,597}{\sqrt{F_y}} = \frac{1,597}{\sqrt{250}} = 101.0 \right)$

In addition, there are no intermediate transverse stiffeners placed between the cross-frame connection plates.

Specimen B9: This doubly symmetric specimen has the same effective web slenderness ratio as Specimen B1. The effective compression-flange slenderness ratio is approximately at the upper limit specified for sections with compact compression flanges fabricated from 50-ksi (345-MPa) steel in the Load Factor Design portion of the 1993 AASHTO Guide Specification. This limit is as follows:

Compression flange: $\frac{b}{t} = \frac{3,200}{\sqrt{F_y}} = \frac{3,200}{\sqrt{50,000}} = 14.3 \quad \left(\frac{b}{t} = \frac{265.5}{\sqrt{F_y}} = \frac{265.5}{\sqrt{345}} = 14.3 \right)$

This specimen was placed last in the series because it was anticipated to have the largest bending capacity.

Specimen B9 was used in many of the earlier non-linear ABAQUS models of the test frame to perform some of the preliminary analytical investigations discussed previously. Specimen B9 was also incorporated in most of the ABAQUS analyses of the single-girder test set-up.

As the project progressed, however, budget and scheduling constraints again became a factor. Upon further review at this stage of the project, it was felt that the available time and budget would not support the analysis, fabrication and testing of nine bending component specimens in addition to all of the other future work that was planned. Therefore, the decision was made to pare the number of bending component specimens in this initial series down to six, which led to the development of the final set of bending component specimens that were initially tested (Table 2.5).

A brief description of each of the final Specimens B1 through B6 is given below. The arc length of each specimen is reduced to approximately 25.4 ft (7.7 m) to ensure that the bolted field splices used to insert each specimen into G3 would clear the cross-frame connection plates on G3 at cross-frame Lines 5L and 5R. The L/R ratio for each specimen is retained at 0.075 (note: this ratio is expressed as R/L = 13.333 in Table 2.5 so that the ratio would be more conveniently expressed as a number greater than 1.0). The L/b ratio of each specimen is approximately 11.0. The ratio of area of the top (compression) flange to the area of the web ranges from approximately 0.73 to 1.28. Again, all transverse stiffeners are placed on the side

Table 2.5. Final Bending Component Specimens B1 through B6

ID	Cross Sectional Dimensions						Girder Geometry and Geometric Properties								Material		M_u by various predictor equations				Section Capacities				
	Top Flange (Comp.)		Web		Bottom Flange (Tens)												AASHTO	YOO	HANSHIN	FUKOMOTO					
	b_{cf} (in)	t_{cf} (in)	d_w (in)	t_w (in)	b_{tf} (in)	t_{tf} (in)	L (ft)	L/b_{cf}	R (ft)	D_c/D	R/L	$(2*D_c/t_w)*(F_{yf}/F_{yn})^{0.5}$	$(b_{cf}/t_{cf})*(F_{yf}/F_{yn})^{0.5}$	$A_{top\ flg}/A_{web}$	$F_{y\text{-}Nom}$ (ksi)	$F_{y\text{-}Expct}$ (ksi)	(K-ft)	(K-ft)	(K-ft)	(K-ft)	M_p ($F_{y\text{-}E}$) (K-ft)	M_y ($F_{y\text{-}E}$) (K-ft)	f_w/f_b	M_p ($F_{y\text{-}N}$) (K-ft)	M_p ($F_{y\text{-}E}$) (K-ft)
Main Girders																									
G3	24	2 ¼	48	½	24	2 ¼	15.66	7.83	208.75	0.500	13.333	100.69	11.19	2.250	50	55	12053	12699	9025	11626	13758	12716	0.360	12507	
G2	20	1 3/16	48	½	20	1 3/16	7.50	4.50	200.00	0.500	26.667	99.37	17.43	0.990	70	75	6664	8273	7308	8682	9101	8274	0.114	8494	
G1	16	1 1/16	48	7/16	16	1 1/16	7.17	5.38	191.25	0.500	26.667	115.07	15.79	0.810	50	55	3504	4479	3862	4718	4977	4479	0.142	4978	
Specimens: Bending Series																									
B1	17 ½	¾	48	5/16	17 ½	¾	15.66	10.74	208.75	0.500	13.333	161.10	24.47	0.875	50	55	1661	3375	2110	2876	3758	3422	0.564	3416	3758
B2	17 ½	¾	48	38	17 ½	¾	15.66	10.74	208.75	0.500	13.333	134.25	24.47	0.729	50	55	1700	3525	2152	2992	3923	3528	0.581	3566	3923
B3	Same as B2 except no intermediate stiffeners.																								
B4	17 ½	¾	48	5/16	20	1 ¼	15.66	10.74	208.75	0.616	13.333	198.46	24.47	0.875	50	55	1719	3442	2207	3601	4596	3658	0.599	4178	4596
B5	16 7/16	15/16	48	5/16	16 7/16	15/16	15.66	11.43	208.75	0.500	13.333	161.10	18.39	1.027	50	55	1846	3875	2387	3200	4281	3921	0.583	3892	4281
B6	16 3/16	1 3/16	48	5/16	16 3/16	1 3/16	15.66	11.61	208.75	0.500	13.333	161.10	14.30	1.282	50	55	4266	4710	2913	3855	5159	4756	0.573	4690	5159

Notes: 1) Intermediate transverse stiffeners will be on the inside of girder web only and will be cut back 1" from the tension flange.

2) All specimens except B3 will have intermediate transverse stiffeners spaced at 0.98D.

3) Specimen B3 will have no intermediate transverse stiffeners.

4) Specimens will be inserted at the center of girder G3 and will be subject to a near constant vertical moment along their length.

5) Specimen length is approximately 25.4'.

6) Vertical loads will be applied to the bottom flange of each girder, approximately 26.8 feet (G1), 28.5 (G2), and 20.3 feet (G3) from each abutment.

7) M_y is computed as the expected yield stress multiplied by the section modulus to the top flange, assuming a uniform stress in the flange.

However, yielding is expected to occur first at the flange tips due to lateral flange bending. M_p is the plastic moment capacity for vertical bending only.

of the web facing the inside of the curve and are welded to the top (compression) flange. However, the decision was made to cut back all intermediate transverse stiffeners (not serving as cross frame connection plates) a distance of 1 in. (25 mm) from the bottom (tension) flange. This detail is often used in practice for economy and would represent a lower-bound case if it is eventually determined that the configuration of the transverse stiffeners does indeed have a significant effect on the bending capacity of curved I girders. However, since the stiffener configuration was felt to be of lesser significance, it was decided not to directly study its effect in this initial series of tests. The transverse stiffeners are again spaced at a distance approximately equal to the web depth D, unless otherwise noted.

Specimen B1 (Final): This doubly symmetric specimen has an effective web slenderness ratio that is approximately at the upper limit specified for sections with non-compact webs fabricated from 50-ksi (345-MPa) steel in the Load Factor Design portion of the 1993 AASHTO Guide Specification. This limit is as follows:

Web: $\frac{D}{t_w} = \frac{36{,}500}{\sqrt{F_y}} = \frac{36{,}500}{\sqrt{50{,}000}} = 163.2 \quad \left(\frac{D}{t_w} = \frac{3{,}030}{\sqrt{F_y}} = \frac{3{,}030}{\sqrt{345}} = 163.1 \right)$

The specified reduction factor to be applied to the web slenderness limit, $[1-8.6(d_o/R)+34(d_o/R)^2]$, is again ignored. The theoretical elastic web bend-buckling stress at the actual effective web slenderness is 36.2 ksi (249.6 MPa).

The effective compression-flange slenderness ratio is approximately at the limit of 26.9 given in the First Edition of the AISC LRFD Specifications for flanges of I-shaped sections fabricated from 50-ksi (345-MPa) steel under uniform compression to reach the yield stress prior to elastic local flange buckling (see the preceding Specimen B2 description) adjusted by the following reduction factor proposed by Yoo et al. (*39*) to account for the effects of curvature on the local-buckling capacity:

$$\varphi_{cv} = \left[1.05 - \frac{l_{br}^2}{4Rb_f} \right] = 0.85 \qquad (3)$$

where: l_{br} = cross frame spacing
R = girder radius
b_f = compression flange width

$$\left(\frac{b}{t}\right)_{cv} = \left(\frac{b}{t}\right)_{st} \sqrt{\varphi_{cv}} = 26.9\sqrt{0.85} = 24.8$$

It is noted that the maximum compression-flange slenderness permitted for non-compact flanges in the NCHRP 12-38 Recommended Specifications as of this writing is 23.0.

Specimen B2 (Final): This doubly symmetric specimen has the same effective compression-flange slenderness ratio as Specimen B1. The effective web slenderness ratio is reduced to 134.25. The theoretical elastic web bend-buckling stress at this effective web slenderness is 52.1 ksi (359.2 MPa), which is above the specified minimum yield stress. Therefore, web bend-buckling would be expected to occur earlier in Specimen B1.

Specimen B3 (Final): This doubly symmetric specimen has the same proportions as Specimen B2, only with no intermediate transverse stiffeners between the cross-frame connection plates. The resulting panel width between the cross-frame connection plates is approximately 3.9D. Therefore, the web in this region is considered to be unstiffened. The NCHRP 12-38 Recommended Specifications limit the slenderness of unstiffened webs to 100 when the minimum radius within the panel is less than 700 ft (213.4 m). The permitted slenderness increases linearly with increasing radius up to a maximum of 150 at a minimum radius of 2,000 ft (609.6 m), which is the maximum permitted slenderness for unstiffened webs in tangent girders. There have been no tests of unstiffened webs with web slenderness ratios greater than about 70 on curved girders prior to this research program.

Specimen B4 (Final): This singly symmetric specimen has the same effective compression-flange slenderness ratio as Specimens B1 and B2. The effective web slenderness ratio, based on the elastic depth of the web in compression D_c, is 198.46, which is representative of the web slenderness of a steel section in a composite girder subject to positive bending prior to the hardening of the concrete deck. The ratio of D_c to D is 0.616. The theoretical elastic web bend-buckling stress at this effective web slenderness is 23.9 ksi (164.8 MPa).

Specimen B5 (Final): This doubly symmetric specimen has the same effective web slenderness ratio as Specimen B1. The effective compression-flange slenderness ratio is approximately at the upper limit specified for compact sections in tangent girders fabricated from 50-ksi (345-MPa) steel in the Load Factor Design portion of the AASHTO Standard Specifications. This limit is as follows:

Compression flange: $\frac{b}{t} = \frac{4{,}110}{\sqrt{F_y}} = \frac{4{,}110}{\sqrt{50{,}000}} = 18.4 \quad \left(\frac{b}{t} = \frac{341}{\sqrt{F_y}} = \frac{341}{\sqrt{345}} = 18.4 \right)$

It is noted that the maximum compression-flange slenderness permitted for compact flanges in the NCHRP 12-38 Recommended Specifications as of this writing is 18.0.

Specimen B6 (Final): This doubly symmetric specimen has the same effective web slenderness ratio as Specimen B1. The effective compression-flange slenderness ratio is approximately at the upper limit specified for sections with compact compression flanges fabricated from 50-ksi (345-MPa) steel in the Load Factor Design portion of the 1993 AASHTO Guide Specification. This limit is as follows:

Compression flange: $\frac{b}{t} = \frac{3{,}200}{\sqrt{F_y}} = \frac{3{,}200}{\sqrt{50{,}000}} = 14.3 \quad \left(\frac{b}{t} = \frac{265.5}{\sqrt{F_y}} = \frac{265.5}{\sqrt{345}} = 14.3 \right)$

This specimen was placed last in the series because it was anticipated to have the largest bending capacity.

Figure 2.52 shows a plot of the effective web slenderness of each specimen versus the effective compression-flange slenderness. The figure also indicates the relationship of the effective slenderness ratios for each specimen to the respective web and compression-flange slenderness limits given in the 1993 Guide Specification (for F_y = 50 ksi (345 MPa) steel) and the NCHRP 12-38 Recommended Specifications (which are independent of F_y). As should be evident from this figure, an attempt was made in the design of these

specimens to vary the slenderness ratios in a rational manner.

Elevation views of each of the six component specimens are given in Figures 2.53 and 2.54. The table of maximum possible flange plate widths, discussed previously, is also shown in each figure. The derivation of the plate widths in this table is described in more detail in the previous section of this report on the G3 bolted flange splice design.

For the intermediate transverse stiffeners on the specimens (not serving as cross-frame connection plates), 7/16″ x 5″ (11 mm x 127 mm) plates were chosen. As described earlier, these plates had previously been designed to serve as intermediate transverse stiffeners on G1 and G2. These stiffeners were all specified to be fillet welded to the top flange and cut-back 1 in. (25 mm) from the bottom flange (refer to Section E-E and Detail 3 in Figure 2.55), except for the stiffeners adjacent to the bolted field splice at each end. In order to clear the flange splice plates, the end stiffeners were specified to be cut-back 3 in. (76 mm) from the top and bottom flange (refer to Section G-G and Detail 2 in Figure 2.55). To minimize the distortion of the flange and web plates during the fabrication of the specimens, ¼″ (6 mm) fillet welds were specified for the flange-to-web welds (refer to Section D-D in Figure 2.55) and all intermediate transverse stiffener welds. Less overall heat input is required to make these smaller welds resulting in less weld shrinkage and plate distortion. At the suggestion of the Lincoln Electric Co., it was specified that where ¼″ (6 mm) fillet welds were to be used, both pieces at the joint were to be preheated to 125° F (101.4° C) to ensure quality welds. In addition, the fabricator was required to submit a welding sequence and distortion control program for the component specimens for review prior to their fabrication.

For the cross-frame connection plates on the specimens, 5/8″ x 7″ (16 mm x 178 mm) plates were specified. These plates had previously been designed to serve as cross frame connection plates on G1. The plates were placed on one side of the web only (facing the inside of the curve). Multiplying the maximum predicted shear stress of 32.0 ksi (220.6 MPa) at the connection plate-to-flange joints at Lines 6L and 6R from the ABAQUS non-linear model of the test frame by the cross-sectional area of the connection plate resulted in a design force of 140 kips (622.7 kN). Complete joint penetration (CJP) welds were conservatively specified for the connection plate-to-flange welds on all six specimens to resist this force. 5/16″ (8 mm) fillet welds were specified for the connection plate-to-web welds (refer to Section B-B and Detail 1 in Figure 2.55).

After the tests of these six specimens were successfully completed, it was decided to revise and repair two of the specimens in order to perform two additional bending component tests. In both cases, the distortions in the web were repaired by carefully applying heat and the distorted top flanges were completely replaced. Brief descriptions of these two additional specimens are given below:

Specimen B7 (Final): This doubly symmetric specimen is Specimen B1 (Final) with a heat-repaired web and a new 5/8″ x 21″ (16 mm x 533 mm) top flange resulting in an effective compression-flange slenderness ratio of 35.2. The area of the replacement flange is the same as the area of the original ¾″ x 17-1/2″ (19 mm x 444.5 mm) top flange on Specimen B1.

Specimen B8 (Final): This singly symmetric specimen is Specimen B4 (Final) with a heat-repaired web and a new ¾″ x 17-1/2″ (19 mm x 444.5 mm) top flange (the same size top flange as was previously used on Specimen B4). In addition, a single longitudinal web stiffener is added on the outside of the web at a distance of 11-13/16″ (300 mm), or approximately $2D_c/5$, from the bottom of the top flange. A 5/8″ x 4″ (16 mm x 102 mm) plate is used for the longitudinal stiffener.

The proportions, geometric properties and predicted capacities of Specimens B7 and B8 are summarized in Table 2.6. It is emphasized that the geometric properties and predicted capacities of the eight specimens shown in Table 2.6 are based on nominal plate dimensions and on an assumed static yield stress of 55 ksi (379 MPa). Properties and predicted capacities of the specimens based on actual measured plate dimensions and average measured values of the static yield stress for the actual plate material are reported elsewhere in other project reports. Figure 2.56 graphically shows the relationship of Specimens B7 and B8 to the original six specimens.

Table 2.6. Final Bending Component Specimens B1 through B8

ID	Cross Sectional Dimensions						Girder Geometry and Geometric Properties								Material		M_u by various predictor equations				Section Capacities				
	Top Flange (Comp.)		Web		Bottom Flange (Tens)												AASHTO	YOO	HANSHIN	FUKOMOTO					
	b_{cf} (in)	t_{cf} (in)	d_w (in)	t_w (in)	b_{tf} (in)	t_{tf} (in)	L (ft)	L/b_{cf}	R (ft)	D_c/D	R/L	$(2*D_c/t_w)*(F_{yf}/F_{yn})^{0.5}$	$(b_{cf}/t_{cf})*(F_{yf}/F_{yn})^{0.5}$	$A_{top\ flg}/A_{web}$	$F_{y\text{-}Nom}$ (ksi)	$F_{y\text{-}Expct}$ (ksi)	(K-ft)	(K-ft)	(K-ft)	(K-ft)	M_p ($F_{y\text{-}E}$) (K-ft)	M_y ($F_{y\text{-}E}$) (K-ft)	f_w/f_b	M_p ($F_{y\text{-}N}$) (K-ft)	M_p ($F_{y\text{-}E}$) (K-ft)
Main Girders																									
G3	24	2 ¼	48	½	24	2 ¼	15.66	7.83	208.75	0.500	13.333	100.69	11.19	2.250	50	55	12053	12699	9025	11626	13758	12716	0.360	12507	
G2	20	1 3/16	48	½	20	1 3/16	7.50	4.50	200.00	0.500	26.667	99.37	17.43	0.990	70	75	6664	8273	7308	8682	9101	8274	0.114	8494	
G1	16	1 1/16	48	7/16	16	1 1/16	7.17	5.38	191.25	0.500	26.667	115.07	15.79	0.810	50	55	3504	4479	3862	4718	4977	4479	0.142	4978	
Specimens: Bending Series																									
B1	17 ½	¾	48	5/16	17 ½	¾	15.66	10.74	208.75	0.500	13.333	161.10	24.47	0.875	50	55	1661	3375	2110	2876	3758	3422	0.564	3416	3758
B2	17 ½	¾	48	3/8	17 ½	¾	15.66	10.74	208.75	0.500	13.333	134.25	24.47	0.729	50	55	1700	3525	2152	2992	3923	3528	0.581	3566	3923
B3	Same as B2 except no intermediate stiffeners.																								
B4	17 ½	¾	48	5/16	20	1 ¼	15.66	10.74	208.75	0.616	13.333	198.46	24.47	0.875	50	55	1719	3442	2207	3601	4596	3658	0.599	4178	4596
B5	16 7/16	15/16	48	5/16	16 7/16	15/16	15.66	11.43	208.75	0.500	13.333	161.10	18.39	1.027	50	55	1846	3875	2387	3200	4281	3921	0.583	3892	4281
B6	16 3/16	1 3/16	48	5/16	16 3/16	1 3/16	15.66	11.61	208.75	0.500	13.333	161.10	14.30	1.282	50	55	4266	4710	2913	3855	5159	4756	0.573	4690	5159
B7	21	5/8	48	5/16	17 ½	¾	15.66	8.95	208.75	0.500	13.333	161.10	35.24	0.875	50	55	1819	3334	2250	3037	3754	3427	0.471		
B8	17 ½	1 3/16	48	5/16	16 3/16	1 ¼	15.66	10.74	208.75	0.616	13.333	161.10	24.47	0.875	50	55	1719	3442	2207	3601	4596	3658	0.599		

Notes: 1) All notes in Table 2.5 apply.

2) Specimen B8 has a single 5/8" x 4" longitudinal stiffener on the outside of the web at a vertical distance of 11-13/16" (2Dc/5) from the bottom of the top flange.

Predicted Capacities: The bending strength of a horizontally curved I girder is dependent on several factors. A curved girder begins to twist and deflect laterally with the initial application of a vertical load. Resistance to the lateral deflection results in the development of lateral flange bending moments. Amplification of the lateral deflections of the girder away from the center of curvature causes additional lateral bending. As the lateral deflection of the compression flange increases, the lateral flange bending continues to increase until a failure of the compression flange occurs either by local buckling or yielding (or a combination of both). If the girder is nearly straight and the web is slender, the girder may fail in bend-buckling. However, it is common for the curved girder to fail by lateral buckling of the compression flange before any significant plastification of the web occurs. Complicating the issue further is the fact that the cross-section of a curved girder typically deforms when subjected to bending and torsion. Bowing of the web has been shown to cause a decrease in the stiffness of the girder compared to the stiffness computed using strength of materials assumptions. This decrease in stiffness may lead to shedding of load from the web to the compression flange. The flanges of a curved I-girder also can rake with respect to the web because the web is generally not stiff enough to retain the shape of the cross-section when the flanges are subjected to lateral bending. The flanges rotate and are no longer parallel to each other and the web takes an S-shape and is no longer perpendicular to the flanges. When the raking effect becomes significant is not presently known. Both of these effects reduce the overall torsional stiffness further from that computed from strength of materials assumptions.

Clearly, the capacity of at least some curved girders is not as closely related to the vertical bending capacity of a curved girder as it is to the lateral bending strength of the compression flange. The lateral bending capacity is a function of both the vertical bending stress and the lateral bending moment. The lateral bending moment is a function of the strength of materials bimoment and the additional lateral moment due to the amplification of the first-order lateral moment caused by the second-order distortion of the cross section. Hence, the strength of a curved girder is related to the lateral moment capacity of the compression flange, but the magnitude of the lateral moment is related to many factors including the strength and stiffness of the web.

Several different predictor equations have been developed to estimate the bending capacity of a curved I-girder, while in some instances trying to directly account for the effects of some of these complex phenomena. Some of the equations are theoretical in nature while other equations are semi-empirical and theoretical. Tables 2.3 through 2.6 list predicted capacities of the bending component specimens according to some of these predictor equations. The predicted capacities in Tables 2.4 through 2.6 are computed using the expected or assumed value of the static yield stress. A computer program, CKMU2, was developed to compute the predicted capacities based on these equations. The following describes each of the equations in more detail.

AASHTO: The equations in the 1993 AASHTO Guide Specification and the NCHRP 12-38 Recommended Specifications are based on the work of McManus (*40*). In Load Factor Design, separate equations are given for sections with compact flanges and for sections with non-compact flanges. Compact flanges are partially braced compression flanges that are permitted to achieve full plastification under combined vertical and lateral bending prior to failure. In fact, most sections fail by plastification of the compression flange with little yielding occurring in the web. Non-compact flanges are partially braced compression flanges that are assumed to reach the yield stress at the flange tip prior to local buckling. According to the research, the webs of the so-called compact sections (or sections with compact flanges) need not be subject to compactness requirements. Compact sections that are subjected to plastification are limited to plastification of the compression flange. The strength of these sections in vertical bending is limited to first yield to ensure that the web is not subjected to yielding. Compact flanges are limited to steels having a specified minimum yield stress not exceeding 50 ksi (345 MPa) since the original research that led to the development of the empirical strength equation for compact flanges was limited to these steels.

In the 1993 Guide Specification, compact flanges are limited to a slenderness b/t of

$3{,}200/\sqrt{F_y}$ with F_y taken in psi ($265.5/\sqrt{F_y}$ with F_y taken in MPa). In the NCHRP 12-38 Recommended Specifications, b/t for compact flanges is currently limited to 18 (the limit is independent of F_y). The critical vertical flange bending stress for a compact compression flange is computed as follows:

$$F_{cr} = F_{bs}\bar{\rho}_B\bar{\rho}_w \tag{4}$$

where:

$F_{bs} = F_y\left(1-3\lambda^2\right)$

$\lambda = \frac{1}{\pi}\left(\frac{l}{0.9b}\right)\sqrt{\frac{F_y}{E}}$

$$\bar{\rho}_B = \frac{1}{1+\frac{l}{b}\left(1+\frac{l}{6b}\right)\left(\frac{l}{R}-0.01\right)^2}$$

$$\bar{\rho}_w = 0.95+18\left[0.1-\frac{l}{R}\right]^2+\frac{\frac{f_w}{f_b}\left[0.3-0.1\frac{l}{R}\frac{l}{b}\right]}{\bar{\rho}_B\left(F_{bs}/F_y\right)}$$

b = compression-flange width
l = arc length between compression-flange brace points
R = girder radius.
(f_w/f_b)= ratio of the lateral flange bending stress to the vertical bending stress (positive when the lateral flange moment is a restoring force)

The critical stress is limited to the yield stress by limiting the product of $\bar{\rho}_B$ and $\bar{\rho}_w$ to 1.0. The product can actually be as large as 1.13 when the lateral flange bending stress is zero. This apparent excess capacity beyond the yield stress is directly related to the shape factor (or ratio of M_p to M_y) for a doubly symmetric I-section. However, for the reason stated above, the critical vertical bending stress is limited to the yield stress in the specifications.

The strength of materials assumption of a rigid cross section is not made in the AASHTO provisions. The development of these equations considered a State 2, which is the name given to a condition resulting from amplification of the lateral deflection of the compression flange due to arch action. State 1 is defined as a distorted state based on strength of materials assumptions as determined by Dabrowski (*41*). However, the State 1 computations were made for a doubly symmetric section. State 2 does not require a doubly symmetric section since the arching is applied only to the compression flange.

At the time the CURT work was done, the AASHTO LFD Specification had a requirement to reduce the width of the compression flanges of singly symmetric sections by 10 percent (*42*). The reason that this assumption was made is that the compressive strength of a partially braced girder was assumed to be a function of the compression flange and a portion of the web. This assumption tacitly assumes that the girder cross section is not maintained. (It should be noted that for certain sections, the AASHTO specifications for tangent girders include an equation to determine the strength of

partially braced I-girders that is based on the strength of materials assumption that the cross-section does not deform). Thus, the flange width b used in the computation of the term λ (given above) was taken as 0.9b for singly symmetric sections in the development of program CKMU2 (note: this use of 0.9b was also reinstated in the NCHRP 12-38 Recommended Specifications). The term λ is used in the computation of the lateral buckling stress F_{bs}. F_{bs} is the lateral buckling equation for tangent-girder compression flanges that existed in the Load Factor portion of the Standard Specifications at the time the Guide Specification was originally developed. Although the use of 0.9b in this equation was prescribed in the Standard Specifications for singly-symmetric sections, the use of this reduced width was not prescribed in the original Guide Specification. This lateral buckling equation has since been replaced in the Standard Specifications but was retained in the 1993 Guide Specification.

In the 1993 Guide Specification, the flange tip stress is not limited for compact compression flanges. Thus, if a compact compression flange is subject to an average stress equal to the yield stress, there is theoretically no capacity remaining in the flange to resist the lateral bending. In the NCHRP 12-38 Recommended Specifications, the critical vertical bending stress for a compact flange is also limited to F_y minus 1/3 of the lateral flange bending stress. The factor of 1/3 is derived from the plastic capacity of the flange under combined vertical and lateral bending (*43*, *44*). A small portion of the web is permitted to yield. Yielding of the web is theoretically precluded if a factor of ½ is used instead of 1/3. Tip stresses are not considered, however, in computing the predicted capacities of the specimens with compact flanges in Tables 2.3 through 2.6. It should be noted that the lateral bending stresses, used to compute the f_w/f_b ratios shown in the tables, are first-order elastic stresses at the brace points. Failure of most curved I girders occurs at mid-span between brace points. Under large vertical bending moments, the lateral bending stresses are actually higher at midpoint than at the brace points because of the arching effect, which causes additional lateral bending as discussed above.

Since the AASHTO equations actually deal with the compression flange, the tension flange must be treated separately. The critical vertical bending stress for a partially braced tension flange on a section with a compact compression flange is specified to be F_y in the 1993 Guide Specification. Again, by limiting only the average normal tension stress to F_y, regardless of the magnitude of the lateral bending stress, there may be insufficient capacity remaining for the tension flange to resist lateral bending without yielding of the web. Since there are no provisions covering yielding of the web, the section may be considered overstressed in such cases. In the original research, it was assumed that the vertical bending stress in a partially braced tension flange should be conservatively limited to F_y times the product of the ρ factors since only doubly symmetric sections were studied. Therefore, in the NCHRP 12-38 Recommended Specifications, the ρ factors were reinstated in determining the critical vertical bending stress for partially braced tension flanges. The $\overline{\rho}$ factors specified for compact flanges are used. The flange tip stress is also limited to F_y minus 1/3 times the lateral flange bending stress in the Recommended Specifications; the same as for compact compression flanges.

In the 1993 Guide Specification, non-compact flanges are limited to a slenderness b/t of $4{,}400/\sqrt{F_y}$ with F_y taken in psi ($365/\sqrt{F_y}$ with F_y taken in MPa). In the NCHRP 12-38 Recommended Specifications, b/t for non-compact flanges is currently limited to $1.02\sqrt{E/(f_b + f_w)} \le 23$. The critical vertical flange bending stress for a non-compact compression flange is computed as follows:

$$F_{cr} = F_{bs}\rho_B\rho_w \tag{5}$$

where:

F_{bs} = $F_y\left(1-3\lambda^2\right)$

λ = $\frac{1}{\pi}\left(\frac{l}{0.9b}\right)\sqrt{\frac{F_y}{E}}$

ρ_B = $\frac{1}{1+\left(\frac{l}{R}\right)\left(\frac{l}{b}\right)}$

ρ_w = if (f_w/f_b) is positive, the smaller of:

$$\rho_{w1} = \frac{1}{1-\left(\frac{f_w}{f_b}\right)\left(1-\frac{\frac{l}{b}}{75}\right)}$$

$$\rho_{w2} = \frac{0.95+\frac{\frac{l}{b}}{\left(30+8000\left(0.1-\frac{l}{R}\right)^2\right)}}{1+0.6\left(\frac{f_w}{f_b}\right)}$$

If (f_w/f_b) is negative, use ρ_{w1}.

The ρ_B factor reflects the effects of vertical bending stress and curvature and the ρ_w factor reflects the effects of the lateral flange bending stress and curvature. The research leading to the development of the ρ factors was based on the study of sections that were doubly symmetric. For both compact and non-compact flanges, the ρ factors are applicable only within the limits of the parameters l/b ($\leq$ 25), l/R ($\leq$ 0.1) and f_w/f_b ($\leq$ 0.5) because these limits were imposed on the empirical study used in the development of the equations. f_b is defined as the largest vertical bending stress at either brace point and f_w is the total lateral flange bending stress at the critical brace point. Only stresses at brace points are considered since the stress condition midway between brace points was implicitly considered in the original derivation of the equations. Changes in flange size between brace points were not considered in the development of the equations. The NCHRP 12-38 Recommended Specifications further clarify that the f_w/f_b ratio need only be checked at locations where f_b exceeds the greater of $0.33F_y$ or 17 ksi (117.2 MPa); that is, at sections where strength may be critical. The empirical basis of these equations requires that the straight girder capacity be used with the rho factors.

For non-compact compression flanges, the flange tip stresses, $f_b + f_w$, are also limited to F_y in both the 1993 Guide Specification and the NCHRP 12-38 Recommended Specifications. When Equation 2 is used to compute M_w, the relationship between f_b and f_w can be expressed as follows:

$$f_w = f_b\left[\frac{3Sl^2}{5Rhtb^2}\right] \quad (6)$$

where:

S = section modulus about the strong axis of the section
l = arc length between compression-flange brace points
R = girder radius
h = vertical distance between flange centerlines
t = compression-flange thickness
b = compression-flange width

Therefore, a second critical vertical bending stress for non-compact compression flanges can be computed as follows based on limiting the flange tip stresses to F_y:

$$F_{cr} = \frac{F_y}{\left[1+\frac{3Sl^2}{5Rhtb^2}\right]} \quad (7)$$

The lower of the values from Equation 5 and Equation 7 governs. Tip stresses are also limited to F_y in a partially braced tension flange on a section with a non-compact compression flange in the 1993 Guide Specification.

The predicted moment capacities in Tables 2.3 through 2.6 under the ″AASHTO″ column are computed as the critical vertical bending stress from either Equation 4 or the lesser of Equations 5 and 7, as applicable, times the section modulus with respect to the compression flange. The capacities of Specimens T3, T4, T7, T8 and T9 in Table 2.3, Specimens B8 and B9 in Table 2.4, and Specimen B6 in Tables 2.5 and 2.6 are computed using Equation 4. The capacity of G3 in Tables 2.4 through 2.6 is also computed using Equation 4. All other capacities are computed using Equations 5 and 7. In several cases, the equations are extrapolated slightly since they do not apply to cases where the f_w/f_b ratio exceeds 0.5 and/or the b/t of the compression flange exceeds 23 according to the current specifications.

<u>*Yoo*</u>: Yoo et al. (*45*) proposed a formula to predict the vertical bending capacity of a horizontally curved I girder as the lateral-torsional buckling capacity of a tangent girder reduced by an empirical factor, which is a function of the central angle. The reduction factor is a regression equation based on the results of a number of finite-element analyses. The capacity is computed as follows:

$$M_u = F_{by}S_{cf} \quad (8)$$

in which: $F_{by} = YF_{bs}$ (9)

where:

S_{cf} = section modulus with respect to the compression flange
F_{bs} = lateral-torsional buckling stress for a tangent girder from Article 10.48.4.1 of the AASHTO Standard Specifications

Y = $\left(1.0-\gamma X^{\beta}\right)^{\alpha}$
γ = 0.1058

β = 2.129
α = 2.152
X = central angle = *l*/R

Hanshin: The Hanshin Guidelines (*6*) proposed the following interaction relationship relating the vertical and lateral flange bending stresses. Since the provisions of the Hanshin Guidelines are in a working stress design format, the factors of safety have been removed in the following for better comparison with the strength predictor equations of Fukomoto (*46*) and the AASHTO Guide Specifications.

$$\frac{f_b}{F_b} + \frac{f_w}{F_y} \le 1.0 \tag{10}$$

where: f_b = vertical bending stress
f_w = lateral flange bending stress (computed from Equation 2-2)
F_b = allowable vertical bending stress = $F_y \Psi$

$$\Psi = \{1.0 \ \ if \ \ \phi < 0.02\alpha_s\}$$
$$= \left\{1.0 - 1.05\sqrt{\alpha_c}\left(\phi + 4.52\phi^2\right) \ \ if \ \ 0.02\alpha_s \le \phi \le 0.2\right\}$$

ϕ = central angle = *l*/R
l = arc length between compression-flange brace points
R = girder radius

$$\alpha_s = \frac{2}{\pi}\sqrt{3 + \frac{A_w}{2A_c}}\left(\frac{l}{b}\right)\sqrt{\frac{F_y}{E}}$$

b = compression-flange width
A_w = web area = Dt_w
D = web depth
t_w = web thickness
A_c = compression-flange area
α_c = $\gamma\alpha_s$

$$\gamma = \{1.0 \ \ if \ \ \phi < 0.02\alpha_s\}$$
$$= \left\{1.0 - 1.97\phi^{1/3} + 4.25\phi - 26.3\phi^3 \ \ if \ \ 0.02\alpha_s \le \phi \le 0.2\right\}$$

The vertical bending capacity is computed by solving for f_b from Equation 10 and multiplying the result by the section modulus with respect to the compression flange. The Hanshin Guidelines limit the b/t of the compression flange to $4{,}700/\sqrt{F_y}$ with F_y taken in psi ($390/\sqrt{F_y}$ with F_y taken in MPa). Therefore, Equation 10 is extrapolated to cases where the b/t of the specimen exceeds this limit.

Fukomoto: Fukomoto and Nishida (46) developed a quartic equation to predict the vertical bending capacity of a doubly symmetric curved I-beam that must be solved using an iterative process. The predictor equation is unique in that it is not related to the existing lateral-torsional buckling equation for a tangent girder. The equation is as follows:

$$\lambda^4\delta^4 - \left(\left[1 + \frac{P_e(d - t_{cf})}{2M_p}\left(\frac{l^2}{2Rb_{cf}}\right)\right]\lambda^4 + 1\right)\delta^2 - \left(\frac{l^2}{2Rb_{cf}}\right)\delta + 1 = 0 \tag{11}$$

where:

d = depth of the girder
t_{cf} = compression-flange thickness
b_{cf} = compression-flange width
l = arc length between compression-flange brace points
R = girder radius

$$\lambda = \sqrt{M_p / M_e}$$

M_p = plastic moment capacity of the section

$$M_e = \sqrt{\left(\frac{\pi^2 EI_y}{l^2}\right)\left(GJ + \frac{\pi^2 EC_w}{l^2}\right)}$$

I_y = weak-axis moment of inertia of the section
G = shear modulus
C_w = warping constant = $I_y h^2 / 4$
h = distance between flange centerlines
J = St. Venant torsional constant = $\frac{Dt_w^3 + \sum bt^3}{3}$
D = web depth
t_w = web thickness
b = flange width
t = flange thickness

$$P_e = \frac{\pi^2 EI_y}{l^2}$$

$$\delta = M_u / M_p$$

The quartic equation is solved for the quantity δ using an iterative procedure (the CKMU2 program uses the Newton-Raphson approximation). The vertical bending capacity is then computed as δ times the plastic moment capacity M_p.

Nakai: Nakai et al. (47) proposed the following equation for the vertical bending capacity of a horizontally curved I girder:

$$M_u = \left[1.92 + 0.357\frac{l^2}{Rb_{cf}}\right]M_a \qquad (12)$$

where:

l = arc length between compression-flange brace points
R = girder radius
b_{cf} = compression-flange width
M_a = minimum of M_{af} and M_{aw}
M_{af} = bending capacity of the flange = $F_{af}S$
S = section modulus of the entire section about the strong axis

$$F_{af} = \left\{F_u / 1.7 \;\; if \;\; l/b_{cf} \le c\right\}$$
$$= \left\{F_u \Big/ 1.7 - a\left(\frac{l}{b} - c\right) \;\; if \; c < l/b_{cf} \le c_o\right\}$$

$$F_u = \{F_y \quad if \quad \alpha < 0.2\}$$
$$= \{F_y[1.0 - 0.412\alpha] \quad if \quad 0.2 \le \alpha < \sqrt{2}\}$$
$$= \{F_y / \alpha^2 \quad if \quad \alpha \ge \sqrt{2}\}$$

a = 0.34 + 0.019(F_y – 33.7 ksi)

c; c_o = constants specified for different Japanese steel grades (for 50-ksi steel, use c = 4.0; c_o = 30)

$$\alpha = \frac{2}{\pi}\sqrt{3 + \frac{A_w}{2A_c}}\left(\frac{l}{b_{cf}}\right)\sqrt{\frac{F_y}{E}}$$

A_w = web area = Dt_w

A_c = compression-flange area

M_{aw} = bending capacity of the web = $\frac{F_{awr} I_x}{(D/2)}$

$F_{aw} = F_y/1.7$

I_x = moment of inertia of the entire section about the strong axis

D = web depth

t_w = web thickness

Nishida: Nishida et al. (*48*) applied large-deflection theory to derive the following approximate critical elastic moment for a curved I-beam subject to two equal end moments:

$$M_{cr} = \sqrt{\left(1 - \frac{l}{\pi^2 R^2}\right)\left(\frac{\pi^2 EI_y}{l^2}\right)\left(GJ + \frac{\pi^2 EC_w}{l^2}\right)} \qquad (13)$$

where:

l = arc length between compression-flange brace points

R = girder radius

I_y = weak-axis moment of inertia of the section

G = shear modulus

C_w = warping constant = $I_y h^2/4$

h = distance between flange centerlines

J = St. Venant torsional constant = $\frac{Dt_w^3 + \sum bt^3}{3}$

D = web depth

t_w = web thickness

b = flange width

t = flange thickness

In this formulation, M_{cr} approaches the elastic critical buckling moment for a tangent girder as the radius R approaches infinity.

An investigation was conducted to determine the effect of the central angle, *l*/R, on the results from the above predictor equations. The study was conducted using the initial set of specimens – Specimens T1 through T9 (Table 2.3). The Nishida equation (Equation 13), which represents an elastic buckling solution only, was not included in this investigation. The results from this equation were also not included with the predicted capacities of the specimens given in Tables 2.3 through 2.6.

The central angle can be varied by either holding *l* constant and varying R, or by holding R constant

and varying *l*. Therefore, the effect of each of these cases on the results from the predictor equations was examined. Figure 2.57 shows plots of the results for Specimen T3 (doubly symmetric specimen) with R varied and *l* held constant. The ordinate of the plots is the ratio of the predicted vertical bending capacity, M_u, to the plastic moment capacity, M_p, and the abscissa is *l*/R. Similar plots for Specimen T7 (singly symmetric specimen) are shown in Figure 2.58. Note that the results from the Nakai equation (Equation 12) increase with increasing *l*/R when R is varied. Because of this unusual behavior, the results from the Nakai equation were not included with the predicted capacities of the specimens given in Tables 2.4 through 2.6. The results from the Yoo formulation (Equations 8 and 9) are relatively unaffected by *l*/R when R is varied. Figures 2.59 and 2.60 show the results for Specimens T3 and T7, respectively, with *l* varied and R held constant. In this case, the results from each of the equations are somewhat closer and follow a similar pattern with increasing *l*/R.

Estimated Design Quantities

The final estimated design quantities for the test frame and its components, the component specimens and the loading fixtures are summarized below. All steel is Grade 50 (Grade 345) steel unless otherwise noted. (Note: 1 lb = 4.4482 N; 1 ksi = 6.8948 MPa).

Test Frame:	Girder 1 (G1):	Flanges and web	16,107	lbs
		Connection plates	774	lbs
		Loading fixture stiffeners	238	lbs
		Intermediate transverse stiffeners	357	lbs
		Bearing stiffeners	286	lbs
		Total	17,762	lbs
	Girder 2 (G2):	Flanges and web (Grade 70W)	21,897	lbs
		Connection plates	2,586	lbs
		Loading fixture stiffeners	398	lbs
		Intermediate transverse stiffeners	357	lbs
		Bearing stiffeners	490	lbs
		Total (Grade 70W steel)	21,897	lbs
		(Grade 50 steel)	3,831	lbs
			25,728	lbs
	Girder 3 (G3):	Flanges and web	42,198	lbs
		Connection plates	1,293	lbs
		Loading fixture stiffeners	398	lbs
		Intermediate transverse stiffeners	714	lbs
		Bearing stiffeners	1,469	lbs
		Total	46,072	lbs
		Center section of G3	11,400	lbs
	Cross Frames: (26 Total)	Pipe (ASTM A513 Type 5 DOM)	4,498	lbs
		Gusset plates and end plates	22,542	lbs
		Total (1,040 lbs/cross frame)	27,040	lbs
	Lateral Bracing:	Structural tees	1,337	lbs
	Splice Plates:	Top outside plate	210	lbs
		Top inside plates	287	lbs
		Bottom inside plates	472	lbs
		Bottom outside plate	357	lbs
		Total (per set)	1,326	lbs
		(4 sets)	5,304	lbs

	Tangential Support Frame:	Wide-flange sections	440	lbs
		Base plate	2,272	lbs
		Connection plates	28	lbs
		Total	2,740	lbs
Component Specimens:	Specimen B1:	Flanges and web	3,663	lbs
		Connection plates	119	lbs
		Intermediate transverse stiffeners	149	lbs
		Total	3,931	lbs
	Specimen B2:	Flanges and web	3,929	lbs
		Connection plates	119	lbs
		Intermediate transverse stiffeners	149	lbs
		Total	4,197	lbs
	Specimen B3:	Flanges and web	3,929	lbs
		Connection plates	119	lbs
		Total	4,048	lbs
	Specimen B4:	Flanges and web	4,718	lbs
		Connection plates	119	lbs
		Intermediate transverse stiffeners	149	lbs
		Total	4,986	lbs
	Specimen B5:	Flanges and web	4,069	lbs
		Connection plates	119	lbs
		Intermediate transverse stiffeners	149	lbs
		Total	4,337	lbs
	Specimen B6:	Flanges and web	4,746	lbs
		Connection plates	119	lbs
		Intermediate transverse stiffeners	149	lbs
		Total	5,014	lbs
	Specimen B7:	Flanges and web	3,663	lbs
		Connection plates	119	lbs
		Intermediate transverse stiffeners	149	lbs
		Total	3,931	lbs
	Specimen B8:	Flanges and web	4,718	lbs
		Connection plates	119	lbs
		Intermediate transverse stiffeners	149	lbs
		Longitudinal stiffener	222	lbs
		Total	5,208	lbs
		Total (8 specimens)	35,652	lbs
Loading Fixtures:		MC12 cross beams	720	lbs
		MC12 end beams	1,440	lbs
		C10 lateral braces	184	lbs
		Details	46	lbs
		Total (per fixture)	2,390	lbs
		(6 fixtures)	14,340	lbs

SUMMARY

This report has reviewed in detail the philosophy and design of the I-girder bending component tests for the FHWA Curved Steel Bridge Research Project. The evolution of a test configuration that would allow the tests to be conducted in a safe and efficient manner and still provide meaningful results was accomplished over a significant period of time in several interrelated stages. Coordination was required amongst several parties in order to perform the numerous iterations that were required at each stage to arrive at the successful tests.

The project employed the full capabilities of the laboratory, modern analytical techniques and instrumentation. The cost of the project and its inherent safety risks required careful planning, design and execution of the plan. The tests are historic in that they are the first tests known to the researchers that tested components to failure as part of a structure that remained elastic and was reusable. The total benefit of the plan will not be realized until the frame is employed to test moment-shear specimens followed by testing of the frame with a composite concrete deck. The original plan to examine skewed supports would be another application that would yield worthwhile information.

The use of a full-size three-girder bridge as a test frame to test multiple components is a unique concept. The complexities introduced by horizontal curvature only added to the challenge. To address the many unknowns in such an ambitious test program, careful integration of analysis was required throughout the entire design process. The extent of the analyses that were employed in the design of this test was unprecedented to ensure that such an endeavor could be safely carried out for the first time, while at the same time providing the desired results without any premature failures of any test-frame components. As detailed above, several different concepts and schemes were given serious consideration for the design of nearly every component of this test, including the overall scheme used to conduct the tests. Although not every investigation necessarily led to visible results, each step along the way still made a worthwhile contribution to the overall knowledge that eventually led to the successful development of the final design concept.

The FHWA Structures Laboratory at the Turner-Fairbank Highway Research Center, with its large test floor, provided the opportunity to construct a full-size horizontally curved structure that could be loaded under controlled conditions. Using a full-size curved bridge as a test frame ensures for the first time that realistic boundary conditions are provided for the component specimen testing. Further, parts of the bridge can later be re-used for testing of the bridge as a full-size composite curved-bridge structure. The testing of this full-size simple-span three-girder structure, with its over 4-ft (1.2-m) deep girders and a total weight of nearly 60 tons (54.4 tonnes), represents one of the single largest civil-engineering related structural laboratory tests ever undertaken. As such, the design of this historically significant test provided an exceptional challenge that makes for an interesting story unto itself.

ACKNOWLEDGMENTS

The detailed design of the test frame, component specimens and load fixtures was coordinated and conducted by the Pittsburgh, PA office of HDR Engineering, Inc. The Project Engineer for the design was John M. Yadlosky, P.E. of the Pittsburgh, PA office of HDR. The principal design engineers for HDR were Domenic A. Coletti, P.E. (currently with the Raleigh, NC office of HDR) and James D. Carnahan, P.E of the Pittsburgh, PA office of HDR. The ABAQUS analyses of the three-girder test frame and the single-girder test were performed by Mr. James D. Burrell under the direction of Professor Abdul H. Zureick of the Georgia Institute of Technology. The BSDI 3D System analyses were performed by A. Richard Lawin of Bridge Software Development International, Ltd. in Coopersburg, PA. The MSC/NASTRAN analyses were performed by Dr. Jim Davidson (currently at Auburn University) under the direction of the late Professor Chai H. Yoo of Auburn University. Drafting services were provided by Kevin A. Stiffey, June E. Marcum and Steven W. Magill of the Pittsburgh office of HDR. The Contractor's Office Technical Representative (COTR) for the FHWA was Ms. Sheila R. Duwadi. The counsel of Dr.Arthur W. Hedgren, P.E. of HDR, William N. Poellet, P.E. of HDR, Deane M. Smith of HDR, Duane K. Miller, P.E. of the Lincoln Electric Company, Cleveland, OH, Lloyd R. Cayes (formerly with the FHWA), William J. Wright, P.E. (formerly with the FHWA), Richard D. Geyer, former President of the Williams Bridge Company, Manassas, VA, Richard Johnson, formerly with the Williams Bridge Company, Richmond, VA, and the various members of the FHWA Research Council on Curved Bridges (RCCB) was also very much appreciated.

REFERENCES

1. Consortium of University Research Teams, "Tentative Design Specifications for Horizontally Curved Highway Bridges." CURT Report, Part of Final Report, Research Project HPR2-(111) (March 1975).

2. Galambos, T.V., "Tentative Load Factor Design Criteria for Curved Steel Bridges, Research Report No. 50." Department of Civil Engineering, Washington University, St. Louis, MO (May 1978).

3. AASHTO, *Guide Specifications for Horizontally Curved Highway Bridges*. Washington, D.C. (1980).

4. Hall, D.H., Grubb, M.A. and Yoo, C.H., "Improved Design Specifications for Horizontally Curved Steel Girder Highway Bridges." NCHRP Report 424, Transportation Research Board, Washington, D.C. (1999).

5. AASHTO, *LRFD Bridge Design Specifications*, First Edition, Washington, D.C. (1994).

6. Hanshin Expressway Public Corporation and Steel Structures Study Committee, "Guidelines for the Design of Horizontally Curved Girder Bridges (Draft)." Hanshin Expressway Public Corporation (October 1988).

7. Mozer, J., Cook, J., and Culver, C.G., "Horizontally Curved Highway Bridges, Stability of Curved Plate Girders." Report No. P3, U.S. DOT, FHWA (August 1975).

8. Simpson, M.D., "Analytical Investigation of Curved Steel Girder Behaviour." Thesis presented to the University of Toronto in partial fulfillment of the requirements for the degree of Doctor of Philosophy, Department of Civil Engineering, University of Toronto, (2000).

9. ANSYS Procedures Manual, the ANSYS Corporation, Pittsburgh, PA.

10. Mozer, J. and Culver, C.G., "Horizontally Curved Highway Bridges, Stability of Curved Plate Girders." Report No. P1, U.S. DOT, FHWA (August 1975).

11. Mozer, J., Ohlson, R., and Culver, C.G., "Horizontally Curved Highway Bridges, Stability of Curved Plate Girders." Report No. P2, U.S. DOT, FHWA (August 1975).

12. American Welding Society, "Bridge Welding Code." ANSI/AASHTO/AWS D1.5-96 (1996).

13. Fukomoto, Y., Itoh, Y., and Kubo, M., "Strength Variation of Laterally Unsupported Beams." *Journal of the Structural Division*, American Society of Civil Engineers, Vol. 106, No. ST1 (1980).

14. Nakai, H., Kitada, T., and Ohminami, R., "Experimental Study on Buckling and Ultimate Strength of Curved Girders Subjected to Combined Loads of Bending and Shear." *Proceedings of Japan Society of Civil Engineers*, No. 356/I-3 (April 1985).

15. Daniels, J.H., Zettlemoyer, N., Abraham, D., and Batcheler, R.P., "Fatigue of Curved Steel Bridge Elements – Analysis and Design of Plate Girder and Box Girder Test Assemblies." Lehigh University, Bethlehem, PA, DOT-FH-11-8198.1 (1979).

16. Daniels, J.H., Fisher, J.W., Batcheler, R.P., and Maurer, J.K., "Fatigue of Curved Steel Bridge Elements – Ultimate Strength Tests of Horizontally Curved Plate and Box Girders." Lehigh University. Bethlehem, PA, DOT-FH-11-8198.7 (1979).

17. Nakai, H. and Kotoguchi, H., "A Study on Lateral Buckling Strength and Design Aid for Horizontally Curved I-Girder Bridges." *Proceedings of Japan Society of Civil Engineers*, No. 339 (November 1983).

18. Pi, Y.L., Bradford, M.A., and Trahair, N.S., "Inelastic Analysis and Behavior of Steel I-Beams Curved in Plan." *Journal of Structural Engineering*, American Society of Civil Engineers, Vol. 126, No. 7, (July 2000).

19. Beal, D.B., "Horizontally Curved Bridges: New York Field Testing and Design Studies, Final Report on Research Project 42-1." Engineering Research and Development Bureau, New York State DOT, Research Report 61 (1978).

20. Gambrell, S.C., Jr., and Skelton, T.J., "Structural Behavior of the Homewood Bridge after Fourteen Years Traffic." The University of Alabama-Birmingham, Department of Engineering Mechanics (August 1986).

21. Buchanan, J.D., Yoo, C.H., and Heins, C.P., "Field Study of a Curved Box Beam Bridge." University of Maryland, Department of Civil Engineering (September 1974).

22. Galambos, T.V., Hajjar, J.F., Leon, R.T., Huang, W., Pulver, B., and Rudie, B.J., "Stresses in Steel Curved Girder Bridges." University of Minnesota Center for Transportation Studies, Research Report No. 96-28 (August 1996).

23. AASHTO, *Guide Specifications for Horizontally Curved Highway Bridges*. Washington, D.C. (1993).

24. AASHTO, *Standard Specifications for Highway Bridges*, 15th Edition (1992) with 1993 Interim Specifications, Washington, D.C.

25. Pennsylvania Department of Transportation, "Design Manual – Part 4: Volume 1, Part B – Design Specifications." Harrisburg, PA (1994).

26. BRIDGE-SYSTEM, 3D System User Manual, Bridge Software Development International, Ltd., Coopersburg, PA.

27. GTSTRUDL User Manual, Georgia Institute of Technology, Atlanta, GA.

28. MDX User Manual, MDX, Columbia, MO.

29. VANCK User Manual, National Steel Bridge Alliance, Chicago, IL.

30. ABAQUS Manual, Hibbitt, Karlsson & Sorenson, Pawtucket, RI.

31. MSC/NASTRAN Reference Manual, the Mac-Neal-Schwindler Corporation, Los Angeles, CA.

32. *Load and Resistance Factor Design Specification for Structural Steel Buildings*. Second Edition, American Institute of Steel Construction, Chicago, IL (December 1, 1993).

33. U.S. Steel Highway Structures Design Handbook, Vol. I, Chapter 12, "Horizontally Curved Girder." chapter available from M.A. Grubb & Associates, LLC, Wexford, PA (1965).

34. "SSRC Technical Memorandum No. 7: Tension Testing." *Guide to Stability Design Criteria for Metal Structures*, Fourth Edition, Edited by T.V. Galambos, John Wiley & Sons, New York, NY (1988).

35. Nakai, H., Kitada, T., and Ohminami, R., "Experimental Study on Bending Strength of Web Plate of Horizontally Curved Girder Bridges." *Proceedings of Japan Society of Civil Engineers*, No. 340 (1983).

36. Nakai, H., Kitada, T., Ohminami, R., and Kawai, T., "A Study on Analysis and Design of Web Plates in Curved Girder Bridges Subjected to Bending." *Proceedings of Japan Society of Civil Engineers*, No.

368/1-5 (1986).

37. Hall, D.H., and Yoo, C.H., "Recommended Specifications for Steel Curved-Girder Bridges." NCHRP Project 12-38, Transportation Research Board, Washington, D.C. (December 1988).

38. *Load and Resistance Factor Design Specification for Structural Steel Buildings*. First Edition, American Institute of Steel Construction, Chicago, IL (September 1, 1986).

39. Davidson, J.S., and Yoo, C.H., "Local Buckling of Curved I-Girder Flanges." *Journal of Structural Engineering*, American Society of Civil Engineers, Vol. 122, No. 8, (August 1996).

40. McManus, P.F., "Lateral Buckling of Curved Plate Girders." Thesis presented to Carnegie Mellon University in partial fulfillment of the requirements for the degree of Doctor of Philosophy, Pittsburgh, PA (1971).

41. Dabrowski, R., *Curved Thin-Walled Girders, Theory and Analysis*, Cement and Concrete Association, London, England (1968) (translated from German).

42. Vincent, G.S., "Tentative Criteria for Load Factor Design of Steel Highway Bridges." Bulletin No. 15, American Iron and Steel Institute, Washington, D.C. (March 1969).

43. Hall, D.H. and Yoo, C.H., "I Girder Curvature Study." Interim Report, NCHRP Project 12-38, Transportation Research Board, Washington, D.C. (June 1996).

44. Schilling, C.G., "Yield-Interaction Relationships for Curved I-Girders." *Journal of Bridge Engineering*, American Society of Civil Engineers, Vol. 1, No. 1 (February 1996).

45. Yoo, C.H., Kang, Y.J., and Davidson, J.S., "Buckling Analysis of Curved Beams by Finite Element Discretization.", *Journal of Structural Engineering*, American Society of Civil Engineers, Vol. 122, No. 8 (August 1996).

46. Fukomoto, Y. and Nishida, S., "Ultimate Load Behavior of Curved I-Beams." *Journal of the Engineering Mechanics Division*, American Society of Civil Engineers, Vol. 107, No. EM2 (1981).

47. Kitada, T., Ohminami, R., and Nakai, H., "Criteria for Designing Web and Flange Plates of Horizontally Curved Plate Girders." *Proceedings of the SSRC 1986 Annual Technical Session* (1986).

48. Nishida, S., Yoshida, H., and Fukomoto, Y., "Large Deflection Analysis of Curved Members with Thin-Walled Open Cross-Section." *24th Symposium of Structural Engineering* (February 1978) (in Japanese).

2.71

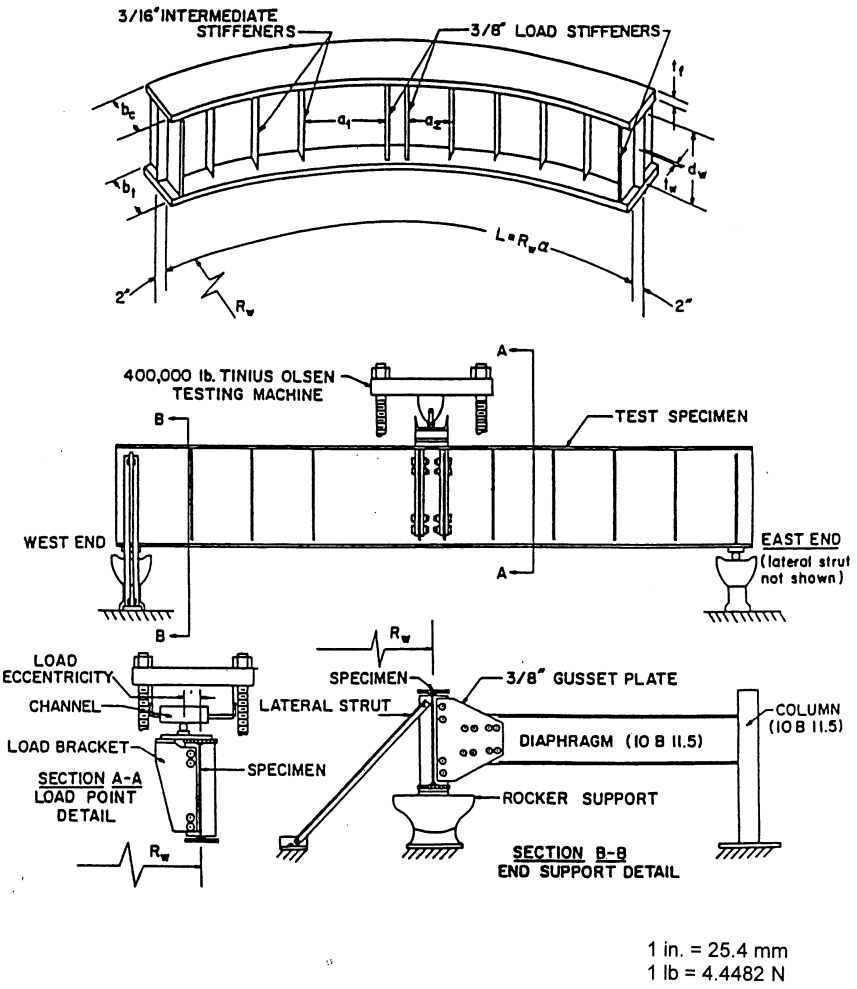

1 in. = 25.4 mm
1 lb = 4.4482 N

Figure 2.1. Mozer-Culver Tests – C and D Series

2.72

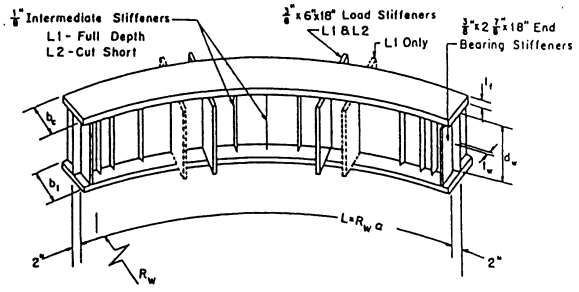

Specimens L1, L2

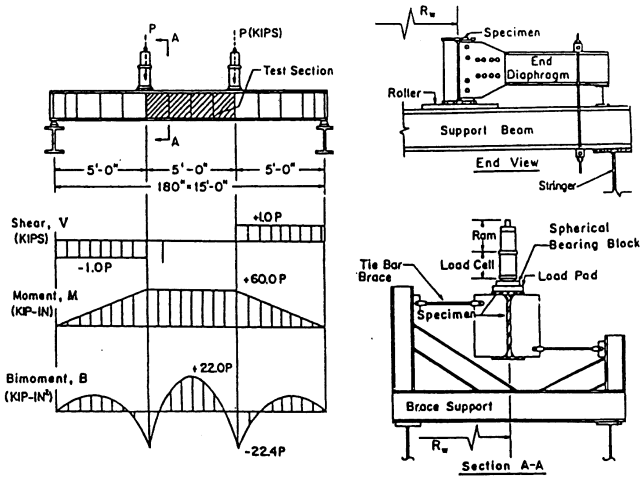

Tests L1-A, L2-A

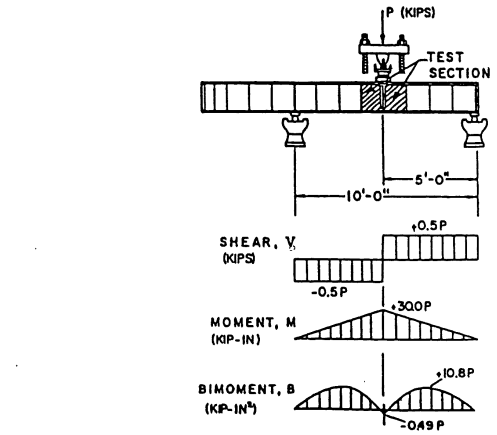

Tests L2-B, L2-C

1 ft = 0.3048 m
1 in. = 25.4 mm
1 kip = 4.4482 kN
1 kip-in. = 0.11298 kN-m
1 kip-in.^{2} = 0.00287 kN-m^2

Figure 2.2. Mozer-Culver Tests – Specimens L1 and L2

2.73

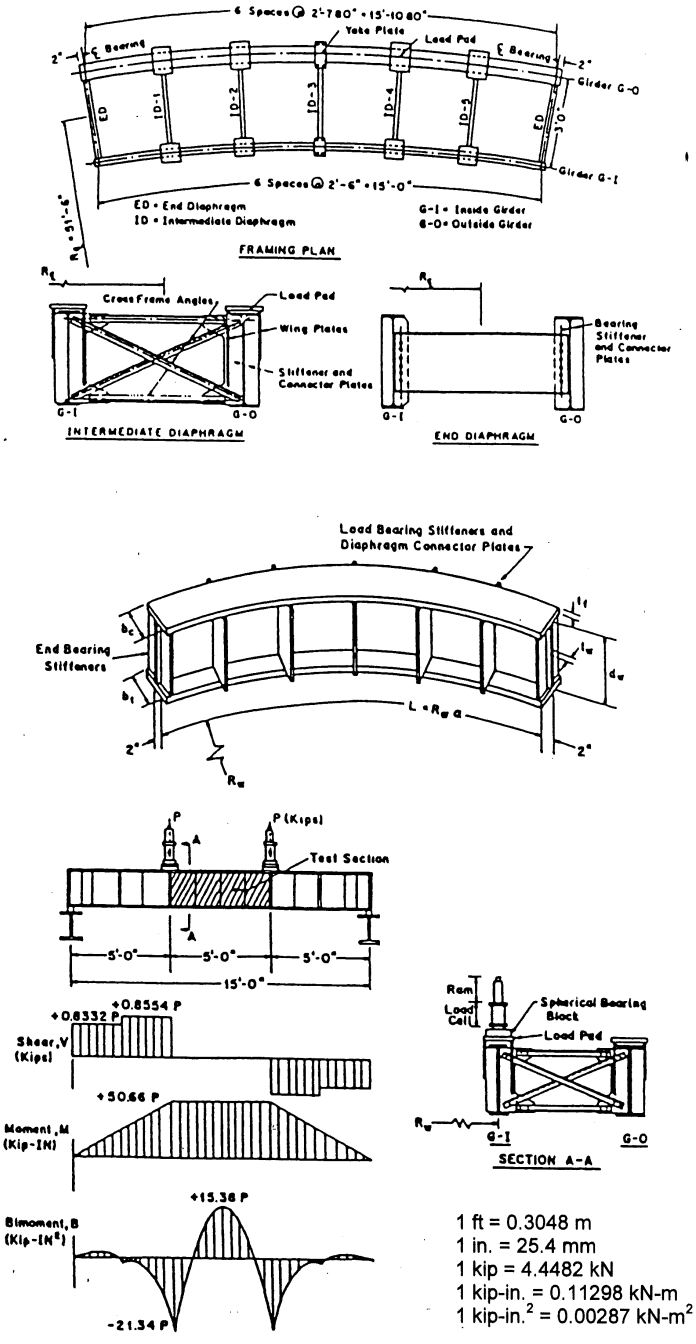

1 ft = 0.3048 m
1 in. = 25.4 mm
1 kip = 4.4482 kN
1 kip-in. = 0.11298 kN-m
1 kip-in.^{2} = 0.00287 kN-m^2

Figure 2.3 Mozer-Culver Two-Girder Tests

2.74

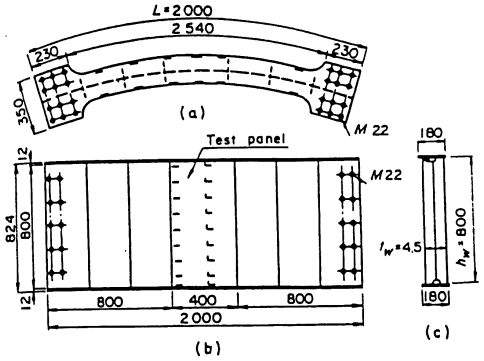

Detail of a test girder under bending (in mm): (a) plan, (b) side elevation, and (c) cross section.

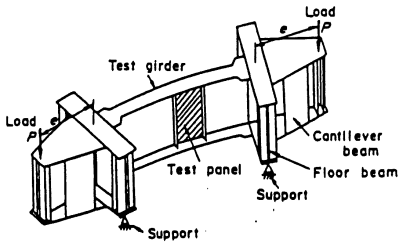

1 mm = 0.03937 in.

Figure 2.4 Nakai Tests

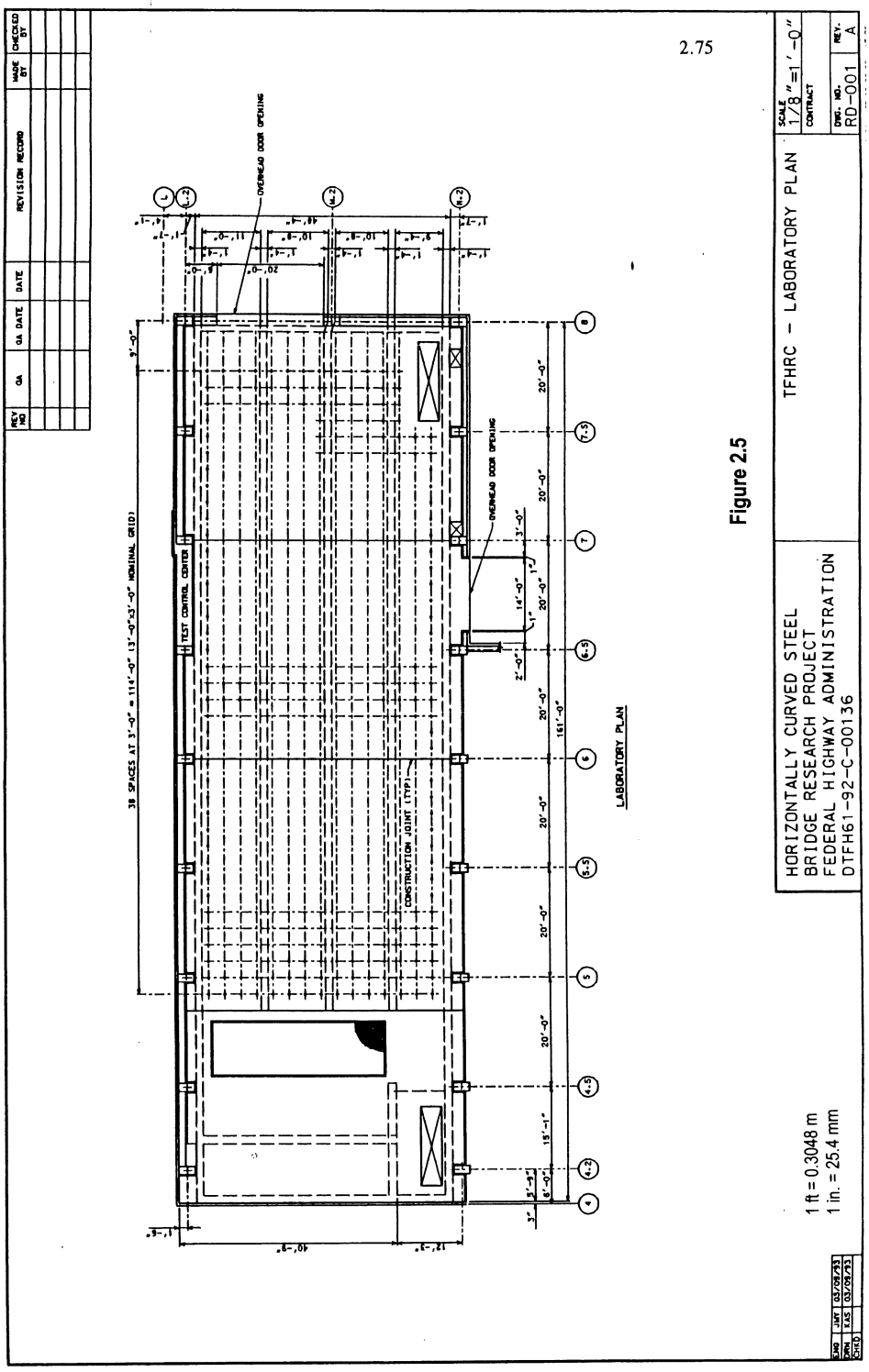
2.75
TFHRC – LABORATORY PLAN
HORIZONTALLY CURVED STEEL
BRIDGE RESEARCH PROJECT
FEDERAL HIGHWAY ADMINISTRATION
DTFH61-92-C-00136
LABORATORY PLAN
TEST CONTROL CENTER
CONSTRUCTION JOINT (TYP.)
OVERHEAD DOOR OPENING
38 SPACES AT 3'-0" = 114'-0" (3'-0"x3'-0" NOMINAL GRID)
1 ft = 0.3048 m
1 in. = 25.4 mm
REVISION RECORD
CHECKED BY
MADE BY
DATE
QA DATE
QA
REV NO
SCALE 1/8"=1'-0"
CONTRACT
DWG. NO. RD-001
REV. A

Figure 2.5

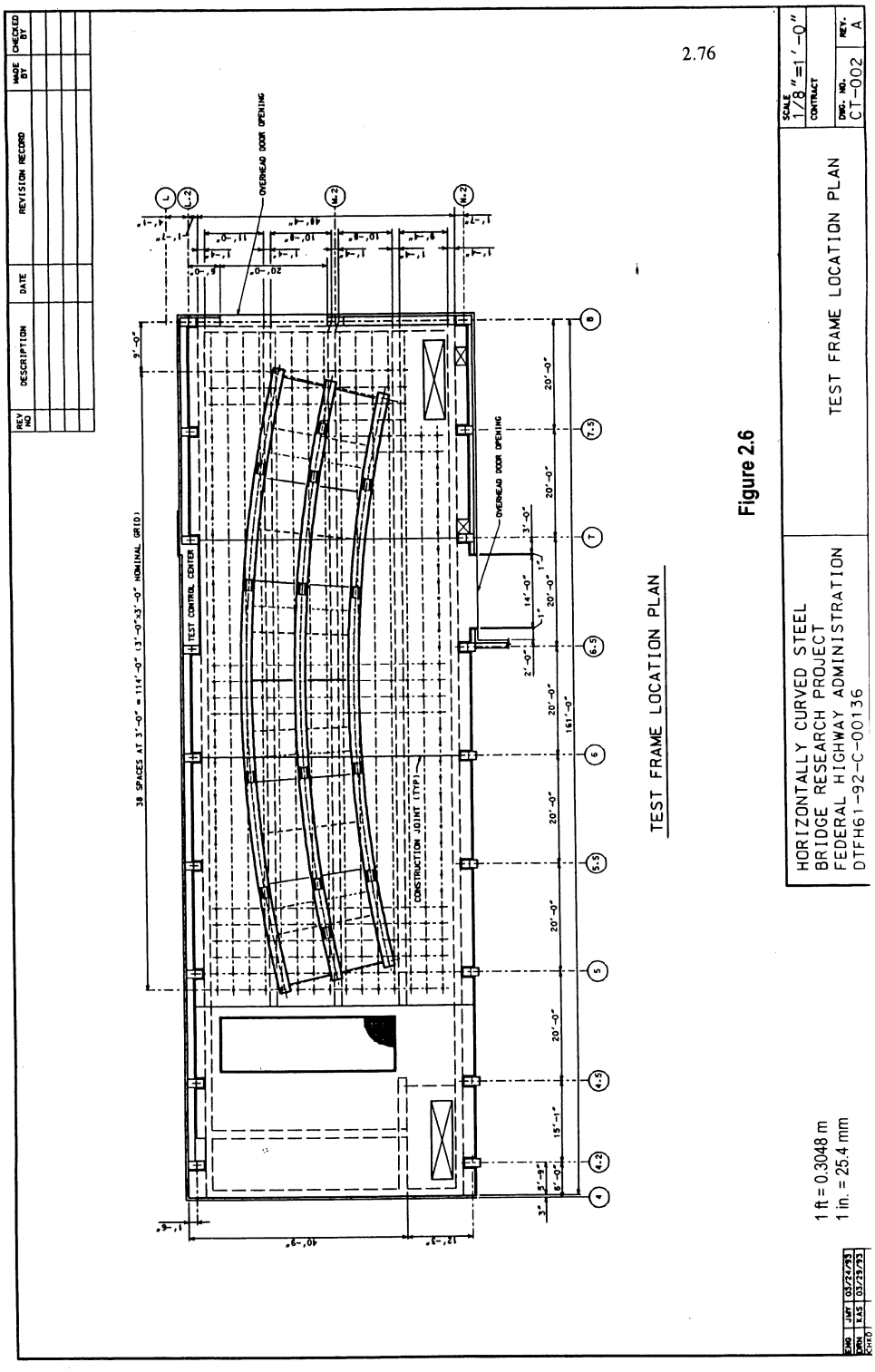
2.76
TEST FRAME LOCATION PLAN
TEST CONTROL CENTER
OVERHEAD DOOR OPENING
CONSTRUCTION JOINT (TYP)
38 SPACES AT 3'-0" = 114'-0" (3'-0"x3'-0" NOMINAL GRID)
HORIZONTALLY CURVED STEEL
BRIDGE RESEARCH PROJECT
FEDERAL HIGHWAY ADMINISTRATION
DTFH61-92-C-00136
TEST FRAME LOCATION PLAN
SCALE 1/8"=1'-0"
CONTRACT
DWG. NO. CT-002
REV. A
1 ft = 0.3048 m
1 in. = 25.4 mm

Figure 2.6

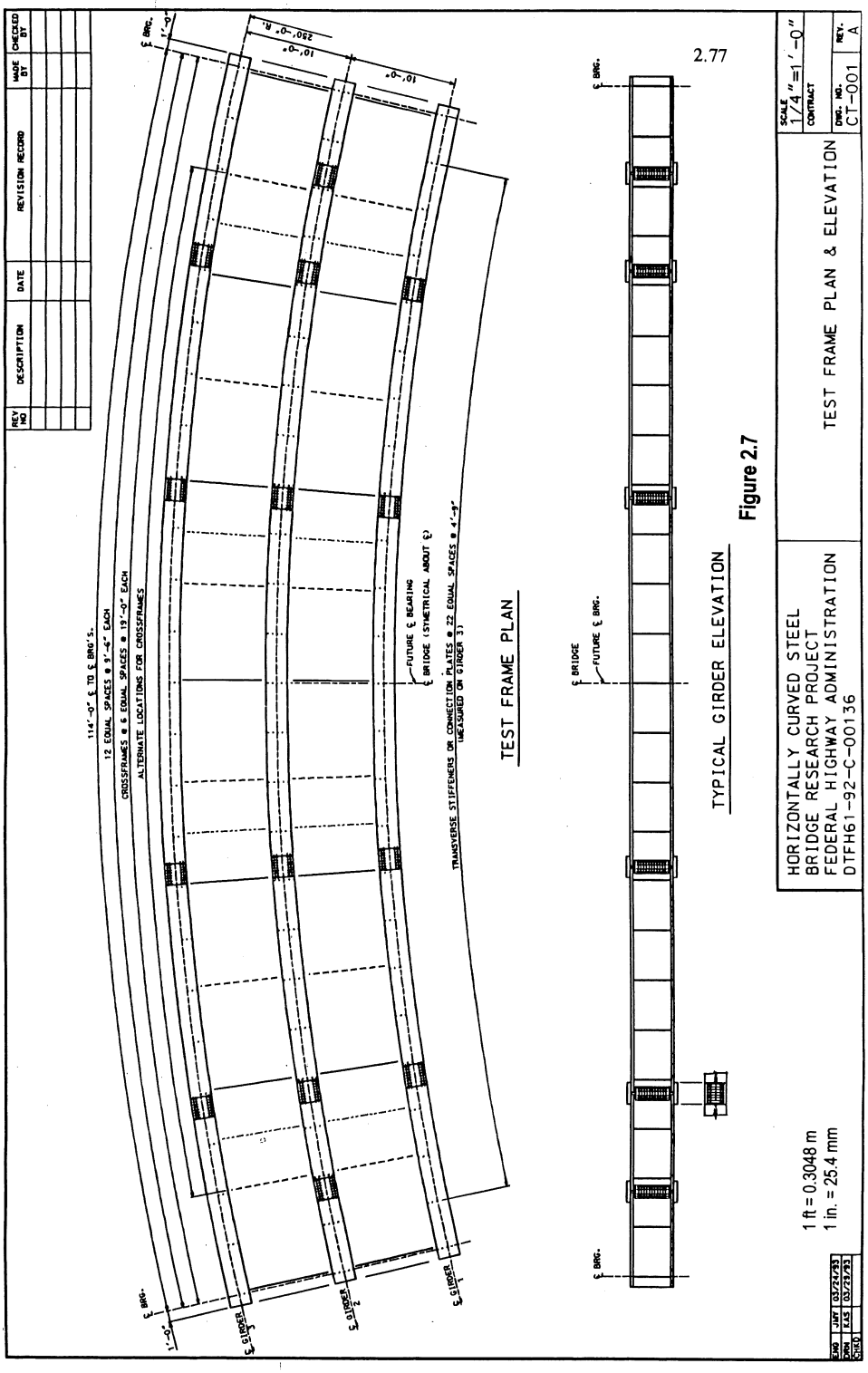
REV NO
DESCRIPTION
DATE
REVISION RECORD
MADE BY
CHECKED BY
114'-0" ℄ TO ℄ BRG'S.
12 EQUAL SPACES @ 9'-4" EACH
CROSSFRAMES @ 6 EQUAL SPACES @ 19'-0" EACH
ALTERNATE LOCATIONS FOR CROSSFRAMES
℄ BRG.
1'-0"
250'-0" R.
10°-0"
8°-0"
℄ BRG.
℄ GIRDER 3
℄ GIRDER 2
℄ GIRDER 1
FUTURE ℄ BEARING
℄ BRIDGE (SYMETRICAL ABOUT ℄)
TRANSVERSE STIFFENERS OR CONNECTION PLATES @ 22 EQUAL SPACES @ 4'-9"
(MEASURED ON GIRDER 3)
TEST FRAME PLAN
℄ BRG.
℄ BRIDGE
FUTURE ℄ BRG.
℄ BRG.
TYPICAL GIRDER ELEVATION
2.77
Figure 2.7
HORIZONTALLY CURVED STEEL
BRIDGE RESEARCH PROJECT
FEDERAL HIGHWAY ADMINISTRATION
DTFH61-92-C-00136
TEST FRAME PLAN & ELEVATION
SCALE 1/4"=1'-0"
CONTRACT
DRG. NO. CT-001
REV. A
1 ft = 0.3048 m
1 in. = 25.4 mm
ENG JMF 03/27/93
DRN EAS 03/27/93
CHKD

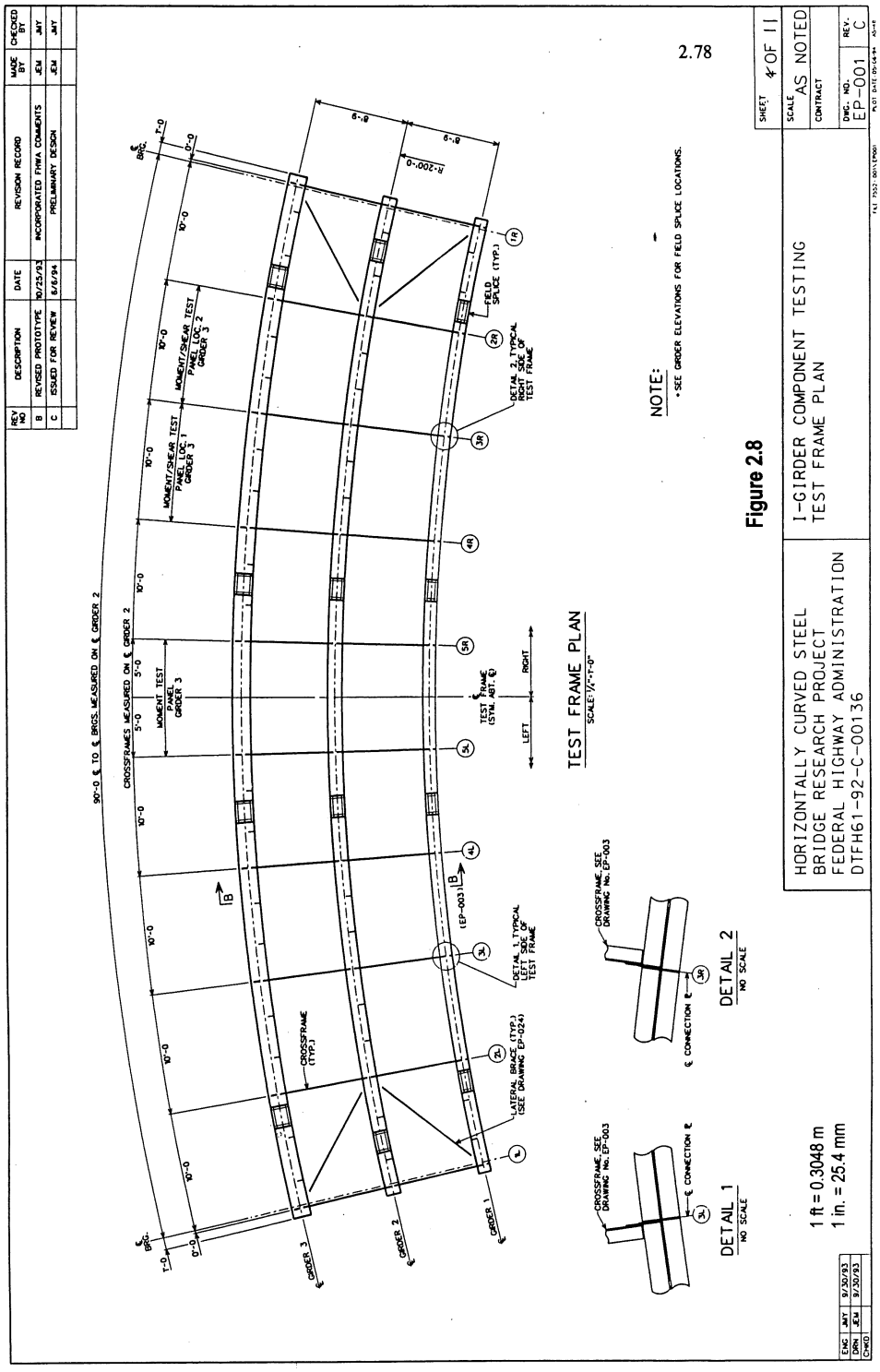

2.78

Figure 2.8

2.79

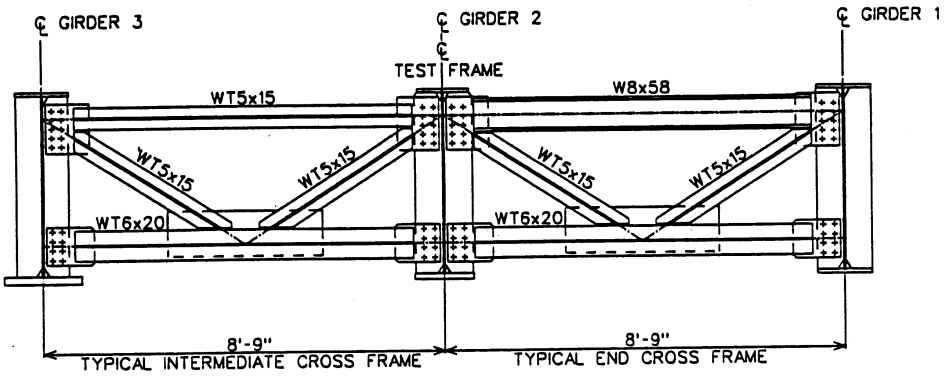

TYPICAL SECTION
PROTOTYPE

1 ft = 0.3048 m
1 in. = 25.4 mm
1 lb/ft = 1.4882 kg/m

Figure 2.9

2.80

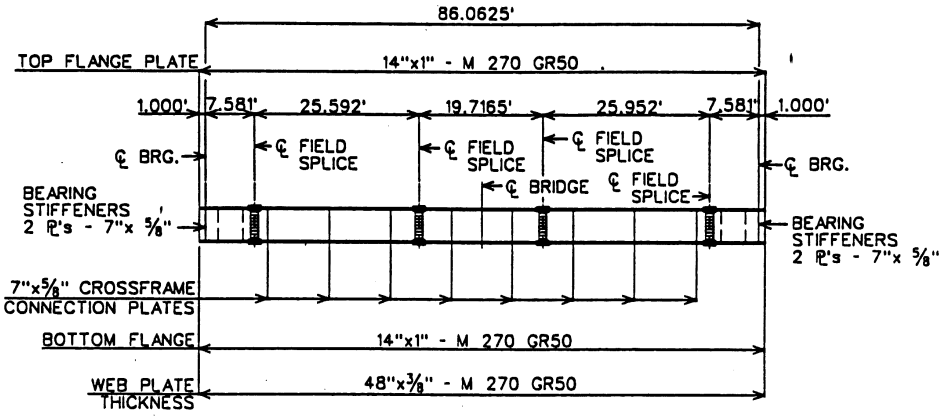

ELEVATION - GIRDER G1
PROTOTYPE

1 ft = 0.3048 m
1 in. = 25.4 mm
1 ksi = 6.8948 MPa

Figure 2.10

2.81

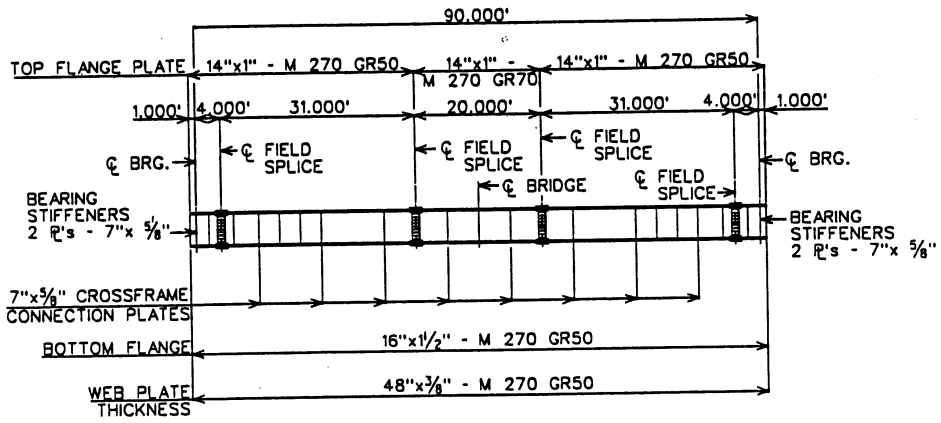

ELEVATION - GIRDER G2
PROTOTYPE

1 ft = 0.3048 m
1 in. = 25.4 mm
1 ksi = 6.8948 MPa

Figure 2.11

2.82

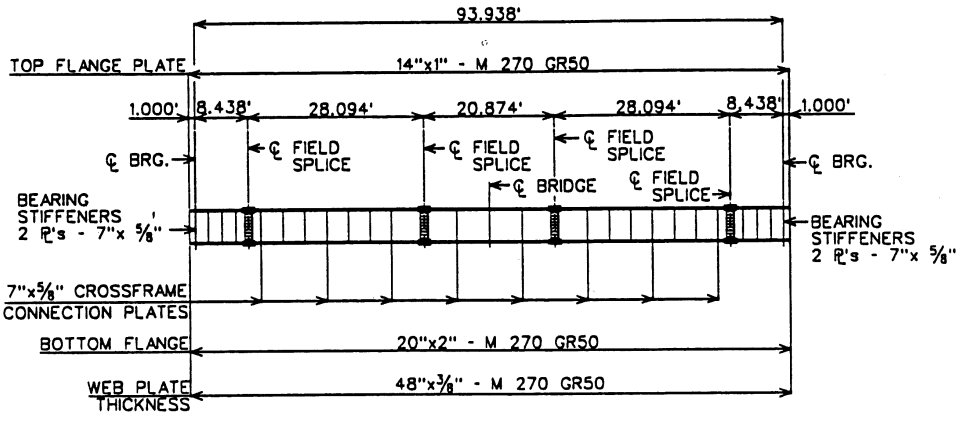

ELEVATION - GIRDER G3
PROTOTYPE

1 ft = 0.3048 m
1 in. = 25.4 mm
1 ksi = 6.8948 MPa

Figure 2.12

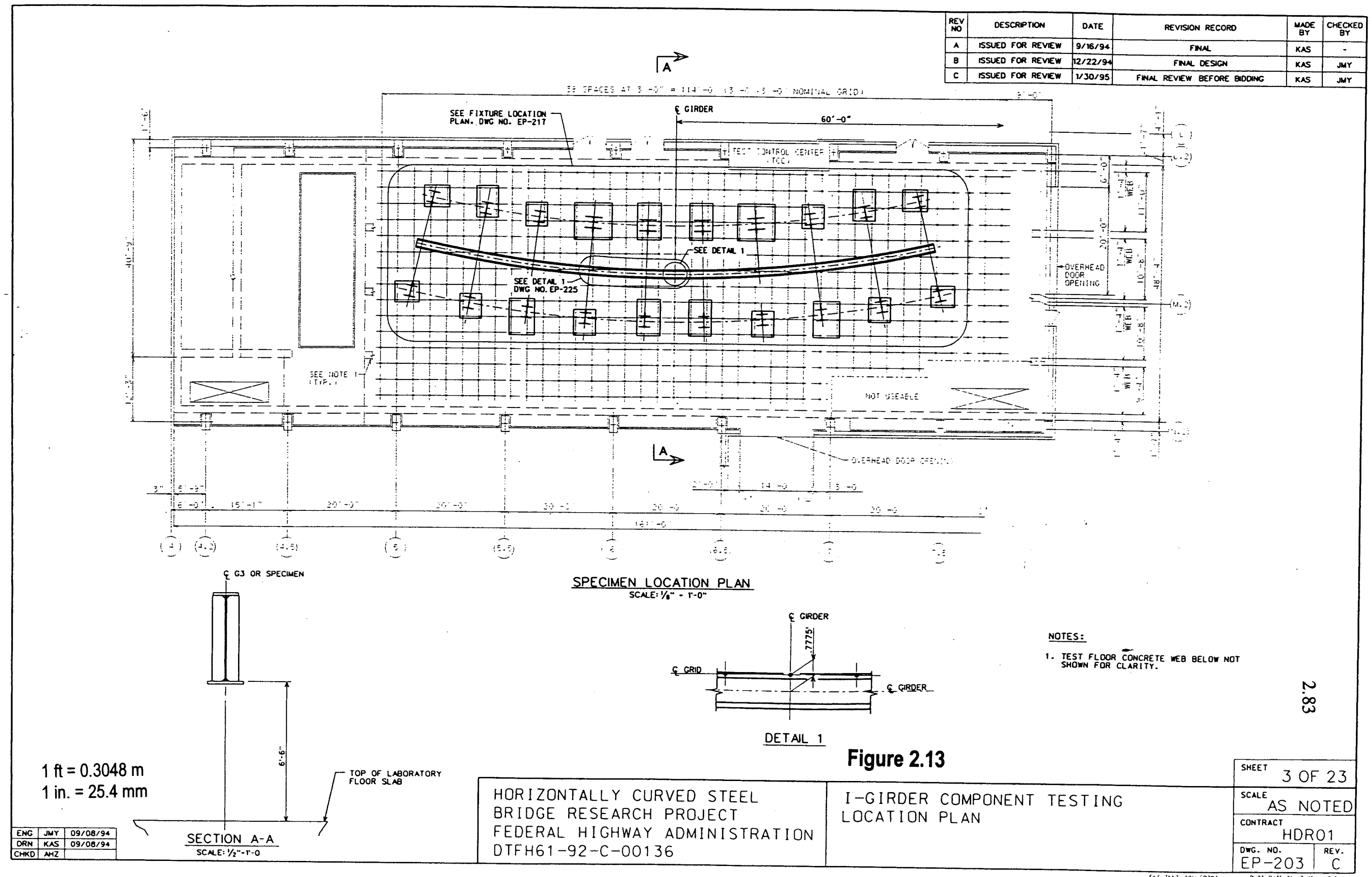

REV NO | DESCRIPTION | DATE | REVISION RECORD | MADE BY | CHECKED BY
A | ISSUED FOR REVIEW | 9/16/94 | FINAL | KAS | -
B | ISSUED FOR REVIEW | 12/22/94 | FINAL DESIGN | KAS | JMY
C | ISSUED FOR REVIEW | 1/30/95 | FINAL REVIEW BEFORE BIDDING | KAS | JMY
SEE FIXTURE LOCATION PLAN. DWG NO. EP-217
℄ GIRDER
60'-0"
SEE DETAIL 1
SEE DETAIL 1 DWG NO. EP-225
OVERHEAD DOOR OPENING
NOT USEABLE
SPECIMEN LOCATION PLAN
SCALE: 1/8" - 1'-0"
℄ G3 OR SPECIMEN
6'-6"
TOP OF LABORATORY FLOOR SLAB
SECTION A-A
SCALE: 1/2"-1'-0
℄ GIRDER
.7775'
℄ GRID
℄ GIRDER
DETAIL 1
NOTES:
1. TEST FLOOR CONCRETE WEB BELOW NOT SHOWN FOR CLARITY.
2.83
1 ft = 0.3048 m
1 in. = 25.4 mm
ENG JMY 09/08/94
DRN KAS 09/08/94
CHKD AHZ
HORIZONTALLY CURVED STEEL BRIDGE RESEARCH PROJECT
FEDERAL HIGHWAY ADMINISTRATION
DTFH61-92-C-00136
I-GIRDER COMPONENT TESTING LOCATION PLAN
SHEET 3 OF 23
SCALE AS NOTED
CONTRACT HDR01
DWG. NO. EP-203
REV. C

Figure 2.13

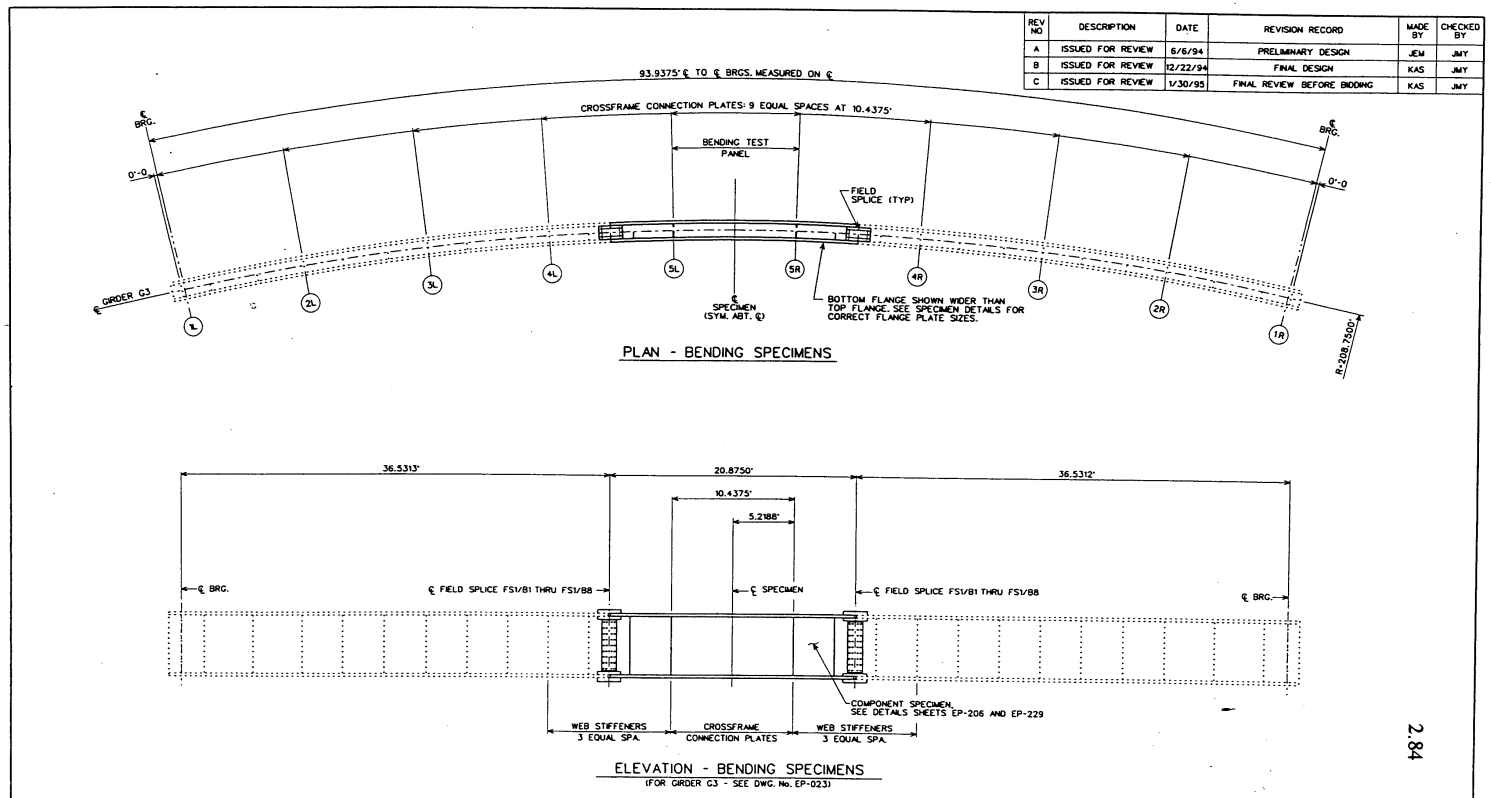

REV NO	DESCRIPTION	DATE	REVISION RECORD	MADE BY	CHECKED BY
A	ISSUED FOR REVIEW	6/6/94	PRELIMINARY DESIGN	JEM	JMY
B	ISSUED FOR REVIEW	12/22/94	FINAL DESIGN	KAS	JMY
C	ISSUED FOR REVIEW	1/30/95	FINAL REVIEW BEFORE BIDDING	KAS	JMY

2.84

Figure 2.14

ENG	JMY	4/26/94
DRN	JEM	4/26/94
CHKD	AHZ	

1 ft = 0.3048 m
1 in. = 25.4 mm

HORIZONTALLY CURVED STEEL BRIDGE RESEARCH PROJECT
FEDERAL HIGHWAY ADMINISTRATION
DTFH61-92-C-00136

I-GIRDER COMPONENT TESTING
PLAN AND ELEVATION - COMPONENT SETUP

SHEET 7 OF 23
SCALE 1/4"=1'-0"
CONTRACT HDR01
DWG. NO. EP-028
REV. C

FILE 7552-001\EP028 PLOT DATE 31-17-95

REV NO	DESCRIPTION	DATE	REVISION RECORD	MADE BY	CHECKED BY
A	ISSUED FOR REVIEW	12/22/94	FINAL DESIGN	KAS	JMY
B	ISSUED FOR REVIEW	1/30/95	FINAL REVIEW BEFORE BIDDING	KAS	JMY

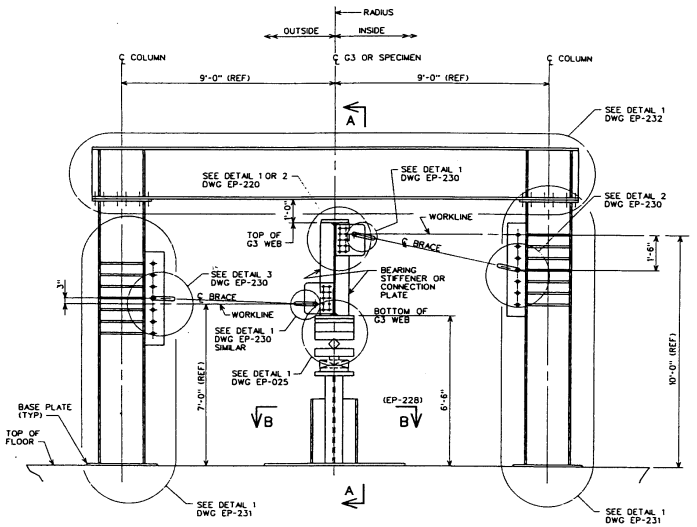

SECTION A-A AT END BRACING

SECTION B-B AT INTERIOR BRACING SIMILAR

TAKEN ON EP-217

SCALE: ½"-1'-0"

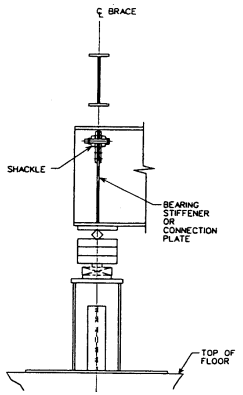

SECTION A-A

SCALE: ½"-1'-0"

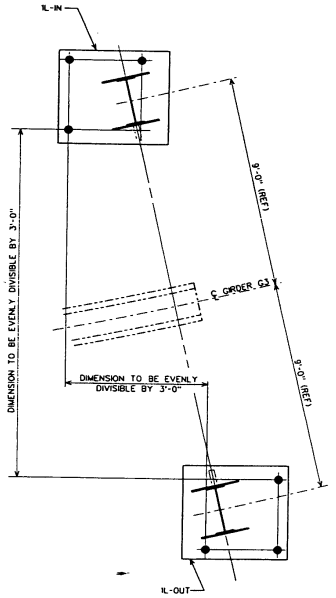

FIGURE 1

2.85

NOTE:

PERFORM A CHECK ASSEMBLY OF ALL FRAMES BEFORE SHIPPING TO LABORATORY. CHECK THAT THE RELATIVE DIMENSIONING OF THE HOLES IN THE BASE PLATES BETWEEN IN COLUMNS AND OUT COLUMNS ARE TO THE DIMENSIONS DETERMINED FROM DRAWING EP-217. SEE FIGURE 1 FOR AN EXAMPLE.

Figure 2.15

1 ft = 0.3048 m

1 in. = 25.4 mm

ENG	JMY	12/01/94
DRN	KAS	12/01/94
CHKD	AHZ	

HORIZONTALLY CURVED STEEL BRIDGE RESEARCH PROJECT
FEDERAL HIGHWAY ADMINISTRATION
DTFH61-92-C-00136

I-GIRDER COMPONENT TESTING
BRACING TYPICAL SECTION

SHEET	14 OF 23
SCALE	AS NOTED
CONTRACT	HDR01
DWG. NO.	EP-213
REV.	B

FILE: 7552 DGN:EP213 PLOT DATE: 01 JUL 95 AS:24

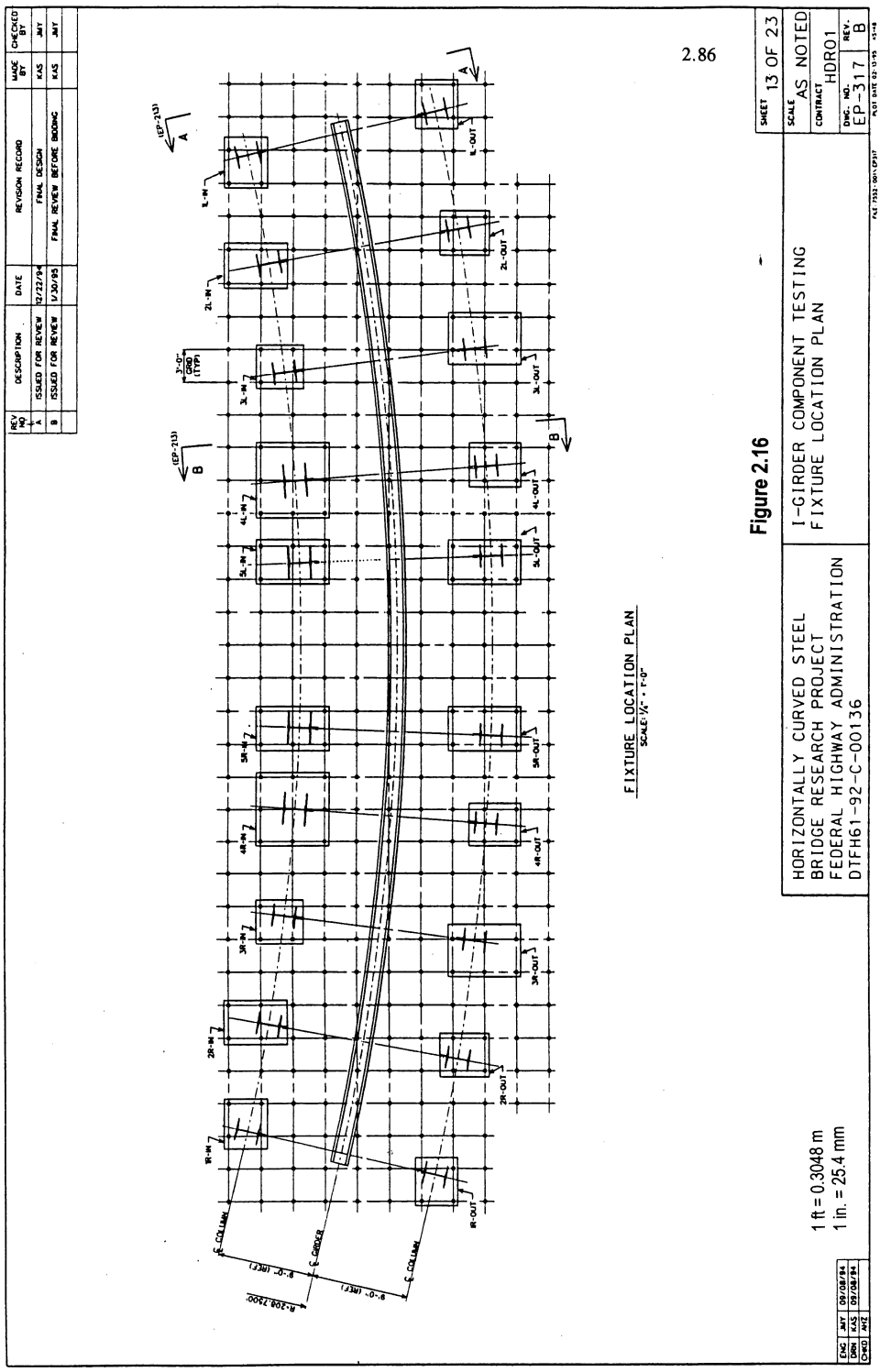

2.86

Figure 2.16

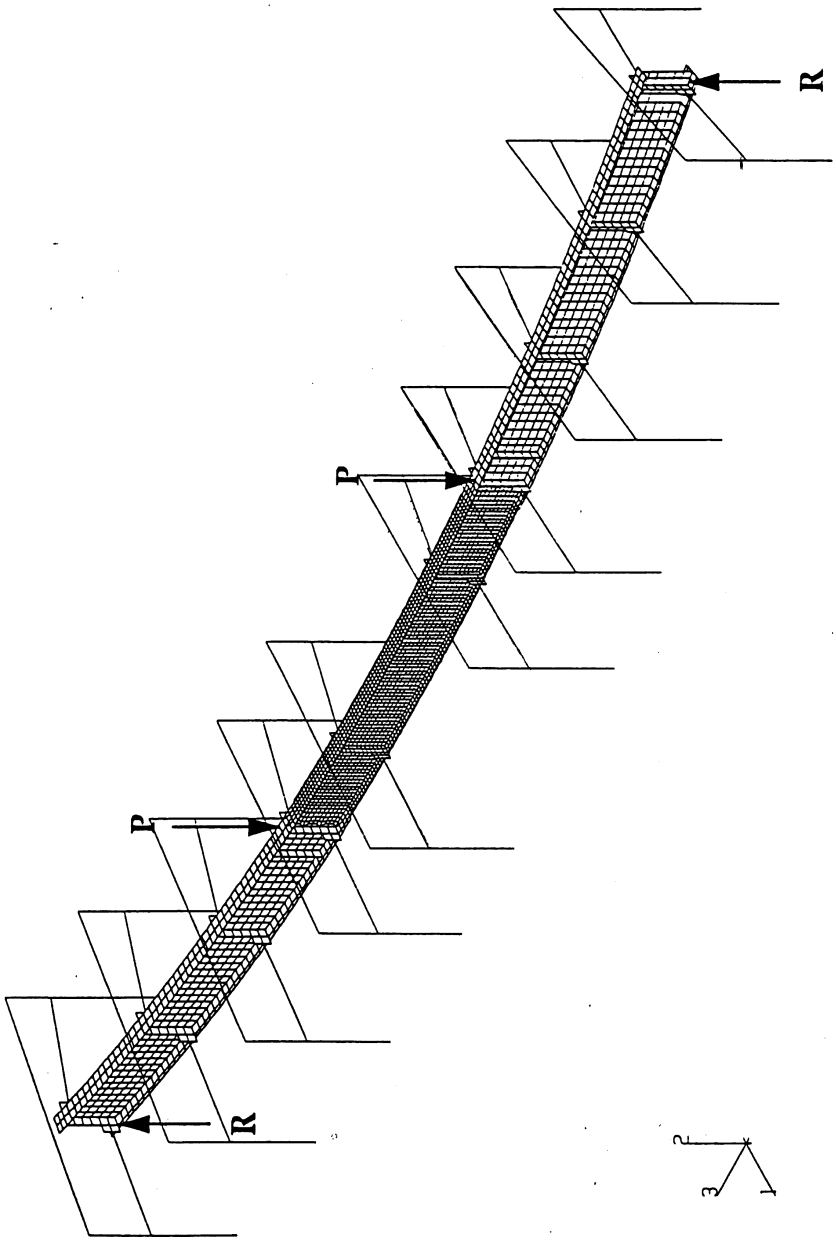

Figure 2.17. ABAQUS Model of Single Girder Test Set-Up

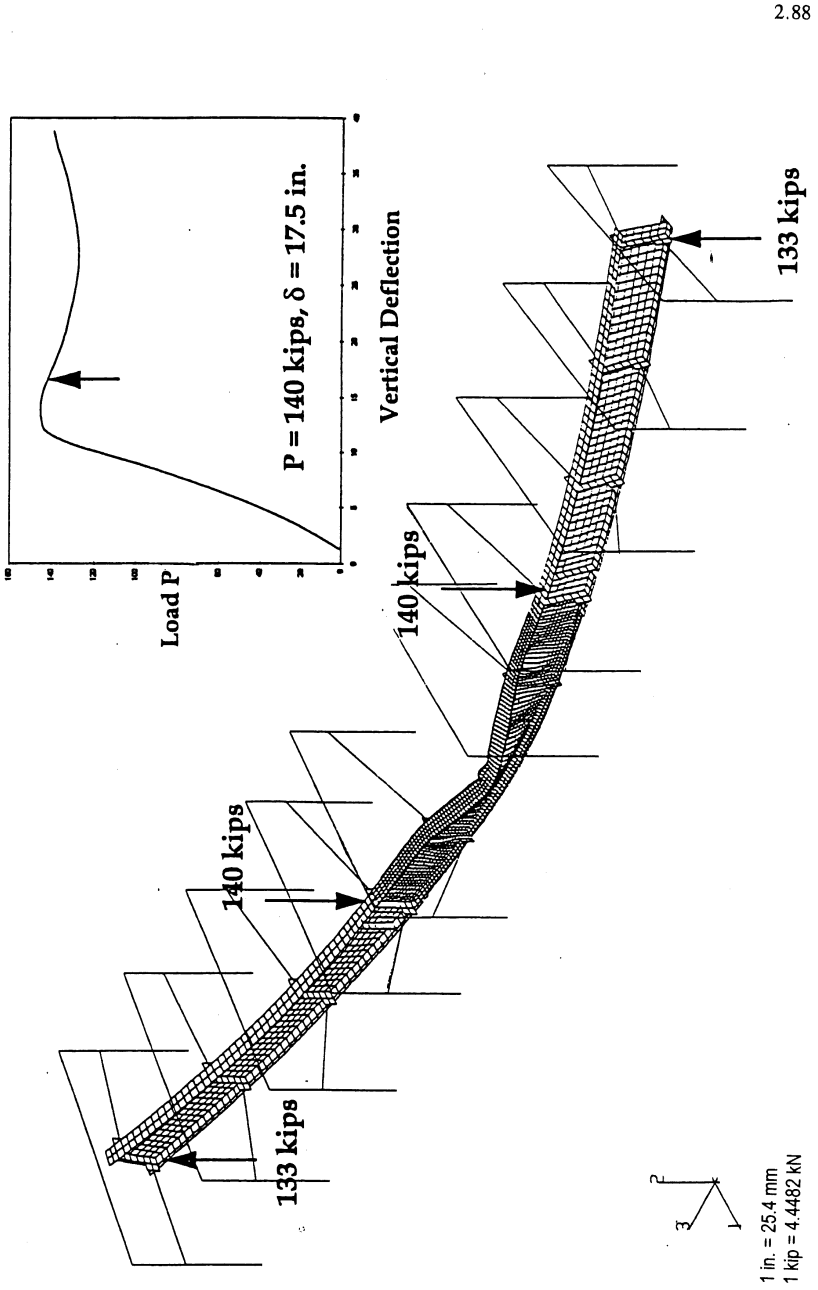

Figure 2.18. ABAQUS Plot of Deformed Single-Girder Test Component Specimen at P = 140 kips with Plot of Load vs. Maximum Vertical Deflection

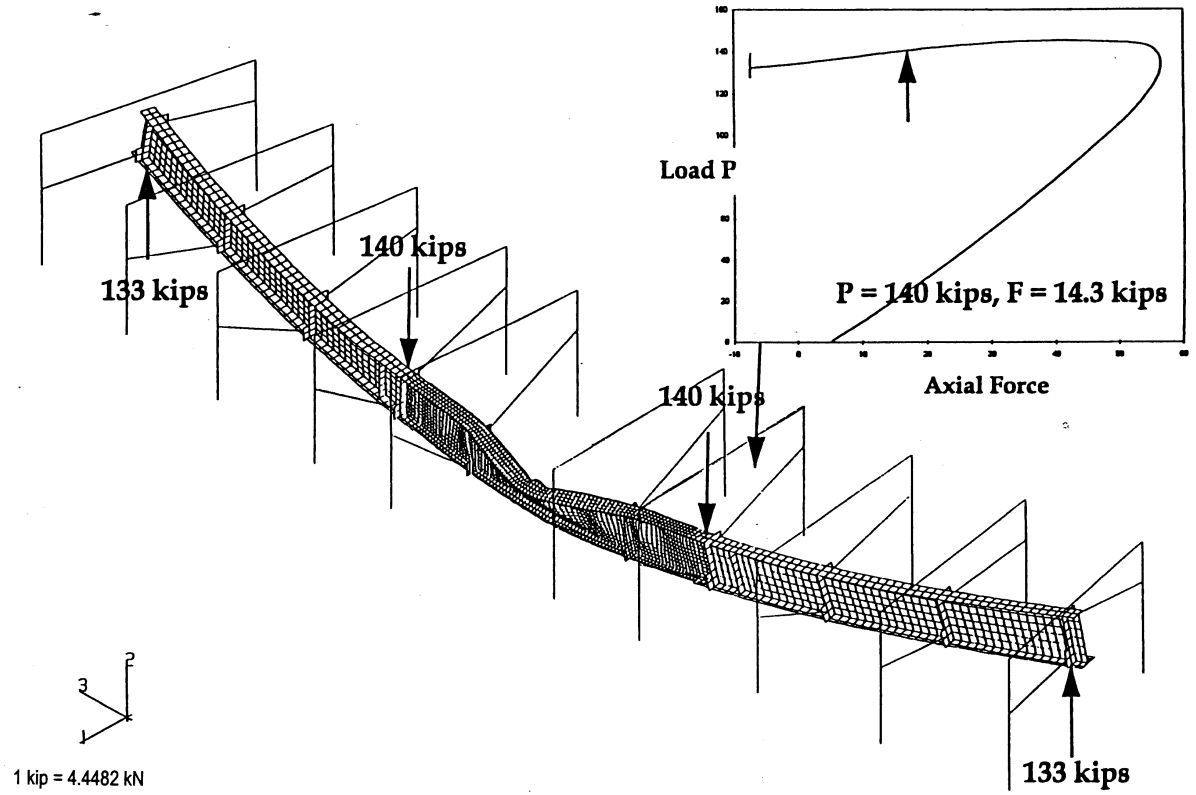

Figure 2.19. ABAQUS Plot of Deformed Single-Girder Test Component Specimen at P = 140 kips with Plot of Load vs. Axial Force in a Bracing Member on the Inside of the Curve Near the Load Point

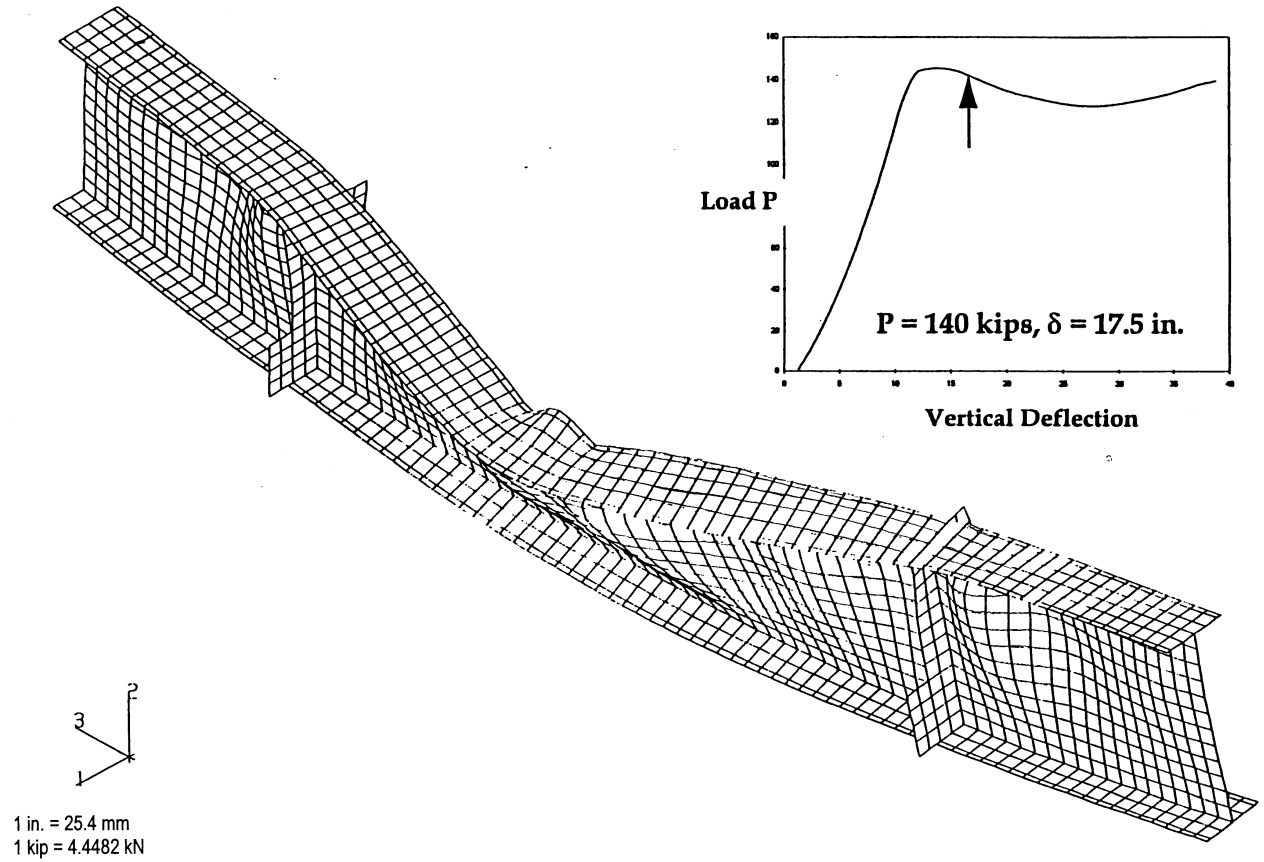

Figure 2.20 ABAQUS Close-Up Plot of Deformed Single-Girder Test Component Specimen

REV NO	DESCRIPTION	DATE	REVISION RECORD	MADE BY	CHECKED BY
1	REMOVE CROSS-FRAME TYPE AND ADDED CONNECTION PLATES	6/2/95	ADDENDUM TO BID DOCUMENTS	DAC	MAG
2	REMOVED CROSS-FRAMES AT LINES 6aL & 6aR & ADDED NOTES 4,5 & 6	2/23/96	ADDENDUM #2 TO CONTRACT	DAC	MAG
3	REMOVED STIFFENERS ON FASCIA SIDE OF G1 & G3 AT CROSS FRAME LINES	10/8/96	ADDENDUM #3 TO CONTRACT	MAG	JDC

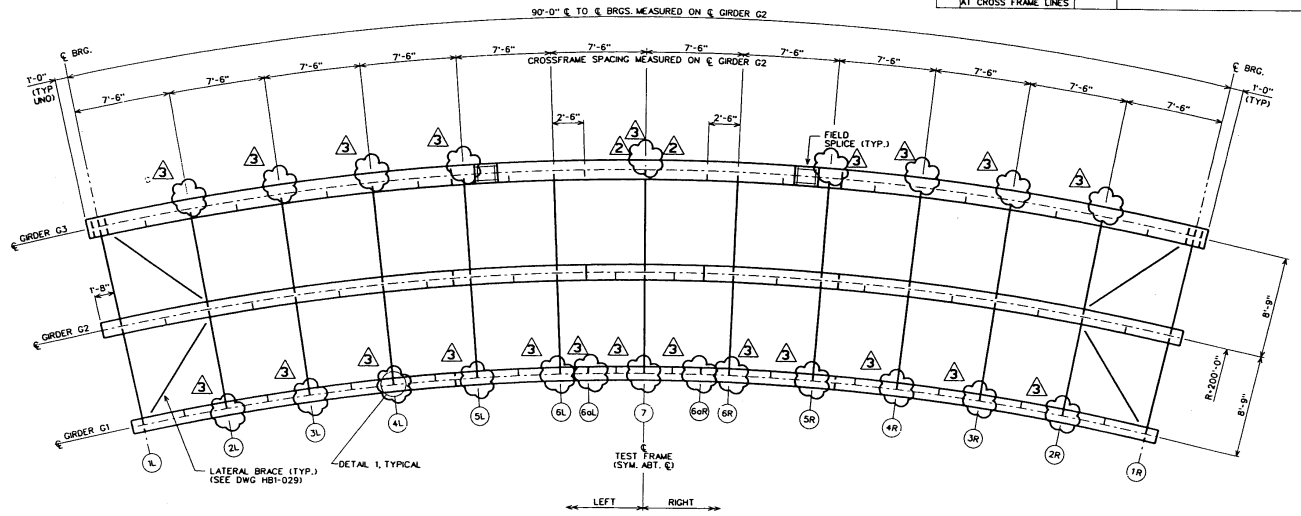

TEST FRAME PLAN
SCALE: 1/4"=1'-0"

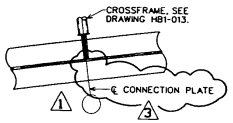

DETAIL 1
NO SCALE

NOTES:

1. SEE ELEVATION OF GIRDER G3, DWG HB1-006, FOR FIELD SPLICE LOCATIONS.
2. IF GIRDERS G2 AND G1 CANNOT BE SHIPPED IN THE LENGTHS SHOWN ON THE PLANS, FIELD SPLICES WILL BE PERMITTED WITH THE APPROVAL OF THE ENGINEER.
3. FABRICATE AND TEST FIT ALL CROSSFRAMES IN THE SHOP. NOTE THAT NOT ALL CROSSFRAMES WILL BE ERECTED IN THE LABORATORY. AN ERECTION PLAN FOR THE TEST FRAME IN THE LABORATORY IS SHOWN ON DWG HB1-027.
4. THE CROSS FRAME BETWEEN GIRDERS G2 AND G3 AT CROSS FRAME LINE 7 WILL ONLY BE CONNECTED TO THE G3 GIRDER SECTION, NEVER TO COMPONENT SPECIMENS B1 THROUGH B6.
5. THE CROSS FRAMES BETWEEN GIRDERS G2 AND G3 AT CROSS FRAME LINES 6L AND 6R WILL ONLY BE CONNECTED TO THE COMPONENT SPECIMEMS B1 THROUGH B6, NEVER TO THE G3 GIRDER SECTION.
6. DO NOT DRILL HOLES IN THE CONNECTION PLATES ON GIRDERS G1 AND G2 AT LINES 6aL AND 6aR.

2.91

Figure 2.21

ENG	DAC	5/1/95
DRN	KAS	5/1/95
CHKD	MAG	5/1/95

1 ft = 0.3048 m
1 in. = 25.4 mm

HORIZONTALLY CURVED STEEL BRIDGE RESEARCH PROJECT
FEDERAL HIGHWAY ADMINISTRATION
[illegible]61-92-C-00136

I-GIRDER COMPONENT TESTING
TEST FRAME PLAN

SHEET 4 OF 27
SCALE AS NOTED
CONTRACT HDR01
DWG. NO. HB1-003
REV. 3

REV NO	DESCRIPTION	DATE	REVISION RECORD	MADE BY	CHECKED BY
1	REVISED NO. OF SHEETS	2/23/96	ADDENDUM #2 TO CONTRACT	DAC	MAG

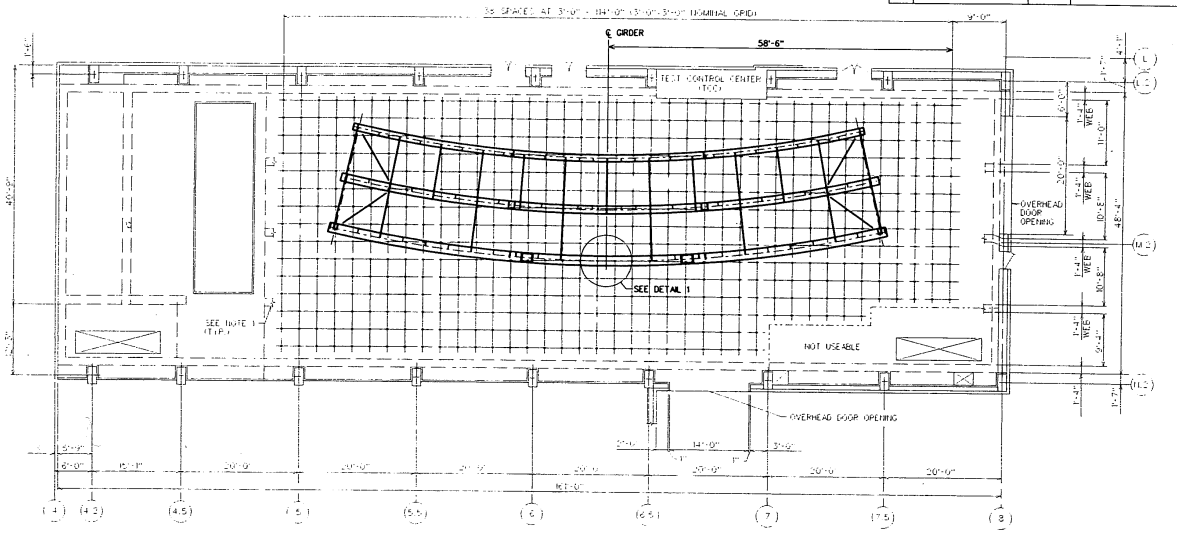

TEST FRAME LOCATION PLAN

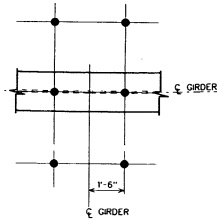

DETAIL 1
SCALE-½"-1'-0"

NOTE:
1. THIS PLAN TO BE USED IN PLACING THE TEST FRAME IN THE LABORATORY.

2.92

1 ft = 0.3048 m
1 in. = 25.4 mm

ENG	DAC	5/1/95
DRN	KAS	5/1/95
CHKD	MAG	5/1/95

Figure 2.22

HORIZONTALLY CURVED STEEL BRIDGE RESEARCH PROJECT
FEDERAL HIGHWAY ADMINISTRATION
DTFH61-92-C-00136

I-GIRDER COMPONENT TESTING LOCATION PLAN

SHEET 3 OF 27
SCALE AS NOTED
CONTRACT HDR01
DWG. NO. HB1-002
REV. 1

REV NO	DESCRIPTION	DATE	REVISION RECORD	MADE BY	CHECKED BY
1	REMOVE CROSS-FRAME TYPE AND ADDED CONNECTION PLATES	6/2/95	ADDENDUM TO BID DOCUMENTS	DAC	MAG
2	REVISED SUPPORT STRUCTURES AND ADDED ABUT CA1 & CA2	2/23/96	ADDENDUM #2 TO CONTRACT	DAC	MAG
3	REMOVED STIFFENERS ON FASCIA SIDE OF G1 & G3 AT CROSS FRAME LINES	10/7/96	ADDENDUM #3 TO CONTRACT	MAG	JDC

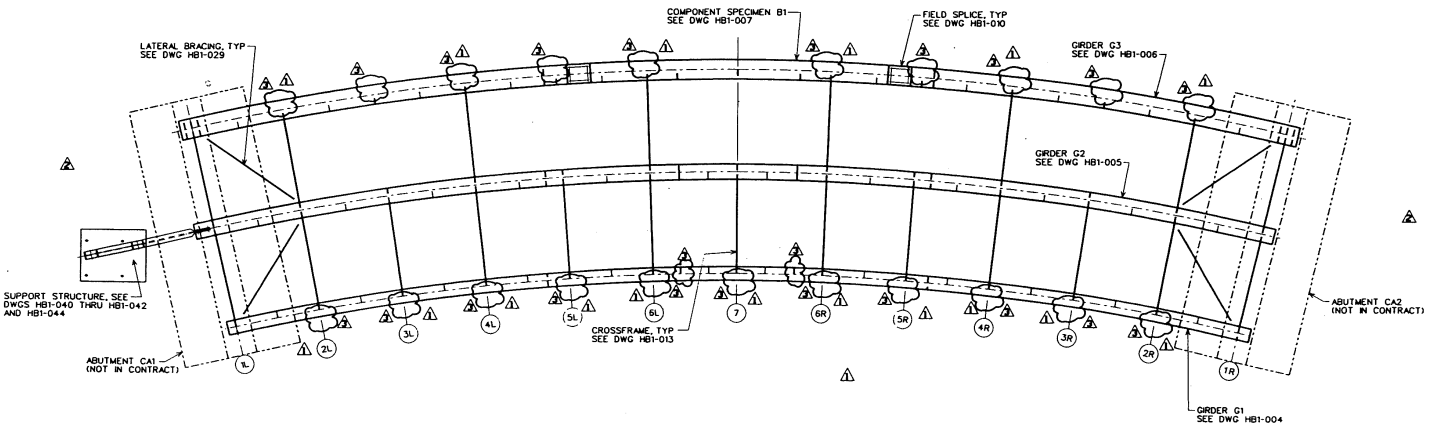

TEST FRAME ERECTION PLAN
SCALE: 1/4" - 1'-0"

NOTES:
1. FOR LOCATION OF TEST FRAME IN LABORATORY, SEE DWG HB1-002.
2. MARK EACH PIECE CLEARLY WITH AN INDELIBLE MARK, INCLUDING EXTRA PIECES NOT TO BE INSTALLED ACCORDING TO THIS ERECTION PLAN. PROVIDE A LIST OF THE MARKS WITH THE SHOP DRAWINGS.

2.93

Figure 2.23

ENG	MAG	5/1/95
DRN	KAS	5/1/95
CHKD	DAC	5/1/95

HORIZONTALLY CURVED STEEL BRIDGE RESEARCH PROJECT
FEDERAL HIGHWAY ADMINISTRATION
DTFH61-92-C-00136

I-GIRDER COMPONENT TESTING
ERECTION PLAN

SHEET 5 OF 27
SCALE AS NOTED
CONTRACT HDR01
DWG. NO. HB1-027
REV. 3

REV NO	DESCRIPTION	DATE	REVISION RECORD	MADE BY	CHECKED BY
1	REV DIMENSIONS	7/21/95	ADDENDUM TO BID DOCUMENTS	DAC	MAG
2	REVISED NO. OF SHEETS	2/23/96	ADDENDUM #2 TO CONTRACT	DAC	MAG
3	REMOVED STIFFENERS ON FASCIA SIDE OF G3 AT CROSS FRAME LINES	10/8/96	ADDENDUM #3 TO CONTRACT	MAG	JDC

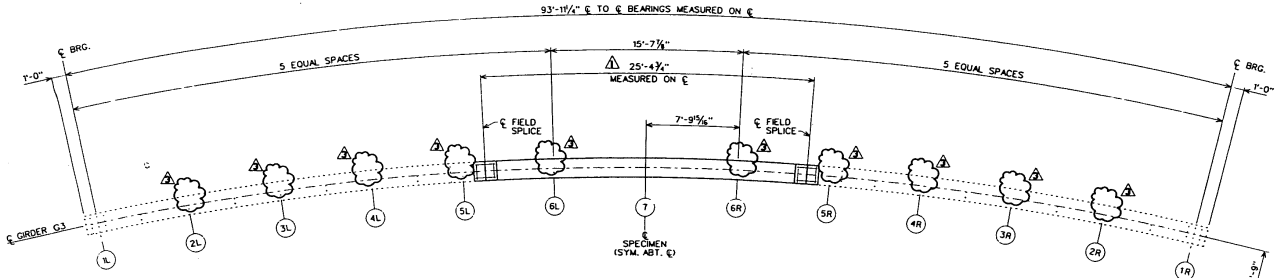

PLAN - BENDING SPECIMEN INSTALLATION

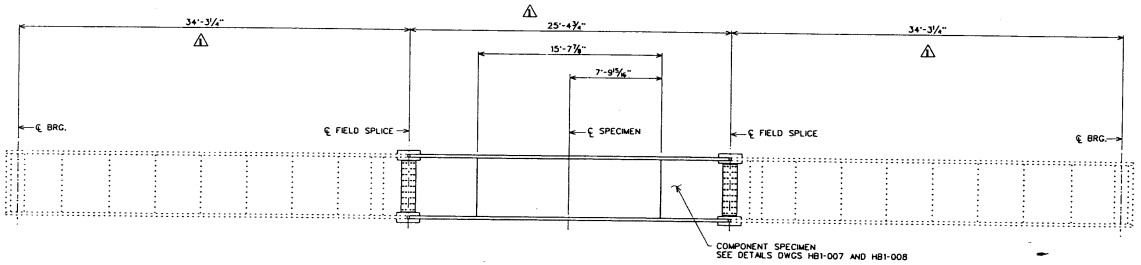

ELEVATION - BENDING SPECIMEN INSTALLATION
(FOR GIRDER G3 - SEE DWG. HB1-006)

2.94

NOTES:
1. SEE DWG HB1-010 FOR FIELD SPLICE DETAILS.
2. ALL LONGITUDINAL DIMENSIONS ARE ARC LENGTHS MEASURED ON THE GIRDER AND SPECIMEN CENTERLINES.

Figure 2.24

1 ft = 0.3048 m
1 in. = 25.4 mm

ENG	MAG	5/1/95
DRN	KAS	5/1/95
CHKD	DAC	5/1/95

HORIZONTALLY CURVED STEEL BRIDGE RESEARCH PROJECT
FEDERAL HIGHWAY ADMINISTRATION
DTFH61-92-C-00136

I-GIRDER COMPONENT TESTING
PLAN AND ELEVATION - COMPONENT SETUP

SHEET 9 OF 27
SCALE 1/4"=1'-0"
CONTRACT HDR01
DWG. NO. HB1-009
REV. 3

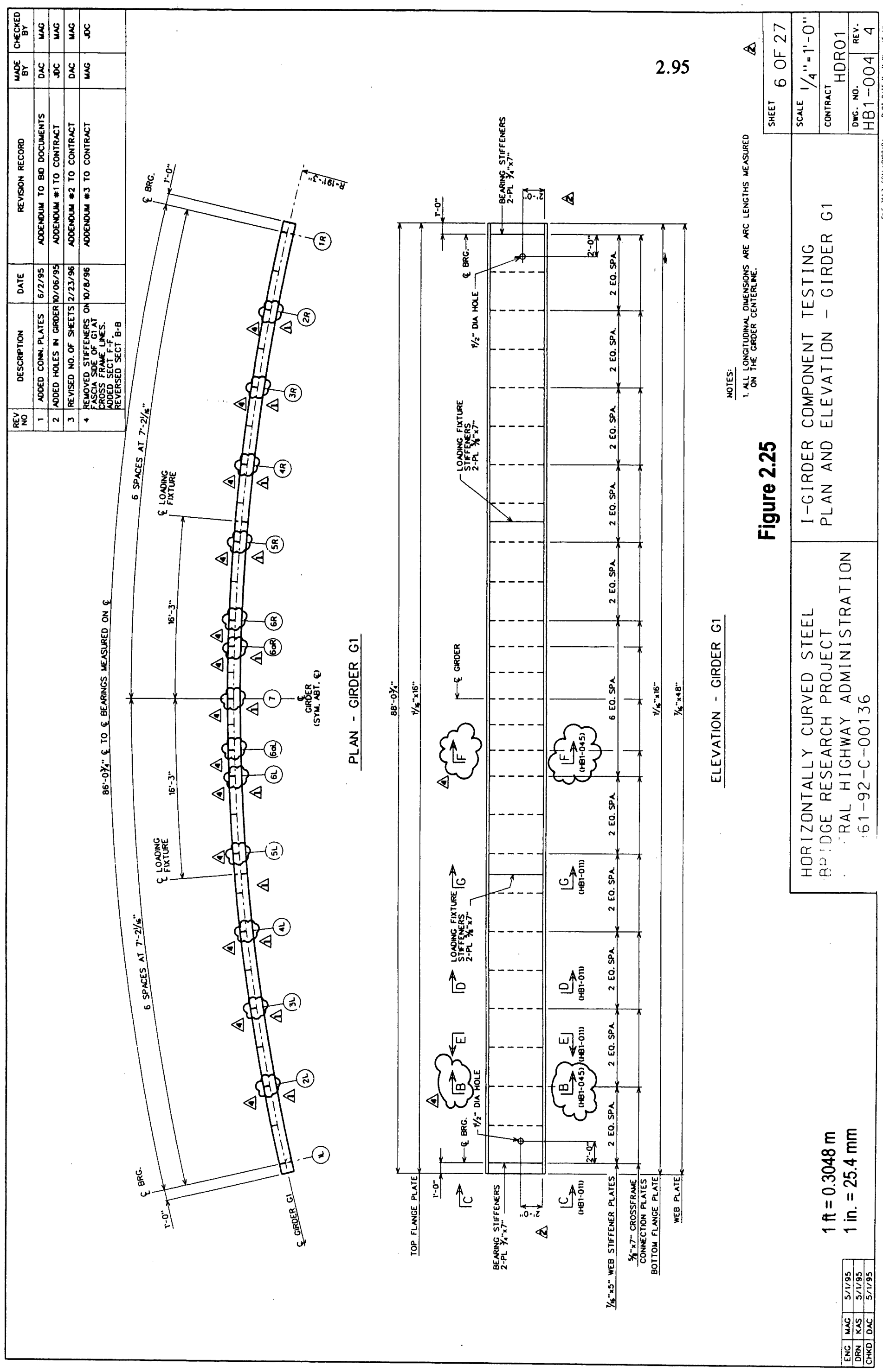
PLAN - GIRDER G1
ELEVATION - GIRDER G1
86'-0¾" ℄ TO ℄ BEARINGS MEASURED ON ℄
6 SPACES AT 7'-2¼"
88'-0¾"
I-GIRDER COMPONENT TESTING
PLAN AND ELEVATION - GIRDER G1
SHEET 6 OF 27
SCALE ¼"=1'-0"
CONTRACT HDR01
DWG. NO. HB1-004
REV. 4
NOTES:
1. ALL LONGITUDINAL DIMENSIONS ARE ARC LENGTHS MEASURED ON THE GIRDER CENTERLINE.
1 ft = 0.3048 m
1 in. = 25.4 mm
2.95
Figure 2.25

1 ft = 0.3048 m
1 in. = 25.4 mm
1 ksi = 6.8948 MPa

REV NO	DESCRIPTION	DATE	REVISION RECORD	MADE BY	CHECKED BY
1	REV CONN PLATE	7/21/95	ADDENDUM TO BID DOCUMENTS	DAC	MAG
2	ADDED HOLES IN GIRDER	10/06/95	ADDENDUM #1 TO CONTRACT	JDC	MAG
3	REV LOAD FIXTURE CONN DETAILS, REV SEC MARK, ADDED HOLE IN GIRDER & ADDED SHOP SPLICES	2/23/96	ADDENDUM #2 TO CONTRACT	DAC	MAG
4	CHANGED SECT B-B TO SECT H-H, ADDED SECT V-V, CHANGED SECT C-C TO SECT L-L, ADDED NOTE 2.	10/8/96	ADDENDUM #3 TO CONTRACT	MAG	JDC

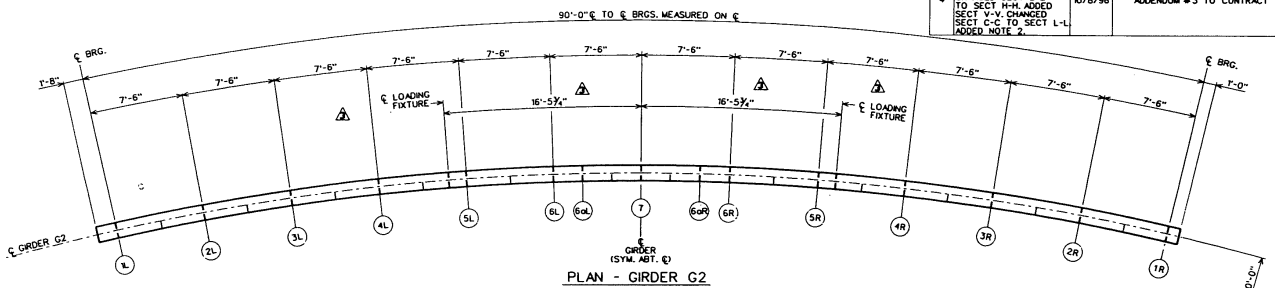

PLAN - GIRDER G2

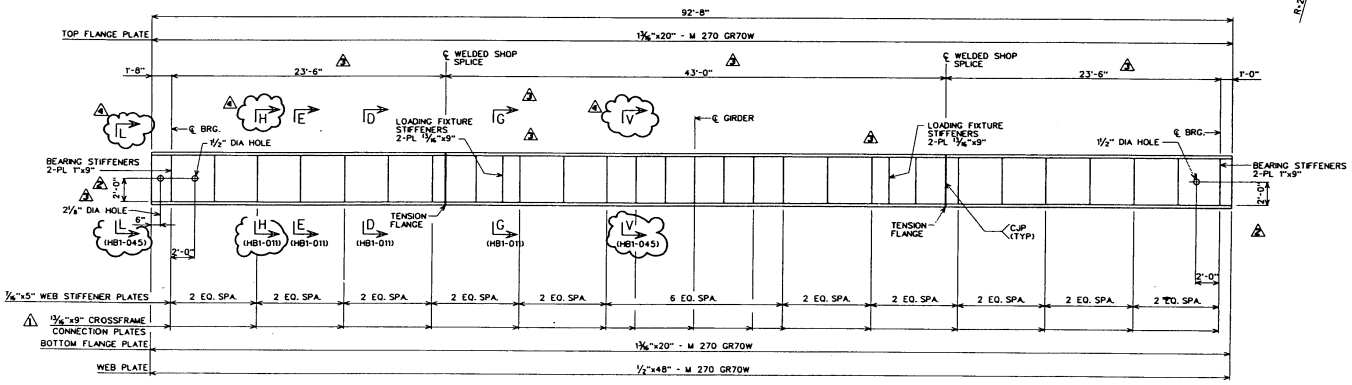

ELEVATION - GIRDER G2

2.96

Figure 2.26

NOTES:
1. ALL LONGITUDINAL DIMENSIONS ARE ARC LENGTHS MEASURED ON THE GIRDER CENTERLINE.
2. AT WELDED SHOP SPLICES, OFFSET FLANGE AND WEB SPLICES LONGITUDINALLY BY 1'-0".

ENG	MAG	5/1/95
DRN	KAS	5/1/95
CHKD	DAC	5/1/95

HORIZONTALLY CURVED STEEL BRIDGE RESEARCH PROJECT
FEDERAL HIGHWAY ADMINISTRATION
DTFH61-92-C-00136

I-GIRDER COMPONENT TESTING
PLAN AND ELEVATION - GIRDER G2

SHEET 7 OF 27
SCALE 1/4"=1'-0"
CONTRACT HDR01
DWG. NO. HB1-005
REV. 4

REV NO	DESCRIPTION	DATE	REVISION RECORD	MADE BY	CHECKED BY
1	ADDED CONN. PLATES	6/2/95	ADDENDUM TO BID DOCUMENTS	DAC	MAG
2	REV DIMENSIONS	7/21/95	ADDENDUM TO BID DOCUMENTS	DAC	MAG
3	ADDED HOLES IN GIRDER	10/06/95	ADDENDUM #1 TO CONTRACT	JDC	MAG
4	REPLACED CONN. PLATES WITH STIFFENERS.	2/23/96	ADDENDUM #2 TO CONTRACT	DAC	MAG
5	REMOVED STIFFENERS ON FASCIA SIDE OF G3 AT CROSS FRAME LINES. CHANGED SECT B-B TO SECT J-J & SECT C-C TO SECT M-M. ADDED SECT K-K.	10/8/96	ADDENDUM #3 TO CONTRACT	MAG	JDC

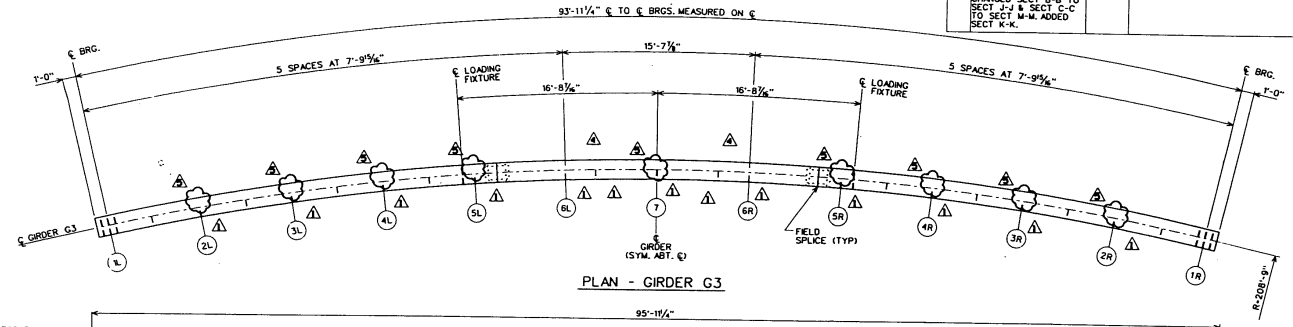

PLAN - GIRDER G3

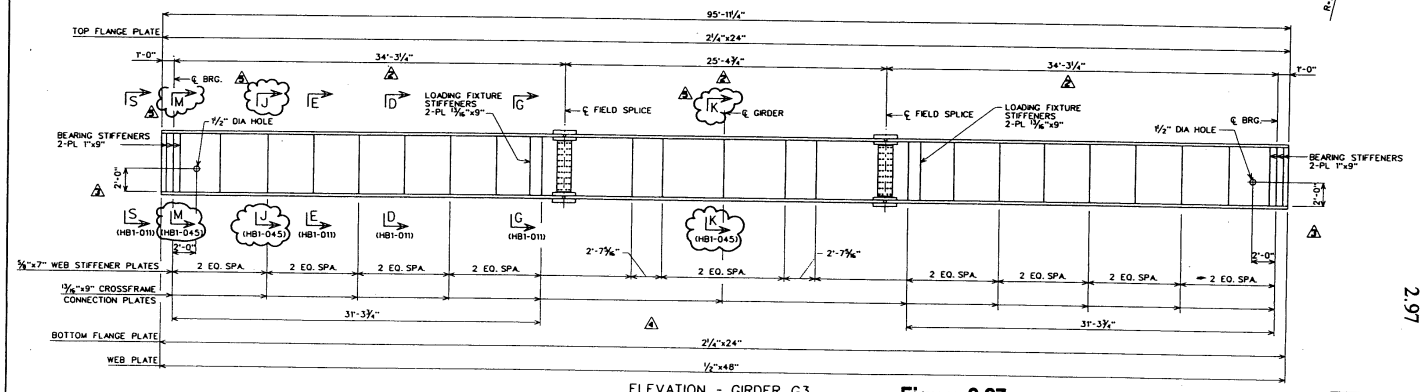

ELEVATION - GIRDER G3

Figure 2.27

2.97

1 ft = 0.3048 m
1 in. = 25.4 mm

NOTES:
1. SEE DWG HB1-010 FOR FIELD SPLICE DETAILS.
2. ALL LONGITUDINAL DIMENSIONS ARE ARC LENGTHS MEASURED ON THE GIRDER CENTERLINE.

ENG	MAG	5/1/95
DRN	KAS	5/1/95
CHKD	DAC	5/1/95

HORIZONTALLY CURVED STEEL BRIDGE RESEARCH PROJECT
FEDERAL HIGHWAY ADMINISTRATION
DTFH61-92-C-00136

I-GIRDER COMPONENT TESTING
PLAN AND ELEVATION - GIRDER G3

SHEET 8 OF 27
SCALE 1/4"=1'-0"
CONTRACT HDR01
DWG. NO. HB1-006
REV. 5

REV NO	DESCRIPTION	DATE	REVISION RECORD	MADE BY	CHECKED BY
1	REVISED CAMBERS FOR FUTURE DECK	9/21/95	ADDENDUM #1 TO CONTRACT	JDC	MAG
2	REVISED CAMBERS AND REVISED NO. OF SHEETS	2/23/96	ADDENDUM #2 TO CONTRACT	DAC	MAG

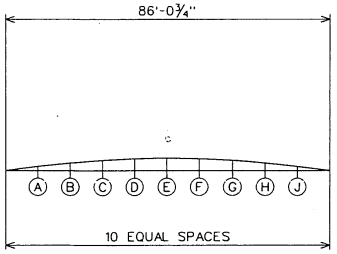

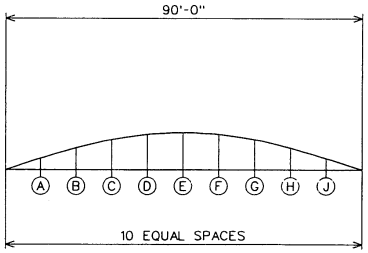

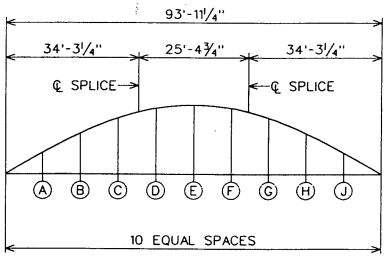

⚠1

GIRDER G1	
LOCATION	"Y" IN INCHES
℄ BRG	0.000
A	0.370
B	0.690
C	0.940
D	1.100
E	1.150
F	1.100
G	0.940
H	0.690
J	0.370
℄ BRG	0.000

⚠2

⚠1

GIRDER G2	
LOCATION	"Y" IN INCHES
℄ BRG	0.000
A	0.710
B	1.350
C	1.850
D	2.170
E	2.280
F	2.170
G	1.850
H	1.350
J	0.710
℄ BRG	0.000

⚠2

⚠1

GIRDER G3	
LOCATION	"Y" IN INCHES
℄ BRG	0.000
A	1.060
B	2.020
C	2.780
℄ SPLICE	3.110
D	3.290
E	3.470
F	3.290
℄ SPLICE	3.110
G	2.780
H	2.020
J	1.060
℄ BRG	0.000

⚠2

2.98

Figure 2.28

1 ft = 0.3048 m
1 in. = 25.4 mm

ENG	DAC	5/1/95
DRN	JEM	5/1/95
CHKD	MAG	5/1/95

HORIZONTALLY CURVED STEEL
BRIDGE RESEARCH PROJECT
FEDERAL HIGHWAY ADMINISTRATION
DTFH61-92-C-00136

I-GIRDER COMPONENT TESTING
CAMBER DIAGRAM

SHEET 26 OF 27
SCALE AS NOTED
CONTRACT HDR01
DWG. NO. HB1-025 REV. 2

I&E 7552 DGN: HB1025R2 PLOT DATE: 02-28-96 AS-2+

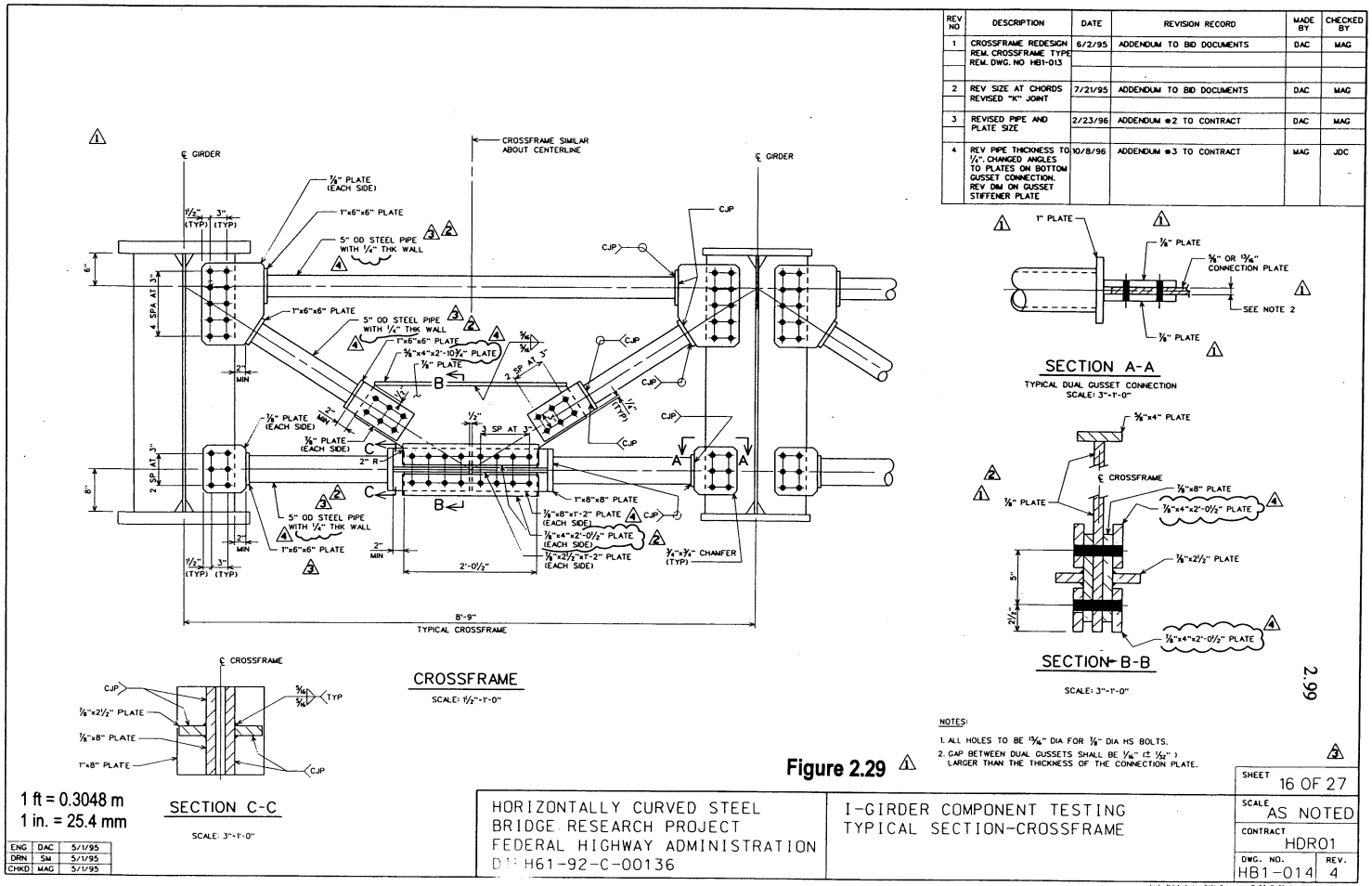

CROSSFRAME

SCALE: ½"-1'-0"

SECTION C-C

SCALE: 3"-1'-0"

REV NO	DESCRIPTION	DATE	REVISION RECORD	MADE BY	CHECKED BY
1	CROSSFRAME REDESIGN REM. CROSSFRAME TYPE REM. DWG. NO H61-013	6/2/95	ADDENDUM TO BID DOCUMENTS	DAC	MAG
2	REV SIZE AT CHORDS REVISED "K" JOINT	7/21/95	ADDENDUM TO BID DOCUMENTS	DAC	MAG
3	REVISED PIPE AND PLATE SIZE	2/23/96	ADDENDUM #2 TO CONTRACT	DAC	MAG
4	REV PIPE THICKNESS TO ½", CHANGED ANGLES TO PLATES ON BOTTOM GUSSET CONNECTION. REV DIM ON GUSSET STIFFENER PLATE	10/8/96	ADDENDUM #3 TO CONTRACT	MAG	JDC

SECTION A-A

TYPICAL DUAL GUSSET CONNECTION

SCALE: 3"-1'-0"

SECTION B-B

SCALE: 3"-1'-0"

2.99

NOTES:

1. ALL HOLES TO BE 13/16" DIA FOR ⅞" DIA HS BOLTS.
2. GAP BETWEEN DUAL GUSSETS SHALL BE ¼" (± ⅛") LARGER THAN THE THICKNESS OF THE CONNECTION PLATE.

Figure 2.29

1 ft = 0.3048 m
1 in. = 25.4 mm

ENG	DAC	5/1/95
DRN	SM	5/1/95
CHKD	MAG	5/1/95

HORIZONTALLY CURVED STEEL BRIDGE RESEARCH PROJECT
FEDERAL HIGHWAY ADMINISTRATION
D[illegible] H61-92-C-00136

I-GIRDER COMPONENT TESTING
TYPICAL SECTION-CROSSFRAME

SHEET 16 OF 27
SCALE AS NOTED
CONTRACT HDR01
DWG. NO. HB1-014
REV. 4

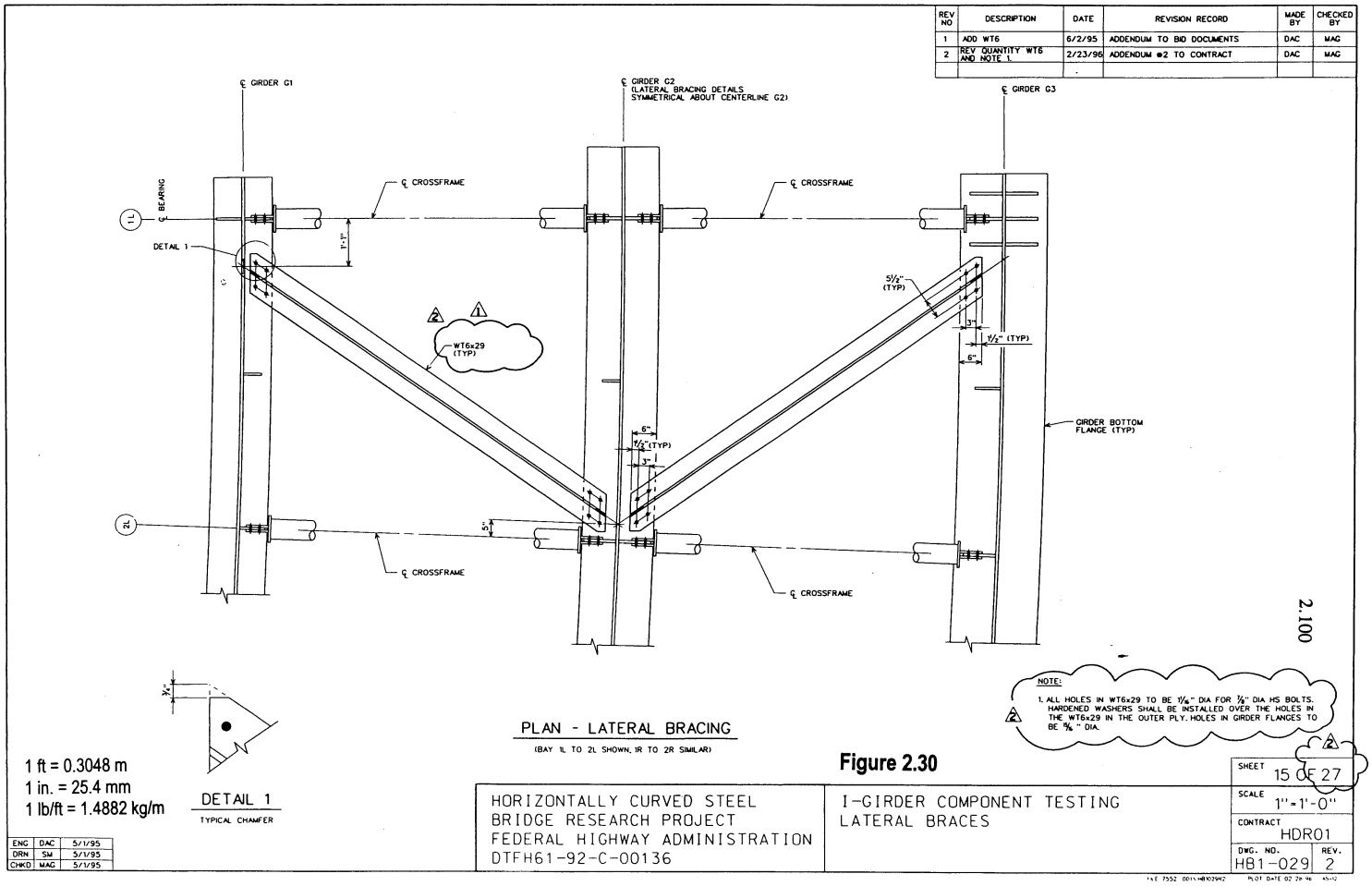
REV NO | DESCRIPTION | DATE | REVISION RECORD | MADE BY | CHECKED BY
1 | ADD WT6 | 6/2/95 | ADDENDUM TO BID DOCUMENTS | DAC | MAC
2 | REV QUANTITY WT6 AND NOTE 1 | 2/23/96 | ADDENDUM #2 TO CONTRACT | DAC | MAC
℄ GIRDER G1
℄ GIRDER G2 (LATERAL BRACING DETAILS SYMMETRICAL ABOUT CENTERLINE G2)
℄ GIRDER G3
℄ BEARING
℄ CROSSFRAME
DETAIL 1
WT6x29 (TYP)
5½" (TYP)
1½" (TYP)
GIRDER BOTTOM FLANGE (TYP)
2.100
NOTE:
1. ALL HOLES IN WT6x29 TO BE 15/16" DIA FOR ⅞" DIA HS BOLTS. HARDENED WASHERS SHALL BE INSTALLED OVER THE HOLES IN THE WT6x29 IN THE OUTER PLY. HOLES IN GIRDER FLANGES TO BE ⅞" DIA.
PLAN - LATERAL BRACING
(BAY 1L TO 2L SHOWN, 1R TO 2R SIMILAR)
DETAIL 1
TYPICAL CHAMFER
1 ft = 0.3048 m
1 in. = 25.4 mm
1 lb/ft = 1.4882 kg/m
ENG DAC 5/1/95
DRN SM 5/1/95
CHKD MAC 5/1/95
HORIZONTALLY CURVED STEEL BRIDGE RESEARCH PROJECT
FEDERAL HIGHWAY ADMINISTRATION
DTFH61-92-C-00136
I-GIRDER COMPONENT TESTING
LATERAL BRACES
SHEET 15 OF 27
SCALE 1"=1'-0"
CONTRACT HDR01
DWG. NO. HB1-029
REV. 2

Figure 2.30

REV NO	DESCRIPTION	DATE	REVISION RECORD	MADE BY	CHECKED BY
1	REMOVED 2 DETAILS, REV REMAINING DETAILS & NOTES	10/06/95	ADDENDUM #1 TO CONTRACT	JDC	MAG
2	REVISED NOTES 1 AND 2, REVISED NO. OF SHEETS	2/23/96	ADDENDUM #2 TO CONTRACT	DAC	MAG

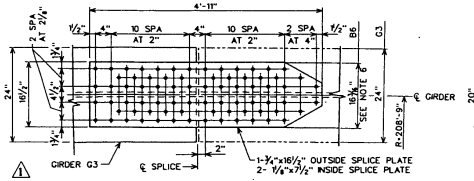

TOP FLANGE SPLICE PLATES
TOP FLANGE BOLTING DETAIL
FOR GIRDER G3 AND SPECIMEN B6

SCALE: 1"-1'-0"

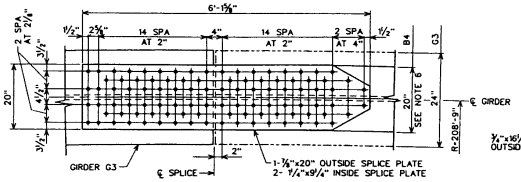

BOTTOM FLANGE SPLICE PLATES
BOTTOM FLANGE BOLTING DETAIL
FOR GIRDER G3 AND SPECIMEN B4

SCALE: 1"-1'-0"

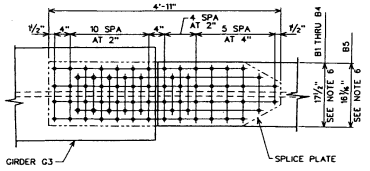

TOP FLANGE BOLTING DETAIL
FOR SPECIMENS B1 THRU B5

(FOR INFORMATION AND DETAILS NOT SHOWN, SEE DETAIL ABOVE)

SCALE: 1"-1'-0"

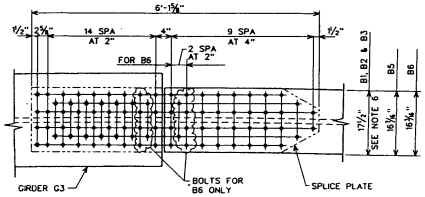

BOTTOM FLANGE BOLTING DETAIL
FOR SPECIMENS B1, B2, B3, B5 AND B6

(FOR INFORMATION AND DETAILS NOT SHOWN, SEE DETAIL ABOVE)

SCALE: 1"-1'-0"

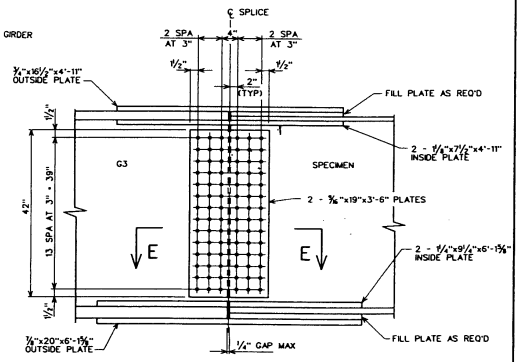

TYPICAL FIELD SPLICE ELEVATION

SCALE: 1"-1'-0"

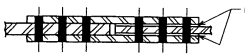

SECTION E-E

NO SCALE

NOTES:

2. 1. ALL HOLES TO BE ⅝" DIA FOR ⅞" DIA HS BOLTS, (UNLESS NOTED).
2. ALL STEEL TO BE AASHTO M270 GRADE 50 (EXCEPT FILL PLATES). FILL PLATES SHALL BE ASTM A36 STEEL.
3. THE SAME SPLICE PLATES ARE USED TO SPLICE EACH SPECIMEN INTO GIRDER G3. SPLICE PLATES WILL BE REUSED IN EACH TEST.
4. NEW BOLTS WILL BE USED TO SPLICE EACH SPECIMEN INTO GIRDER G3. NO BOLTS ARE TO BE REUSED.
5. PREPARE ONE (1) COMPLETE DUPLICATE SET OF FLANGE AND WEB SPLICE PLATES.
1. 6. DIMENSIONS GIVEN FOR SPECIMEN FLANGES MAY VARY DEPENDING ON THE RESULTS FROM THE TENSILE TESTS AND THE ACTUAL MEASURED FLANGE PLATE THICKNESSES. MAXIMUM POSSIBLE FLANGE-PLATE WIDTHS ARE GIVEN IN THE TABLES ON DWGS HB1-007 AND HB1-008. 2

2.101

Figure 2.31

ENG	JDC	5/1/95
DRN	SM	5/1/95
CHKD	MAG	5/1/95

1 ft = 0.3048 m
1 in. = 25.4 mm

LEGEND:
● - PROVIDE BOLT
○ - DO NOT PROVIDE BOLT

HORIZONTALLY CURVED STEEL BRIDGE RESEARCH PROJECT
FEDERAL HIGHWAY ADMINISTRATION
D[illegible]-92-C-00136

I-GIRDER COMPONENT TESTING
FIELD SPLICES

SHEET 12 OF 27
SCALE AS NOTED
CONTRACT HDR01
DWG. NO. HB1-010 REV. 2

REV NO	DESCRIPTION	DATE	REVISION RECORD	MADE BY	CHECKED BY

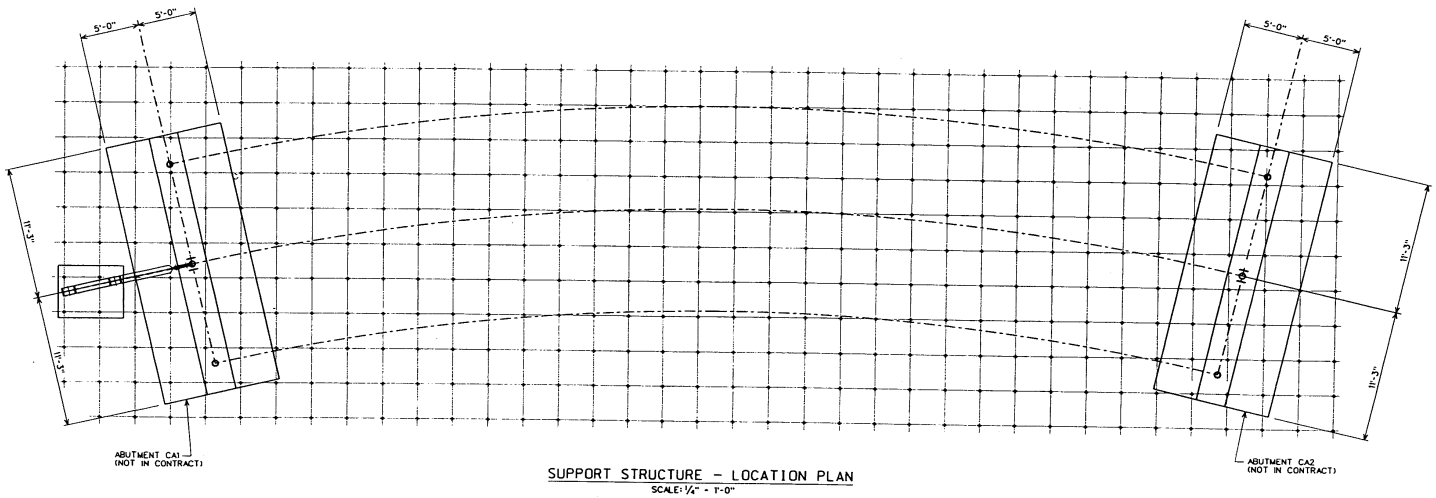

SUPPORT STRUCTURE - LOCATION PLAN
SCALE: 1/4" = 1'-0"

LEGEND:

O - NON-GUIDED BEARING

O - GUIDED BEARING (IN DIRECTION INDICATED)

NOTES:

1. FOR SUPPORT STRUCTURE DETAILS, SEE DRAWINGS HB1-040, HB1-041 AND HB1-042.
2. FOR BEARING DETAILS, SEE DRAWING HB1-044.

2.102

Figure 2.32

ENG	DAC	2/23/96
DRN	KAS	2/23/96
CHKD	MAG	2/23/96

1 ft = 0.3048 m
1 in. = 25.4 mm

HORIZONTALLY CURVED STEEL
BRIDGE RESEARCH PROJECT
FEDERAL HIGHWAY ADMINISTRATION
DTFH61-92-C-00136

I-GIRDER COMPONENT TESTING
SUPPORT STRUCTURE - LOCATION PLAN

SHEET	17 OF 27
SCALE	AS NOTED
CONTRACT	HDR01
DWG. NO.	HB1-039
REV.	0

REV NO	DESCRIPTION	DATE	REVISION RECORD	MADE BY	CHECKED BY

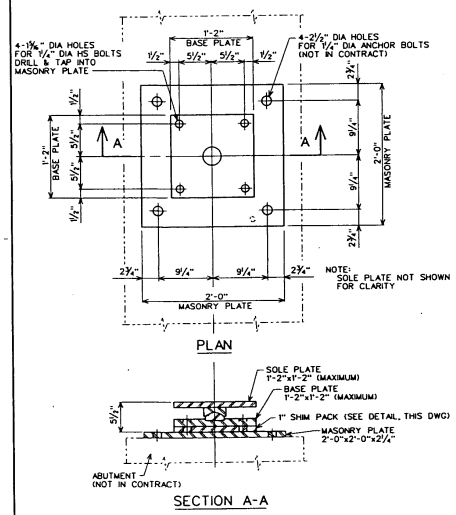

BEARING AT GIRDER G1
SCALE: 3"-1'-0"

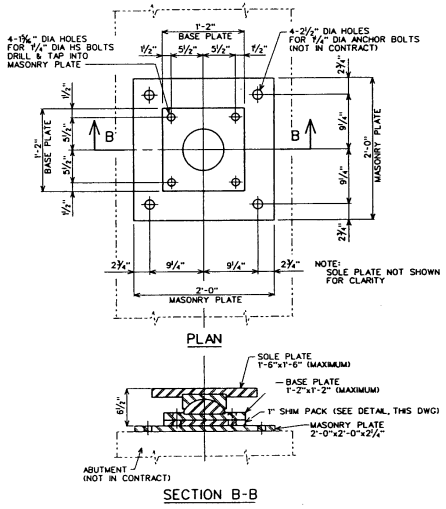

BEARING AT GIRDER G2
SCALE: 3"-1'-0"

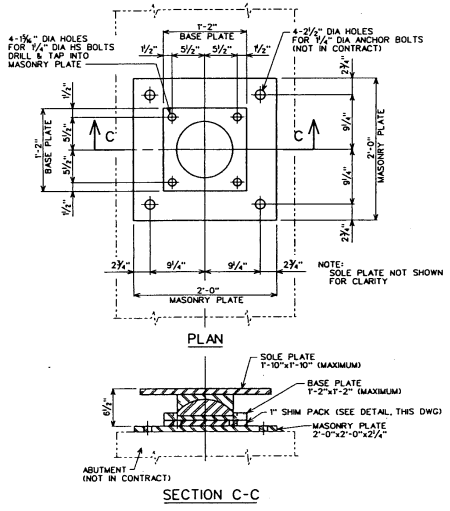

BEARING AT GIRDER G3
SCALE: 3"-1'-0"

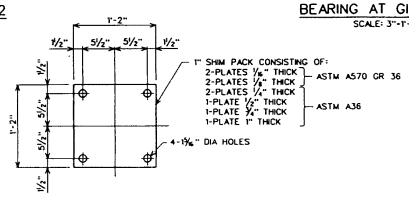

DETAIL - SHIM PACK
SCALE: 3"-1'-0"

NOTES:
1. USE MERRIMAN "LUBRITE F" SPHERICAL EXPANSION BEARINGS OR EQUAL APPROVED BY THE ENGINEER.
   UNIT LOAD - 6.0 ksi
2. SEE ALSO PART IV SECTION D.1(A) OF THE TECHNICAL SPECIFICATIONS RELATED TO THE BEARINGS.

2.103

1 ft = 0.3048 m
1 in. = 25.4 mm
1 kip = 4.4482 kN
1 ksi = 6.8948 MPa

Figure 2.33

BEARING DESIGN PARAMETERS

GIRDER	MAXIMUM VERTICAL LOAD	MINIMUM DEAD LOAD	MAXIMUM HORIZONTAL LOAD	MAXIMUM ROTATIONS		MAXIMUM MOVEMENTS	
				ABOUT RADIAL AXIS	ABOUT LONGIT AXIS	RADIAL	LONGIT
G1	100k	3k	10k	2.1°	1.5°	0.8"	1.8"
G2	275k	14k	38k	4.5°	1.5°	FIXED	2.3"
G3	375k	29k	38k	6.0°	1.5°	0.8"	1.8"

ENG	DAC	2/23/96
DRN	KAS	2/23/96
CHKD	MAG	2/23/96

HORIZONTALLY CURVED STEEL BRIDGE RESEARCH PROJECT
FEDERAL HIGHWAY ADMINISTRATION
(TFH61-92-C-00136

I-GIRDER COMPONENT TESTING
SUPPORT STRUCTURE - BEARING DETAILS

SHEET	21 OF 27
SCALE	AS NOTED
CONTRACT	HDR01
DWG. NO.	HB1-044
REV.	0

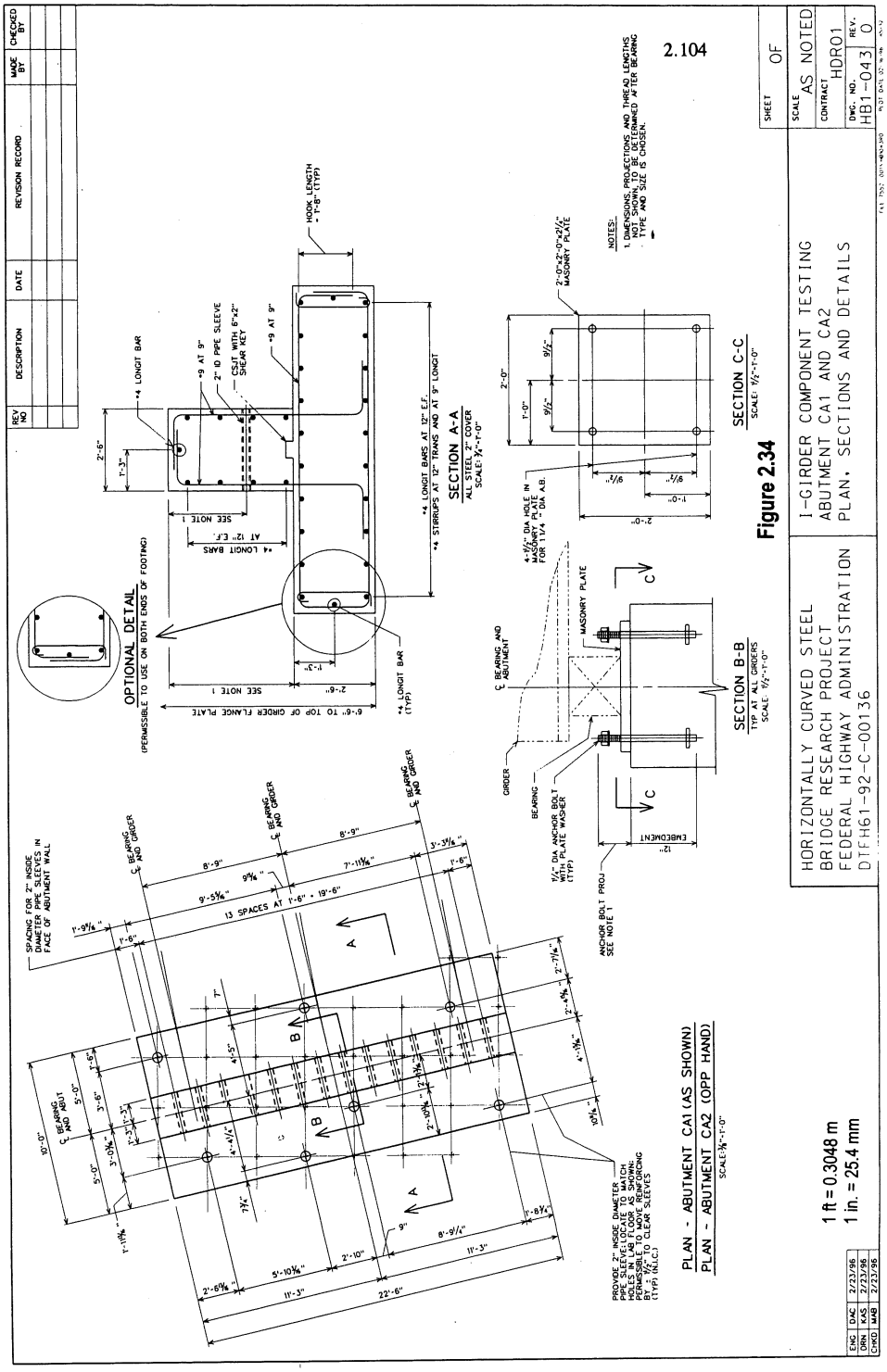
2.104
HORIZONTALLY CURVED STEEL
BRIDGE RESEARCH PROJECT
FEDERAL HIGHWAY ADMINISTRATION
DTFH61-92-C-00136
I-GIRDER COMPONENT TESTING
ABUTMENT CA1 AND CA2
PLAN. SECTIONS AND DETAILS
SCALE AS NOTED
CONTRACT HDR01
DWG. NO. HB1-043
REV. 0
SHEET OF
REV NO
DESCRIPTION
DATE
REVISION RECORD
MADE BY
CHECKED BY
ENG DAC 2/23/96
DRN KAS 2/23/96
CHKD MAB 2/23/96
PLAN - ABUTMENT CA1 (AS SHOWN)
PLAN - ABUTMENT CA2 (OPP HAND)
SCALE: 3/4"=1'-0"
OPTIONAL DETAIL
(PERMISSIBLE TO USE ON BOTH ENDS OF FOOTING)
SECTION A-A
ALL STEEL 2" COVER
SCALE: 3/4"=1'-0"
SECTION B-B
TYP AT ALL GIRDERS
SCALE: 1/2"=1'-0"
SECTION C-C
SCALE: 1/2"=1'-0"
NOTES:
1. DIMENSIONS, PROJECTIONS AND THREAD LENGTHS NOT SHOWN, TO BE DETERMINED AFTER BEARING TYPE AND SIZE IS CHOSEN.
Figure 2.34
1 ft = 0.3048 m
1 in. = 25.4 mm

REV NO	DESCRIPTION	DATE	REVISION RECORD	MADE BY	CHECKED BY
1	CHANGE SHEET NUMBER	6/2/95	ADDENDUM TO BID DOCUMENTS	DAC	MAG

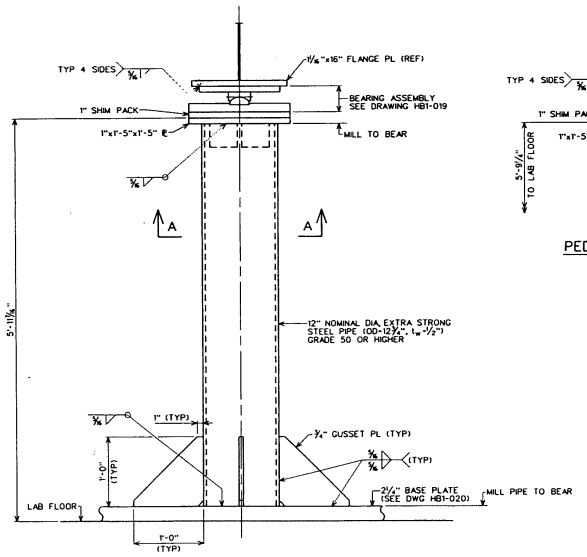

ELEVATION B-B
PEDESTAL AT GIRDER G1R AND G1L
TAKEN FROM DWG HB1-020
SCALE: 1½"-1'-0"

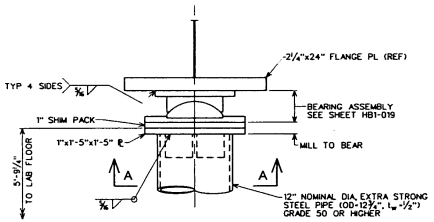

PARTIAL ELEVATION C-C
PEDESTAL AT GIRDER G3R AND G3L
TAKEN FROM DWG HB1-020
SCALE: 1½"-1'-0"
FOR INFORMATION NOT SHOWN, SEE ELEVATION B-B

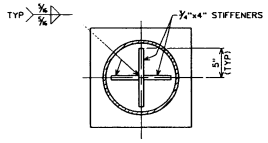

SECTION A-A
SCALE: 1½"-1'-0"

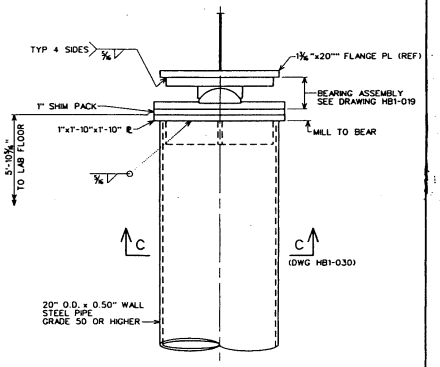

PARTIAL ELEVATION D-D
PEDESTAL AT GIRDER G2R
TAKEN FROM DWG HB1-020
SCALE: 1½"-1'-0"
FOR INFORMATION NOT SHOWN, SEE ELEVATION B-B, DWG HB1-030

2.105

Figure 2.35

1 ft = 0.3048 m
1 in. = 25.4 mm

ENG	JDC	5/1/95
DRN	JEM	5/1/95
CHKD	DAC	5/1/95

HORIZONTALLY CURVED STEEL BRIDGE RESEARCH PROJECT
FEDERAL HIGHWAY ADMINISTRATION
DTFH61-92-C-00136

I-GIRDER COMPONENT TESTING
SUPPORT STRUCTURE G1L AND G1R, G2R, G3L AND G3R - ELEVATIONS

SHEET 21 OF 31
SCALE AS NOTED
CONTRACT HDR01
DWG. NO. HB1-017
REV. 1

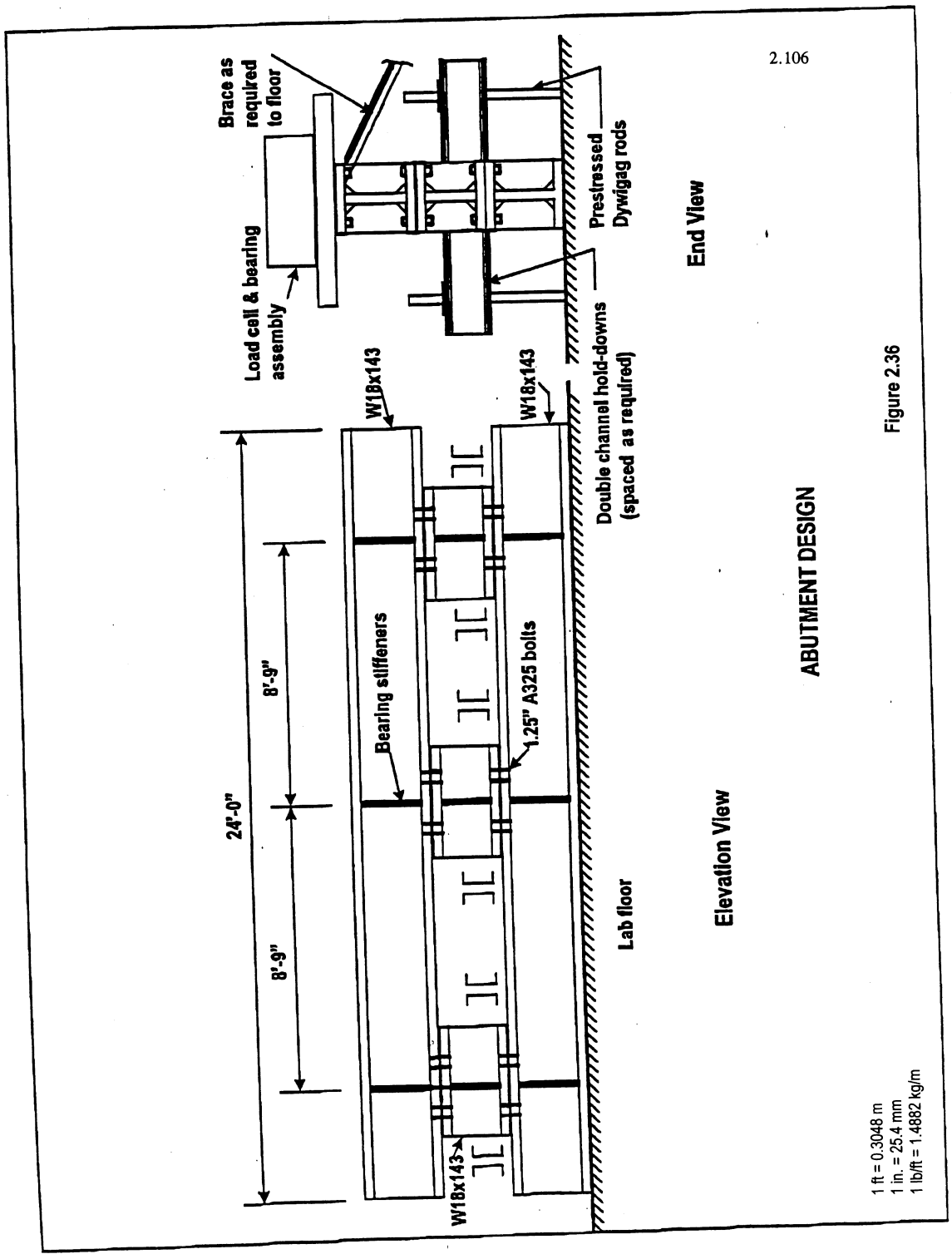
2.106
Brace as required to floor
Load cell & bearing assembly
Prestressed Dywigag rods
End View
W18x143
W18x143
Double channel hold-downs (spaced as required)
24'-0"
8'-9"
8'-9"
Bearing stiffeners
1.25" A325 bolts
W18x143
Lab floor
Elevation View
ABUTMENT DESIGN
Figure 2.36
1 ft = 0.3048 m
1 in. = 25.4 mm
1 lb/ft = 1.4882 kg/m

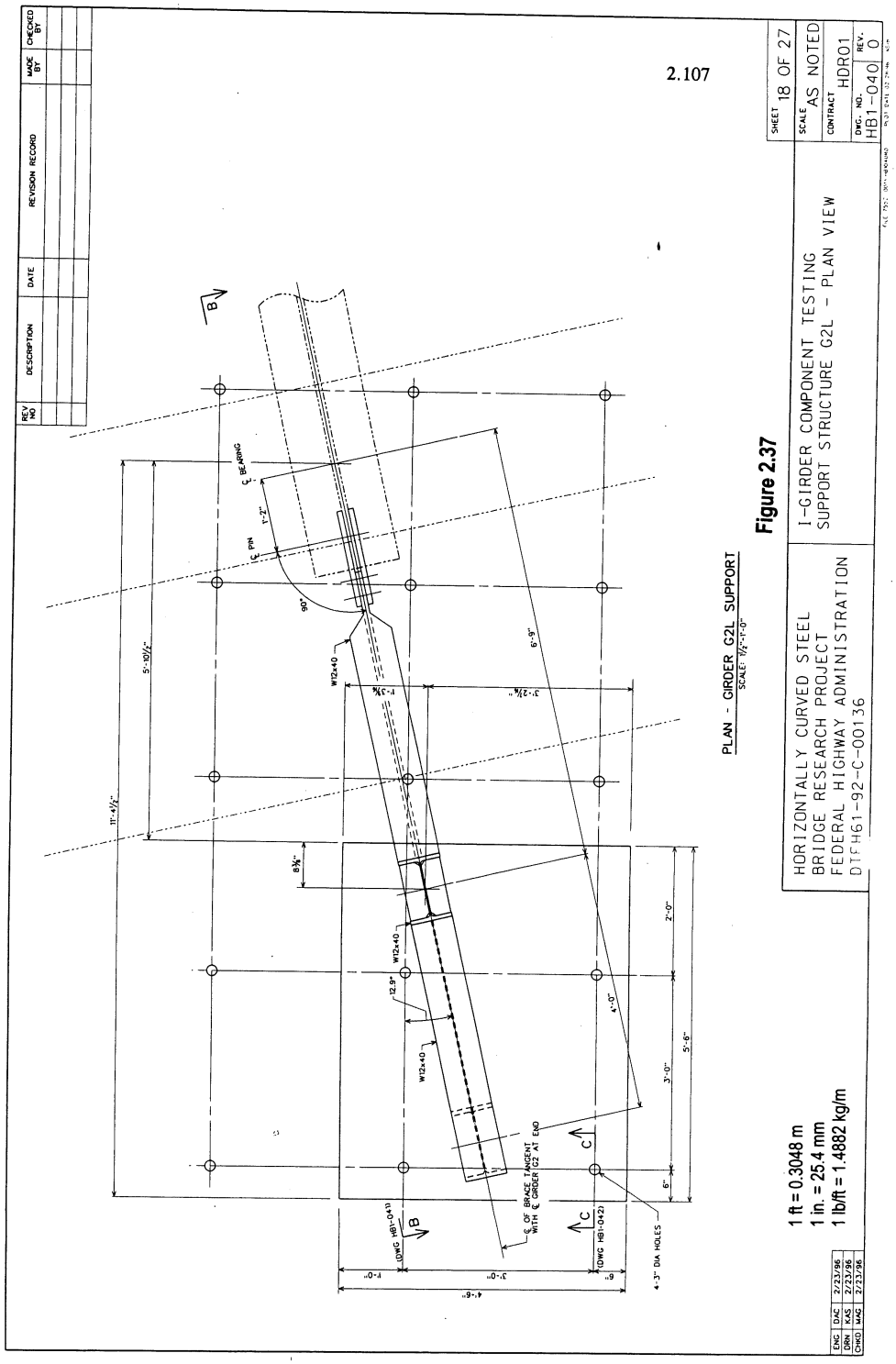
2.107
PLAN - GIRDER G2L SUPPORT
SCALE: 1½"=1'-0"
HORIZONTALLY CURVED STEEL
BRIDGE RESEARCH PROJECT
FEDERAL HIGHWAY ADMINISTRATION
DTFH61-92-C-00136
I-GIRDER COMPONENT TESTING
SUPPORT STRUCTURE G2L - PLAN VIEW
SHEET 18 OF 27
SCALE AS NOTED
CONTRACT HDR01
DWG. NO. HB1-040
REV. 0
REVISION RECORD
DESCRIPTION
DATE
MADE BY
CHECKED BY
1 ft = 0.3048 m
1 in. = 25.4 mm
1 lb/ft = 1.4882 kg/m

Figure 2.37

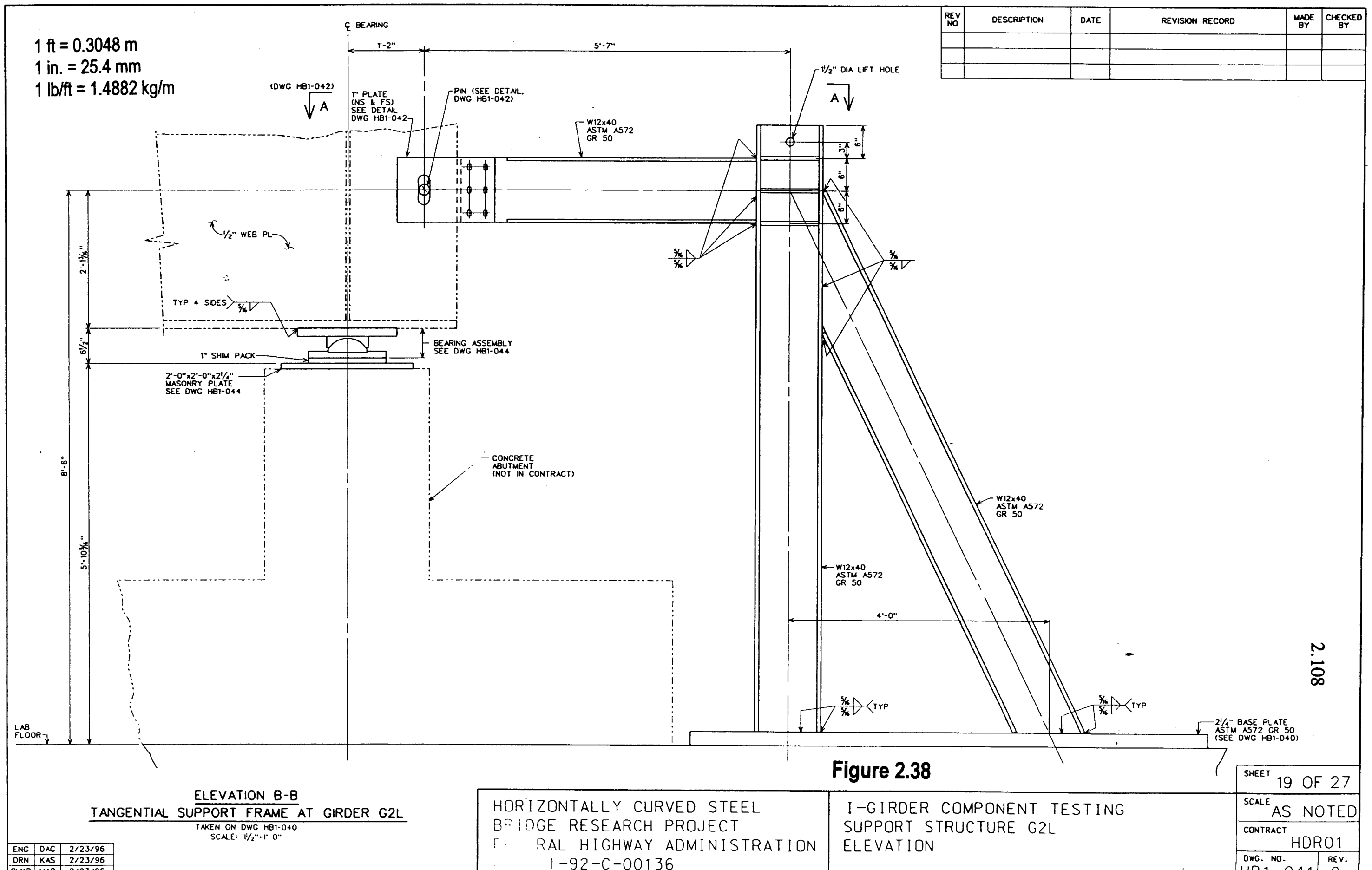
1 ft = 0.3048 m
1 in. = 25.4 mm
1 lb/ft = 1.4882 kg/m
℄ BEARING
1'-2"
5'-7"
(DWG HB1-042)
A
1" PLATE (NS & FS) SEE DETAIL DWG HB1-042
PIN (SEE DETAIL, DWG HB1-042)
W12x40 ASTM A572 GR 50
1/2" DIA LIFT HOLE
1/2" WEB PL
TYP 4 SIDES
BEARING ASSEMBLY SEE DWG HB1-044
1" SHIM PACK
2'-0"x2'-0"x2 1/4" MASONRY PLATE SEE DWG HB1-044
CONCRETE ABUTMENT (NOT IN CONTRACT)
2'-1 3/8"
6 1/2"
8'-6"
5'-10 3/8"
4'-0"
TYP
2 1/4" BASE PLATE ASTM A572 GR 50 (SEE DWG HB1-040)
LAB FLOOR
2.108
ELEVATION B-B
TANGENTIAL SUPPORT FRAME AT GIRDER G2L
TAKEN ON DWG HB1-040
SCALE: 1/2"-1'-0"
ENG DAC 2/23/96
DRN KAS 2/23/96
CHKD MAG 2/23/96
HORIZONTALLY CURVED STEEL
BRIDGE RESEARCH PROJECT
FEDERAL HIGHWAY ADMINISTRATION
1-92-C-00136
I-GIRDER COMPONENT TESTING
SUPPORT STRUCTURE G2L
ELEVATION
SHEET 19 OF 27
SCALE AS NOTED
CONTRACT HDR01
DWG. NO. HB1-041
REV. 0
REV NO
DESCRIPTION
DATE
REVISION RECORD
MADE BY
CHECKED BY

Figure 2.38

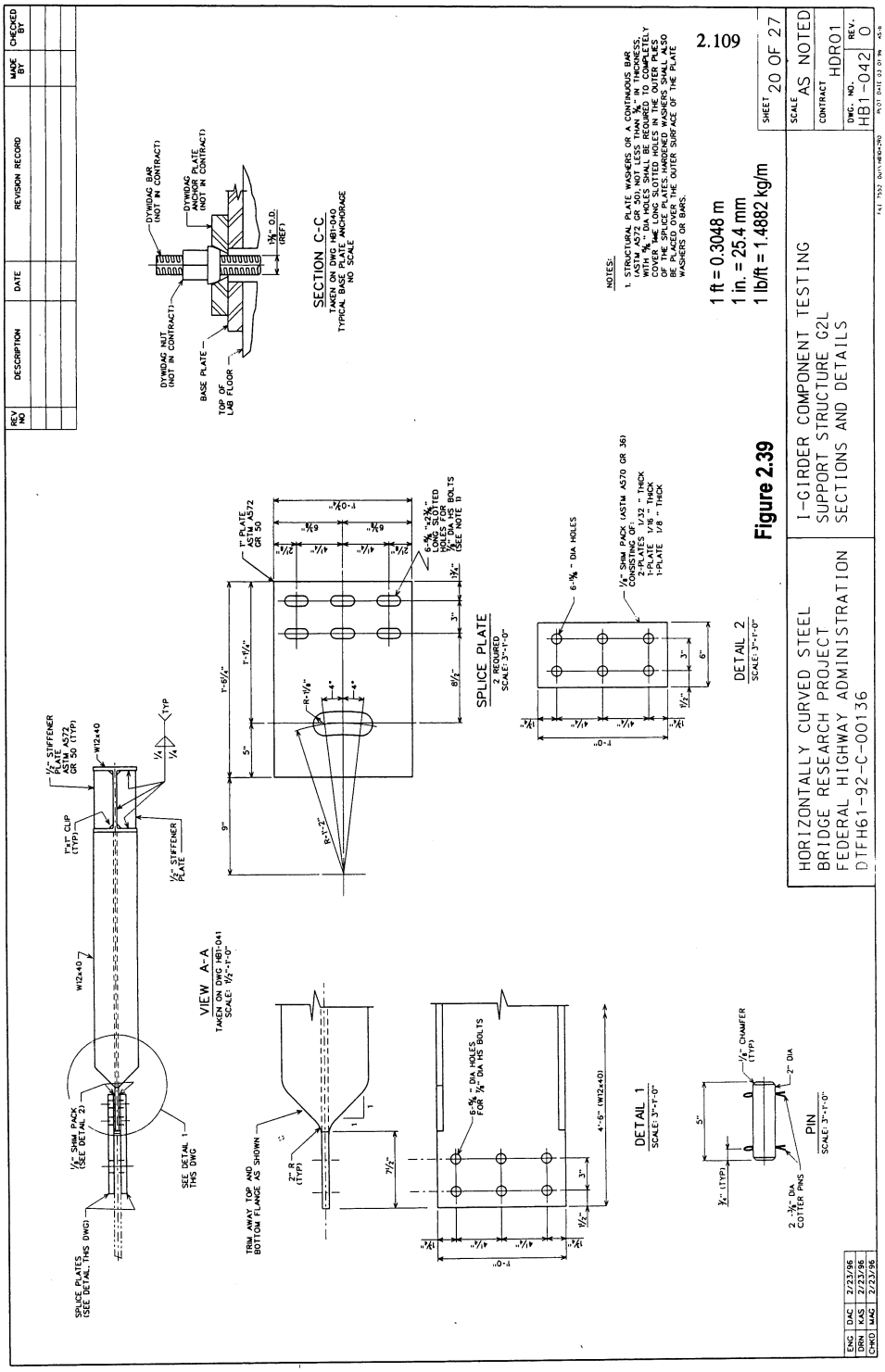
SECTION C-C
TAKEN ON DWG HB1-040
TYPICAL BASE PLATE ANCHORAGE
NO SCALE
DYWIDAG BAR (NOT IN CONTRACT)
DYWIDAG ANCHOR PLATE (NOT IN CONTRACT)
DYWIDAG NUT (NOT IN CONTRACT)
BASE PLATE
TOP OF LAB FLOOR
SPLICE PLATE
2 REQUIRED
SCALE: 3"-1'-0"
1" PLATE ASTM A572 GR 50
DETAIL 2
SCALE: 3"-1'-0"
DETAIL 1
SCALE: 3"-1'-0"
PIN
SCALE: 3"-1'-0"
VIEW A-A
TAKEN ON DWG HB1-041
SCALE: 1½"-1'-0"
NOTES:
1. STRUCTURAL PLATE WASHERS OR A CONTINUOUS BAR WITH 3/8" DIA HOLES SHALL BE REQUIRED TO COMPLETELY COVER THE LONG SLOTTED HOLES IN THE OUTER PLIES OF THE SPLICE PLATES. HARDENED WASHERS SHALL ALSO BE PLACED OVER THE OUTER SURFACE OF THE PLATE WASHERS OR BARS.
2.109
1 ft = 0.3048 m
1 in. = 25.4 mm
1 lb/ft = 1.4882 kg/m
HORIZONTALLY CURVED STEEL
BRIDGE RESEARCH PROJECT
FEDERAL HIGHWAY ADMINISTRATION
DTFH61-92-C-00136
I-GIRDER COMPONENT TESTING
SUPPORT STRUCTURE G2L
SECTIONS AND DETAILS
SCALE AS NOTED
CONTRACT HDR01
DWG. NO. HB1-042
REV. 0
SHEET 20 OF 27
ENG DAC 2/23/96
DRN KAS 2/23/96
CHKD MAG 2/23/96

Figure 2.39

REV NO	DESCRIPTION	DATE	REVISION RECORD	MADE BY	CHECKED BY
1	REV SPREADER BEAMS	6/2/95	ADDENDUM TO BID DOCUMENTS	JDC	MAG

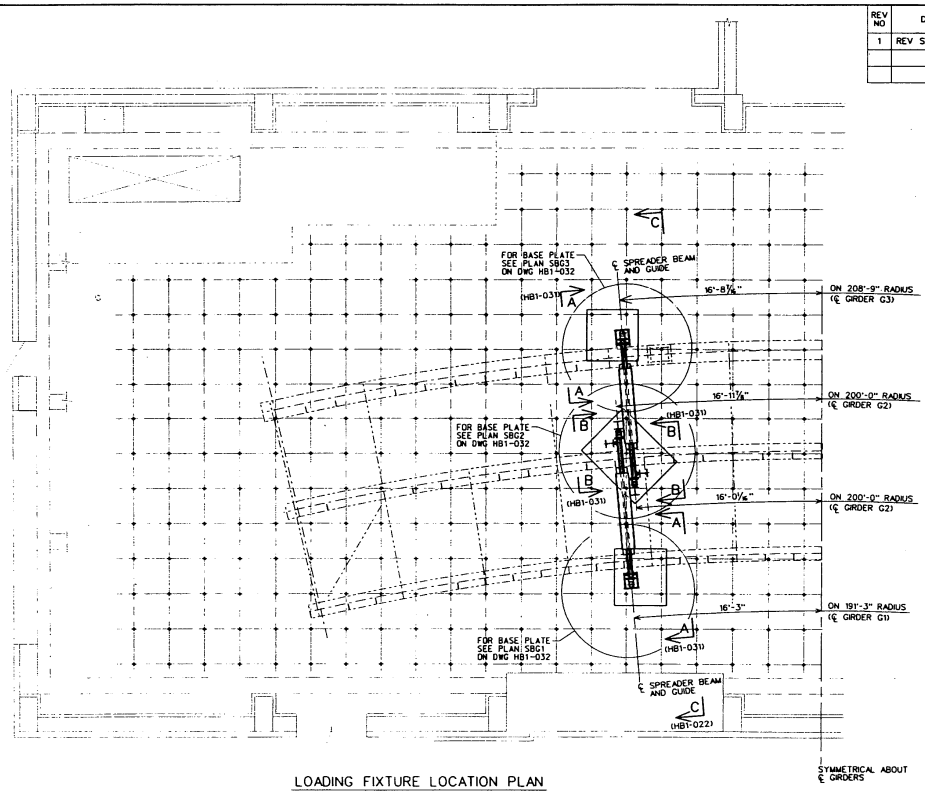

LOADING FIXTURE LOCATION PLAN

2.110

Figure 2.40

ENG	DAC	5/1/95
DRN	KAS	5/1/95
CHKD	MAG	5/1/95

1 ft = 0.3048 m
1 in. = 25.4 mm

HORIZONTALLY CURVED STEEL BRIDGE RESEARCH PROJECT
FEDERAL HIGHWAY ADMINISTRATION
DTFH61-92-C-00136

I-GIRDER COMPONENT TESTING
LOADING FIXTURE - LOCATION PLAN

SHEET 23 OF 31
SCALE AS NOTED
CONTRACT HDR01
DWG. NO. HB1-021
REV. 1

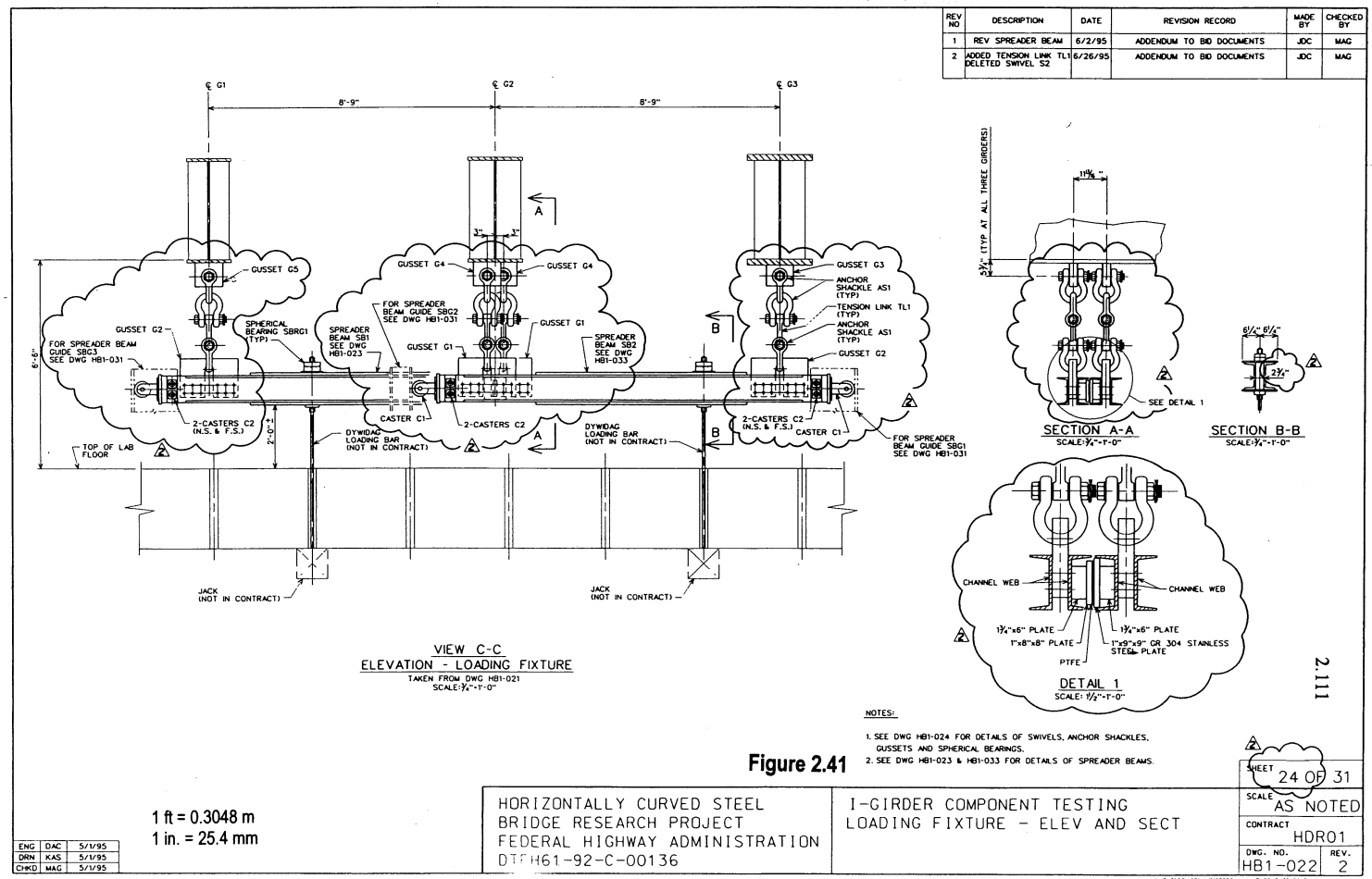
REV NO | DESCRIPTION | DATE | REVISION RECORD | MADE BY | CHECKED BY
1 | REV SPREADER BEAM | 6/2/95 | ADDENDUM TO BID DOCUMENTS | JDC | MAG
2 | ADDED TENSION LINK TL1 DELETED SWIVEL S2 | 6/26/95 | ADDENDUM TO BID DOCUMENTS | JDC | MAG
℄ G1
℄ G2
℄ G3
8'-9"
8'-9"
GUSSET G5
GUSSET G2
SPHERICAL BEARING SBRG1 (TYP)
FOR SPREADER BEAM GUIDE SBG3 SEE DWG HB1-031
GUSSET G4
GUSSET G4
FOR SPREADER BEAM GUIDE SBG2 SEE DWG HB1-031
SPREADER BEAM SB1 SEE DWG HB1-023
GUSSET G1
GUSSET G1
SPREADER BEAM SB2 SEE DWG HB1-033
GUSSET G3
ANCHOR SHACKLE AS1 (TYP)
TENSION LINK TL1 (TYP)
ANCHOR SHACKLE AS1 (TYP)
GUSSET G2
6'-6"
2'-0"
TOP OF LAB FLOOR
2-CASTERS C2 (N.S. & F.S.)
CASTER C1
2-CASTERS C2
DYWIDAG LOADING BAR (NOT IN CONTRACT)
DYWIDAG LOADING BAR (NOT IN CONTRACT)
2-CASTERS C2 (N.S. & F.S.)
CASTER C1
FOR SPREADER BEAM GUIDE SBG1 SEE DWG HB1-031
JACK (NOT IN CONTRACT)
JACK (NOT IN CONTRACT)
VIEW C-C
ELEVATION - LOADING FIXTURE
TAKEN FROM DWG HB1-021
SCALE: 3/4"-1'-0"
5 3/4" (TYP AT ALL THREE GIRDERS)
11 3/4"
SEE DETAIL 1
SECTION A-A
SCALE: 3/4"-1'-0"
6 1/4" 6 1/4"
2 3/4"
SECTION B-B
SCALE: 3/4"-1'-0"
CHANNEL WEB
CHANNEL WEB
1 3/4"x6" PLATE
1"x8"x8" PLATE
1 3/4"x6" PLATE
1"x9"x9" OR 304 STAINLESS STEEL PLATE
PTFE
DETAIL 1
SCALE: 1 1/2"-1'-0"
NOTES:
1. SEE DWG HB1-024 FOR DETAILS OF SWIVELS, ANCHOR SHACKLES, GUSSETS AND SPHERICAL BEARINGS.
2. SEE DWG HB1-023 & HB1-033 FOR DETAILS OF SPREADER BEAMS.
2.111
1 ft = 0.3048 m
1 in. = 25.4 mm
ENG DAC 5/1/95
DRN KAS 5/1/95
CHKD MAG 5/1/95
HORIZONTALLY CURVED STEEL BRIDGE RESEARCH PROJECT
FEDERAL HIGHWAY ADMINISTRATION
DTFH61-92-C-00136
I-GIRDER COMPONENT TESTING
LOADING FIXTURE - ELEV AND SECT
SHEET 24 OF 31
SCALE AS NOTED
CONTRACT HDR01
DWG. NO. HB1-022
REV. 2

Figure 2.41

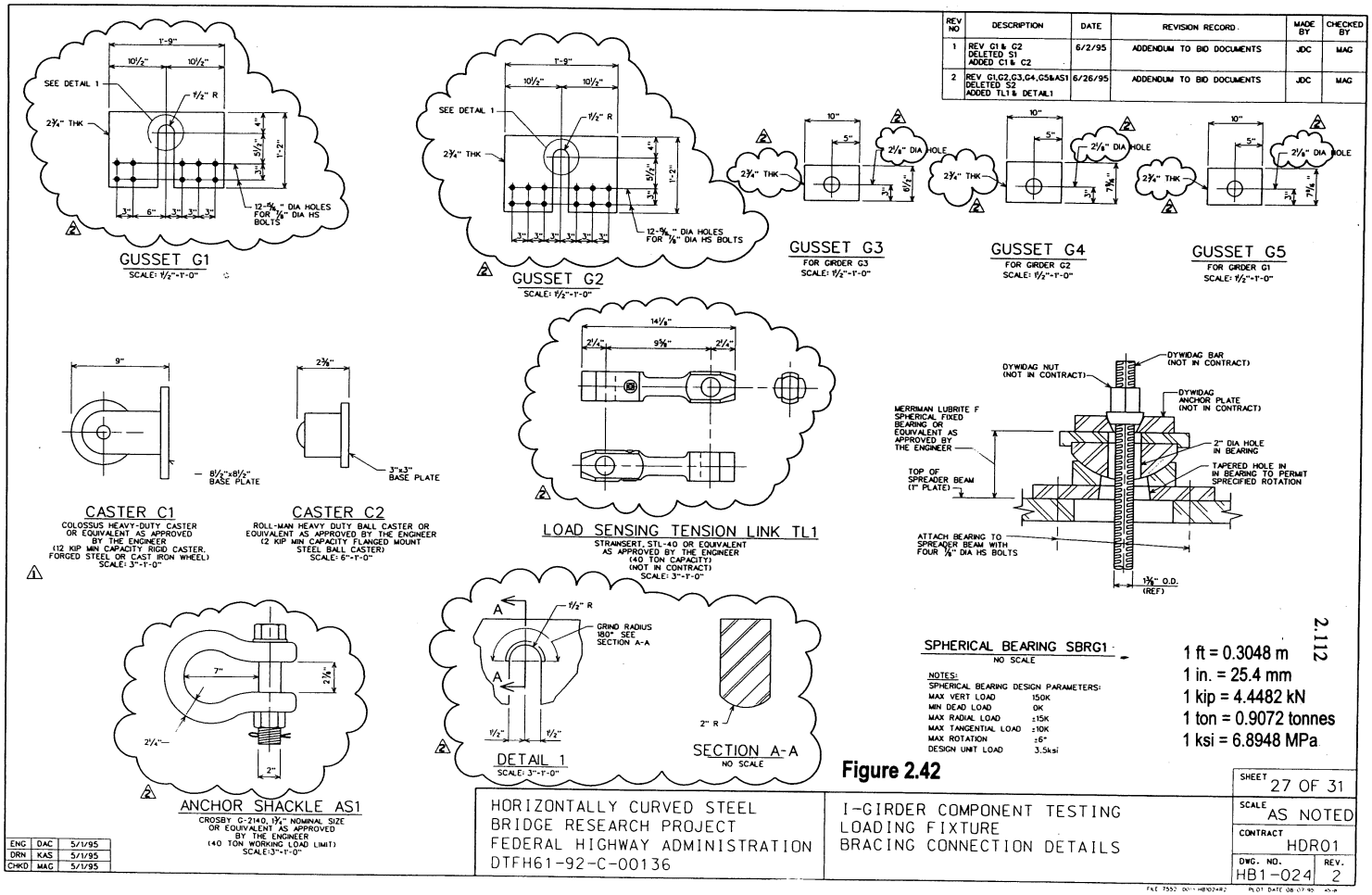

Figure 2.42

2.112

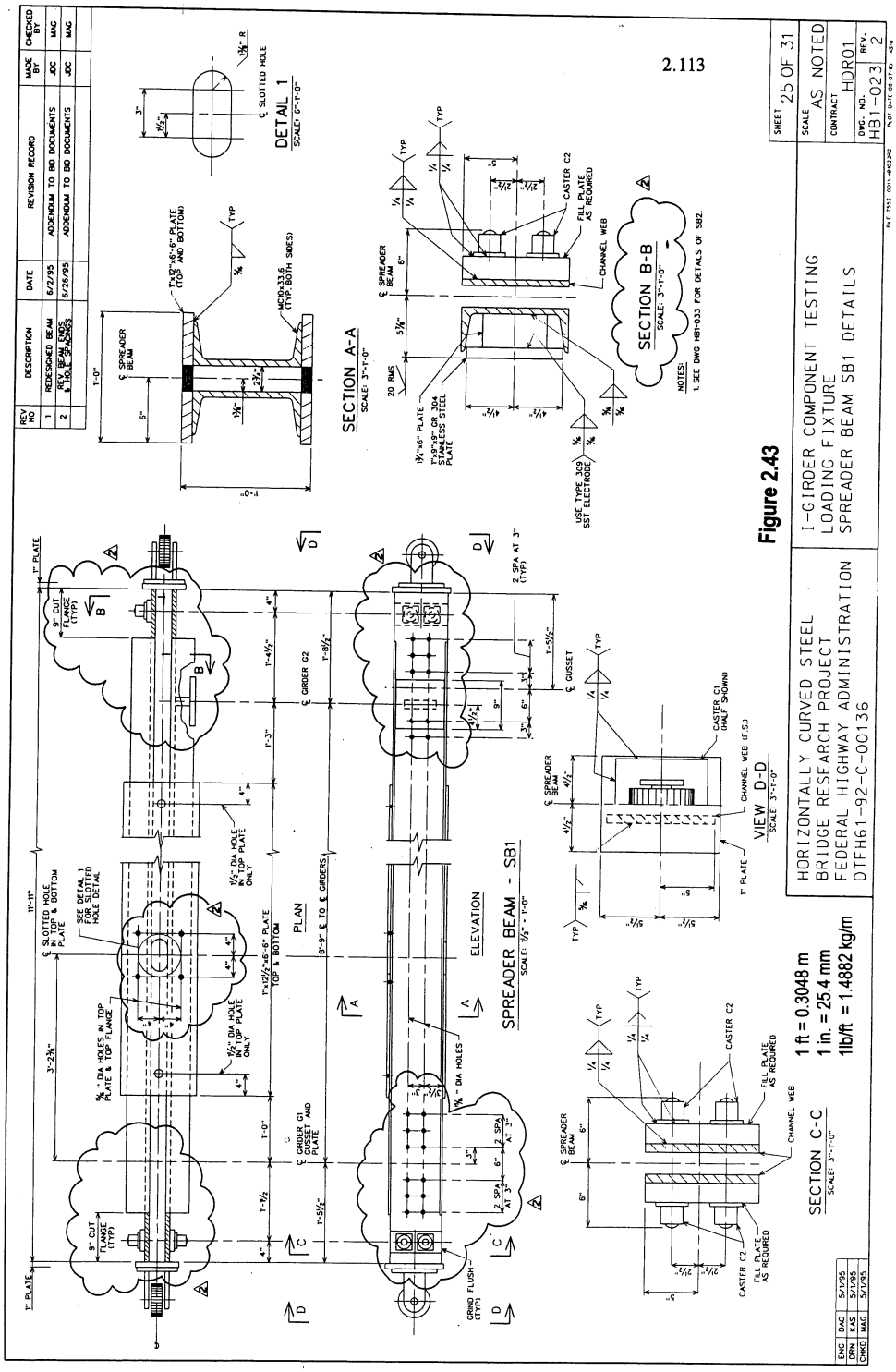
2.113
SPREADER BEAM - SB1
SCALE: 1½" = 1'-0"
PLAN
ELEVATION
SECTION A-A
SECTION B-B
SECTION C-C
VIEW D-D
DETAIL 1
HORIZONTALLY CURVED STEEL
BRIDGE RESEARCH PROJECT
FEDERAL HIGHWAY ADMINISTRATION
DTFH61-92-C-00136
I-GIRDER COMPONENT TESTING
LOADING FIXTURE
SPREADER BEAM SB1 DETAILS
1 ft = 0.3048 m
1 in. = 25.4 mm
1lb/ft = 1.4882 kg/m

Figure 2.43

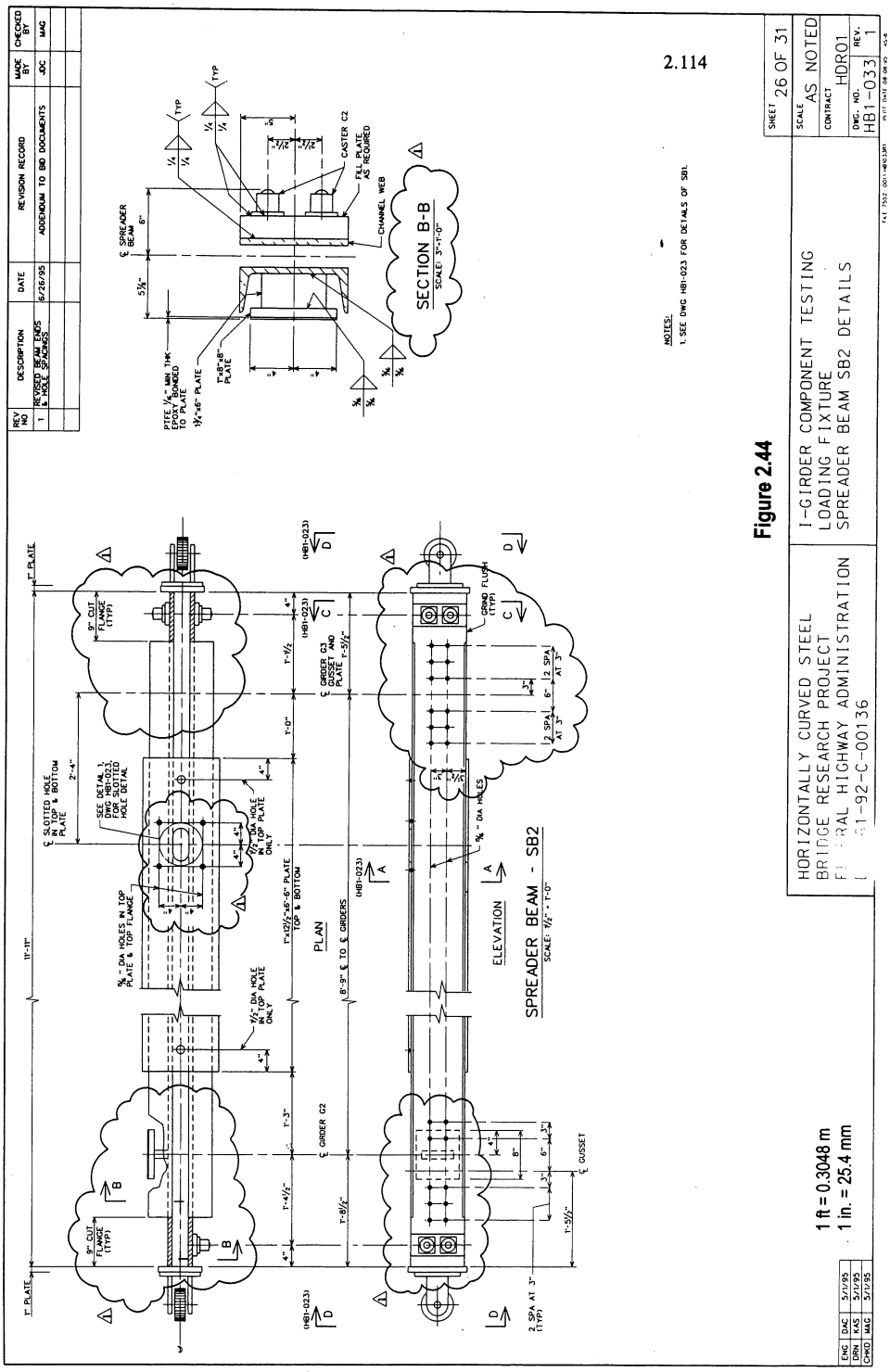
2.114
SECTION B-B
SCALE: 3"-1'-0"
SPREADER BEAM - SB2
SCALE: ½" - 1'-0"
PLAN
ELEVATION
NOTES:
1. SEE DWG HB1-023 FOR DETAILS OF SB1.
HORIZONTALLY CURVED STEEL
BRIDGE RESEARCH PROJECT
FEDERAL HIGHWAY ADMINISTRATION
I-GIRDER COMPONENT TESTING
LOADING FIXTURE
SPREADER BEAM SB2 DETAILS
1 ft = 0.3048 m
1 in. = 25.4 mm

Figure 2.44

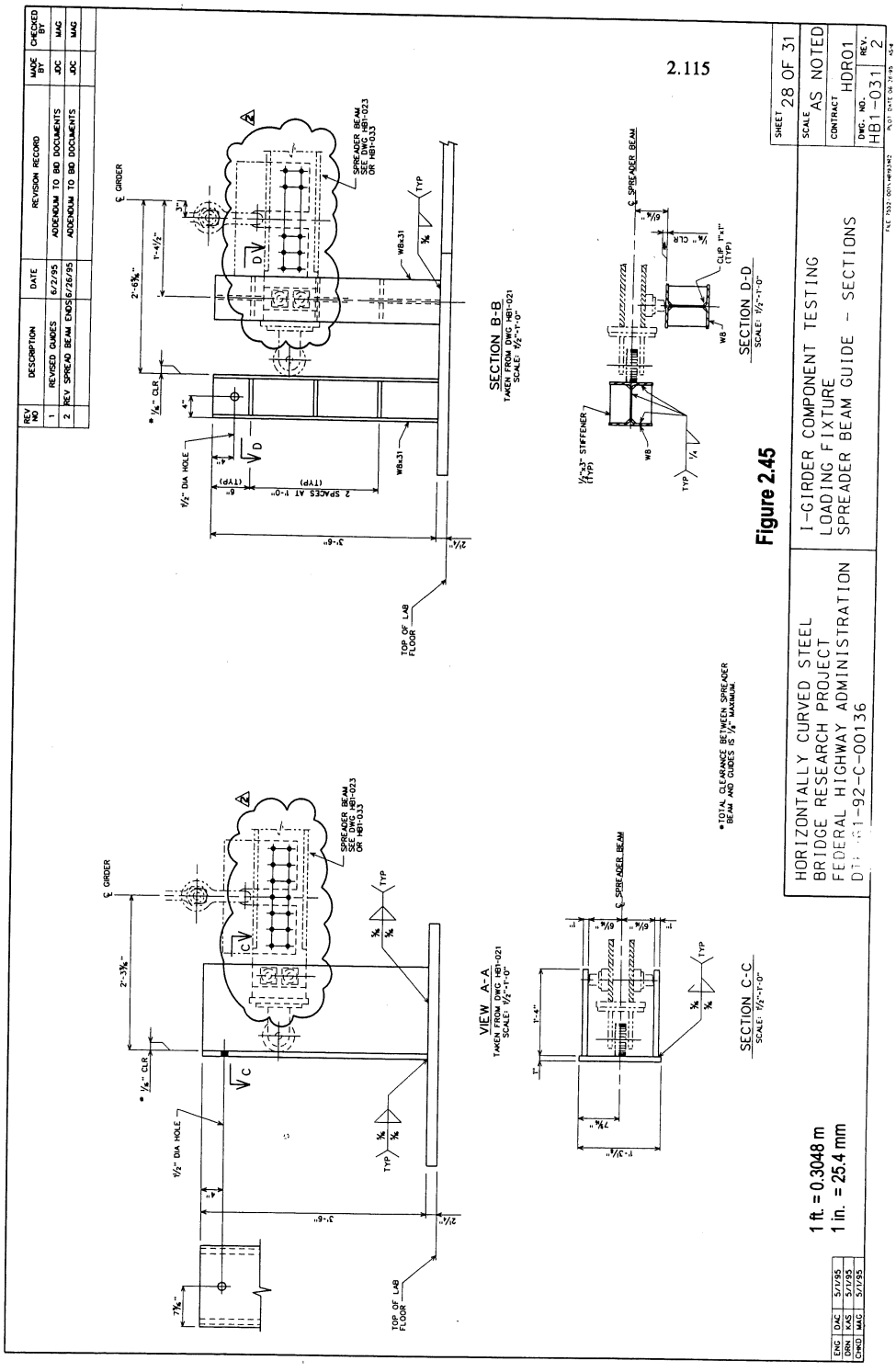
2.115
SECTION B-B
TAKEN FROM DWG HB1-021
SCALE: ½"=1'-0"
SECTION D-D
SCALE: ½"=1'-0"
VIEW A-A
TAKEN FROM DWG HB1-021
SCALE: ½"=1'-0"
SECTION C-C
SCALE: ½"=1'-0"
SPREADER BEAM SEE DWG HB1-023 OR HB1-033
TOP OF LAB FLOOR
*TOTAL CLEARANCE BETWEEN SPREADER BEAM AND GUIDE IS ¼" MAXIMUM.
HORIZONTALLY CURVED STEEL
BRIDGE RESEARCH PROJECT
FEDERAL HIGHWAY ADMINISTRATION
DTFH61-92-C-00136
I-GIRDER COMPONENT TESTING
LOADING FIXTURE
SPREADER BEAM GUIDE - SECTIONS
SHEET 28 OF 31
SCALE AS NOTED
CONTRACT HDR01
DWG. NO. HB1-031
REV. 2
1 ft. = 0.3048 m
1 in. = 25.4 mm

Figure 2.45

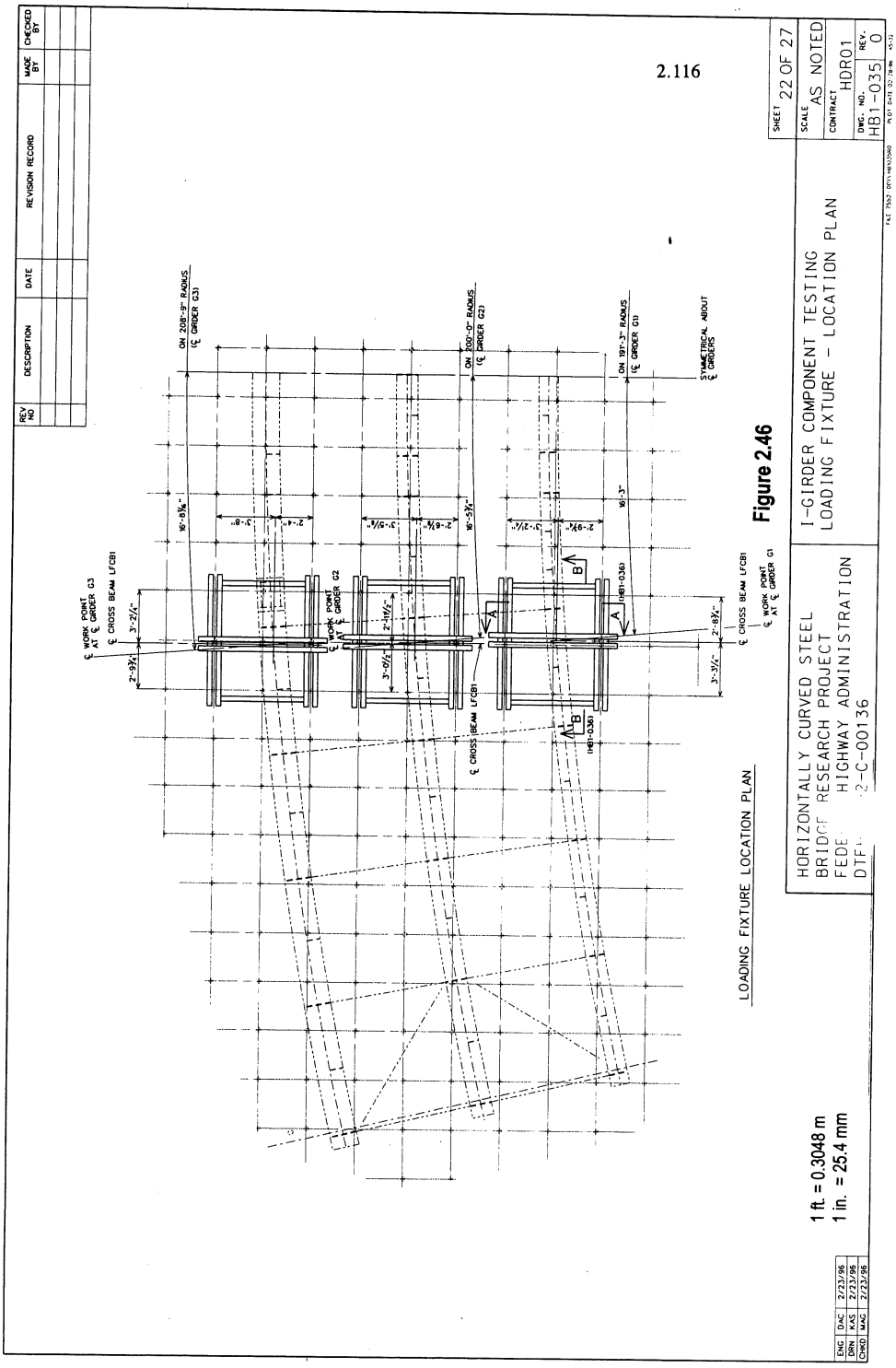
2.116
REV NO
DESCRIPTION
DATE
REVISION RECORD
MADE BY
CHECKED BY
ON 208'-9" RADIUS (℄ GIRDER G3)
ON 200'-0" RADIUS (℄ GIRDER G2)
ON 191'-3" RADIUS (℄ GIRDER G1)
SYMMETRICAL ABOUT ℄ GIRDER
WORK POINT AT ℄ GIRDER G3
WORK POINT AT ℄ GIRDER G2
WORK POINT AT ℄ GIRDER G1
℄ CROSS BEAM LFCB1
℄ CROSS BEAM LFCB1
℄ CROSS BEAM LFCB1
(HB1-036)
(HB1-036)
A
B
LOADING FIXTURE LOCATION PLAN
Figure 2.46
HORIZONTALLY CURVED STEEL
BRIDGE RESEARCH PROJECT
FEDE HIGHWAY ADMINISTRATION
DTF 2-C-00136
I-GIRDER COMPONENT TESTING
LOADING FIXTURE - LOCATION PLAN
SHEET 22 OF 27
SCALE AS NOTED
CONTRACT HDR01
DWG. NO. HB1-035
REV. 0
ENG DAC 2/23/96
DRN KAS 2/23/96
CHKD MAG 2/23/96
1 ft. = 0.3048 m
1 in. = 25.4 mm

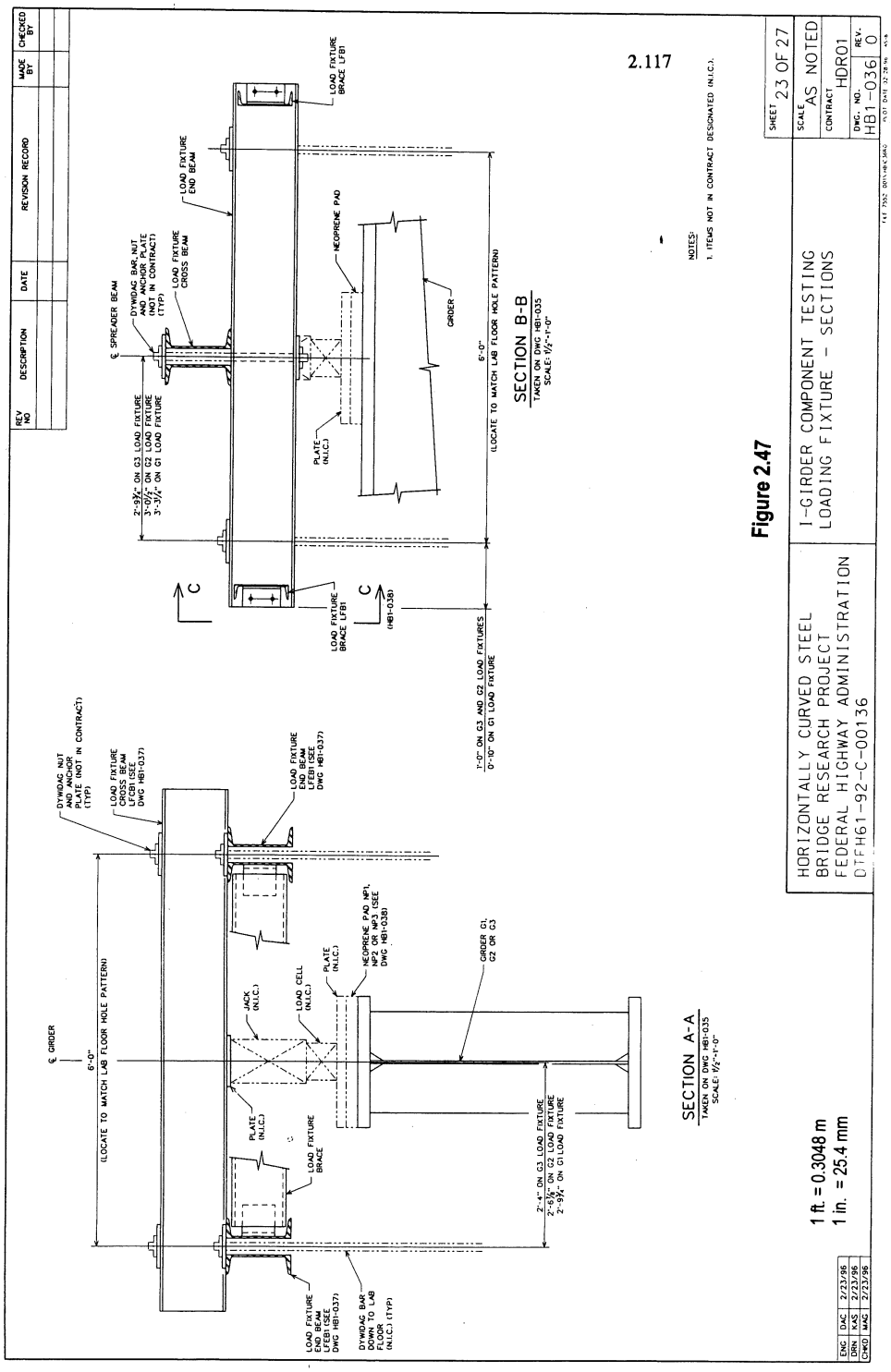
2.117
SECTION B-B
TAKEN ON DWG HB1-035
SCALE 1/2"=1'-0"
SECTION A-A
TAKEN ON DWG HB1-035
SCALE 1/2"=1'-0"
NOTES:
1. ITEMS NOT IN CONTRACT DESIGNATED (N.I.C.).
HORIZONTALLY CURVED STEEL
BRIDGE RESEARCH PROJECT
FEDERAL HIGHWAY ADMINISTRATION
DTFH61-92-C-00136
I-GIRDER COMPONENT TESTING
LOADING FIXTURE - SECTIONS
SCALE AS NOTED
CONTRACT HDR01
DWG. NO. HB1-036
REV. 0
SHEET 23 OF 27
1 ft. = 0.3048 m
1 in. = 25.4 mm

Figure 2.47

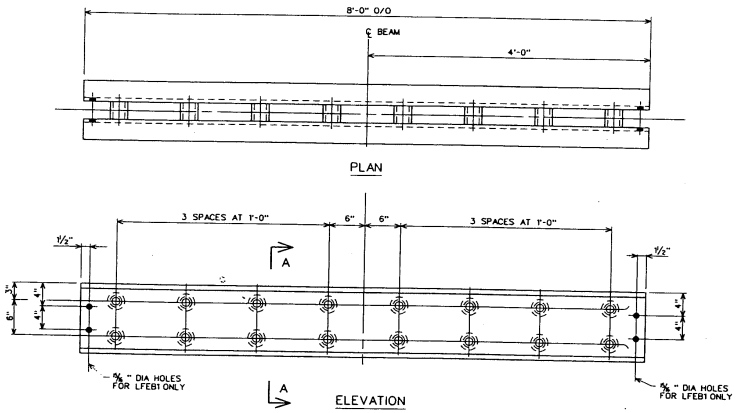

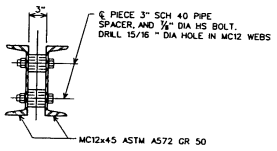

SECTION A-A

LOAD FIXTURE CROSS BEAM - LFCB1 (AS SHOWN & NOTED)
LOAD FIXTURE END BEAM - LFEB1 (AS SHOWN & NOTED)
SCALE: ½" - 1'-0"

REV NO	DESCRIPTION	DATE	REVISION RECORD	MADE BY	CHECKED BY

2.118

1 ft. = 0.3048 m
1 in. = 25.4 mm
1 ksi = 6.8948 MPa
1 lb/ft = 1.4882 kg/m

ENG	DAC	2/23/96
DRN	KAS	2/23/96
CHKD	MAG	2/23/96

Figure 2.48

HORIZONTALLY CURVED STEEL BRIDGE RESEARCH PROJECT
FEDERAL HIGHWAY ADMINISTRATION
DTFH61-92-C-00136

I-GIRDER COMPONENT TESTING
LOADING FIXTURE - DETAILS
SHEET 1 OF 2

SHEET 24 OF 27
SCALE AS NOTED
CONTRACT HDR01
DWG. NO. HB1-037
REV. 0

REV NO	DESCRIPTION	DATE	REVISION RECORD	MADE BY	CHECKED BY

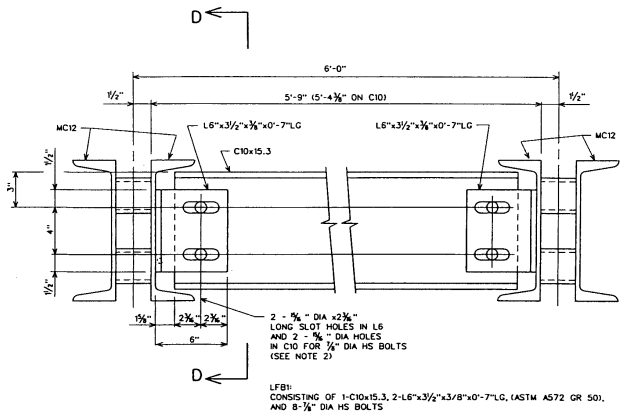

VIEW C-C
TAKEN ON DWG HB1-036
SCALE: 3"-1'-0"

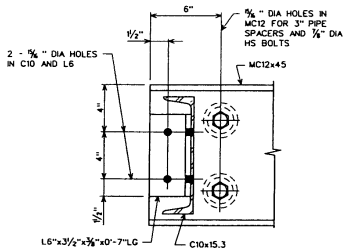

SECTION D-D
SCALE: 3"-1'-0"

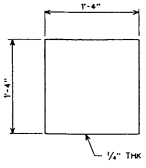

NEOPRENE PAD - NP1
FOR USE WITH GIRDER G1
SCALE: 3"-1'-0"

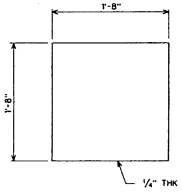

NEOPRENE PAD - NP2
FOR USE WITH GIRDER G2
SCALE: 3"-1'-0"

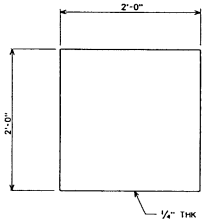

NEOPRENE PAD - NP3
FOR USE WITH GIRDER G3
SCALE: 3"-1'-0"

NOTES:

1. NEOPRENE PADS SHALL BE 50 ± 5 DUROMETER GRADE 0 AND SHALL SATISFY THE REQUIREMENTS OF ARTICLE 18.2.3.1 OF DIVISION II (CONSTRUCTION) OF THE AASHTO STANDARD SPECIFICATIONS FOR HIGHWAY BRIDGES.
2. STRUCTURAL PLATE WASHERS OR A CONTINUOUS BAR (ASTM A572 GR 50), NOT LESS THAN 5/16 " IN THICKNESS, WITH 15/16 " DIA HOLES SHALL BE REQUIRED TO COMPLETELY COVER THE LONG-SLOTTED HOLES IN THE OUTER PLY OF THE CONNECTION ANGLES. HARDENED WASHERS SHALL ALSO BE PLACED OVER THE OUTER SURFACE OF THE PLATE WASHERS OR BARS.

2.119

Figure 2.49

1 ft. = 0.3048 m
1 in. = 25.4 mm
1 ksi = 6.8948 MPa
1 lb/ft = 1.4882 kg/m

ENG	DAC	2/23/96
DRN	KAS	2/23/96
CHKD	MAG	2/23/96

HORIZONTALLY CURVED STEEL BRIDGE RESEARCH PROJECT
FEDERAL HIGHWAY ADMINISTRATION
DTFH61-92-C-00136

I-GIRDER COMPONENT TESTING LOADING FIXTURE - DETAILS SHEET 2 OF 2

SHEET 25 OF 27
SCALE AS NOTED
CONTRACT HDR01
DWG. NO. HB1-038
REV. 0

FILE 7532 DGN-HB103BRD PLOT DATE 03-01-96 AS-B

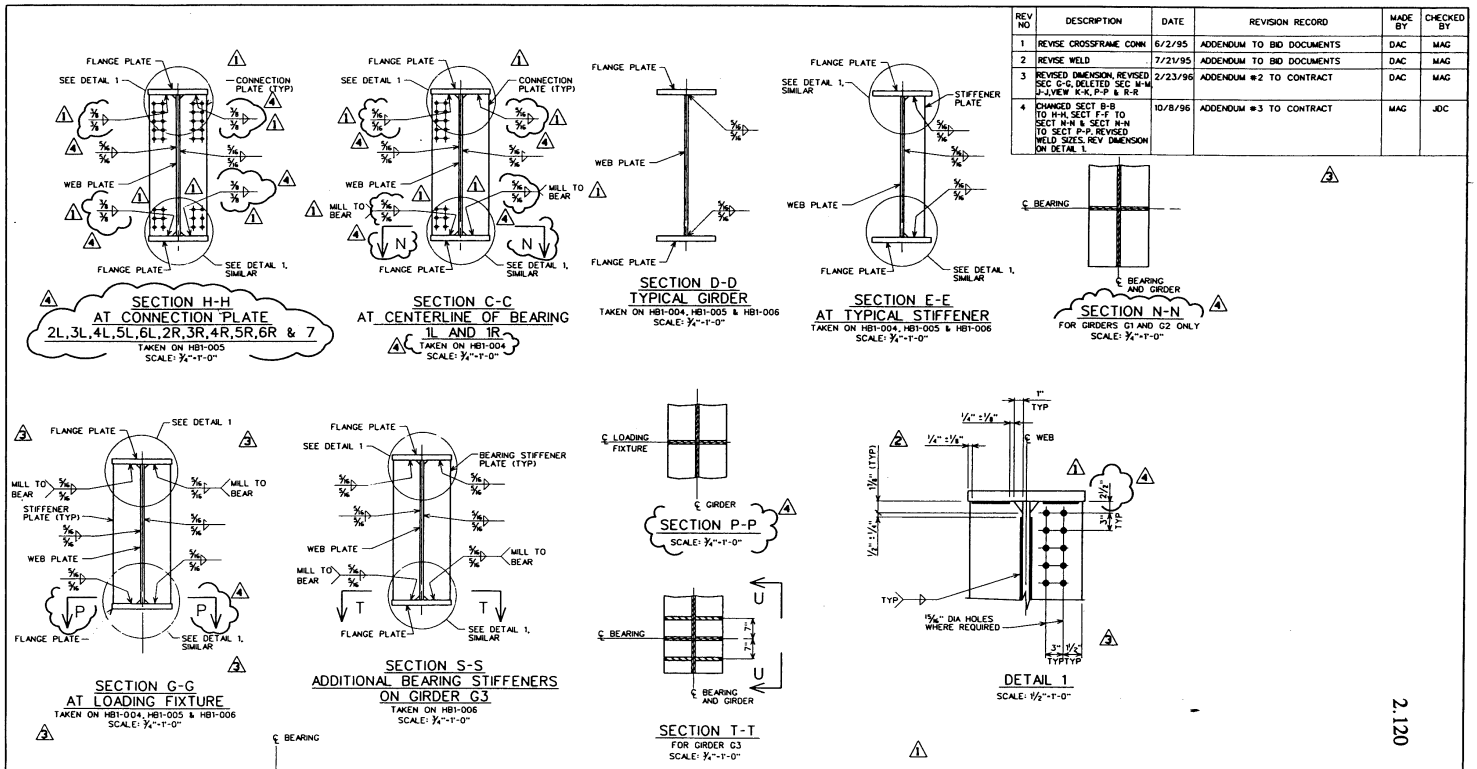
SECTION H-H
AT CONNECTION PLATE
2L,3L,4L,5L,6L,2R,3R,4R,5R,6R & 7
TAKEN ON HB1-005
SCALE: 3/4"-1'-0"
SECTION C-C
AT CENTERLINE OF BEARING
1L AND 1R
TAKEN ON HB1-004
SCALE: 3/4"-1'-0"
SECTION D-D
TYPICAL GIRDER
TAKEN ON HB1-004, HB1-005 & HB1-006
SCALE: 3/4"-1'-0"
SECTION E-E
AT TYPICAL STIFFENER
TAKEN ON HB1-004, HB1-005 & HB1-006
SCALE: 3/4"-1'-0"
SECTION N-N
FOR GIRDERS G1 AND G2 ONLY
SCALE: 3/4"-1'-0"
SECTION G-G
AT LOADING FIXTURE
TAKEN ON HB1-004, HB1-005 & HB1-006
SCALE: 3/4"-1'-0"
SECTION S-S
ADDITIONAL BEARING STIFFENERS
ON GIRDER G3
TAKEN ON HB1-006
SCALE: 3/4"-1'-0"
SECTION P-P
SCALE: 3/4"-1'-0"
SECTION T-T
FOR GIRDER G3
SCALE: 3/4"-1'-0"
DETAIL 1
SCALE: 1 1/2"-1'-0"
VIEW U-U
SCALE: 3/4"-1'-0"
1 ft. = 0.3048 m
1 in. = 25.4 mm
REV NO | DESCRIPTION | DATE | REVISION RECORD | MADE BY | CHECKED BY
1 | REVISE CROSSFRAME CONN | 6/2/95 | ADDENDUM TO BID DOCUMENTS | DAC | MAG
2 | REVISE WELD | 7/21/95 | ADDENDUM TO BID DOCUMENTS | DAC | MAG
3 | REVISED DIMENSION, REVISED SEC C-C, DELETED SEC M-M, J-J, VIEW K-K, P-P & R-R | 2/23/96 | ADDENDUM #2 TO CONTRACT | DAC | MAG
4 | CHANGED SECT B-B TO H-H, SECT F-F TO SECT N-N & SECT N-N TO SECT P-P, REVISED WELD SIZES, REV DIMENSION ON DETAIL 1. | 10/8/96 | ADDENDUM #3 TO CONTRACT | MAG | JDC
ENG DAC 5/1/95
DRN KAS 5/1/95
CHKD MAG 5/1/95
HORIZONTALLY CURVED STEEL
BRIDGE RESEARCH PROJECT
FEDERAL HIGHWAY ADMINISTRATION
DTFH61-92-C-00136
I-GIRDER COMPONENT TESTING
TYPICAL DETAILS - GIRDERS G1, G2 & G3
SHEET 13 OF 27
SCALE AS NOTED
CONTRACT HDR01
DWG. NO. HB1-011
REV. 4
2.120

Figure 2.50

REV NO	DESCRIPTION	DATE	REVISION RECORD	MADE BY	CHECKED BY

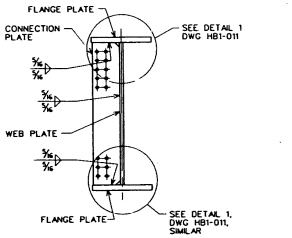

SECTION B-B
AT CONNECTION PLATE
2L, 3L, 4L, 5L, 6L, 2R, 3R, 4R, 5R, 6R & 7
TAKEN ON HB1-004
SCALE: 3/4"-1'-0"

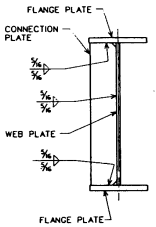

SECTION F-F
AT CONNECTION PLATE
6aL & 6aR
TAKEN ON HB1-004
SCALE: 3/4"-1'-0"

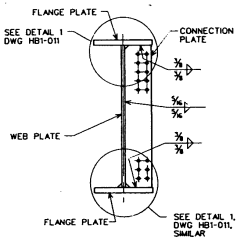

SECTION J-J
AT CONNECTION PLATE
2L,3L,4L,2R,3R & 4R
TAKEN ON HB1-006
SCALE: 3/4"-1'-0"

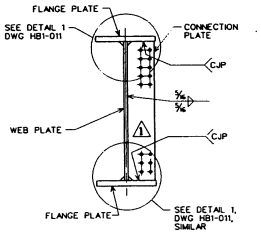

SECTION K-K
AT CONNECTION PLATE
5L, 5R & 7
TAKEN ON HB1-006
SCALE: 3/4"-1'-0"

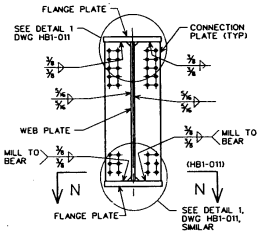

SECTION L-L
AT CENTERLINE OF BEARING
1L AND 1R
TAKEN ON HB1-005
SCALE: 3/4"-1'-0"

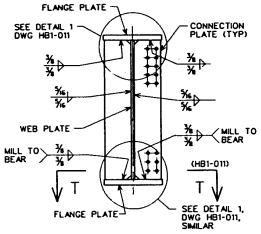

SECTION M-M
AT CENTERLINE OF BEARING
1L AND 1R
TAKEN ON HB1-006
SCALE: 3/4"-1'-0"

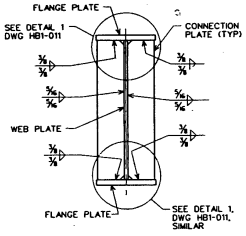

SECTION V-V
AT CONNECTION PLATE
6aL & 6aR
TAKEN ON HB1-005
SCALE: 3/4"-1'-0"

2.121

Figure 2.51

ENG	JDC	10/8/96
DRN	KAS	10/8/96
CHKD	MAG	10/8/96

1 ft. = 0.3048 m
1 in. = 25.4 mm

HORIZONTALLY CURVED STEEL
BRIDGE RESEARCH PROJECT
FEDERAL HIGHWAY ADMINISTRATION
[illegible]61-92-C-00136

I-GIRDER COMPONENT TESTING
TYPICAL DETAILS - GIRDERS G1, G2 & G3

SHEET 13A OF 27
SCALE AS NOTED
CONTRACT HDR01
DWG. NO. HB1-045 REV. 0

FILE: 7552-001\HB1045R0 PLOT DATE: 11-19-96 AS-IS

Bending Specimens

B1 through B6

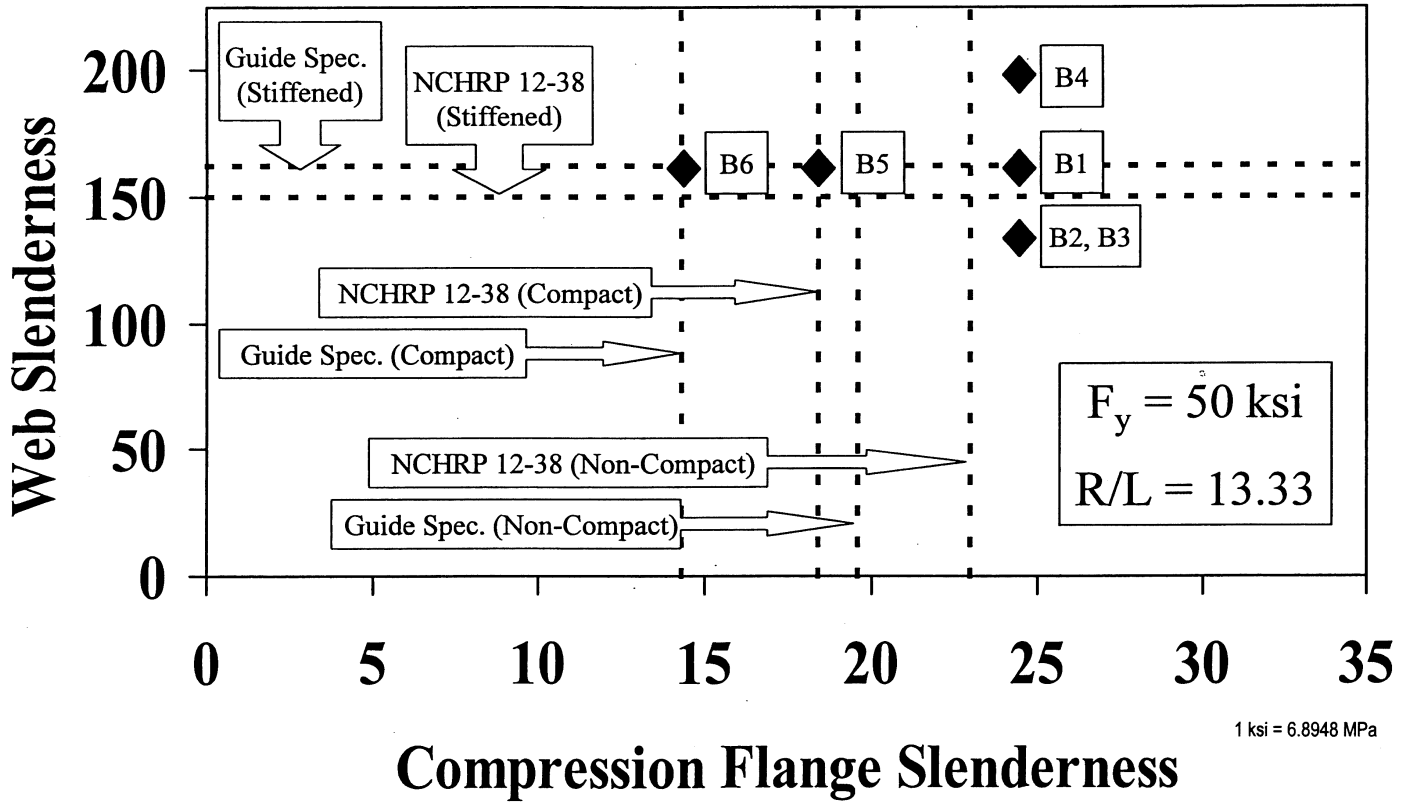

1 ksi = 6.8948 MPa

2.122

Figure 2.52

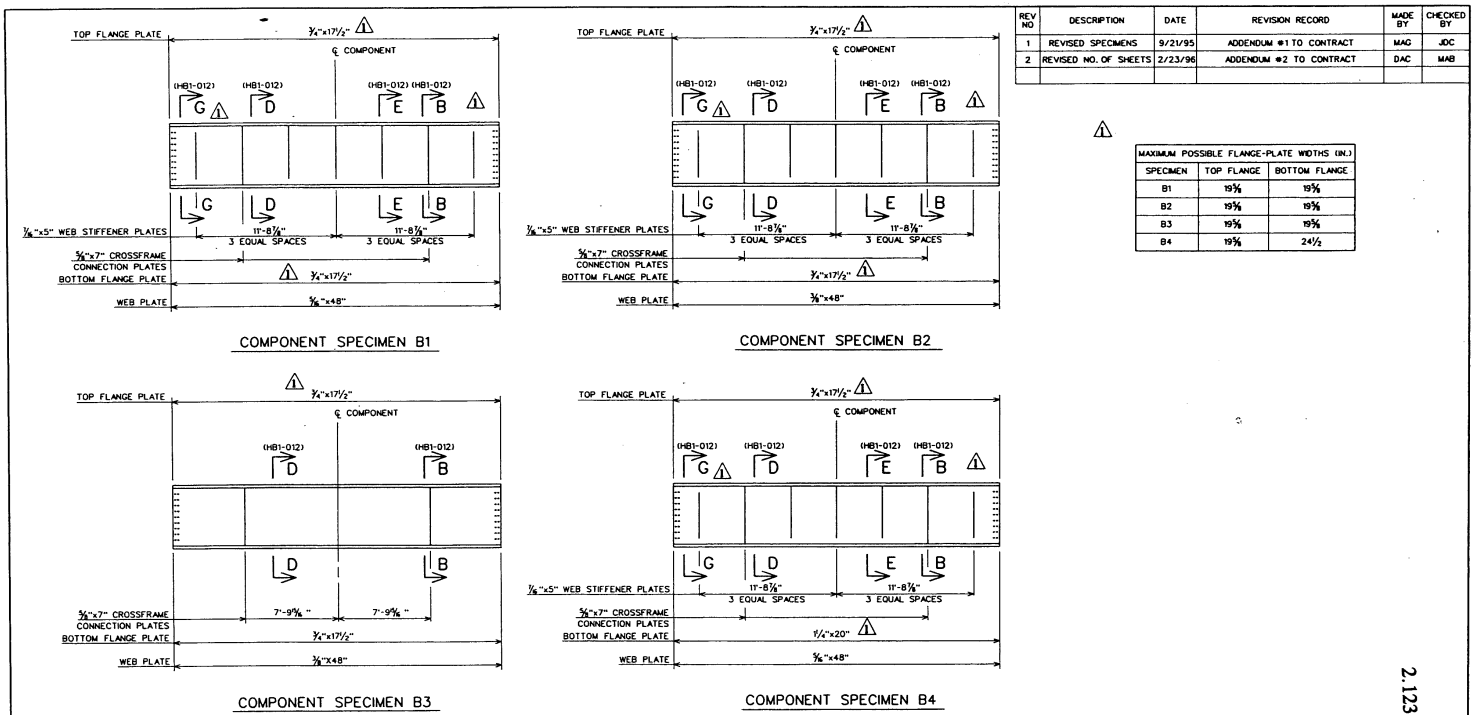

REV NO	DESCRIPTION	DATE	REVISION RECORD	MADE BY	CHECKED BY
1	REVISED SPECIMENS	9/21/95	ADDENDUM #1 TO CONTRACT	MAG	JDC
2	REVISED NO. OF SHEETS	2/23/96	ADDENDUM #2 TO CONTRACT	DAC	MAB

⚠

MAXIMUM POSSIBLE FLANGE-PLATE WIDTHS (IN.)		
SPECIMEN	TOP FLANGE	BOTTOM FLANGE
B1	19⅜	19⅜
B2	19⅜	19⅜
B3	19⅜	19⅜
B4	19⅜	24½

2.123

NOTES:
1. ALL LONGITUDINAL DIMENSIONS ARE ARC LENGTHS MEASURED ON THE SPECIMEN CENTERLINE

Figure 2.53

ENG	MAG	5/1/95
DRN	KAS	5/1/95
CHKD	DAC	5/1/95

1 ft. = 0.3048 m
1 in. = 25.4 mm

HORIZONTALLY CURVED STEEL BRIDGE RESEARCH PROJECT
FEDERAL HIGHWAY ADMINISTRATION
DTFH61-92-C-00136

I-GIRDER COMPONENT TESTING
ELEVATIONS - COMPONENT SPECIMENS
B1, B2, B3 AND B4

SHEET 10 OF 27
SCALE 1/4"=1'-0"
CONTRACT HDR01
DWG. NO. HB1-007
REV. 2

FILE: 7552-001\HB100782 PLOT DATE: 02-21-96 AS-48

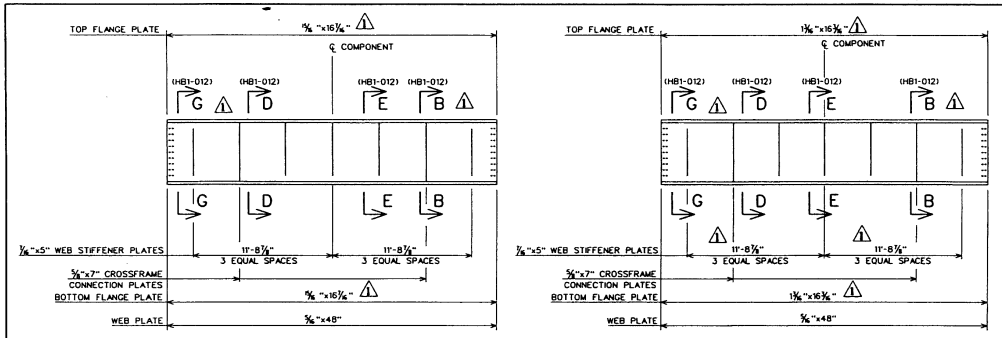

COMPONENT SPECIMEN B5

COMPONENT SPECIMEN B6

REV NO	DESCRIPTION	DATE	REVISION RECORD	MADE BY	CHECKED BY
1	REVISED SPECIMENS	9/21/95	ADDENDUM #1 TO CONTRACT	MAG	JDC
2	REVISED NO. OF SHEETS	2/23/96	ADDENDUM #2 TO CONTRACT	DAC	MAG

1

MAXIMUM POSSIBLE FLANGE-PLATE WIDTHS (IN.)		
SPECIMEN	TOP FLANGE	BOTTOM FLANGE
B5	17 7/8	17 7/8
B6	17 7/8	17 7/8

2.124

NOTES:
1. ALL LONGITUDINAL DIMENSIONS ARE ARC LENGTHS MEASURED ON THE SPECIMEN CENTERLINE.

2

Figure 2.54

1 ft. = 0.3048 m
1 in. = 25.4 mm

ENG	MAG	5/1/95
DRN	KAS	5/1/95
CHKD	DAC	5/1/95

HORIZONTALLY CURVED STEEL BRIDGE RESEARCH PROJECT
FEDERAL HIGHWAY ADMINISTRATION
DTFH61-92-C-00136

I-GIRDER COMPONENT TESTING
ELEVATIONS - COMPONENT SPECIMENS B5 AND B6

SHEET 11 OF 27
SCALE 1/4"=1'-0"
CONTRACT HDR01
DWG. NO. HB1-008 REV. 2

FILE: 7552-001\HB1008R2 PLOT DATE: 02-21-96 AS-48

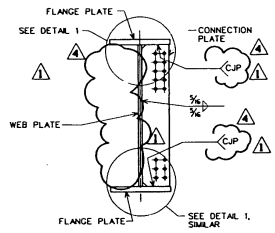

SECTION B-B
AT CONNECTION PLATE
TAKEN ON HB1-007 & HB1-008
SCALE: 3/4"=1'-0"

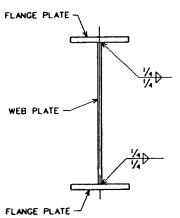

SECTION D-D
TYPICAL SPECIMEN
TAKEN ON HB1-007 & HB1-008
SCALE: 3/4"=1'-0"

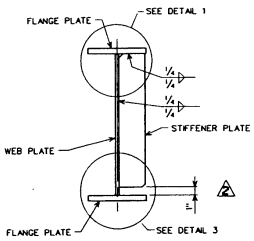

SECTION E-E
AT TYPICAL STIFFENER
TAKEN ON HB1-007 & HB1-008
SCALE: 3/4"=1'-0"

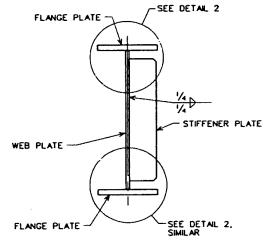

SECTION G-G
AT STIFFENER NEAR FIELD SPLICE
TAKEN ON HB1-007 & HB1-008
SCALE: 3/4"=1'-0"

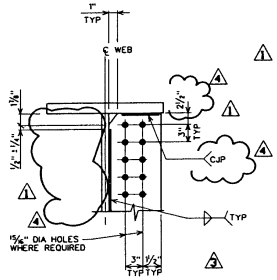

DETAIL 1
SCALE: 1½"=1'-0"

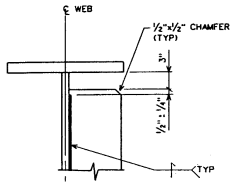

DETAIL 2
SCALE: 1½"=1'-0"

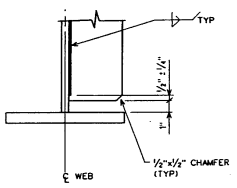

DETAIL 3
SCALE: 1½"=1'-0"

REV NO	DESCRIPTION	DATE	REVISION RECORD	MADE BY	CHECKED BY
1	REVISE CROSSFRAME CONN	6/2/95	ADDENDUM TO BID DOCUMENTS	DAC	MAG
2	REMOVED SECT F-F, REV SECT E-E & ADDED DET 3	9/21/95	ADDENDUM #1 TO CONTRACT	MAG	JDC
3	REVISED DIMENSION	2/23/96	ADDENDUM #2 TO CONTRACT	DAC	MAG
4	REMOVED STIFFENERS ON FASCIA SIDE OF THE SPECIMENS AT CROSS FRAME LINES, REV WELDS, REV DIM & WELD ON DET 1.	10/8/96	ADDENDUM #3 TO CONTRACT	MAG	JDC

2.125

NOTES:

1. WHERE PIECES ARE TO BE CONNECTED WITH 1/4" FILLET WELD, PREHEAT BOTH PIECES AT THE JOINT TO 125°F.

Figure 2.55

ENG	DAC	5/1/95
DRN	KAS	5/1/95
CHKD	MAG	5/1/95

1 ft. = 0.3048 m
1 in. = 25.4 mm

HORIZONTALLY CURVED STEEL
BRIDGE RESEARCH PROJECT
FEDERAL HIGHWAY ADMINISTRATION
DTFH61-92-C-00136

I-GIRDER COMPONENT TESTING
TYPICAL DETAILS-COMPONENT SPECIMENS

SHEET 14 OF 27
SCALE AS NOTED
CONTRACT HDR01
DWG. NO. HB1-012 REV. 4

FILE: 7552-001\HB1012R4 PLOT DATE: 11-11-96 -S-16

Bending Specimens

Additional Specimens B7 and B8

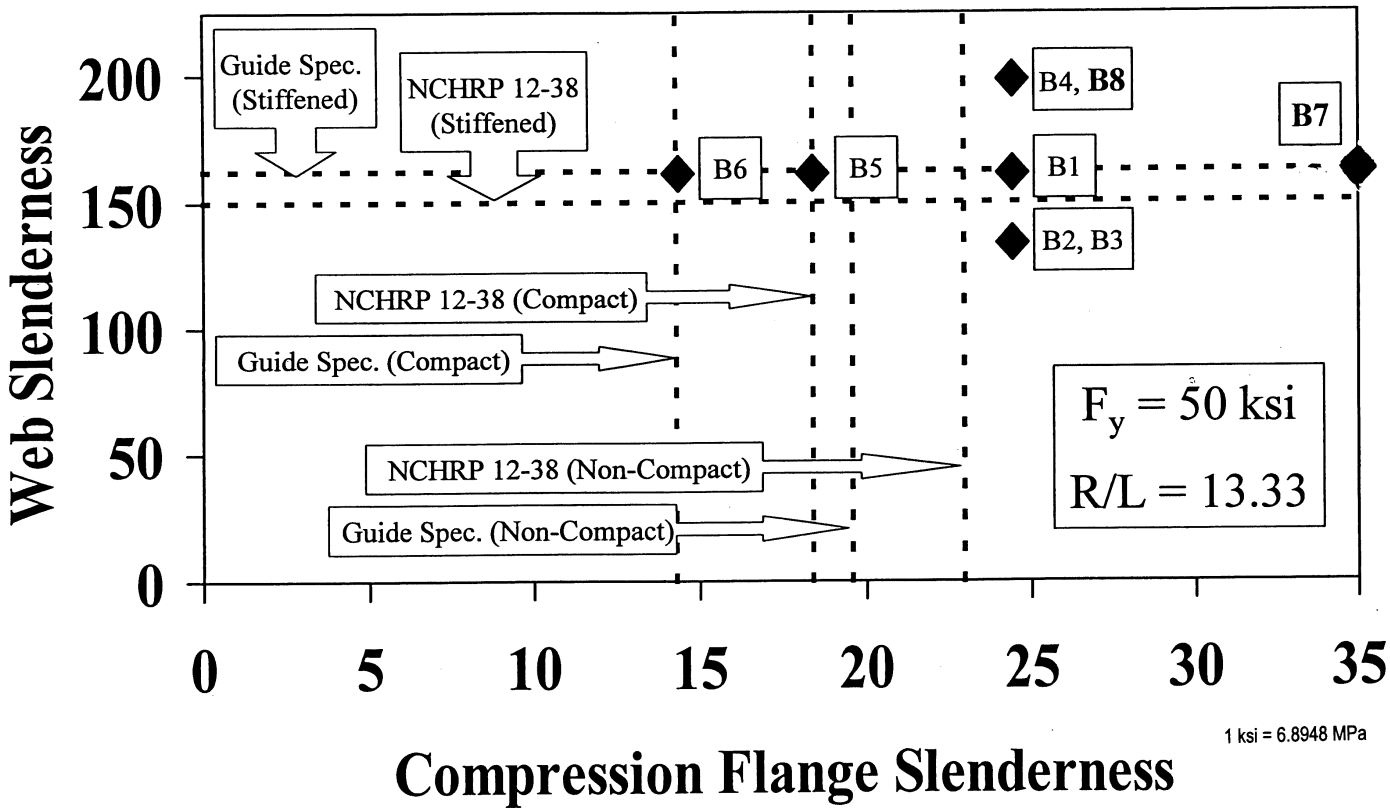

2.126

Figure 2.56

2.127

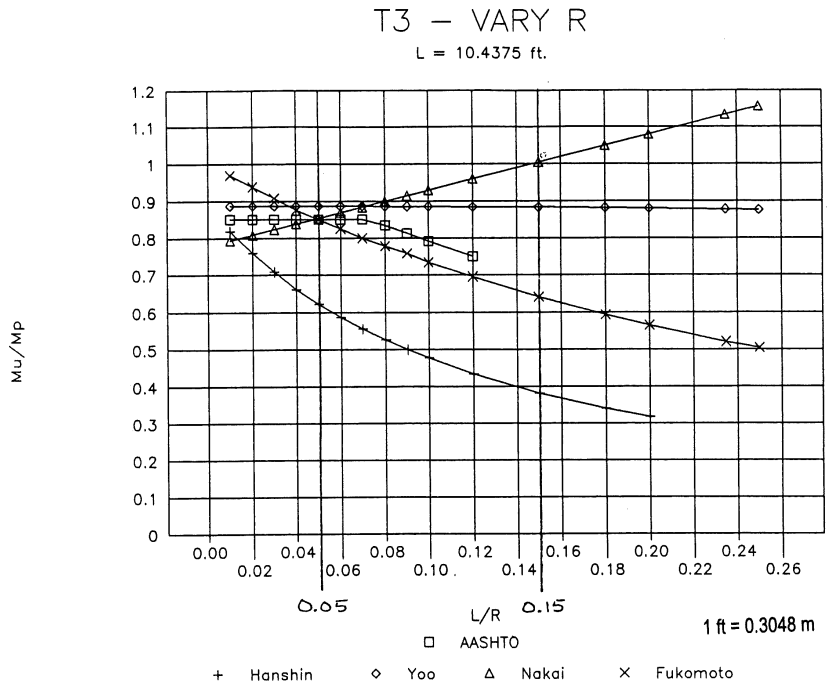

Figure 2.57. Preliminary Bending Component Specimen T3 – Predicted Capacities vs. L/R with R Varied and L Held Constant

2.128

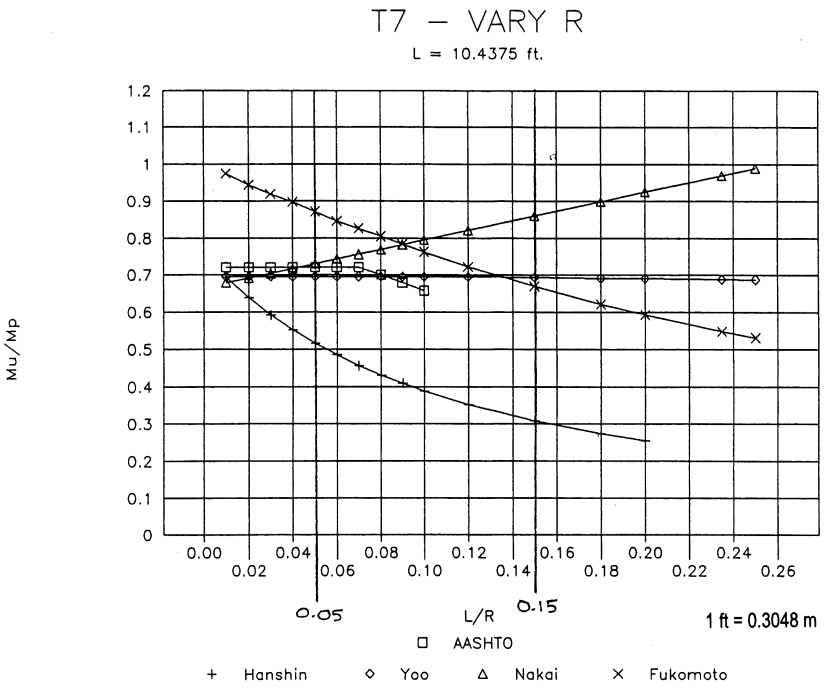

Figure 2.58. Preliminary Bending Component Specimen T7 – Predicted Capacities vs. L/R with R Varied and L Held Constant

2.129

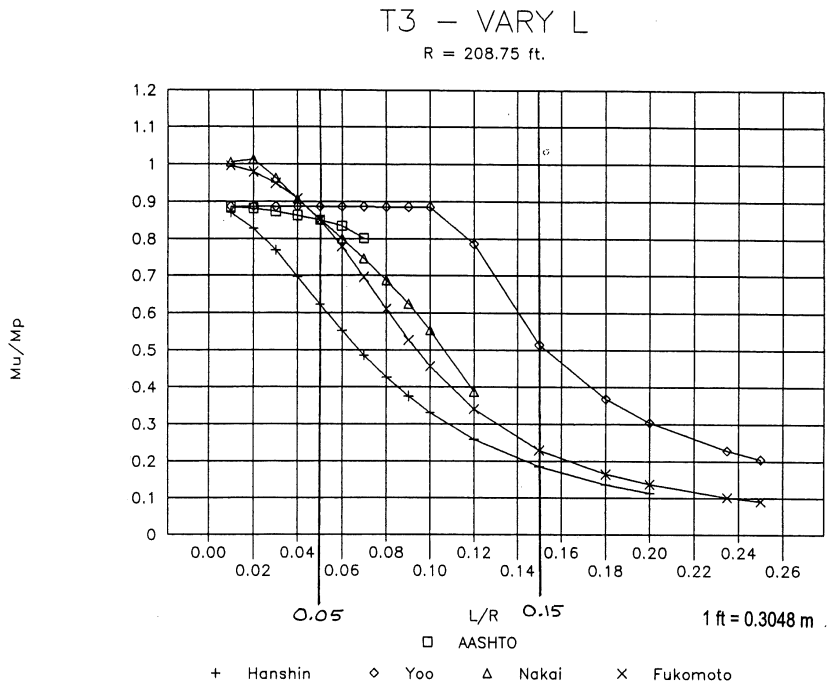

Figure 2.59. Preliminary Bending Component Specimen T3 – Predicted Capacities vs. L/R with L Varied and R Held Constant

2.130

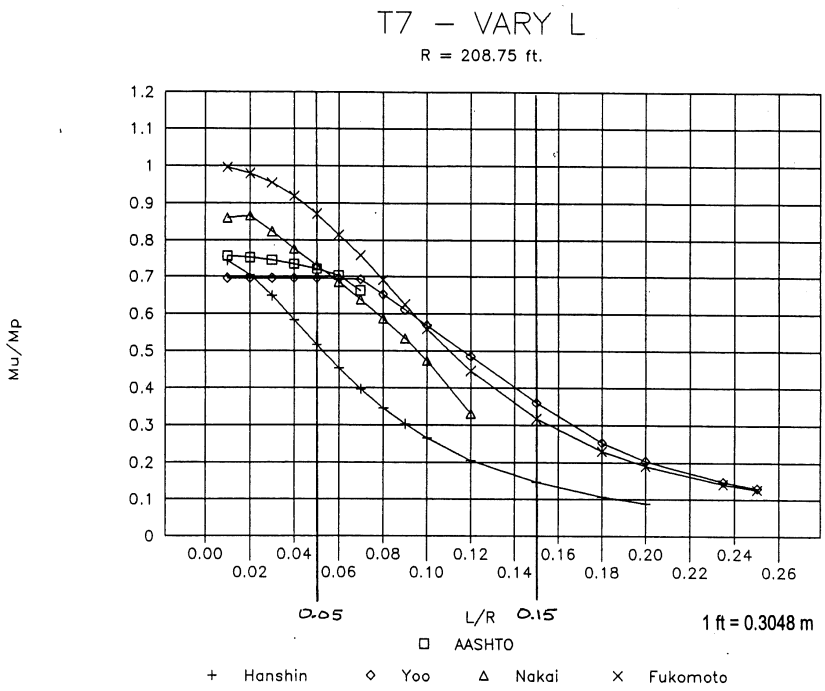

Figure 2.60. Preliminary Bending Component Specimen T7 – Predicted Capacities vs. L/R with L Varied and R Held Constant

APPENDIX A: ELASTIC ANALYSIS RESULTS FOR THE THREE-GIRDER TEST FRAME
(Preliminary Concept)

by Michael A. Grubb, P.E.[1] and Dann H. Hall[2]

Introduction

Detailed elastic analyses were carried out on the preliminary concept for the simple-span horizontally curved I-girder prototype bridge that was originally intended to serve as the test frame for the component specimen testing. A plan view of the three-girder prototype bridge is shown in Figure A.1. A cross section of the bridge is shown in Figure A.2. The girder spacing is set at 8′-9″ (2.7 m), with deck overhangs (not shown) set at 2′-9″ (0.84 m), for a total out-to-out width of 23′-0″ (7.0 m). An 8-inch (200 mm) cast-in-place concrete deck (with no integral wearing surface) spans the 8′-9″ (2.7 m) girder spacing. The deck is assumed flared from the edge of the deck haunch over the outermost and innermost girders to a thickness of 9.5 inches (240 mm) at the edge of the deck overhangs. The deck haunch is assumed to be 14-inches (355 mm) wide by 3-inches (76 mm) thick over each girder. The thickness of the haunch is measured from the top of the web to the bottom of the deck. Elevation views of each of the three girders are shown in Figures A.3 through A.5. The span length along the longitudinal centerline of the bridge (along Girder 2 or G2) is 90 feet (27.4 m), and the radius to the longitudinal centerline is 200 feet (61.0 m). The two end supports are radial. Girder 1 (G1) is located inside of the longitudinal centerline and Girder 3 (G3) is located outside of the longitudinal centerline. Superimposed dead loads include two 1′-6″ (0.46 m) wide parapets, each with a unit weight of 505 lbs/ft (752 kg/m), placed at the extreme edges of the deck, which results in a roadway width of 20′-0″ (6.1 m). A future wearing surface of 25 psf (122 kg/m^2) is also assumed. The bridge is designed for AASHTO H20 live loading. All live loads are assumed to be placed in 10-ft (3.05 m) design lanes and include impact.

Elastic analyses were carried out on full three-dimensional models of the bridge, which included the concrete deck. These analyses were conducted using the commercially available BSDI BRIDGE SYSTEM 3D finite-element analysis software (a comprehensive software package for the full three-dimensional analysis and design of bridge structures) (*1*), and with the general-purpose finite-element analysis software GTSTRUDL (*2*). The prototype bridge was also analyzed using the two-dimensional grid-analysis capability provided in the commercially available MDX software (*3*). Finally, the bridge was analyzed with the NSBA software package VANCK (*4*), which performs a V-load analysis that isolates and analyzes each girder in the system as a straight one-dimensional girder with a span length equal to the curved-girder arc length.

The results of each of these analyses are given in the following sections; listed for each girder are the vertical bending moments and vertical deflections at tenth points along the span, vertical end reactions, and the lateral-flange bending moments and maximum cross-frame forces at cross-frame Line 5L (Figure A.1). In most cases, actions are listed for the non-composite dead load (DL1), the composite dead load (DL2), and the maximum live load plus impact (LL+I). The results are for the *unfactored* loads. Since the bridge is symmetrical about midspan, actions at tenth points are only listed up to midspan, and vertical end reactions are only listed at one end of the bridge. For the three-dimensional finite-element analyses, dead-load displacements in three orthogonal directions are also given in the local coordinate system at the top and bottom of each girder web at each cross-frame line.

BSDI 3D System Analysis

This section summarizes the results of the three-dimensional elastic analysis of the prototype bridge using the BSDI BRIDGE SYSTEM 3D finite-element software (3D System). The model was developed in

---

[1] Bridge Software Development International, Ltd. (now with M.A. Grubb & Associates, LLC), Wexford, PA 15090

[2] Bridge Software Development International, Ltd. (now retired), Coopersburg, PA 18036

accordance with Figure A.1, with the exception that the bottom lateral bracing in the end bays was not included in the original model. A detailed description of the model is given in Chapter 2.

***Vertical Bending Moments*:** Table A1.1 lists the vertical bending moments in each girder at the tenth points computed from the 3D System results. The listed live load plus impact moments are the maximum envelope values. The governing live-load moments were caused by lane loading (lane loading governed on this rather short bridge because H20 loading was specified for the live load. According to AASHTO, H20 lane loading is specified to be the same as the HS20 lane loading). It was noted that small negative live load plus impact moments (not shown) resulted in Girder 1 from the placement of the live load at extreme positions on the influence surface relative to Girder 1.

Tenth Pt	GIRDER 1			GIRDER 2			GIRDER 3		
	DL1	DL2	LL+I	DL1	DL2	LL+I	DL1	DL2	LL+I
1	110	79	191	396	159	319	735	348	504
2	171	124	315	694	289	540	1313	604	898
3	204	150	393	909	388	695	1753	806	1207
4	216	162	434	1039	448	788	2022	928	1407
5	222	167	450	1083	468	821	2113	970	1475

Table A1.1 – BSDI 3D System Vertical Bending Moments at Tenth Points (k-ft)
(1 k-ft = 1.35582 kN-m)

***Vertical Deflections*:** Table A1.2 lists the computed vertical deflections in each girder at the tenth points from the BSDI 3D System. LL+I deflections are only given at midspan.

Tenth Pt	GIRDER 1			GIRDER 2			GIRDER 3		
	DL1	DL2	LL+I	DL1	DL2	LL+I	DL1	DL2	LL+I
1	0.42	0.11	--	0.93	0.19	--	1.46	0.29	--
2	0.77	0.21	--	1.77	0.37	--	2.77	0.54	--
3	1.05	0.29	--	2.42	0.50	--	3.80	0.74	--
4	1.24	0.34	--	2.83	0.59	--	4.45	0.87	--
5	1.30	0.35	0.43	2.97	0.62	0.69	4.68	0.91	0.95

Table A1.2 – BSDI 3D System Vertical Deflections at Tenth Points (in.)
(1 in. = 25.4 mm)

***Vertical End Reactions*:** Table A1.3 lists the computed vertical end reactions from the BSDI 3D System at Line 1L (Figure A.1). For the reactions due to live load plus impact, the first (negative) number represents the maximum upward reaction that resists the maximum downward force at the bearing under consideration. The second (positive or zero) number represents the maximum downward reaction that resists the maximum uplift force with the live load positioned to cause the maximum uplift at the bearing under consideration. This downward reaction would be appropriately combined with the total vertical dead load reaction at the bearing under consideration to determine if an uplift condition actually exists.

GIRDER 1			GIRDER 2			GIRDER 3		
DL1	**DL2**	**LL+I**	**DL1**	**DL2**	**LL+I**	**DL1**	**DL2**	**LL+I**
-16	-10	-33/9	-48	-17	-49/0	-81	-41	-64/0

Table A1.3 – BSDI 3D System Vertical End Reactions at Line 1L (kips)
(1 kip = 4.4482 kN)

***Lateral Flange Bending Moments*:** Table A1.4 lists the absolute value of the bottom-flange lateral bending moments, M_l, at cross-frame Line 5L computed from the BSDI 3D System results using the following approximate formula (5):

$$M_l = \frac{Md^2}{10\,hR} \qquad \text{(A-1)}$$

where: M = vertical bending moment in the curved girder at the cross frame
d = cross-frame spacing
R = girder radius
h = vertical distance between flange centerlines

GIRDER 1			GIRDER 2			GIRDER 3		
DL1	**DL2**	**LL+I**	**DL1**	**DL2**	**LL+I**	**DL1**	**DL2**	**LL+I**
2.58	1.93	5.23	13.03	5.64	9.89	26.39	12.11	18.47

Table A1.4 – BSDI 3D System Bottom-Flange Lateral Bending Moments at Line 5L from Equation A-1 (k-ft) (1 k-ft = 1.35582 kN-m)

Table A1.5 lists the lateral moments in the top and bottom flanges of Girder 3 at each cross-frame line and halfway in-between each cross-frame line due to the non-composite dead load (DL1), as obtained directly from the BSDI 3D System output. A negative moment is assumed to cause compression on the outside or convex tip of the flange.

SECTION	TOP FLANGE	BOTTOM FLANGE
1L	0	0
	4	-4
2L	-5	5
	10	-12
3L	-9	8
	16	-17
4L	-13	10
	18	-21
5L	-14	12
	20	-22

Table A1.5 – Lateral DL1 Flange Moments (G3) Obtained from BSDI 3D System Output (k-ft) – No Bottom Flange Lateral Braces (1 k-ft = 1.35582 kN-m)

Table A1.6 lists the same moments with the bottom flange lateral braces (Figure A.1) included in the model in the end bays. WT 6 x 20 (WT155 x 30) structural tees were assumed for the lateral bracing members. Note the influence of the braces on the distribution of the bottom flange lateral bending moments.

SECTION	TOP FLANGE	BOTTOM FLANGE
1L	0	0
	5	-1
2L	-4	12
	12	-5
3L	-9	16
	16	-10
4L	-12	17
	20	-13
5L	-13	19
	20	-14

Table A1.6 – Lateral DL1 Flange Moments (G3) Obtained from BSDI 3D System Output (k-ft) – With Bottom Flange Lateral Braces (1 k-ft = 1.35582 kN-m)

***Cross-Frame Forces*:** Table A1.7 lists the computed maximum cross-frame forces from the BSDI 3D System at cross-frame Line 5L. Note that the reported live load plus impact responses are not necessarily caused by coincident loads. G1-G2 refers to the cross frame between Girders 1 and 2 and G2-G3 refers to the cross frame between Girders 2 and 3. Positive values are tensile forces and negative values are

compressive forces. The figure below may be used as a key for matching the reported responses with each member.

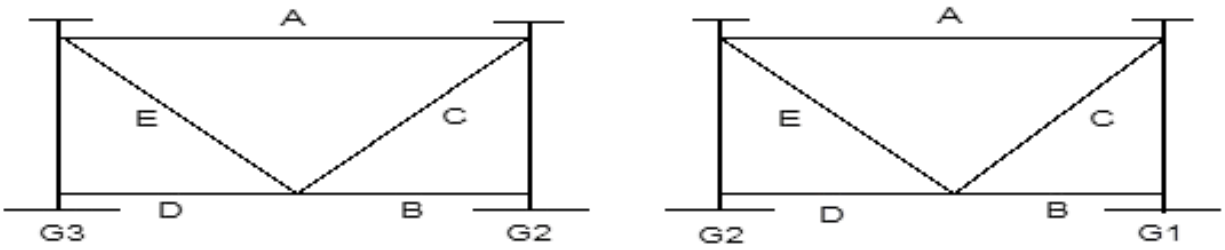

Member	G2 – G3				G1 – G2			
	DL1	DL2	LL+I		DL1	DL2	LL+I	
			(+)	(-)			(+)	(-)
Top Strut - A	14	-1	2	0	7	-3	1	-1
Diagonal - C	-14	-1	0	-12	-13	-10	0	-8
Diagonal - E	14	1	12	0	13	10	8	0
Bot. Strut - B	-3	-9	6	-3	2	2	5	-1
Bot. Strut - D	-25	-10	0	-16	-16	-14	2	-8

Table A1.7 – BSDI 3D System Cross-Frame Forces at Line 5L (kips)
(1 kip = 4.4482 kN)

***Local Web Displacements*:** Tables A1.8 through A1.10 list the computed displacements from the BSDI 3D System in three orthogonal directions at the bottom and top of the web of Girders 1 through 3, respectively. The displacements are given at each cross-frame line due to the dead load of the structural steel and the dead load of the concrete deck. All displacements are indicated in the element or local coordinate system. Positive tangential and radial displacements are in the directions shown in Figure A.1 (L = tangential and R = radial). Downward vertical displacements are negative. These results were obtained from a separate analysis of the bridge using the finite-element solver contained within the 3D System software. In this analysis, the boundary conditions corresponded to the boundary conditions used in the GTSTRUDL analysis model (described later). The bottom lateral bracing was also included in the model in the end bays. WT6 x 20 (WT155 x 30) structural tees were again assumed for the lateral bracing members.

***Variations to the Base Model*:** In addition to the base configuration of the model described above, a number of parametric variations to the geometry were made and analyzed with the BSDI 3D System software. The specific variations that were made and the results of those analyses are discussed in detail in Appendix B.

CROSS-FRAME LINE	TOP OF WEB					
	DEAD LOAD - STEEL			DEAD LOAD - DECK		
	TANGENTIAL	RADIAL	VERTICAL	TANGENTIAL	RADIAL	VERTICAL
1L	0.057	0.001	0.000	0.210	0.002	-0.002
2L	0.055	0.088	-0.085	0.201	0.240	-0.375
3L	0.047	0.160	-0.158	0.177	0.441	-0.695
4L	0.037	0.211	-0.211	0.141	0.584	-0.927
5L	0.025	0.238	-0.238	0.099	0.658	-1.048
5R	0.012	0.238	-0.238	0.055	0.658	-1.048
4R	0.000	0.212	-0.211	0.012	0.584	-0.927
3R	-0.011	0.160	-0.158	-0.023	0.441	-0.695
2R	-0.017	0.087	-0.085	-0.047	0.241	-0.375
1R	-0.020	0.000	0.000	-0.056	0.002	-0.002

CROSS-FRAME LINE	BOTTOM OF WEB					
	DEAD LOAD - STEEL			DEAD LOAD - DECK		
	TANGENTIAL	RADIAL	VERTICAL	TANGENTIAL	RADIAL	VERTICAL
1L	0.021	-0.001	0.000	0.052	-0.002	0.000
2L	0.006	0.027	-0.085	0.013	0.069	-0.375
3L	0.002	0.038	-0.158	0.005	0.095	-0.696
4L	-0.001	0.044	-0.211	-0.001	0.112	-0.927
5L	-0.004	0.046	-0.239	-0.007	0.122	-1.049
5R	-0.006	0.045	-0.239	-0.011	0.126	-1.049
4R	-0.007	0.042	-0.211	-0.013	0.125	-0.927
3R	-0.006	0.034	-0.158	-0.010	0.118	-0.696
2R	-0.004	0.024	-0.085	0.002	0.108	-0.375
1R	0.017	-0.001	0.000	0.102	-0.002	0.000

Table A1.8 – BSDI 3D System Local Web Displacements in Girder 1 (in.)
(1 in. = 25.4 mm)

CROSS-FRAME LINE	TOP OF WEB					
	DEAD LOAD - STEEL			DEAD LOAD - DECK		
	TANGENTIAL	RADIAL	VERTICAL	TANGENTIAL	RADIAL	VERTICAL
1L	0.094	0.001	-0.001	0.318	0.002	-0.005
2L	0.089	0.088	-0.235	0.302	0.241	-0.798
3L	0.075	0.161	-0.438	0.259	0.443	-1.488
4L	0.056	0.213	-0.586	0.196	0.587	-1.994
5L	0.032	0.239	-0.665	0.120	0.662	-2.261
5R	0.007	0.239	-0.665	0.041	0.662	-2.261
4R	-0.017	0.213	-0.586	-0.035	0.587	-1.994
3R	-0.036	0.160	-0.438	-0.099	0.443	-1.488
2R	-0.050	0.087	-0.235	-0.141	0.242	-0.798
1R	-0.055	0.000	-0.001	-0.157	0.002	-0.005

CROSS-FRAME LINE	BOTTOM OF WEB					
	DEAD LOAD - STEEL			DEAD LOAD - DECK		
	TANGENTIAL	RADIAL	VERTICAL	TANGENTIAL	RADIAL	VERTICAL
1L	0.000	0.000	0.000	0.000	0.000	0.000
2L	0.001	0.018	-0.235	0.006	0.043	-0.798
3L	0.005	0.031	-0.438	0.020	0.072	-1.489
4L	0.010	0.037	-0.587	0.041	0.088	-1.995
5L	0.016	0.041	-0.665	0.066	0.095	-2.262
5R	0.023	0.041	-0.665	0.093	0.095	-2.262
4R	0.029	0.037	-0.587	0.119	0.088	-1.996
3R	0.034	0.030	-0.438	0.141	0.072	-1.489
2R	0.038	0.018	-0.235	0.154	0.043	-0.798
1R	0.039	0.000	0.000	0.161	0.000	0.000

Table A1.9 – BSDI 3D System Local Web Displacements in Girder 2 (in.)
(1 in. = 25.4 mm)

CROSS-FRAME LINE	TOP OF WEB					
	DEAD LOAD - STEEL			DEAD LOAD - DECK		
	TANGENTIAL	RADIAL	VERTICAL	TANGENTIAL	RADIAL	VERTICAL
1L	0.136	0.001	-0.002	0.442	0.002	-0.007
2L	0.129	0.089	-0.387	0.419	0.245	-1.229
3L	0.107	0.163	-0.722	0.355	0.449	-2.296
4L	0.077	0.215	-0.969	0.259	0.594	-3.079
5L	0.040	0.242	-1.099	0.145	0.670	-3.494
5R	0.001	0.242	-1.099	0.023	0.670	-3.494
4R	-0.036	0.215	-0.969	-0.092	0.594	-3.079
3R	-0.067	0.163	-0.722	-0.187	0.449	-2.296
2R	-0.088	0.089	-0.387	-0.251	0.245	-1.229
1R	-0.095	0.001	-0.002	-0.274	0.002	-0.007

CROSS-FRAME LINE	BOTTOM OF WEB					
	DEAD LOAD - STEEL			DEAD LOAD - DECK		
	TANGENTIAL	RADIAL	VERTICAL	TANGENTIAL	RADIAL	VERTICAL
1L	-0.011	0.001	0.000	-0.025	0.001	0.000
2L	-0.009	0.018	-0.387	-0.018	0.040	-1.229
3L	-0.004	0.029	-0.723	0.001	0.067	-2.297
4L	0.005	0.035	-0.970	0.030	0.082	-3.082
5L	0.015	0.039	-1.100	0.066	0.089	-3.497
5R	0.025	0.038	-1.100	0.102	0.088	-3.497
4R	0.036	0.035	-0.970	0.137	0.082	-3.082
3R	0.044	0.029	-0.723	0.166	0.068	-2.297
2R	0.050	0.017	-0.387	0.186	0.041	-1.229
1R	0.052	0.001	0.000	0.193	0.001	0.000

Table A1.10 – BSDI 3D System Local Web Displacements in Girder 3 (in.)
(1 in. = 25.4 mm)

GTSTRUDL Analysis

This section summarizes the results of the three-dimensional elastic analysis of the original prototype bridge using the general-purpose finite-element software GTSTRUDL. The model was developed in accordance with Figure A.1. In addition, the model was developed with the following boundary conditions at the end bearings:

Girder 1: Girder 1 was fixed against vertical translation and was free to translate in the tangential and radial directions at Lines 1L and 1R (Figure A.1).

Girder 2: Girder 2 was fixed against translation in all three orthogonal directions at Line 1L. At Line 1R, Girder 2 was fixed against translation in the vertical and radial directions but was free to translate in the tangential direction.

Girder 3: Girder 3 was fixed against vertical translation and was free to translate in the tangential and radial directions at Lines 1L and 1R.

All restraints were applied in the element or local coordinate system. The girders were free to rotate about their local X, Y, and Z-axes at both Lines 1L and 1R. For the boundary conditions defined above, it was necessary to include the bottom lateral bracing in the end bays (Figure A.1) in the model to provide stability and prevent numerical singularities in the stiffness matrix when the concrete deck elements were not included in the model. WT6 x 20 (WT155 x 30) structural tees were assumed for the lateral bracing members.

The basic model was developed using the steel-girder module of the commercially available SC-BRIDGE preprocessor (*6*) to GTSTRUDL. Variations to this basic model were then made as required. Top and bottom flanges were modeled as straight beam elements, and the web and concrete deck were modeled as straight rectangular plate elements; all elements have six degrees of freedom at each node. A single plate element was used to model the web through the depth. In the transverse direction, nodes were located at girders, midway between the girders, and at the edge of the deck overhangs at the elevation of the mid-thickness of the concrete deck, which resulted in a total of six plate elements in the transverse direction to model the deck. At cross-frame lines, a single node was also defined at the elevation of the bottom of the web in-between each girder in the transverse direction to accommodate the inverted K-type cross frames. In the longitudinal direction, nodes were defined at cross-frame locations and midway between cross-frame locations, which resulted in a total of 18 sets of elements along each girder. The centroid of each of the top- and bottom-flange beam elements was offset from the upper and lower edges of the web plate-element nodes. Beam elements were also used to define the concrete deck haunch; eccentricities from the top web nodes to the centroid of the deck-haunch beams were again defined to offset the haunch elements above the web. Rigid beam elements, with a large moment of inertia relative to the flange and deck-haunch elements, were defined between the deck-haunch beams and the mid-surface of the deck elements to constrain the deck and girder elements to act together structurally. Cross-frame members were modeled as beam elements that were connected directly to the top and bottom web nodes. Pinned end connections were approximated by releasing all internal moments at the ends of each cross frame member, with the exception of the torsional moment at one end (a limitation of the particular beam element that was used in the analysis is that at least one moment at one end of the member cannot be released in order to provide numerical stability). The bottom strut was defined as a continuous member at the intersection with the diagonals. The cross-frame connection plates were not included in the model.

Analyses were run for the dead load of the structural steel, the dead load of the concrete deck, and the composite dead load (barriers and curbs). The self-weight of the structural steel members was applied as body forces. The weight of the concrete deck and deck haunches was applied as equivalent uniformly distributed loads to the top-flange elements of the steel superstructure. In the composite dead-load analysis, the elastic modulus of the concrete was divided by 3 to account in an approximate fashion for the effects of concrete creep. The bottom lateral bracing members were also removed. The barriers were applied as a surface load to the top of the deck elements representing the deck overhangs. The future wearing surface

load was applied as a surface load to the remaining deck elements. Live-load analyses were not run on the GTSTRUDL model because of the substantial effort that would have been required to generate the required influence surfaces and moment envelopes. Thus, results for live load plus impact are not given below.

***Vertical Bending Moments*:** Table A2.1 lists the vertical bending moments in each girder at the tenth points computed from the GTSTRUDL results. The vertical bending moments at sections halfway in-between the element nodes in the longitudinal direction were determined from the calculated curvatures at those sections. The listed moments at the tenth points, which did not coincide with those locations, were then determined by linear interpolation (or extrapolation).

Tenth Pt	GIRDER 1			GIRDER 2			GIRDER 3		
	DL1	DL2	LL+I	DL1	DL2	LL+I	DL1	DL2	LL+I
1	106	62	--	361	154	--	669	311	--
2	161	93	--	639	279	--	1222	550	--
3	187	109	--	840	369	--	1631	727	--
4	197	116	--	958	422	--	1882	836	--
5	201	119	--	1011	446	--	1994	884	--

Table A2.1 -- GTSTRUDL Vertical Bending Moments at Tenth Points (k-ft)
(1 k-ft = 1.35582 kN-m)

***Vertical Deflections*:** Table A2.2 lists the computed vertical deflections in each girder at the tenth points computed from the GTSTRUDL results. The listed values were determined by linear interpretation (or extrapolation) of the computed nodal values.

Tenth Pt	GIRDER 1			GIRDER 2			GIRDER 3		
	DL1	DL2	LL+I	DL1	DL2	LL+I	DL1	DL2	LL+I
1	0.39	0.10	--	0.89	0.19	--	1.39	0.30	--
2	0.74	0.18	--	1.67	0.36	--	2.62	0.56	--
3	1.00	0.25	--	2.28	0.50	--	3.58	0.76	--
4	1.16	0.29	--	2.67	0.58	--	4.19	0.89	--
5	1.24	0.31	--	2.84	0.62	--	4.47	0.94	--

Table A2.2 -- GTSTRUDL Vertical Deflections at Tenth Points (in.)
(1 in. = 25.4 mm)

***Vertical End Reactions*:** Table A2.3 lists the computed vertical end reactions at Line 1L (Figure A.1) from GTSTRUDL.

GIRDER 1			GIRDER 2			GIRDER 3		
DL1	DL2	LL+I	DL1	DL2	LL+I	DL1	DL2	LL+I
-16	-9	--	-50	-18	--	-80	-38	--

Table A2.3 -- GTSTRUDL Vertical End Reactions at Line 1L (kips)
(1 kip = 4.4482 kN)

Lateral Flange Bending Moments: Table A2.4 lists the absolute value of the bottom-flange lateral bending moments at cross-frame Line 5L computed from the GTSTRUDL results. The lateral flange bending moments, M_l, in this table were computed using the following approximate formula (7):

$$M_l = \frac{Md^2}{12\,hR} \tag{A-2}$$

where: M = vertical bending moment in the curved girder at the cross frame
d = cross-frame spacing
R = girder radius
h = vertical distance between flange centerlines

GIRDER 1			GIRDER 2			GIRDER 3		
DL1	DL2	LL+I	DL1	DL2	LL+I	DL1	DL2	LL+I
1.9	1.1	--	10.0	4.4	--	20.4	9.0	--

Table A2.4 -- Computed GTSTRUDL Bottom-Flange Lateral Bending Moments at Line 5L from Equation A-2 (k-ft) (1 k-ft = 1.35582 kN-m)

Table A2.5 lists the lateral moments in the top and bottom flanges of Girder 3 at each cross-frame line and halfway in-between each cross-frame line due to the non-composite dead load, as obtained directly from the GTSTRUDL output. A negative moment is assumed to cause compression on the outside or convex tip of the flange. Recall that the bottom flange lateral braces are included in the model in the end bays.

SECTION	TOP FLANGE	BOTTOM FLANGE
1L	0.0	0.0
	4.6	-1.7
2L	-4.7	11.2
	11.1	-5.0
3L	-8.8	15.1
	16.3	-10.6
4L	-11.6	17.2
	18.7	-13.5
5L	-12.9	18.2
	20.0	-15.0

Table A2.5 – Lateral DL1 Flange Moments (G3) Obtained from GTSTRUDL Output (k-ft) – With Bottom Flange Lateral Braces (1 k-ft = 1.35582 kN-m)

The above-listed moments include the effects of lateral bending of the flanges in-between each cross frame and lateral bending of the entire girder in-between the end supports. To reduce the latter component, a separate analysis was run with artificial rigid radial restraints included in the model at the top and bottom flange of each girder at each cross-frame line. Table A2.7 lists the noncomposite dead load lateral moment in each flange of Girder 3 obtained directly from the GTSTRUDL output for this analysis.

SECTION	TOP FLANGE	BOTTOM FLANGE
1L	0.0	0.0
	2.2	-2.7
2L	-3.9	4.7
	5.3	-5.5
3L	-6.7	7.3
	7.8	-8.2
4L	-8.6	9.2
	8.9	-9.3
5L	-9.4	10.0
	9.5	-9.9

Table A2.6 – Lateral DL1 Flange Moments (G3) Obtained from GTSTRUDL Output (k-ft) – With Bottom Flange Lateral Braces & Rigid Radial Restraints at the Cross Frames (1 k-ft = 1.35582 kN-m)

With the contribution of the lateral bending of the girder between end supports reduced, the lateral moments in each flange are more nearly equal at each section. Note that the contribution of lateral bending of the girder is fairly significant in this example and that its effect is currently not directly comprehended in computing lateral flange bending moments using the approximate formulas A1 or A2. The resulting moments at cross-frame Line 5L from Table A2.6 are about one-half of the value computed from the approximate formula A2 (Table A2.4). The BSDI 3D System and GTSTRUDL models included only two elements in-between each cross frame to model the flanges; additional refinement of the models would likely lead to a more accurate computation of the lateral flange bending moments (*7*), but at the same time, would add to the size and complexity of the models.

***Cross-Frame Forces*:** Table A2.7 lists the computed maximum cross-frame forces at cross-frame Line 5L from GTSTRUDL. The format for the table is the same as that described previously for Table A1.7. Note that the DL1 forces in the diagonals are not equal because the bottom strut was assumed to be continuous at the intersection with the diagonals, which introduces a small moment and shear forces at that location.

Member	G2 – G3				G1 – G2			
	DL1	DL2	LL+I		DL1	DL2	LL+I	
			(+)	(-)			(+)	(-)
Top Strut - A	12	-1	--	--	6	-1	--	--
Diagonal - C	-12	-3	--	--	-11	-8	--	--
Diagonal - E	17	3	--	--	14	8	--	--
Bot. Strut - B	-3	-9	--	--	3	2	--	--
Bot. Strut - D	-25	-10	--	--	-16	-10	--	--

Table A2.7 -- GTSTRUDL Cross-Frame Forces at Line 5L (kips)
(1 kip = 4.4482 kN)

***Local Web Displacements*:** Tables A2.8 through A2.10 list the computed displacements from GTSTRUDL in three orthogonal directions at the bottom and top of the web of Girders 1 through 3, respectively. The displacements are given at each cross-frame line due to the dead load of the structural steel and the dead load of the concrete deck. All displacements are indicated in the element or local coordinate system. Positive tangential and radial displacements are in the directions shown in Figure A.1 (L = tangential and R = radial). Downward vertical displacements are negative.

***Variations to the Base Model*:** Variations to the base GTSTRUDL model were made to observe their effects on the results. All studies were made for the non-composite dead load case. In the first variation, cross-frame connection plates were included in the model on all girders. The connection plates were modeled with beam elements that were rigidly connected to the top and bottom web nodes. On exterior girders, the connection plates were on one side of the web only. The maximum vertical deflection at the midspan of Girder 3 was reduced from 4.47 inches (113.5 mm) to 4.34 inches (110.2 mm). Including additional transverse stiffeners on one side of the web halfway in-between each cross frame (rigidly connected to the top and bottom web nodes) reduced this deflection further to 4.22 inches (107.2 mm). Removing the intermediate transverse stiffeners on the web and all moment releases at the ends of the cross-frame members to simulate rigid connections of the members to the connection plates resulted in a maximum vertical deflection of 3.38 inches (85.9 mm).

In another study, the ends of all the cross-frame members were offset vertically from the top and bottom web nodes. The top strut and the top ends of the diagonals were lowered 6.5 inches (165 mm) and the bottom strut and lower ends of the diagonals were raised 8 inches (203 mm) to correspond to the actual locations of the centerline of the cross-frame connections. The maximum vertical deflection at midspan of Girder 3 increased from 4.47 (113.5 mm) inches to 8.20 inches (208.3 mm). The maximum radial deflection increased from 0.9 inches (23 mm) to 2.8 inches (71 mm). The vertical bending moments in Girders 1, 2, and 3 changed slightly to 216.0 (293.0), 1019.0 (1381.6), and 1951.0 (2645.2) k-ft (N-mm), respectively. The cross-frame forces in some members at Line 5L increased as much as 30 percent. Doubling the top and bottom offsets to 13.0 (330.2) and 16.0 (406.4) inches (mm) increased the vertical and radial deflections to 40.2 (1021.1) and 22.4 (569.0) inches (mm), respectively. Removing the moment releases at the ends of all the cross-frame members to simulate rigid connections reduced the maximum vertical deflection to 3.5 inches (88.9 mm) and the maximum radial deflection to 0.3 inches (7.6 mm). The vertical bending moments in Girders 1, 2, and 3 were 520.7 (706.0), 1037.2 (1406.3), and 1648.8 (2235.5) k-ft (N-mm), respectively, for this case. The cross-frame forces were also reduced significantly to values generally below the values in the base model.

CROSS-FRAME LINE	TOP OF WEB					
	DEAD LOAD - STEEL			DEAD LOAD - DECK		
	TANGENTIAL	RADIAL	VERTICAL	TANGENTIAL	RADIAL	VERTICAL
1L	0.054	0.001	0.000	0.198	0.001	-0.002
2L	0.052	0.084	-0.081	0.192	0.230	-0.357
3L	0.045	0.153	-0.149	0.168	0.423	-0.662
4L	0.035	0.204	-0.198	0.134	0.561	-0.882
5L	0.024	0.229	-0.224	0.094	0.633	-0.996
5R	0.012	0.229	-0.224	0.051	0.632	-0.996
4R	0.000	0.203	-0.198	0.012	0.562	-0.882
3R	-0.010	0.154	-0.149	-0.022	0.423	-0.662
2R	-0.017	0.084	-0.081	-0.046	0.230	-0.357
1R	-0.019	0.001	0.000	-0.053	0.001	-0.002

CROSS-FRAME LINE	BOTTOM OF WEB					
	DEAD LOAD - STEEL			DEAD LOAD - DECK		
	TANGENTIAL	RADIAL	VERTICAL	TANGENTIAL	RADIAL	VERTICAL
1L	0.020	-0.001	0.000	0.049	-0.002	0.000
2L	0.005	0.026	-0.081	0.013	0.065	-0.357
3L	0.002	0.035	-0.149	0.005	0.090	-0.662
4L	-0.001	0.041	-0.198	-0.001	0.107	-0.882
5L	-0.004	0.044	-0.224	-0.007	0.117	-0.996
5R	-0.006	0.043	-0.224	-0.011	0.119	-0.996
4R	-0.007	0.039	-0.198	-0.013	0.118	-0.882
3R	-0.006	0.033	-0.149	-0.010	0.112	-0.662
2R	-0.004	0.022	-0.081	0.002	0.102	-0.357
1R	0.015	-0.001	0.000	0.095	-0.002	0.000

Table A2.8 – GTSTRUDL Local Web Displacements in Girder 1 (in.)
(1 in. = 25.4 mm)

CROSS-FRAME LINE	TOP OF WEB					
	DEAD LOAD - STEEL			DEAD LOAD - DECK		
	TANGENTIAL	RADIAL	VERTICAL	TANGENTIAL	RADIAL	VERTICAL
1L	0.089	0.001	-0.001	0.301	0.002	-0.005
2L	0.085	0.084	-0.224	0.289	0.232	-0.764
3L	0.072	0.155	-0.418	0.248	0.426	-1.424
4L	0.053	0.204	-0.560	0.187	0.564	-1.908
5L	0.030	0.231	-0.635	0.114	0.636	-2.163
5R	0.006	0.231	-0.635	0.038	0.636	-2.163
4R	-0.016	0.204	-0.560	-0.035	0.564	-1.908
3R	-0.035	0.154	-0.418	-0.096	0.426	-1.424
2R	-0.048	0.084	-0.224	-0.137	0.232	-0.764
1R	-0.052	0.000	-0.001	-0.149	0.001	-0.005

CROSS-FRAME LINE	BOTTOM OF WEB					
	DEAD LOAD - STEEL			DEAD LOAD - DECK		
	TANGENTIAL	RADIAL	VERTICAL	TANGENTIAL	RADIAL	VERTICAL
1L	0.000	0.000	0.000	0.000	0.000	0.000
2L	0.001	0.017	-0.224	0.006	0.040	-0.764
3L	0.004	0.029	-0.418	0.019	0.068	-1.424
4L	0.010	0.036	-0.560	0.039	0.084	-1.908
5L	0.016	0.039	-0.635	0.063	0.090	-2.163
5R	0.021	0.038	-0.635	0.089	0.090	-2.163
4R	0.027	0.035	-0.560	0.113	0.083	-1.908
3R	0.032	0.029	-0.418	0.133	0.068	-1.424
2R	0.035	0.017	-0.224	0.146	0.041	-0.764
1R	0.037	0.000	0.000	0.152	0.000	0.000

Table A2.9 – GTSTRUDL Local Web Displacements in Girder 2 (in.)
(1 in. = 25.4 mm)

CROSS-FRAME LINE	TOP OF WEB					
	DEAD LOAD - STEEL			DEAD LOAD - DECK		
	TANGENTIAL	RADIAL	VERTICAL	TANGENTIAL	RADIAL	VERTICAL
1L	0.130	0.001	-0.002	0.421	0.002	-0.007
2L	0.123	0.085	-0.370	0.402	0.234	-1.177
3L	0.103	0.156	-0.692	0.341	0.431	-2.199
4L	0.073	0.207	-0.928	0.249	0.571	-2.951
5L	0.037	0.233	-1.053	0.138	0.644	-3.349
5R	0.000	0.233	-1.053	0.020	0.644	-3.349
4R	-0.036	0.207	-0.928	-0.090	0.571	-2.951
3R	-0.065	0.156	-0.692	-0.182	0.431	-2.199
2R	-0.085	0.086	-0.370	-0.244	0.235	-1.177
1R	-0.092	0.001	-0.002	-0.263	0.002	-0.007

CROSS-FRAME LINE	BOTTOM OF WEB					
	DEAD LOAD - STEEL			DEAD LOAD - DECK		
	TANGENTIAL	RADIAL	VERTICAL	TANGENTIAL	RADIAL	VERTICAL
1L	-0.011	0.001	0.000	-0.023	0.001	0.000
2L	-0.009	0.017	-0.370	-0.016	0.038	-1.177
3L	-0.004	0.027	-0.692	0.003	0.064	-2.201
4L	0.005	0.034	-0.928	0.030	0.077	-2.953
5L	0.014	0.037	-1.053	0.062	0.084	-3.350
5R	0.024	0.037	-1.053	0.096	0.083	-3.350
4R	0.034	0.033	-0.928	0.129	0.078	-2.953
3R	0.041	0.027	-0.692	0.156	0.063	-2.201
2R	0.046	0.016	-0.370	0.174	0.038	-1.177
1R	0.049	0.000	0.000	0.182	0.001	0.000

Table A2.10 – GTSTRUDL Local Web Displacements in Girder 3 (in.)
(1 in. = 25.4 mm)

MDX Grid Analysis

This section summarizes the results of the prototype analysis using the two-dimensional grid-analysis capability provided in the commercially available MDX software. The model was developed in accordance with Figure A.1, with the exception that the bottom lateral bracing in the end bays was not included in the model. At the time this analysis was run, there were no provisions in the software to model these lateral-bracing members. At each support, the software assumed that the support acted as a ″ball joint″ type bearing; that is, each support joint provided translational restraint in the vertical direction normal to the plane of the grid, while allowing free rotation about the radial and tangential axes in the plane of the grid. At the ends of each member in the grid, three degrees of freedom of movement are permitted; translation normal to the grid and rotation about the two axes in the plane of the grid. In a grid analysis, the translations in the radial and tangential directions and the rotation about the vertical axis are not active degrees of freedom.

The defined grid consisted of the girders and cross-frame members. All girder elements were assumed to be straight between nodes and cross-frame members were assumed to be rigidly connected to the girders so that moment was transferred at the connection. In the longitudinal direction, nodes were generated at cross-frame lines resulting in 9 elements per span per girder. The appropriate moments of inertia for each girder element were calculated internally for each loading condition, including composite moments of inertia for the composite dead-load and live-load analyses. In the transverse direction, nodes were generated at girder lines resulting in one cross-frame element between each girder. The bending stiffness of the cross-frame members to be input into the analysis was calculated by analyzing the cross frame as an indeterminate frame. In this analysis, the end connections on one side of the frame were assumed to be pinned. On the other side of the frame, the members were released at the top of the frame and were supported by a roller support at the bottom of the frame. A unit end moment was applied at the released end of the cross frame and the resulting angle of rotation, theta, was calculated based on the horizontal displacements of the top and bottom cross-frame members. This rotation was then used to calculate the equivalent bending stiffness of a prismatic beam for input into the analysis according to the following relationship:

$$\theta = ML/4EI \qquad \text{(A-3)}$$

The concrete deck was not included in the computed bending stiffness.

A comparison of the cross-frame member forces generated by the grid analysis with the forces generated from the 3D analyses showed good correlation. In addition, the vertical deflections generated from the grid analysis and the vertical deflections generated from the 3D analyses also showed good correlation. Therefore, the computed bending stiffness based on the method described above is considered reasonable.

The self-weight of the cross frames was estimated, converted to an equivalent uniform loading per foot of girder, and included in the model as an additional superimposed non-composite dead load. The self-weight of the girders and the weight of the concrete deck were computed internally and applied as equivalent uniformly distributed loads directly over each girder line. For the composite dead loads, the parapet loads and an estimated portion of the future wearing surface were applied as uniformly distributed loads directly over Girders 1 and 3. The remainder of the future wearing surface was applied as a uniformly distributed load over Girder 2. For the live-load analyses, influence surfaces for vertical bending moment, shear, torque, deflections, vertical end reactions, and cross-frame forces were generated and loaded to develop maximum and minimum effects.

Cross-frame member forces were determined in a separate analysis by enforcing statics at each cross-frame joint and assuming that the end connections of all cross-frame members at each joint were pinned. Vertical moments at the cross-frame connections were resolved into force couples acting at the top and bottom struts. Shear was assumed to be carried through the diagonals.

The maximum and minimum live load moments and shears generated at the ends of the cross frames will differ in magnitude and direction. The reported forces are not concurrent due to the various positions of the live load required to cause maximum effects in the individual grid elements. Specifically, each end of the cross frame is analyzed separately for the maximum reported loading at that end and the member forces at that end are determined by enforcing statics ″locally″ at the joints. The most severe forces in each member are drawn from the separate analyses at each end of the cross frame. It is understood that because the live load forces are not concurrent, equilibrium of the entire cross frame cannot be attained from the analysis with the reported loading at each end. However, by considering the two ends of the cross frame separately, the maximum member forces are determined.

***Vertical Bending Moments*:** Table A3.1 lists the computed vertical bending moments in each girder at the tenth points from MDX. The listed live load plus impact moments are the maximum envelope values. The governing live-load moments were caused by lane loading. It was noted that small negative live load plus impact moments (not shown) resulted in Girder 1 from the placement of the live load at extreme positions on the influence surface relative to Girder 1.

Tenth Pt	GIRDER 1			GIRDER 2			GIRDER 3		
	DL1	DL2	LL+I	DL1	DL2	LL+I	DL1	DL2	LL+I
1	110	61	190	383	165	316	721	335	484
2	171	93	321	678	301	538	1310	604	901
3	202	108	405	889	401	689	1746	802	1221
4	214	114	451	1014	462	777	2015	924	1423
5	218	115	466	1054	482	806	2106	965	1492

Table A3.1 -- MDX Vertical Bending Moments at Tenth Points (k-ft)
(1 k-ft = 1.35582 kN-m)

***Vertical Deflections*:** Table A3.2 lists the computed vertical deflections in each girder at the tenth points from MDX.

Tenth Pt	GIRDER 1			GIRDER 2			GIRDER 3		
	DL1	DL2	LL+I	DL1	DL2	LL+I	DL1	DL2	LL+I
1	0.40	0.09	0.11	0.90	0.19	0.20	1.43	0.32	0.31
2	0.75	0.18	0.21	1.70	0.37	0.38	2.70	0.60	0.58
3	1.02	0.24	0.28	2.33	0.50	0.52	3.72	0.82	0.80
4	1.19	0.28	0.33	2.74	0.59	0.62	4.37	0.96	0.94
5	1.25	0.29	0.35	2.88	0.62	0.65	4.59	1.01	0.99

Table A3.2 -- MDX Vertical Deflections at Tenth Points (in.)
(1 in.= 25.4 mm)

***Vertical End Reactions*:** Table A3.3 lists the computed vertical end reactions from MDX at Line 1L (Figure A.1). For the reactions due to live load plus impact, the first (negative) number represents the maximum upward reaction that resists the maximum downward force at the bearing under consideration. The second (positive or zero) number represents the maximum downward reaction that resists the maximum uplift force with the live load positioned to cause the maximum uplift at the bearing under consideration. This downward reaction would be appropriately combined with the total vertical dead load

reaction at the bearing under consideration to determine if an uplift condition actually exists.

GIRDER 1			GIRDER 2			GIRDER 3		
DL1	DL2	LL+I	DL1	DL2	LL+I	DL1	DL2	LL+I
-17	-10	-32/8	-47	-19	-50/0	-82	-39	-61/0

Table A3.3 -- MDX Vertical End Reactions at Line 1L (kips)
(1 kip = 4.4482 kN)

Lateral Flange Bending Moments: Table A3.4 lists the absolute value of the bottom-flange lateral bending moments at cross-frame Line 5L computed from the MDX results. The torque on the girder was determined by dividing the primary vertical bending moment by the radius of curvature of the girder. The lateral distributed load on the flanges was then obtained by converting the torque into a force couple acting on the flanges. For composite sections, the top force was assumed to act at the mid-thickness of the slab. Assuming that the cross frames act as rigid fixed-end supports to the adjacent flange elements, the lateral moments in the flanges given in the table were then calculated using the approximate Equation A-2 given earlier.

GIRDER 1			GIRDER 2			GIRDER 3		
DL1	DL2	LL+I	DL1	DL2	LL+I	DL1	DL2	LL+I
2.0	0.9	4.0	10.6	4.3	7.2	22.0	8.9	13.7

Table A3.4 -- MDX Bottom-Flange Lateral Bending Moments at Line 5L from Equation A-2 (k-ft)
(1 k-ft = 1.35582 kN-m)

***Cross-Frame Forces*:** Table A3.5 lists the maximum cross-frame forces at cross-frame Line 5L computed from the MDX results. The format for the table is the same as that described previously for Table A1.7.

Member	G2 – G3				G1 – G2			
	DL1	DL2	LL+I		DL1	DL2	LL+I	
			(+)	(-)			(+)	(-)
Top Strut - A	15	9	16	-15	7	5	15	-9
Diagonal - C	-15	-4	0	-15	-13	-9	0	-9
Diagonal - E	15	4	15	0	13	9	9	0
Bot. Strut - B	-4	-5	4	-4	3	1	2	-5
Bot. Strut - D	-26	-12	26	-27	-17	-11	16	-19

Table A3.5 -- MDX Cross-Frame Forces at Line 5L (kips)
(1 kip = 4.4482 kN)

***Variations to the Base Model*:** Two properties are used to model the cross frames and diaphragms in a grid analysis; the bending stiffness (I_x) and the torsional constant (J). Depending on the cross-frame depth, the computed bending stiffness can vary dramatically. For example, using the method described above, the

stiffness, I_x, of a 48-in. (1219-mm) deep cross frame is computed to be 2157 in^4 (897.8 x 10^6 mm^4). The calculated stiffness of a 33.5-in. (851-mm) deep cross frame is 1208 in^4 (502.8 x 10^6 mm^4).

Variations to the base model were made in order to determine the effects of cross frame bending and torsional stiffness on the analysis. The following combinations of cross frame properties were studied:

I_x = 1000 in^4 (416.2 x 10^6 mm^4); J = 1.0 in^4 (416.2 x 10^3 mm^4)
I_x = 1000 in^4 (416.2 x 10^6 mm^4); J = 5.0 in^4 (2.08 x 10^6 mm^4)
I_x = 2000 in^4 (832.5 x 10^6 mm^4); J = 5.0 in^4 (2.08 x 10^6 mm^4)
I_x = 4000 in^4 (1.66 x 10^9 mm^4); J = 5.0 in^4 (2.08 x 10^6 mm^4)

The analyses indicated that the dead load moments in Girders 1 and 3 decreased slightly with an increase in the bending stiffness of the cross frames, while the dead-load moments in Girder 2 increased slightly. However, for the range of stiffnesses studied, the maximum decrease in the DL1 moments was only 4% and the maximum decrease in the DL2 moments was only 10% (both in Girder 1). The analyses further indicated that the live-load moments in Girder 1 increased with an increase in the bending stiffness of the cross frames, while the live-load moments in Girder 2 and 3 decreased. The bending stiffness of the cross frames had a negligible effect on the vertical girder deflections for the range of stiffnesses studied. The change in the torsional constant, J, of the cross frames also appeared to have a negligible effect on the vertical bending moments and vertical girder deflections.

VANCK (V-load) Analysis

This section summarizes the results of the prototype analysis using the NSBA software package VANCK, which performs a V-load analysis. In a V-load analysis, each curved girder in the system is analyzed as a straight one-dimensional girder with a span length equal to the curved-girder arc length. The theory behind this approximate analysis approach for curved I-girder bridges is discussed in detail elsewhere (*7*). In essence, the V-load method can best be considered as a two-step process. In the first step, the curved structure is straightened out so that the applied vertical loads are assumed to induce only ordinary bending stresses caused by so-called primary moments. In the second step, additional fictitious forces are applied to the straight structure so that the resulting internal forces are the same as those in the curved structure when it is subjected to vertical loads only. Statics requires that the applied fictitious forces result in no net force on the structure. Thus, these curvature forces on the straight structure -- that result in so-called secondary or V-load moments in each girder -- are treated as self-equilibrating external loads commonly referred to as ″V-Loads″. In the three-girder prototype bridge, the V-Loads on the interior girder (Girder 2) are equal to zero.

The V-load analysis method cannot account for the effects of the bottom lateral bracing members in the end bays of the prototype bridge. In practice, the V-load analysis method should not be applied to structures with a system of horizontal lateral bracing in the plane of one or both flanges, especially structures utilizing a full-length lateral bracing system.

For the dead-load analysis, the self-weight of the structure and the weight of the concrete deck and haunch were applied as uniformly distributed loads to each individual girder. The composite dead loads, consisting of the barriers and future wearing surface, were uniformly distributed to each girder.

For the live-load analysis, wheel loads were distributed to the individual girders using lateral distribution factors. For determining the primary moments due to live load plus impact, the current AASHTO lateral wheel-load distribution factors for straight girders are typically used. For the prototype bridge, the computed AASHTO distribution factors were 1.59 and 1.31 wheels for the interior and exterior girders, respectively. NCHRP Project 12-26 developed formulas giving alternative live-load distribution factors for straight girders that are available in an AASHTO Guide Specification (*8*). Using these formulas, the distribution factors were computed to be 1.38 and 1.25 wheels for the interior and exterior girders, respectively. Each set of factors was then used to compute the primary live-load plus impact effects in independent V-load analyses. For determining the secondary or V-load effects, a separate lateral

distribution factor was used. Since the V-Loads act concurrently on a cross section, the summation of the V-load lateral distribution factors across the section should equal the number of wheels on the structure. Thus, the lateral distribution factor for determining the live-load V-load effects is simply computed by dividing the total number of wheels by the number of girders in the section. Since the V-Loads on Girder 1 tend to reduce the primary effects, only one lane of live loading was conservatively used in calculating this lateral distribution factor when determining the live-load V-load effects on Girder 1.

Cross-frame member forces were determined in a separate analysis by enforcing statics at each cross-frame joint. Net torsional moments at the ends of each cross frame, computed from the final vertical bending moments in each girder, were resolved into force couples acting at the top and bottom struts. It was assumed that the top and bottom struts were separated vertically by a distance equal to the web depth. The cross-frame shears, equivalent to the V-Loads, were resisted by the diagonal members.

Bottom-flange lateral moments at the cross frames were computed in a separate analysis using the approximate Equation A-2 given earlier.

Vertical Bending Moments: Table A4.1 lists the vertical bending moments in each girder at the tenth points computed from the V-load analysis. The listed live load plus impact moments are the maximum envelope values. The governing live-load moments were caused by lane loading. In one column (labeled ″AASHTO″) are the maximum live load plus impact moments computed by using the AASHTO straight-girder distribution factors to calculate the primary moments. In the adjacent column (labeled ″Guide″) are the maximum live load plus impact moments computed by using the AASHTO Guide Specification straight-girder distribution factors to calculate the primary moments. Negative live load plus impact moments in Girder 1 that were calculated in the BSDI 3D System and MDX analyses (from the placement of the live load at extreme positions on the influence surface) were not detected in the V-load analysis because Girder 1 was analyzed as a single isolated simple-span girder.

Tenth Pt	GIRDER 1				GIRDER 2				GIRDER 3			
	DL1	DL2	LL+I (AASHTO)	LL+I (Guide)	DL1	DL2	LL+I (AASHTO)	LL+I (Guide)	DL1	DL2	LL+I (AASHTO)	LL+I (Guide)
1	89	56	215	202	424	183	371	323	684	322	484	469
2	130	87	358	335	753	326	660	574	1245	586	911	884
3	146	102	449	418	988	428	867	753	1661	782	1243	1208
4	149	108	498	463	1129	489	990	861	1917	902	1453	1413
5	150	110	514	477	1176	509	1032	897	2004	943	1525	1483

Table A4.1 -- V-load Analysis Vertical Bending Moments at Tenth Points (k-ft)
(1 k-ft = 1.35582 kN-m)

Vertical Deflections: Table A4.2 lists the computed vertical deflections in each girder at the tenth points from V-load analysis. The V-load method does not directly take into account the effect of girder twist, which causes additional deflections beyond those produced by bending. Thus, vertical deflections may be significantly underestimated when utilizing this method and lateral deflections, which become important on bridges with large spans and/or sharp skews, are not computed.

Tenth Pt	GIRDER 1			GIRDER 2			GIRDER 3		
	DL1	DL2	LL+I	DL1	DL2	LL+I	DL1	DL2	LL+I
1	0.13	0.05	--	0.73	0.16	--	1.10	0.24	--
2	0.24	0.09	--	1.38	0.30	--	2.08	0.45	--
3	0.32	0.12	--	1.89	0.41	--	2.86	0.62	--
4	0.36	0.13	--	2.22	0.48	--	3.35	0.73	--
5	0.38	0.14	-.01	2.33	0.50	0.48	3.52	0.77	0.81

Table A4.2 -- V-load Analysis Vertical Deflections at Tenth Points (in.)
(1 in. = 25.4 mm)

***Vertical End Reactions*:** Table A4.3 lists the computed vertical end reactions from the V-load analysis at Line 1L (Figure A.1). Again, since each girder is isolated and analyzed as a single girder in the V-load analysis, the potential uplift of Girder 1 at the end supports under the live load plus impact, evident from the BSDI 3D System and MDX analyses, cannot be detected in the V-load analysis. It should also be noted that vertical bearing reactions at interior supports on the inside (concave) side of continuous-span curved I-girder bridges are often significantly underestimated when using the V-load analysis.

GIRDER 1				GIRDER 2				GIRDER 3			
DL1	DL2	LL+I (AASHTO)	LL+I (Guide)	DL1	DL2	LL+I (AASHTO)	LL+I (Guide)	DL1	DL2	LL+I (AASHTO)	LL+I (Guide)
-14	-8	-40/0	-38/0	-53	-23	-56/0	-49/0	-79	-37	-59/0	-57/0

Table A4.3 -- V-load Analysis Vertical End Reactions at Line 1L (kips)
(1 kip = 4.4482 kN)

***Lateral Flange Bending Moments*:** Table A4.4 lists the absolute value of the bottom-flange lateral bending moments at cross-frame Line 5L, as computed by the approximate Equation A-2 given earlier.

GIRDER 1				GIRDER 2				GIRDER 3			
DL1	DL2	LL+I (AASHTO)	LL+I (Guide)	DL1	DL2	LL+I (AASHTO)	LL+I (Guide)	DL1	DL2	LL+I (AASHTO)	LL+I (Guide)
1.5	1.1	4.9	4.6	11.7	5.1	10.2	8.9	20.6	9.7	15.6	15.1

Table A4.4 -- V-load Analysis Bottom-Flange Lateral Bending Moments at Line 5L from Equation A-2 (k-ft) (1 k-ft = 1.35582 kN-m)

***Cross-Frame Forces*:** Table A4.5 lists the maximum cross-frame forces computed from the V-load analysis results at cross-frame Line 5L. The live load plus impact cross frame forces were approximately the same for the ″AASHTO″ and ″Guide″ cases; hence, only the ″AASHTO″ values are listed under ″LL+I″. The format for the table is the same as that described previously for Table A1.7.

Member	G2 – G3				G1 – G2			
	DL1	DL2	LL+I		DL1	DL2	LL+I	
			(+)	(-)			(+)	(-)
Top Strut - A	14	7	9	0	8	3	3	0
Diagonal - C	-14	-6	0	-13	-14	-6	0	-13
Diagonal - E	14	6	13	0	14	6	13	0
Bot. Strut - B	-3	-9	6	-3	2	1	6	-1
Bot. Strut - D	-25	-11	0	-19	-18	-8	2	-12

Table A4.5 -- V-load Analysis Cross-Frame Forces at Line 5L (kips)
(1 kip = 4.4482 kN)

Summary

Detailed elastic analyses were carried out on the horizontally curved simple-span I-girder prototype bridge that was originally proposed for testing as part of this project. The analyses were conducted using the BSDI 3D System, GTSTRUDL, the MDX grid-analysis program, and the V-load analysis method. For the most part, the agreement between the results from all the analyses was quite good, except for the vertical deflections computed in the V-load analysis. These deflections were significantly lower than the deflections from the more refined two- and three-dimensional analyses because the V-load method does not directly take into account the deformations caused by twist of the girders in the cross section. The V-load analysis was also unable to detect the small negative live-load plus impact moments in Girder 1 and the potential uplift condition at the end support caused by those moments. The agreement between the V-load live-load plus impact vertical bending moments and the same moments from the more refined analysis methods appeared to significantly improve when the AASHTO Guide Specification lateral-distribution factors were utilized to compute the primary moments. The deviations in the composite dead-load (DL2) results between the V-load and refined analyses were due to the fact that the composite dead loads were assumed to be distributed equally to all the girders in the V-load analysis. In the refined analyses, the barriers were applied either at the extreme edges of the deck overhangs or directly over the two fascia girders. The deformations from the three-dimensional analyses appeared to be sensitive to the restraint assumed at the end connections of the cross frames and appeared to be very sensitive to the vertical location of those connections on the web when pinned end connections were assumed. The modeling of the cross-frame connection plates and transverse stiffeners had a smaller effect.

Acknowledgments

The BSDI 3D System and MDX analyses were coordinated by James D. Carnahan P.E. of the Pittsburgh, PA office of HDR Engineering, Inc. A. Richard Lawin of Bridge Software Development International, Ltd. in Coopersburg, PA performed the 3D System analyses.

References

1. BRIDGE-SYSTEM, 3D System User Manual, Bridge Software Development International, Ltd., Coopersburg, PA.

2. GTSTRUDL User Manual, Georgia Institute of Technology, Atlanta, GA.

3. MDX User Manual, MDX, Columbia, MO.

4. VANCK User Manual, available from M.A. Grubb & Associates, LLC, Wexford, PA.

5. U.S. Steel Highway Structures Design Handbook (1965). Vol. I Chapter 12, "Horizontally Curved Girder", chapter available from M.A. Grubb & Associates, LLC, Wexford, PA.

6. SC-BRIDGE User Manual, SC-SOLUTIONS, Mountain View, CA.

7. AISC Marketing, Inc. Highway Structures Design Handbook (1984). Vol. I Chapter 12, "V-LOAD ANALYSIS: An Approximate Procedure, Simplified and Extended, for Determining Moments and Shears in Designing Horizontally-Curved Open-Framed Highway Bridges," chapter available from the M.A. Grubb & Associates, LLC, Wexford, PA.

8. AASHTO (1994). *Guide Specifications for Distribution of Loads for Highway Bridges*, American Association of State Highway and Transportation Officials, Washington, D.C.

A.25

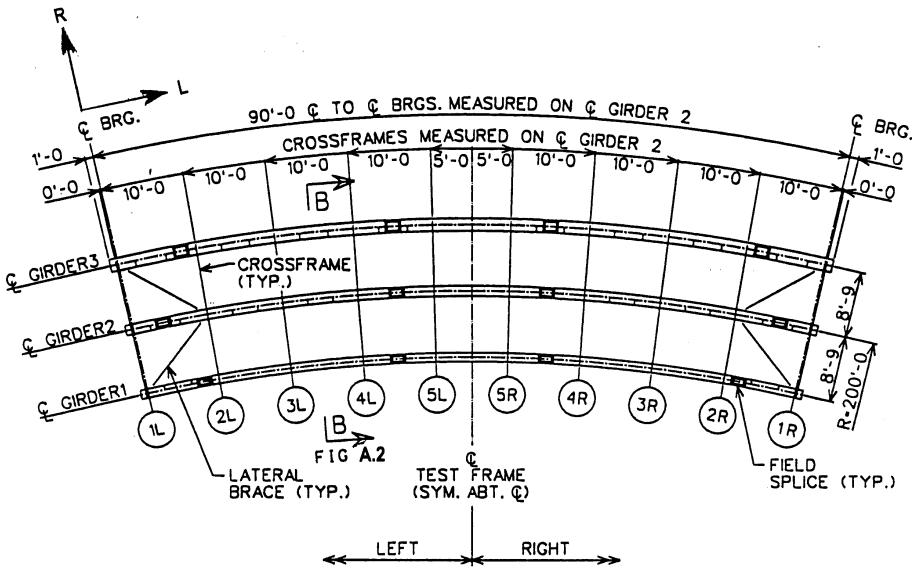

PROTOTYPE PLAN

1 ft = 0.3048 m
1 in. = 25.4 mm

Figure A.1

A.26

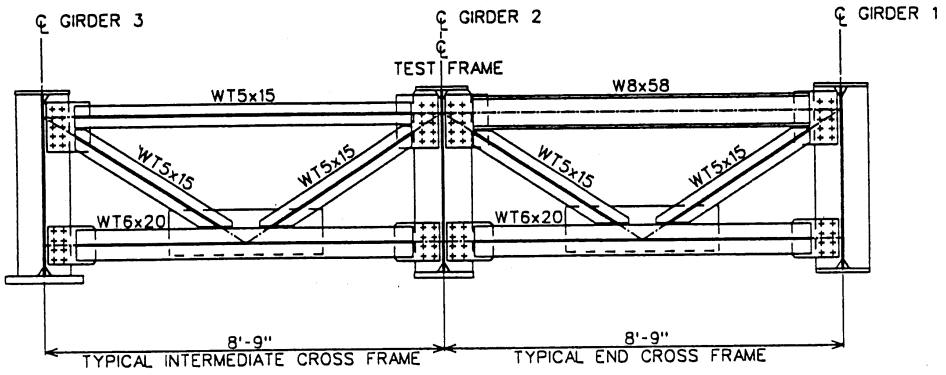

TYPICAL SECTION B-B
PROTOTYPE

1 ft = 0.3048 m
1 in. = 25.4 mm
1 lb/ft = 1.4882 kg/m

Figure A.2

A.27

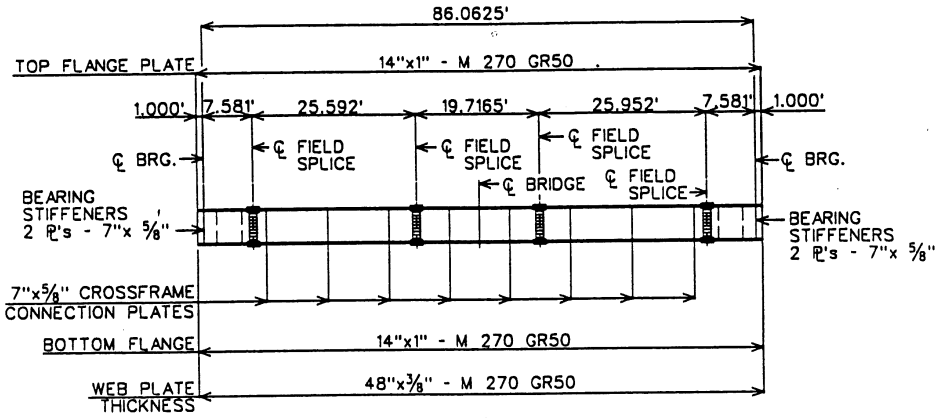

ELEVATION - GIRDER G1
PROTOTYPE

1 ft = 0.3048 m
1 in. = 25.4 mm
1 ksi = 6.8948 MPa

Figure A.3

A.28

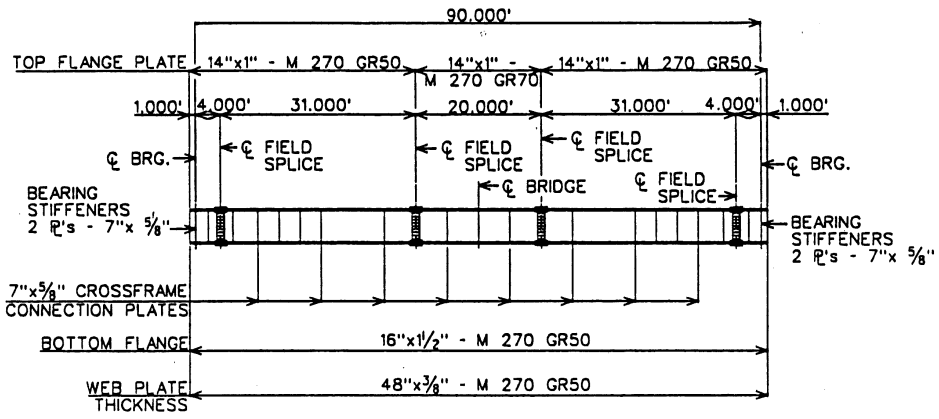

ELEVATION - GIRDER G2
PROTOTYPE

1 ft = 0.3048 m
1 in. = 25.4 mm
1 ksi = 6.8948 MPa

Figure A.4

A.29

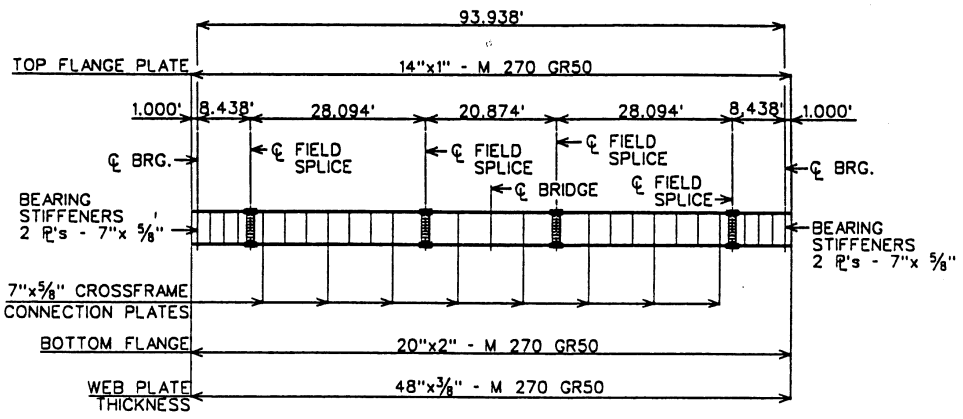

ELEVATION - GIRDER G3
PROTOTYPE

1 ft = 0.3048 m
1 in. = 25.4 mm
1 ksi = 6.8948 MPa

Figure A.5

APPENDIX B: ELASTIC ANALYSIS RESULTS FOR THE THREE-GIRDER TEST FRAME (Preliminary Concept – cont'd): VARIATIONS TO THE BSDI 3D System BASE MODEL

by Michael A. Grubb, P.E.[1] and Dann H. Hall[2]

Introduction

As described in Appendix A, detailed elastic analyses were carried out on the preliminary concept for the simple-span horizontally curved I-girder prototype bridge that was originally intended to serve as the test frame for the component specimen testing. The details of the prototype bridge are shown in Figures B.1 through B.5 and are discussed in Appendix A. The bridge is designed for H20 live loading. The analyses were conducted using four commercially available software packages: the BSDI 3D System (*1*), GTSTRUDL (*2*), MDX (*3*) and VANCK (*4*). After these analyses were completed, the BSDI 3D System base model of the prototype bridge was modified and re-analyzed. Specifically, variations to the base model were made to determine the effects of cross-frame type, cross-frame spacing, radius, skew and bearing orientation (boundary conditions).

The results of each of the analyses are given in the following sections. Among the actions listed for each girder are the vertical bending moments and vertical deflections at tenth points along the span, vertical end reactions, and lateral flange bending moments and maximum cross-frame forces at selected cross-frame lines (Figure B.1). In most cases, actions are listed for the non-composite dead load (DL1), the composite dead load (DL2), and the maximum live load plus impact (LL+I). The results are for the *unfactored* loads. With the exception of the skew and bearing orientation studies, the bridge is symmetrical about midspan. Therefore, for these symmetrical cases, actions at the tenth points are only listed up to midspan, and vertical end reactions are only listed at one end of the bridge. For the skew and bearing orientation studies, more detailed reports are provided as required to completely describe the effects of the variations.

Cross-Frame Type

This section summarizes the results of the analyses that were conducted to investigate the effects of cross-frame type on the behavior of the prototype bridge. The BSDI 3D System model was developed in accordance with Figure B.1, with the exception that the bottom lateral bracing in the end bays was not included in the original model. A detailed description of the model is given in Chapter 2. The girder sizes shown in Figures B.3 through B.5 were also assumed.

Two separate cases were investigated:

1) Case A – with the K-type cross frames shown in Figure B.2 spaced at 10 ft (3.0 m) along the arc span of Girder 2 (G2) – **BASE CASE**
2) Case B – with full-depth solid plate diaphragms spaced at 10 ft (3.0 m) along the arc span of G2. The diaphragms were assumed to have ½″ x 7″ (12.7 mm x 178 mm) top and bottom flanges and a 0.313-in. (8.0 mm) thick web. The total area of each diaphragm is 22.02 in.^{2} (14 206 mm^2) and the moment of inertia of each diaphragm about its strong axis is 7,001 in.^{4} (2.9 x 109 mm^4).

***Vertical Bending Moments*:** Tables B1.1 and B1.2 list the vertical bending moments in each girder at the tenth points computed from the 3D System results for Cases A and B, respectively. Table B1.3 provides

---

[1] Bridge Software Development International, Ltd. (now with M.A. Grubb & Associates, LLC), Wexford, PA 15090

[2] Bridge Software Development International, Ltd. (now retired), Coopersburg, PA 18036

a comparison of the maximum vertical bending moments in each girder from Cases A and B (at midspan). The listed live load plus impact moments are the maximum envelope values. The governing live load plus impact moments were caused by lane loading (lane loading governed on this rather short bridge because H20 loading was specified for the live load. According to AASHTO, H20 lane loading is specified to be the same as HS20 lane loading).

Tenth Pt	GIRDER 1			GIRDER 2			GIRDER 3		
	DL1	DL2	LL+I	DL1	DL2	LL+I	DL1	DL2	LL+I
1	110	79	191	396	159	319	735	348	504
2	171	124	315	694	289	540	1313	604	898
3	204	150	393	909	388	695	1753	806	1207
4	216	162	434	1039	448	788	2022	928	1407
5	222	167	450	1083	468	821	2113	970	1475

Table B1.1 – Case A – K-Type Cross Frames
Vertical Bending Moments at Tenth Points (k-ft)
(1 k-ft = 1.35582 kN-m)

Tenth Pt	GIRDER 1			GIRDER 2			GIRDER 3		
	DL1	DL2	LL+I	DL1	DL2	LL+I	DL1	DL2	LL+I
1	161	82	192	398	171	318	682	326	495
2	267	134	312	709	306	543	1226	576	888
3	331	166	388	933	405	701	1635	772	1194
4	366	184	430	1066	463	796	1883	891	1392
5	378	190	441	1111	482	827	1967	931	1451

Table B1.2 – Case B – Full-Depth Solid Plate Diaphragms
Vertical Bending Moments at Tenth Points (k-ft)
(1 k-ft = 1.35582 kN-m)

Case	GIRDER 1			GIRDER 2			GIRDER 3		
	DL1	DL2	LL+I	DL1	DL2	LL+I	DL1	DL2	LL+I
A	222	167	450	1083	468	821	2113	970	1475
B	378	190	441	1111	482	827	1967	931	1451

Table B1.3 – Case A vs. Case B – Maximum Vertical Bending Moments (k-ft)
(1 k-ft = 1.35582 kN-m)

The data show that for Case B (with solid plate diaphragms), the DL1 and DL2 moments increase in Girder 1 (G1) and G2 and decrease in Girder 3 (G3). The total DL1 moment across the mid-span section in Case B is approximately 1.1 percent higher than for Case A, due primarily to the slightly larger self-weight of the solid plate diaphragms. As expected, the total DL2 moment across the mid-span section is essentially the same for Cases A and B. For Case B, the LL+I moments decrease slightly in G1 and G3 and increase slightly in G2.

***Vertical Deflections*:** Tables B1.4 and B1.5 list the computed vertical deflections in each girder at the tenth points from the BSDI 3D System for Cases A and B, respectively. LL+I deflections are only given at midspan. Table B1.6 provides a comparison of the maximum vertical deflections in each girder from Cases

A and B (at midspan).

Tenth Pt	GIRDER 1			GIRDER 2			GIRDER 3		
	DL1	DL2	LL+I	DL1	DL2	LL+I	DL1	DL2	LL+I
1	0.42	0.11	--	0.93	0.19	--	1.46	0.29	--
2	0.77	0.21	--	1.77	0.37	--	2.77	0.54	--
3	1.05	0.29	--	2.42	0.50	--	3.80	0.74	--
4	1.24	0.34	--	2.83	0.59	--	4.45	0.87	--
5	1.30	0.35	0.43	2.97	0.62	0.69	4.68	0.91	0.95

Table B1.4 – Case A – K-Type Cross Frames
Vertical Deflections at Tenth Points (in.)
(1 in. = 25.4 mm)

Tenth Pt	GIRDER 1			GIRDER 2			GIRDER 3		
	DL1	DL2	LL+I	DL1	DL2	LL+I	DL1	DL2	LL+I
1	0.48	0.12	--	0.90	0.19	--	1.32	0.27	--
2	0.89	0.22	--	1.70	0.36	--	2.51	0.52	--
3	1.22	0.30	--	2.32	0.50	--	3.45	0.70	--
4	1.43	0.35	--	2.72	0.58	--	4.05	0.83	--
5	1.49	0.36	0.44	2.86	0.61	0.68	4.24	0.87	0.92

Table B1.5 – Case B – Full-Depth Solid Plate Diaphragms
Vertical Deflections at Tenth Points (in.)
(1 in. = 25.4 mm)

Case	GIRDER 1			GIRDER 2			GIRDER 3		
	DL1	DL2	LL+I	DL1	DL2	LL+I	DL1	DL2	LL+I
A	1.30	0.35	0.43	2.97	0.62	0.69	4.68	0.91	0.95
B	1.49	0.36	0.44	2.86	0.61	0.68	4.24	0.87	0.92

Table B1.6 – Case A vs. Case B – Maximum Vertical Deflections (in.)
(1 in. = 25.4 mm)

The vertical deflections of G1 are greater for Case B than for Case A. Conversely, the vertical deflections of G2 and G3 are smaller for Case B than for Case A. In all cases, the differences between the DL2 and LL+I vertical deflections (or the composite cases) are less significant.

***Vertical End Reactions*:** Table B1.7 lists the computed vertical end reactions from the BSDI 3D System for Cases A and B at Line 1L (Figure B.1). For the reactions due to live load plus impact, the first (negative) number represents the maximum upward reaction that resists the maximum downward force at the bearing under consideration. The second (positive or zero) number represents the maximum downward reaction that resists the maximum uplift force with the live load positioned to cause the maximum uplift at the bearing under consideration. This downward reaction would be appropriately combined with the total vertical dead load reaction at the bearing under consideration to determine if an uplift condition actually exists.

Case	GIRDER 1			GIRDER 2			GIRDER 3		
	DL1	DL2	LL+I	DL1	DL2	LL+I	DL1	DL2	LL+I
A	-16	-10	-33/9	-48	-17	-49/0	-81	-41	-64/0
B	-18	9	-32/9	-45	-19	-53/0	-83	-40	-63/0

Table B1.7 – Case A vs. Case B – Vertical End Reactions at Line 1L (kips)
(1 kip = 4.4482 kN)

***Lateral Flange Bending Moments*:** Table B1.8 lists the absolute value of the bottom-flange lateral bending moments, M_l, at cross-frame Line 5L computed from the BSDI 3D System results for Cases A and B using the following approximate formula (*5*):

$$M_l = \frac{Md^2}{10\,hR} \tag{B-1}$$

where: M = vertical bending moment in the curved girder at the cross frame
d = cross-frame spacing
R = girder radius
h = vertical distance between flange centerlines

Case	GIRDER 1			GIRDER 2			GIRDER 3		
	DL1	DL2	LL+I	DL1	DL2	LL+I	DL1	DL2	LL+I
A	2.58	1.93	5.23	13.03	5.64	9.89	26.39	12.11	18.47
B	4.39	2.20	5.13	13.36	5.81	9.97	24.57	11.63	18.17

Table B1.8 – Case A vs. Case B – Bottom-Flange Lateral Bending Moments at Line 5L from Equation B-1 (k-ft) (1 k-ft = 1.35582 kN-m)

Cross-Frame Spacing

This section summarizes the results of the analyses that were conducted to investigate the effects of cross-frame spacing on the behavior of the prototype bridge.

Three separate cases were investigated:

1) Case A – with cross frames spaced at 10 ft (3.0 m) along the arc span of Girder 2 (G2) – **BASE CASE**
2) Case B – with cross frames spaced at 15 ft (4.6 m) along the arc span of G2
3) Case C – with cross frames spaced at 25 ft – 20 ft – 20 ft – 25 ft (7.6 m – 6.1 m – 6.1 m – 7.6 m) along the arc span of G2.

In each case, the cross-frame configuration and member sizes shown in Figure B.2 were assumed. The girder sizes shown in Figures B.3 through B.5 were also assumed.

***Vertical Bending Moments*:** Tables B2.1 and B2.2 list the vertical bending moments in each girder at the tenth points computed from the 3D System results for Cases B and C, respectively (Note: the results for the base Case A may be found in Table B1.1). Table B2.3 provides a comparison of the maximum vertical bending moments in each girder from Cases A, B and C (at midspan).

Tenth Pt	GIRDER 1			GIRDER 2			GIRDER 3		
	DL1	DL2	LL+I	DL1	DL2	LL+I	DL1	DL2	LL+I
1	107	84	194	391	152	326	728	355	510
2	170	128	310	686	281	535	1299	607	888
3	201	152	392	900	381	697	1739	810	1211
4	220	167	436	1029	441	791	1996	931	1406
5	216	167	446	1070	463	819	2101	973	1474

Table B2.1 – Case B – Cross-Frame Spacing = 15 ft (4.6 m)
Vertical Bending Moments at Tenth Points (k-ft)
(1 k-ft = 1.35582 kN-m)

Tenth Pt	GIRDER 1			GIRDER 2			GIRDER 3		
	DL1	DL2	LL+I	DL1	DL2	LL+I	DL1	DL2	LL+I
1	121	101	201	390	127	324	705	352	491
2	169	138	316	683	262	537	1287	616	901
3	184	150	387	891	377	685	1749	815	1215
4	219	174	436	1024	432	791	1979	934	1402
5	201	163	441	1064	466	815	2102	974	1480

Table B2.2 – Case C – Cross-Frame Spacing = 25 ft – 20 ft – 20 ft – 25 ft (7.6 m – 6.1 m – 6.1 m – 7.6 m)
Vertical Bending Moments at Tenth Points (k-ft)
(1 k-ft = 1.35582 kN-m)

Case	GIRDER 1			GIRDER 2			GIRDER 3		
	DL1	DL2	LL+I	DL1	DL2	LL+I	DL1	DL2	LL+I
A	222	167	450	1083	468	821	2113	970	1475
B	216	167	446	1070	463	819	2101	973	1474
C	201	163	441	1064	466	815	2102	974	888

Table B2.3 – Case A vs. Case B vs. Case C – Maximum Vertical Bending Moments (k-ft)
(1 k-ft = 1.35582 kN-m)

The vertical bending moments in the girders are essentially unaffected by the cross-frame spacing.

***Vertical Deflections*:** Tables B2.4 and B2.5 list the computed vertical deflections in each girder at the tenth points from the BSDI 3D System for Cases B and C, respectively (Note: the results for the base Case A may be found in Table B1.4). LL+I deflections are only given at midspan. Table B2.6 provides a comparison of the maximum vertical deflections in each girder from Cases A, B and C (at midspan).

Tenth Pt	GIRDER 1			GIRDER 2			GIRDER 3		
	DL1	DL2	LL+I	DL1	DL2	LL+I	DL1	DL2	LL+I
1	0.41	0.12	--	0.94	0.19	--	1.47	0.29	--
2	0.79	0.22	--	1.78	0.37	--	2.80	0.55	--
3	1.07	0.29	--	2.43	0.50	--	3.83	0.75	--
4	1.25	0.34	--	2.85	0.59	--	4.49	0.88	--
5	1.31	0.36	0.44	2.99	0.62	0.70	4.72	0.92	0.96

Table B2.4 – Case B – Cross-Frame Spacing = 15 ft (4.6 m)
Vertical Deflections at Tenth Points (in.)
(1 in. = 25.4 mm)

Tenth Pt	GIRDER 1			GIRDER 2			GIRDER 3		
	DL1	DL2	LL+I	DL1	DL2	LL+I	DL1	DL2	LL+I
1	0.46	0.12	--	1.03	0.20	--	1.63	0.31	--
2	0.84	0.23	--	1.92	0.38	--	3.03	0.57	--
3	1.13	0.31	--	2.59	0.52	--	4.10	0.77	--
4	1.32	0.36	--	3.03	0.60	--	4.79	0.90	--
5	1.38	0.38	0.46	3.18	0.64	0.73	5.02	0.95	0.99

Table B2.5 – Case C -- Cross-Frame Spacing = 25 ft – 20 ft – 20 ft – 25 ft (7.6 m – 6.1 m – 6.1 m – 7.6 m)
Vertical Deflections at Tenth Points (in.)
(1 in. = 25.4 mm)

Case	GIRDER 1			GIRDER 2			GIRDER 3		
	DL1	DL2	LL+I	DL1	DL2	LL+I	DL1	DL2	LL+I
A	1.30	0.35	0.43	2.97	0.62	0.69	4.68	0.91	0.95
B	1.31	0.36	0.44	2.99	0.62	0.70	4.72	0.92	0.96
C	1.38	0.38	0.46	3.18	0.64	0.73	5.02	0.95	0.99

Table B2.6 – Case A vs. Case B vs. Case C – Maximum Vertical Deflections (in.)
(1 in. = 25.4 mm)

As expected, there is a general increase in the vertical deflection of each girder with increasing cross-frame spacing.

***Vertical End Reactions*:** Table B2.7 lists the computed vertical end reactions from the BSDI 3D System for Cases A, B and C at Line 1L (Figure B.1).

Case	GIRDER 1			GIRDER 2			GIRDER 3		
	DL1	DL2	LL+I	DL1	DL2	LL+I	DL1	DL2	LL+I
A	-16	-10	-33/9	-48	-17	-49/0	-81	-41	-64/0
B	-16	-11	-33/9	-47	-16	-49/0	-81	-42	-64/0
C	-16	-12	-33/9	-47	-13	-49/0	-80	-43	-64/0

Table B2.7 – Case A vs. Case B vs. Case C – Vertical End Reactions at Line 1L (kips)
(1 kip = 4.4482 kN)

Note that with increasing cross-frame spacing, less of the composite dead load (DL2) is shed from the fascia girders (G1 and G3) to the center girder G2. The influence of the cross-frame spacing on the LL+I reactions is not evident because the listed reactions are the maximum and minimum reactions for each case.

***Lateral Flange Bending Moments*:** Table B2.8 lists the absolute value of the bottom-flange lateral bending moments, M_l, computed from the BSDI 3D System results for Cases A, B and C using the approximate Equation B-1. For Case A, the lateral flange bending moments are reported at Line 5L and for Cases B and C, the lateral flange bending moments are reported at midspan. These locations, which are relatively close together, correspond to actual cross-frame locations in each case. Equation B-1 is only theoretically valid at cross-frame locations.

Case	GIRDER 1			GIRDER 2			GIRDER 3		
	DL1	DL2	LL+I	DL1	DL2	LL+I	DL1	DL2	LL+I
A	2.58	1.93	5.23	13.03	5.64	9.89	26.39	12.11	18.47
B	5.69	4.40	11.75	29.33	12.69	22.45	59.81	27.70	41.96
C	9.41	7.63	20.70	51.85	22.71	39.72	106.37	49.29	74.90

Table B2.8 – Case A vs. Case B vs. Case C – Bottom-Flange Lateral Bending Moments (k-ft)
at Line 5L for Case A and at Midspan for Cases B and C from Equation B-1
(1 k-ft = 1.35582 kN-m)

According to the approximate Equation B-1, the lateral flange bending moment increases directly in proportion to the square of the cross-frame spacing (assuming all other variables are held constant). Therefore, as illustrated above, the lateral-flange bending moments increase significantly with the cross-frame spacing.

***Cross-Frame Forces*:** Tables B2.9, B2.10 and B2.11 list the computed maximum cross-frame forces from the BSDI 3D System analysis for Cases A, B and C, respectively. Note that the reported live load plus impact responses are ont necessarily caused by coincident loads. G1-G2 refers to the cross frame between Girders 1 and 2 and G2-G3 refers to the cross frame between Girders 2 and 3. For Case A, the cross-frame forces are reported for the cross frames at Line 5L and for Cases B and C, the cross-frame forces are reported for the cross frames at midspan. Positive values are tensile forces and negative values are compressive forces. The figure below may be used for matching the reported responses with each member.

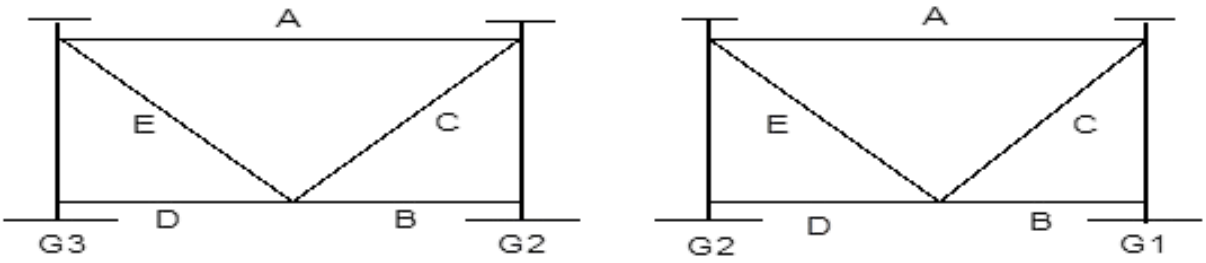

Member	G2 – G3				G1 – G2			
	DL1	DL2	LL+I		DL1	DL2	LL+I	
			(+)	(-)			(+)	(-)
Top Strut - A	14	-1	2	0	7	-3	1	-1
Diagonal - C	-14	-1	0	-12	-13	-10	0	-8
Diagonal - E	14	1	12	0	13	10	8	0
Bot. Strut - B	-3	-9	6	-3	2	2	5	-1
Bot. Strut - D	-25	-10	0	-16	-16	-14	2	-8

Table B2.9 – Case A – Cross-Frame Spacing = 10 ft (3.0 m)
Cross-Frame Forces at Line 5L (kips)
(1 kip = 4.4482 kN)

Member	G2 – G3				G1 – G2			
	DL1	DL2	LL+I		DL1	DL2	LL+I	
			(+)	(-)			(+)	(-)
Top Strut - A	21	-2	2	0	11	-4	2	-1
Diagonal - C	-21	-2	0	-17	-19	-16	0	-11
Diagonal - E	21	2	17	0	19	16	11	0
Bot. Strut - B	-5	-13	8	-4	3	3	7	-2
Bot. Strut - D	-37	-16	0	-24	-24	-20	2	-11

Table B2.10 – Case B – Cross-Frame Spacing = 15 ft (4.6 m)
Cross-Frame Forces at Midspan (kips)
(1 kip = 4.4482 kN)

Member	G2 – G3				G1 – G2			
	DL1	DL2	LL+I		DL1	DL2	LL+I	
			(+)	(-)			(+)	(-)
Top Strut - A	28	-2	3	0	14	-5	2	-1
Diagonal - C	-27	-2	0	-22	-24	-20	0	-15
Diagonal - E	27	2	22	0	24	20	15	0
Bot. Strut - B	-8	-17	10	-5	4	3	9	-2
Bot. Strut - D	-47	-20	0	-30	-32	-27	2	-14

Table B2.11 – Case C -- Cross-Frame Spacing = 25 ft – 20 ft – 20 ft – 25 ft (7.6 m – 6.1 m – 6.1 m – 7.6 m)
Cross-Frame Forces at Midspan (kips)
(1 kip = 4.4482 kN)

As expected, the cross-frame forces increase with increasing cross-frame spacing since there are fewer cross frames available to resist the differential deflection of the girders. Since the moments in the girders remain relatively unaffected by the increased spacing, the forces in the cross frames must increase and the increase can simply be estimated to be approximately inversely proportional to the reduction in the number of cross frames. For example, there are a total of 10 cross frames in Case A and a total of 5 cross frames in Case C. Therefore, the forces in the cross frames increase by a factor of approximately (1/0.5) = 2.0 between Cases A and C.

Radius

This section summarizes the results of the analyses that were conducted to investigate the effects of the radius on the behavior of the prototype bridge.

Five separate cases were investigated:

1) Case A – with a centerline radius (along G2) of 200 ft (61.0 m) – **BASE CASE**
2) Case B – with a centerline radius of 400 ft (121.9 m)
3) Case C – with a centerline radius of 800 ft (243.8 m)
4) Case D – with a centerline radius of 1200 ft (365.8 m)
5) Case E – with the radius of all 3 girders equal to infinity [i.e. tangent girders with a span of 90.0 ft (27.4 m)]

In each case, the cross-frame spacing shown in Figure B.1 and the cross-frame configuration and member sizes shown in Figure B.2 were assumed. The girder sizes shown in Figures B.3 through B.5 were also assumed for all five cases (i.e. the girders were not redesigned to reflect the different radius in each case).

***Vertical Bending Moments*:** Tables B3.1 through B3.4 list the vertical bending moments in each girder at the tenth points computed from the 3D System results for Cases B through E, respectively (Note: the results for the base Case A may be found in Table B1.1). Table B3.6 provides a comparison of the maximum vertical bending moments in each girder from Cases A through E (at midspan).

Tenth Pt	GIRDER 1			GIRDER 2			GIRDER 3		
	DL1	DL2	LL+I	DL1	DL2	LL+I	DL1	DL2	LL+I
1	246	134	236	398	167	329	573	273	415
2	425	226	402	699	304	558	1018	471	734
3	547	288	514	915	409	721	1353	625	980
4	619	323	577	1045	472	821	1555	718	1134
5	643	335	598	1089	494	854	1624	749	1187

Table B3.1 – Case B – Centerline Radius = 400 ft (121.9 m)
Vertical Bending Moments at Tenth Points (k-ft)
(1 k-ft = 1.35582 kN-m)

Tenth Pt	GIRDER 1			GIRDER 2			GIRDER 3		
	DL1	DL2	LL+I	DL1	DL2	LL+I	DL1	DL2	LL+I
1	312	161	267	403	173	335	496	236	371
2	549	274	461	708	316	571	876	407	658
3	715	354	597	929	425	740	1159	537	875
4	814	401	677	1062	491	844	1329	615	1014
5	848	417	704	1106	513	879	1387	641	1061

Table B3.2 – Case C – Centerline Radius = 800 ft (243.8 m)
Vertical Bending Moments at Tenth Points (k-ft)
(1 k-ft = 1.35582 kN-m)

Tenth Pt	GIRDER 1			GIRDER 2			GIRDER 3		
	DL1	DL2	LL+I	DL1	DL2	LL+I	DL1	DL2	LL+I
1	335	169	278	406	176	337	469	225	357
2	589	291	481	713	319	577	828	386	631
3	771	376	624	935	430	749	1094	508	838
4	878	427	711	1069	498	853	1254	581	972
5	915	444	738	1113	520	888	1308	605	1017

Table B3.3 – Case D – Centerline Radius = 1200 ft (365.8 m)
Vertical Bending Moments at Tenth Points (k-ft)
(1 k-ft = 1.35582 kN-m)

Tenth Pt	GIRDER 1			GIRDER 2			GIRDER 3		
	DL1	DL2	LL+I	DL1	DL2	LL+I	DL1	DL2	LL+I
1	378	187	299	410	182	343	419	201	328
2	672	323	522	724	329	588	733	343	582
3	883	421	681	950	444	765	965	450	764
4	1007	479	776	1086	513	873	1104	513	876
5	1051	498	808	1132	537	909	1151	535	917

Table B3.4 – Case E – Radius of all 3 Girders = Infinity
Vertical Bending Moments at Tenth Points (k-ft)
(1 k-ft = 1.35582 kN-m)

The difference in the girder vertical bending moments in Case E (all tangent girders) in this case is due primarily to the difference in the girder stiffnesses. The noncomposite (″Steel″) and composite (″3n″ and ″n″) moments of inertia of the three girders are summarized in Table B3.5.

GIRDER 1			GIRDER 2			GIRDER 3		
Steel	3n	n	Steel	3n	n	Steel	3n	n
20,263	38,312	50,255	25,435	53,171	72,397	30,864	66,324	96,890

Table B3.5 – Girder Moments of Inertia (in.^{4})
(1 in.^{4} = 416 231 mm^4)

Case	GIRDER 1			GIRDER 2			GIRDER 3		
	DL1	DL2	LL+I	DL1	DL2	LL+I	DL1	DL2	LL+I
A	222	167	450	1083	468	821	2113	970	1475
B	643	335	598	1089	494	854	1624	749	1187
C	848	417	704	1106	513	879	1387	641	1061
D	915	444	738	1113	520	888	1308	605	1017
E	1051	498	808	1132	537	909	1151	535	917

Table B3.6 – Case A vs. Case B vs. Case C vs. Case D vs. Case E – Maximum Vertical Bending Moments (k-ft)
(1 k-ft = 1.35582 kN-m)

The results are shown graphically in Figures B.6 through B.8 for DL1, DL2 and LL+I, respectively. Note that with increasing radius, there is a significant increase in the vertical bending moments in G1 and a significant decrease in the vertical bending moments in G3. There is only a slight increase in the vertical bending moments in G2 with increasing radius.

***Vertical Deflections*:** Tables B3.7 through B3.10 list the computed vertical deflections in each girder at the tenth points from the BSDI 3D System for Cases B through E, respectively (Note: the results for the base Case A may be found in Table B1.4). LL+I deflections are only given at midspan. Table B3.11 provides a comparison of the maximum vertical deflections in each girder from Cases A through E (at midspan).

Tenth Pt	GIRDER 1			GIRDER 2			GIRDER 3		
	DL1	DL2	LL+I	DL1	DL2	LL+I	DL1	DL2	LL+I
1	0.54	0.14	--	0.73	0.16	--	0.94	0.19	--
2	1.01	0.27	--	1.39	0.30	--	1.77	0.36	--
3	1.38	0.36	--	1.90	0.42	--	2.42	0.49	--
4	1.61	0.42	--	2.22	0.49	--	2.83	0.58	--
5	1.68	0.44	0.53	2.33	0.51	--	2.97	0.61	0.65

Table B3.7 – Case B – Centerline Radius = 400 ft (121.9 m)
Vertical Deflections at Tenth Points (in.)
(1 in. = 25.4 mm)

Tenth Pt	GIRDER 1			GIRDER 2			GIRDER 3		
	DL1	DL2	LL+I	DL1	DL2	LL+I	DL1	DL2	LL+I
1	0.66	0.17	--	0.70	0.16	--	0.74	0.16	--
2	1.23	0.32	--	1.33	0.30	--	1.42	0.30	--
3	1.69	0.43	--	1.81	0.41	--	1.94	0.41	--
4	1.97	0.50	--	2.12	0.48	--	2.27	0.48	--
5	2.06	0.53	0.62	2.22	0.50	0.58	2.37	0.50	0.54

Table B3.8 – Case C – Centerline Radius = 800 ft (243.8 m)
Vertical Deflections at Tenth Points (in.)
(1 in. = 25.4 mm)

Tenth Pt	GIRDER 1			GIRDER 2			GIRDER 3		
	DL1	DL2	LL+I	DL1	DL2	LL+I	DL1	DL2	LL+I
1	0.71	0.18	--	0.70	0.16	--	0.69	0.15	--
2	1.33	0.34	--	1.32	0.30	--	1.31	0.28	--
3	1.81	0.46	--	1.81	0.41	--	1.79	0.38	--
4	2.12	0.54	--	2.11	0.48	--	2.11	0.45	--
5	2.22	0.56	0.66	2.22	0.50	0.59	2.21	0.47	0.51

Table B3.9 – Case D – Centerline Radius = 1200 ft (365.8 m)
Vertical Deflections at Tenth Points (in.)
(1 in. = 25.4 mm)

Tenth Pt	GIRDER 1			GIRDER 2			GIRDER 3		
	DL1	DL2	LL+I	DL1	DL2	LL+I	DL1	DL2	LL+I
1	0.82	0.20	--	0.71	0.16	--	0.61	0.14	--
2	1.54	0.38	--	1.34	0.31	--	1.14	0.25	--
3	2.11	0.52	--	1.84	0.42	--	1.57	0.34	--
4	2.46	0.61	--	2.15	0.49	--	1.83	0.40	--
5	2.58	0.64	0.74	2.26	0.52	0.61	1.93	0.42	0.47

Table B3.10 – Case E – Radius of all 3 Girders = Infinity
Vertical Deflections at Tenth Points (in.)
(1 in. = 25.4 mm)

Case	GIRDER 1			GIRDER 2			GIRDER 3		
	DL1	DL2	LL+I	DL1	DL2	LL+I	DL1	DL2	LL+I
A	1.30	0.35	0.43	2.97	0.62	0.69	4.68	0.91	0.95
B	1.68	0.44	0.53	2.33	0.51	0.59	2.97	0.61	0.65
C	2.06	0.53	0.62	2.22	0.50	0.58	2.37	0.50	0.54
D	2.22	0.56	0.66	2.22	0.50	0.59	2.21	0.47	0.51
E	2.58	0.64	0.74	2.26	0.52	0.61	1.93	0.42	0.47

Table B3.11 – Case A vs. Case B vs. Case C vs. Case D vs. Case E – Maximum Vertical Deflections (in.)
(1 in. = 25.4 mm)

The results are shown graphically in Figures B.9 through B.11 for DL1, DL2 and LL+I, respectively. Note that with increasing radius, the vertical deflections of G1 increase due to lengthening of the girder in conjunction with the lessening of the curvature effect and the vertical deflections of G3 decrease due to shortening of the girder in conjunction with the lessening of the curvature effect. The only significant effect on the vertical deflections of G2 is the decrease in deflection that occurs as the centerline radius increases from 200 ft (61.0 m) to 400 ft (121.9 m) (i.e. Case A vs. Case B).

***Vertical End Reactions*:** Table B3.12 lists the computed vertical end reactions from the BSDI 3D System for Cases A through E at Line 1L (Figure B.1).

Case	GIRDER 1			GIRDER 2			GIRDER 3		
	DL1	DL2	LL+I	DL1	DL2	LL+I	DL1	DL2	LL+I
A	-16	-10	-33/9	-48	-17	-49/0	-81	-41	-64/0
B	-32	-17	-37/2	-49	-18	-51/0	-65	-33	-52/0
C	-39	-21	-39/0	-49	-19	-51/0	-57	-28	-47/0
D	-41	-22	-41/0	-49	-19	-51/0	-55	-27	-46/0
E	-46	-24	-43/0	-50	-19	-52/0	-50	-24	-42/0

Table B3.12 – Case A vs. Case B vs. Case C vs. Case D vs. Case E – Vertical End Reactions at Line 1L (kips)
(1 kip = 4.4482 kN)

The dead- and live-load reactions increase at G1 and decrease at G3 with increasing radius, with the largest change occurring between a centerline radius of 200 ft (61.0 m) and 400 ft (121.9 m) (i.e. Case A vs. Case B). The G2 reactions are largely unaffected by an increase in the radius.

***Lateral Flange Bending Moments*:** Table B3.13 lists the absolute value of the bottom-flange lateral bending moments, M_l, at Line 5L computed from the BSDI 3D System results for Cases A through E using the approximate Equation B-1.

Case	GIRDER 1			GIRDER 2			GIRDER 3		
	DL1	DL2	LL+I	DL1	DL2	LL+I	DL1	DL2	LL+I
A	2.58	1.93	5.23	13.03	5.64	9.89	26.39	12.11	18.47
B	3.81	1.98	3.54	6.55	2.97	5.14	9.93	4.58	7.25
C	2.54	1.25	2.11	3.33	1.54	2.65	4.20	1.94	3.21
D	1.83	0.89	1.48	2.23	1.04	1.78	2.63	1.22	2.04
E	0	0	0	0	0	0	0	0	0

Table B3.13 – Case A vs. Case B vs. Case C vs. Case D vs. Case E – Bottom-Flange Lateral Bending Moments at Line 5L from Equation B-1 (k-ft)
(1 k-ft = 1.35582 kN-m)

***Cross-Frame Forces*:** Tables B3.14 through B3.17 list the computed maximum cross-frame forces at Line 5L from the BSDI 3D System analysis for Cases B through E, respectively (Note: the results for the base Case A are shown in Table B2.9). Note that the reported live load plus impact responses are not necessarily caused by coincident loads. G1-G2 refers to the cross frame between Girders 1 and 2 and G2-G3 refers to the cross frame between Girders 2 and 3. Positive values are tensile forces and negative values are compressive forces. The figure below may be used as a key for matching the reported responses with each member.

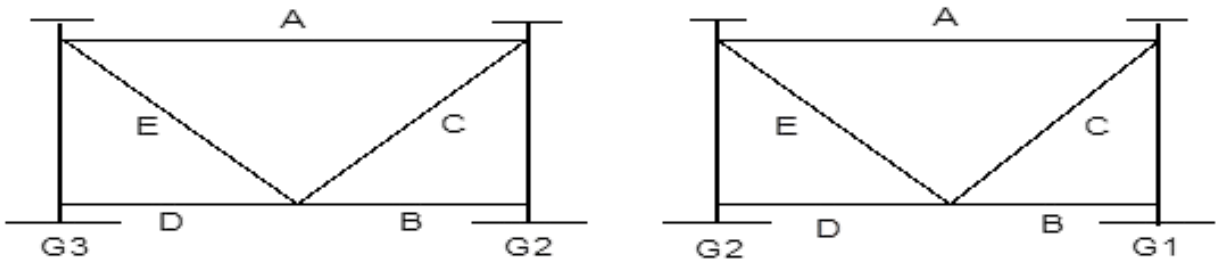

Member	G2 – G3				G1 – G2			
	DL1	DL2	LL+I		DL1	DL2	LL+I	
			(+)	(-)			(+)	(-)
Top Strut - A	4	-2	2	0	0	-2	2	-1
Diagonal - C	-7	2	0	-7	-5	-8	2	-4
Diagonal - E	7	-2	7	0	5	8	4	-2
Bot. Strut - B	2	-7	6	-1	4	2	4	0
Bot. Strut - D	-9	-4	0	-7	-4	-10	4	-2

Table B3.14 – Case B – Centerline Radius = 400 ft (121.9 m)
Cross-Frame Forces at Line 5L (kips)
(1 kip = 4.4482 kN)

Member	G2 – G3				G1 – G2			
	DL1	DL2	LL+I		DL1	DL2	LL+I	
			(+)	(-)			(+)	(-)
Top Strut - A	1	-2	2	0	-1	-2	2	0
Diagonal - C	-4	4	0	-5	-2	-7	3	-2
Diagonal - E	4	-4	5	0	2	7	2	-3
Bot. Strut - B	2	-7	5	0	2	1	2	0
Bot. Strut - D	-4	-2	0	-3	-1	-9	4	-1

Table B3.15 – Case C – Centerline Radius = 800 ft (243.8 m)
Cross-Frame Forces at Line 5L (kips)
(1 kip = 4.4482 kN)

Member	G2 – G3				G1 – G2			
	DL1	DL2	LL+I		DL1	DL2	LL+I	
			(+)	(-)			(+)	(-)
Top Strut - A	0	-2	2	0	-1	-2	2	0
Diagonal - C	-2	4	0	-4	-1	-6	3	-1
Diagonal - E	2	-4	4	0	1	6	1	-3
Bot. Strut - B	2	-7	5	0	2	1	2	0
Bot. Strut - D	-3	-1	0	-2	0	-8	5	-1

Table B3.16 – Case D – Centerline Radius = 1200 ft (365.8 m)
Cross-Frame Forces at Line 5L (kips)
(1 kip = 4.4482 kN)

Member	G2 – G3				G1 – G2			
	DL1	DL2	LL+I		DL1	DL2	LL+I	
			(+)	(-)			(+)	(-)
Top Strut - A	0	-2	2	-1	0	-2	2	0
Diagonal - C	-1	5	0	-4	0	-5	4	-1
Diagonal - E	1	-5	4	0	0	5	1	-4
Bot. Strut - B	1	-8	5	-1	0	0	0	0
Bot. Strut - D	0	0	1	-1	1	-8	5	-1

Table B3.17 – Case E – Radius of all 3 Girders = Infinity
Cross-Frame Forces at Line 5L (kips)
(1 kip = 4.4482 kN)

The maximum cross-frame forces decrease significantly as the radius increases from 200 ft (61.0 m) to 400 ft (121.9 m) (i.e. Case A vs. Case B). As the radius increases beyond 400 ft (121.9), the change in the magnitude of the cross-frame forces becomes less significant. It should be kept in mind, however, that the magnitude of the cross-frame forces is relatively small for this simple bridge with a regular framing plan (i.e. without skew).

Skew

This section summarizes the results of the analyses that were conducted to investigate the effects of support skew on the behavior of the prototype bridge.

Four separate cases were investigated:

1) Case A – with radial supports at Lines 1L and 1R (Figure B.1) – **BASE CASE**

2) Case B – with a radial support at Line 1L and an approximate 30° skew at the right support. The skew extends from Line 2R on G1 to Line 1R on G3 (Figure B.12).
3) Case C – Case B with the cross frame between G1 and G2 at Line 2R eliminated (Figure B.13).
4) Case D – with a radial support at Line 1L and an approximate 50° skew at the right support. The skew extends from Line 3R on G1 to Line 1R on G3 (Figure B.14).

In each case, the cross-frame configuration and member sizes shown in Figure B.2 were assumed. The centerline radius was taken as 200 ft (61.0 m). The girder sizes shown in Figures B.3 through B.5 were also assumed.

For the analyses to determine the bottom-flange lateral bending moments, cross frame forces and end support moments (note: results are summarized below), the boundary conditions given for Case A in the next section of this report were assumed (refer to Case A of Table B5.1 given in the next section of this report entitled 'Bearing Orientation'. See also Figure B.15). The girders were free to rotate about their local X, Y and Z-axes at both Lines 1L and 1R. All restraints were applied in the element or local coordinate system. In addition, bottom flange lateral bracing members were included in the model in the end bays adjacent to the left end only (Line 1L). WT6 x 20 (WT155 x 30) structural tees were assumed for the lateral bracing members.

***Vertical Bending Moments*:** Tables B4.1 through B4.4 list the vertical bending moments in each girder at each cross-frame line computed from the 3D System results for Cases A through D, respectively. Table B4.5 provides a comparison of the vertical bending moments in each girder at Line 5L from Cases A through D.

Line	GIRDER 1			GIRDER 2			GIRDER 3		
	DL1	DL2	LL+I	DL1	DL2	LL+I	DL1	DL2	LL+I
1L	0	0	0	0	0	0	0	0	0
2L	119	87	208	433	176	347	805	382	553
3L	182	132	335	751	316	579	1426	659	974
4L	210	156	410	963	413	733	1863	856	1288
5L	220	166	445	1069	462	811	2085	957	1454
5R	220	165	445	1069	462	811	2085	957	1454
4R	210	155	410	963	413	733	1863	856	1288
3R	181	130	335	751	316	578	1426	659	974
2R	119	85	208	433	176	348	805	382	553
1R	0	0	0	0	0	0	0	0	0

Table B4.1 – Case A – Radial Supports at Lines 1L and 1R
Vertical Bending Moments at Cross-Frame Lines (k-ft)
(1 k-ft = 1.35582 kN-m)

Line	GIRDER 1			GIRDER 2			GIRDER 3		
	DL1	DL2	LL+I	DL1	DL2	LL+I	DL1	DL2	LL+I
1L	0	0	0	0	0	0	0	0	0
2L	142	91	204	420	171	342	749	363	530
3L	228	138	319	723	308	568	1319	622	928
4L	276	163	384	923	404	719	1705	800	1218
5L	300	172	403	1024	454	794	1876	882	1357
5R	299	167	380	1040	459	793	1818	863	1327
4R	268	148	323	981	419	713	1527	743	1138
3R	216	116	242	814	319	528	1028	534	813
2R	0	0	0	400	135	224	465	282	425
1R	--	--	--	--	--	--	0	0	0

Table B4.2 – Case B – Radial Support at Line 1L and 30° Skew at Right Support
Vertical Bending Moments at Cross-Frame Lines (k-ft)
(1 k-ft = 1.35582 kN-m)

Line	GIRDER 1			GIRDER 2			GIRDER 3		
	DL1	DL2	LL+I	DL1	DL2	LL+I	DL1	DL2	LL+I
1L	0	0	0	0	0	0	0	0	0
2L	116	83	204	416	170	341	777	371	536
3L	176	124	322	716	305	567	1373	637	938
4L	198	141	386	915	401	716	1784	822	1234
5L	193	140	408	1019	453	792	1978	911	1380
5R	158	124	388	1047	463	794	1940	898	1357
4R	88	92	324	1008	427	718	1664	786	1173
3R	11	55	206	828	320	529	1203	593	860
2R	0	0	0	324	116	220	680	346	477
1R	--	--	--	--	--	--	0	0	0

Table B4.3 – Case C – Case B w/ G1-G2 Cross Frame Removed at Line 2R
Vertical Bending Moments at Cross-Frame Lines (k-ft)
(1 k-ft = 1.35582 kN-m)

Line	GIRDER 1			GIRDER 2			GIRDER 3		
	DL1	DL2	LL+I	DL1	DL2	LL+I	DL1	DL2	LL+I
1L	0	0	0	0	0	0	0	0	0
2L	163	94	202	408	170	338	702	348	507
3L	269	144	311	701	306	559	1228	592	882
4L	332	170	368	897	404	707	1568	754	1145
5L	362	177	381	1008	460	781	1686	819	1257
5R	356	168	352	1051	475	779	1570	781	1198
4R	322	147	295	1012	440	691	1230	648	986
3R	0	0	0	757	322	482	775	454	675
2R	--	--	--	0	0	0	406	252	351
1R	--	--	--	--	--	--	0	0	0

Table B4.4 – Case D – Radial Support at Line 1L and 50° Skew at Right Support
Vertical Bending Moments at Cross-Frame Lines (k-ft)
(1 k-ft = 1.35582 kN-m)

Case	GIRDER 1			GIRDER 2			GIRDER 3		
	DL1	DL2	LL+I	DL1	DL2	LL+I	DL1	DL2	LL+I
A	220	166	445	1069	462	811	2085	957	1454
B	300	172	403	1024	454	794	1876	882	1357
C	193	140	408	1019	453	792	1978	911	1380
D	362	177	381	1008	460	781	1686	819	1257

Table B4.5 – Case A vs. Case B vs. Case C vs. Case D –Vertical Bending Moments at Line 5L (k-ft)
(1 k-ft = 1.35582 kN-m)

***Vertical Deflections*:** Tables B4.6 through B4.9 list the computed vertical deflections in each girder at the cross-frame lines from the BSDI 3D System for Cases A through D, respectively. LL+I deflections are only given at midspan. Table B4.10 provides a comparison of the vertical deflections in each girder at Line 5L from Cases A through D.

Line	GIRDER 1			GIRDER 2			GIRDER 3		
	DL1	DL2	LL+I	DL1	DL2	LL+I	DL1	DL2	LL+I
1L	0	0	0	0	0	0	0	0	0
2L	0.45	0.13	--	1.03	0.21	--	1.62	0.32	--
3L	0.85	0.23	--	1.93	0.40	--	3.02	0.59	--
4L	1.13	0.31	--	2.59	0.54	--	4.06	0.79	--
5L	1.28	0.35	--	2.92	0.61	--	4.61	0.90	--
CL	--	--	0.43	--	--	0.69	--	--	0.95
5R	1.28	0.35	--	2.92	0.61	--	4.61	0.90	--
4R	1.13	0.31	--	2.59	0.54	--	4.06	0.79	--
3R	0.85	0.23	--	1.93	0.40	--	3.02	0.59	--
2R	0.45	0.13	--	1.03	0.21	--	1.62	0.32	--
1R	0	0	0	0	0	0	0	0	0

Table B4.6 – Case A – Radial Supports at Lines 1L and 1R
Vertical Deflections at Cross-Frame Lines (in.)
(1 in. = 25.4 mm)

Line	GIRDER 1			GIRDER 2			GIRDER 3		
	DL1	DL2	LL+I	DL1	DL2	LL+I	DL1	DL2	LL+I
1L	0	0	0	0	0	0	0	0	0
2L	0.42	0.11	--	0.92	0.20	--	1.43	0.30	--
3L	0.74	0.20	--	1.72	0.37	--	2.67	0.56	--
4L	1.02	0.26	--	2.28	0.49	--	3.58	0.74	--
5L	1.12	0.29	--	2.56	0.55	--	4.02	0.84	--
CL	--	--	0.36	--	--	0.62	--	--	0.89
5R	1.06	0.27	--	2.51	0.54	--	3.99	0.83	--
4R	0.83	0.21	--	2.15	0.46	--	3.47	0.73	--
3R	0.47	0.12	--	1.47	0.31	--	2.55	0.54	--
2R	0	0	0	0.54	0.12	--	1.35	0.29	--
1R	--	--	--	--	--	0	0	0	0

Table B4.7 – Case B – Radial Support at Line 1L and 30° Skew at Right Support
Vertical Deflections at Cross-Frame Lines (in.)
(1 in. = 25.4 mm)

Line	GIRDER 1			GIRDER 2			GIRDER 3		
	DL1	DL2	LL+I	DL1	DL2	LL+I	DL1	DL2	LL+I
1L	0	0	0	0	0	0	0	0	0
2L	0.38	0.11	--	0.96	0.20	--	1.55	0.31	--
3L	0.69	0.19	--	1.79	0.38	--	2.90	0.58	--
4L	0.90	0.25	--	2.38	0.50	--	3.87	0.78	--
5L	0.97	0.27	--	2.67	0.56	--	4.39	0.89	--
CL	--	--	0.34	--	--	0.63	--	--	0.92
5R	0.90	0.25	--	2.63	0.55	--	4.37	0.88	--
4R	0.70	0.19	--	2.25	0.47	--	3.83	0.78	--
3R	0.38	0.11	--	1.54	0.32	--	2.85	0.58	--
2R	0	0	0	0.56	0.12	--	1.53	0.32	--
1R	--	--	--	--	--	0	0	0	0

Table B4.8 – Case C - Case B w/ G1-G2 Cross Frame Removed at Line 2R
Vertical Deflections at Cross-Frame Lines (in.)
(1 in. = 25.4 mm)

Line	GIRDER 1			GIRDER 2			GIRDER 3		
	DL1	DL2	LL+I	DL1	DL2	LL+I	DL1	DL2	LL+I
1L	0	0	0	0	0	0	0	0	0
2L	0.38	0.10	--	0.83	0.19	--	1.30	0.29	--
3L	0.68	0.17	--	1.54	0.34	--	2.41	0.53	--
4L	0.87	0.22	--	2.04	0.45	--	3.22	0.71	--
5L	0.90	0.23	--	2.26	0.50	--	3.60	0.80	--
CL	--	--	0.28	--	--	0.56	--	--	0.84
5R	0.77	0.19	--	2.16	0.48	--	3.55	0.80	--
4R	0.46	0.11	--	1.73	0.39	--	3.07	0.70	--
3R	0	0	0	1.00	0.22	--	2.26	0.52	--
2R	--	--	--	0	0	0	1.20	0.28	--
1R	--	--	--	--	--	--	0	0	0

Table B4.9 – Case D – Radial Support at Line 1L and 50° Skew at Right Support
Vertical Deflections at Cross-Frame Lines (in.)
(1 in. = 25.4 mm)

Case	GIRDER 1			GIRDER 2			GIRDER 3		
	DL1	DL2	LL+I	DL1	DL2	LL+I	DL1	DL2	LL+I
A	1.28	0.35	0.43	2.92	0.61	0.69	4.61	0.90	0.95
B	1.12	0.29	0.36	2.56	0.55	0.62	4.02	0.84	0.89
C	0.97	0.27	0.34	2.67	0.56	0.63	4.39	0.89	0.92
D	0.90	0.23	0.28	2.26	0.50	0.56	3.60	0.80	0.84

Table B4.10 – Case A vs. Case B vs. Case C vs. Case D –Vertical Deflections at Line 5L (in.)
(Note: LL+I Deflections are at Midspan)
(1 k-ft = 1.35582 kN-m)

***Vertical End Reactions*:** Table B4.11 lists the computed vertical end reactions from the BSDI 3D System for Cases A through D at Line 1L (Figure B.1). Table B4.12 lists the computed vertical end reactions from the BSDI 3D System for Cases A through D at the right support.

Case	GIRDER 1			GIRDER 2			GIRDER 3		
	DL1	DL2	LL+I	DL1	DL2	LL+I	DL1	DL2	LL+I
A	-16	-10	-33/9	-48	-17	-49/0	-81	-41	-64/0
B	-19	-10	-32/6	-47	-17	-48/0	-76	-39	-62/0
C	-16	-9	-32/7	-46	-17	-50/0	-79	-40	-62/0
D	-21	-11	-31/5	-45	-17	-59/0	-71	-38	-59/0

Table B4.11 – Case A vs. Case B vs. Case C vs. Case D vs. Case E – Vertical End Reactions at Line 1L (kips)
(1 kip = 4.4482 kN)

Case	GIRDER 1			GIRDER 2			GIRDER 3		
	DL1	DL2	LL+I	DL1	DL2	LL+I	DL1	DL2	LL+I
A	-16	-10	-33/9	-48	-17	-49/0	-81	-41	-64/0
B	19	3	-35/26	-106	-35	-67/0	-51	-32	-53/0
C	-1	-4	-35/19	-72	-24	-59/0	-66	-37	-55/0
D	30	12	-35/35	-111	-40	-81/0	-48	-30	-47/0

Table B4.12 – Case A vs. Case B vs. Case C vs. Case D vs. Case E – Vertical End Reactions at Right Support (kips)
(1 kip = 4.4482 kN)

Note that at the right support (Table B4.12), the support skew results in a significant decrease in the load transferred to G1 and G3 and a significant increase in the load transferred to G2. In fact, the skew results in uplift at the right support of G1 in Cases B, C and D. As noted later, this increased load transfer to G2 is reflected in larger cross frame forces in the region of the skew. Note that removal of the G1-G2 cross frame at Line 2R (Case C) lessens this load transfer somewhat.

***Lateral Flange Bending Moments*:** Tables B4.13 and B4.14 list the absolute value of the bottom-flange lateral bending moments, M_l, at cross-frame Lines 5L and 2R, respectively, computed from the

BSDI 3D System results for Cases A through D using the approximate Equation B-1.

Case	GIRDER 1			GIRDER 2			GIRDER 3		
	DL1	DL2	LL+I	DL1	DL2	LL+I	DL1	DL2	LL+I
A	2.58	1.93	5.23	13.03	5.64	9.89	26.39	12.11	18.47
B	3.51	2.01	4.72	12.48	5.53	9.67	23.73	11.16	17.17
C	2.26	1.64	4.78	12.41	5.52	9.65	25.02	11.53	17.46
D	4.24	2.07	4.46	12.28	5.60	9.51	21.33	10.36	15.90

Table B4.13 – Case A vs. Case B vs. Case C vs. Case D – Bottom-Flange Lateral Bending Moments at Line 5L from Equation B-1 (k-ft)
(1 k-ft = 1.35582 kN-m)

Case	GIRDER 1			GIRDER 2			GIRDER 3		
	DL1	DL2	LL+I	DL1	DL2	LL+I	DL1	DL2	LL+I
A	1.39	1.00	2.44	5.28	1.96	4.24	10.17	4.85	7.01
B	0	0	0	4.87	1.64	2.73	5.88	3.57	5.38
C	0	0	0	3.95	1.41	2.68	8.60	4.38	6.03
D	--	--	--	0	0	0	5.14	3.19	4.44

Table B4.14 – Case A vs. Case B vs. Case C vs. Case D – Bottom-Flange Lateral Bending Moments at Line 2R from Equation B-1 (k-ft)
(1 k-ft = 1.35582 kN-m)

Table B4.15 through B4.18 list the bottom-flange lateral bending moments in each girder at cross-frame Lines 5L through 1R (moving from left to right) and at locations halfway in-between each of these cross-frame lines taken directly from the BSDI 3D System results. A negative moment is assumed to cause compression on the outside or convex tip of the flange. Note that the lateral bending moments due to LL+I were not available at each of the locations halfway in-between cross-frame Lines 5L through 1R.

SECTION	GIRDER 1			GIRDER 2			GIRDER 3		
	DL1	DL2	LL+I	DL1	DL2	LL+I	DL1	DL2	LL+I
5L	1	1	2	6	1	4	12	2	6
	-2	-2	-4	-10	-5	-7	-22	-11	-15
5R	1	0	2	6	1	4	12	2	6
	-2	-2	--	-10	-5	--	-21	-10	--
4R	1	0	2	5	1	4	2	2	6
	-2	-2	--	-8	-4	--	-17	-9	--
3R	1	0	2	4	1	2	8	1	5
	-1	-1	--	-5	-3	--	-12	-6	--
2R	0	0	1	2	1	2	5	1	4
	-1	0	--	-2	-1	--	-4	-2	--
1R	0	0	0	0	0	0	0	0	0

Table B4.15 – Case A – Bottom-Flange Lateral Bending Moments from Line 5L through Line 1R from BSDI 3D System Output (k-ft)
(1 k-ft = 1.35582 kN-m)

SECTION	GIRDER 1			GIRDER 2			GIRDER 3		
	DL1	DL2	LL+I	DL1	DL2	LL+I	DL1	DL2	LL+I
5L	2	1	2	7	2	4	13	2	6
	-2	-2	-4	-9	-5	-7	-17	-10	-14
5R	1	0	2	7	1	4	13	2	6
	-2	-2	--	-8	-4	--	-14	-9	--
4R	2	0	2	8	1	4	12	2	5
	-3	-2	--	-9	-4	--	-10	-8	--
3R	-1	0	1	4	0	2	8	0	2
	-3	-1	--	-3	-1	--	-2	-1	--
2R	0	0	0	11	4	6	11	9	11
	--	--	--	0	0	0	2	2	4
1R	--	--	--	--	--	--	0	0	0

Table B4.16 – Case B – Bottom-Flange Lateral Bending Moments from Line 5L through Line 1R from BSDI 3D System Output (k-ft)
(1 k-ft = 1.35582 kN-m)

SECTION	GIRDER 1			GIRDER 2			GIRDER 3		
	DL1	DL2	LL+I	DL1	DL2	LL+I	DL1	DL2	LL+I
5L	1	1	2	6	1	4	13	2	6
	-2	-2	-4	-9	-5	-7	-18	-10	-14
5R	0	0	2	8	2	4	13	2	6
	-1	-2	--	-10	-5	--	-17	-10	--
4R	1	1	2	4	0	2	12	1	5
	-4	-2	--	-5	-2	--	-12	-7	--
3R	-8	-3	-4	15	5	6	11	4	6
	-4	-2	--	-9	-5	--	-4	-4	--
2R	0	0	0	-16	-11	-9	12	1	4
	--	--	--	0	0	0	0	-2	-2
1R	--	--	--	--	--	--	0	0	0

Table B4.17 – Case C – Bottom-Flange Lateral Bending Moments from Line 5L through Line 1R from BSDI 3D System Output (k-ft)
(1 k-ft = 1.35582 kN-m)

SECTION	GIRDER 1			GIRDER 2			GIRDER 3		
	DL1	DL2	LL+I	DL1	DL2	LL+I	DL1	DL2	LL+I
5L	2	1	2	8	2	4	13	2	6
	-3	-2	-4	-8	-5	-6	-13	-9	-13
5R	2	1	1	8	2	4	12	2	5
	-4	-2	--	-9	-5	--	-11	-9	--
4R	0	0	1	5	1	2	10	1	4
	-4	-2	--	-5	-3	--	-5	-4	--
3R	0	0	0	12	4	6	12	6	9
	--	--	--	-1	0	--	-4	-1	--
2R	--	--	--	0	0	0	-1	2	1
	--	--	--	--	--	--	-4	-1	--
1R	--	--	--	--	--	--	0	0	0

Table B4.18 – Case D – Bottom-Flange Lateral Bending Moments from Line 5L through Line 1R from BSDI 3D System Output (k-ft)
(1 k-ft = 1.35582 kN-m)

From a comparison of the results for Case A at Line 5L from Tables B4.13 and B4.15 and at Line 2R from Tables B4.14 and B4.15, the approximate Equation B-1 appears to yield a conservative estimate of the bottom-flange lateral moments at the cross frame due solely to the effects of curvature. A comparison of the results for Cases A, B and C at Line 2R from Table B4.14 and from Tables B4.15 through B4.17 indicates that support skew introduces additional lateral flange bending in the region of the skew that is not comprehended by the approximate equation. Removal of the G1-G2 cross frame at Line 2R also introduces additional lateral flange bending into G2 (comparing the results for G2 at Line 2R from Case B in Table B4.16 to the results for G2 at Line 2R from Case C in Table B4.17). The additional lateral bending is due to the forces in the G2-G3 cross frame at that line acting on the G2 flange.

***Cross-Frame Forces*:** Tables B4.19 through B4.21 list the computed maximum cross-frame forces at cross-frame Lines 3R, 2R and 1R, respectively, from the BSDI 3D System analysis for Case A. Note that the reported live load plus impact responses are not necessarily caused by coincident loads. G1-G2 refers to the cross frame between Girders 1 and 2 and G2-G3 refers to the cross frame between Girders 2 and 3. Positive values are tensile forces and negative values are compressive forces. The figure below may be used as a key for matching the reported responses with each member.

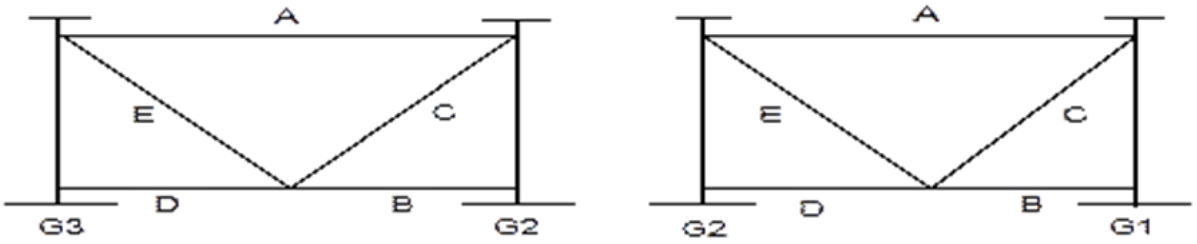

Member	G2 – G3				G1 – G2			
	DL1	DL2	LL+I		DL1	DL2	LL+I	
			(+)	(-)			(+)	(-)
Top Strut - A	9	-2	2	0	4	-3	1	-1
Diagonal - C	-10	0	0	-9	-9	-8	2	-5
Diagonal - E	10	0	9	0	9	8	5	-2
Bot. Strut - B	-2	-7	6	-2	2	2	4	-1
Bot. Strut - D	-17	-7	0	-10	-11	-11	3	-5

Table B4.19 – Case A – Radial Supports at Lines 1L and 1R
Cross-Frame Forces at Line 3R (kips)
(1 kip = 4.4482 kN)

Member	G2 – G3				G1 – G2			
	DL1	DL2	LL+I		DL1	DL2	LL+I	
			(+)	(-)			(+)	(-)
Top Strut - A	5	-2	1	0	3	-2	1	0
Diagonal - C	-6	1	0	-5	-5	-6	2	-3
Diagonal - E	6	-1	5	0	5	6	3	-2
Bot. Strut - B	0	-5	5	-1	1	1	2	-1
Bot. Strut - D	-9	-4	0	-6	-6	7	3	-3

Table B4.20 – Case A – Radial Supports at Lines 1L and 1R
Cross-Frame Forces at Line 2R (kips)
(1 kip = 4.4482 kN)

Member	G2 – G3				G1 – G2			
	DL1	DL2	LL+I		DL1	DL2	LL+I	
			(+)	(-)			(+)	(-)
Top Strut - A	0	-2	1	-2	0	0	4	-1
Diagonal - C	-1	-2	0	-2	0	-1	0	-2
Diagonal - E	1	2	2	0	0	1	2	0
Bot. Strut - B	0	0	2	0	0	0	1	0
Bot. Strut - D	-1	-2	1	-2	0	-2	0	-2

Table B4.21 – Case A – Radial Supports at Lines 1L and 1R
Cross-Frame Forces at Line 1R (kips)
(1 kip = 4.4482 kN)

Tables B4.22 through B4.24 list the computed maximum cross-frame forces at cross-frame Lines 3R, 2R and Along the Skewed Support respectively, from the BSDI 3D System analysis for Case B.

Member	G2 – G3				G1 – G2			
	DL1	DL2	LL+I		DL1	DL2	LL+I	
			(+)	(-)			(+)	(-)
Top Strut - A	13	-2	1	-1	11	-3	1	-1
Diagonal - C	3	4	2	-6	-17	-10	2	-7
Diagonal - E	-3	-4	6	-2	17	10	7	-2
Bot. Strut - B	-15	-10	6	-6	2	1	3	0
Bot. Strut - D	-12	-5	0	-8	-24	-13	3	-9

Table B4.22 – Case B – Radial Support at Line 1L and 30° Skew at Right Support
Cross-Frame Forces at Line 3R (kips)
(1 kip = 4.4482 kN)

Member	G2 – G3				G1 – G2			
	DL1	DL2	LL+I		DL1	DL2	LL+I	
			(+)	(-)			(+)	(-)
Top Strut - A	39	-3	1	-2	73	0	1	-3
Diagonal - C	43	11	11	-4	-5	-4	2	-3
Diagonal - E	-43	-11	4	-11	5	4	3	-2
Bot. Strut - B	-70	-21	4	-21	-69	-17	4	-22
Bot. Strut - D	-7	-5	0	-6	-78	-23	5	-25

Table B4.23 – Case B – Radial Support at Line 1L and 30° Skew at Right Support
Cross-Frame Forces at Line 2R (kips)
(1 kip = 4.4482 kN)

Member	G2 – G3				G1 – G2			
	DL1	DL2	LL+I		DL1	DL2	LL+I	
			(+)	(-)			(+)	(-)
Top Strut - A	-4	-4	1	-2	-45	0	4	-1
Diagonal - C	-4	-1	2	-3	-45	-9	2	-11
Diagonal - E	4	1	3	-2	45	9	11	-2
Bot. Strut - B	7	0	5	-4	81	19	26	-5
Bot. Strut - D	0	0	1	-2	10	5	9	-2

Table B4.24 – Case B – Radial Support at Line 1L and 30° Skew at Right Support
Cross-Frame Forces Along the Skewed Support (kips)
(1 kip = 4.4482 kN)

Tables B4.25 through B4.27 list the computed maximum cross-frame forces at cross-frame Lines 3R, 2R and Along the Skewed Support, respectively, from the BSDI 3D System analysis for Case C.

Member	G2 – G3				G1 – G2			
	DL1	DL2	LL+I		DL1	DL2	LL+I	
			(+)	(-)			(+)	(-)
Top Strut - A	23	-2	1	-1	23	-4	1	-2
Diagonal - C	10	4	2	-6	-28	-13	2	-9
Diagonal - E	-10	-4	6	-2	28	13	9	-2
Bot. Strut - B	-30	-13	6	-8	-2	0	2	-1
Bot. Strut - D	-14	-7	0	-10	-43	-19	4	-14

Table B4.25 – Case C – Case B w/ G1-G2 Cross Frame Removed at Line 2R
Cross-Frame Forces at Line 3R (kips)
(1 kip = 4.4482 kN)

Member	G2 – G3				G1 – G2			
	DL1	DL2	LL+I		DL1	DL2	LL+I	
			(+)	(-)			(+)	(-)
Top Strut - A	5	-5	1	-3	--	--	--	--
Diagonal - C	-5	0	0	-3	--	--	--	--
Diagonal - E	5	0	3	0	--	--	--	--
Bot. Strut - B	-3	-3	2	-2	--	--	--	--
Bot. Strut - D	-9	-3	0	-5	--	--	--	--

Table B4.26 – Case C – Case B w/ G1-G2 Cross Frame Removed at Line 2R
Cross-Frame Forces at Line 2R (kips)
(1 kip = 4.4482 kN)

Member	G2 – G3				G1 – G2			
	DL1	DL2	LL+I		DL1	DL2	LL+I	
			(+)	(-)			(+)	(-)
Top Strut - A	5	-4	1	-1	6	-1	3	-1
Diagonal - C	7	1	2	-1	-9	-3	1	-3
Diagonal - E	-7	-1	1	-2	9	3	3	-1
Bot. Strut - B	-9	-4	1	-4	1	1	4	-1
Bot. Strut - D	0	-3	0	-2	-13	-3	1	-1

Table B4.27 – Case C – Case B w/ G1-G2 Cross Frame Removed at Line 2R
Cross-Frame Forces Along the Skewed Support (kips)
(1 kip = 4.4482 kN)

Finally, Tables B4.28 through B4.30 list the computed maximum cross-frame forces at cross-frame Lines 3R, 2R and Along the Skewed Support, respectively, from the BSDI 3D System analysis for Case D.

Member	G2 – G3				G1 – G2			
	DL1	DL2	LL+I		DL1	DL2	LL+I	
			(+)	(-)			(+)	(-)
Top Strut - A	36	3	1	-2	66	1	1	-2
Diagonal - C	37	10	9	-4	-11	-8	3	-6
Diagonal - E	-37	-10	4	-9	11	8	6	-3
Bot. Strut - B	-64	-20	4	-19	-59	-12	4	-17
Bot. Strut - D	-10	-6	0	-8	-75	-24	3	-23

Table B4.28 – Case D – Radial Support at Line 1L and 50° Skew at Right Support
Cross-Frame Forces at Line 3R (kips)
(1 kip = 4.4482 kN)

Member	G2 – G3				G1 – G2			
	DL1	DL2	LL+I		DL1	DL2	LL+I	
			(+)	(-)			(+)	(-)
Top Strut - A	13	-3	1	-3	--	--	--	--
Diagonal - C	12	6	5	-1	--	--	--	--
Diagonal - E	-12	-6	1	-5	--	--	--	--
Bot. Strut - B	-21	-12	1	-10	--	--	--	--
Bot. Strut - D	-4	-2	0	-3	--	--	--	--

Table B4.29 – Case D – Radial Support at Line 1L and 50° Skew at Right Support
Cross-Frame Forces at Line 2R (kips)
(1 kip = 4.4482 kN)

Member	G2 – G3				G1 – G2			
	DL1	DL2	LL+I		DL1	DL2	LL+I	
			(+)	(-)			(+)	(-)
Top Strut - A	-7	-6	1	-4	-36	-3	0	-1
Diagonal - C	-8	-3	1	-4	-67	-14	1	-16
Diagonal - E	8	3	4	-1	67	14	16	-1
Bot. Strut - B	13	3	6	-3	94	19	28	-6
Bot. Strut - D	-1	-2	1	-2	-21	-5	2	-6

Table B4.30 – Case D – Radial Support at Line 1L and 50° Skew at Right Support
Cross-Frame Forces Along the Skewed Support (kips)
(1 kip = 4.4482 kN)

The support skew results in a significant increase in the cross-frame forces due to the increased differential vertical deflections between the girders, with the magnitude of the forces generally increasing with increasing skew. Removal of the G1-G2 cross frame at Line 2R helped to soften the transverse stiffness of the structure in the region of the obtuse corner. As shown by comparing the reported cross frame forces for Cases B and C, this action resulted in a significant overall reduction of the cross-frame forces in that region. Note however that removal of the G1-G2 cross frame also introduced some additional lateral flange bending into the G2 bottom flange, as discussed previously.

***End Moments*:** Although the prototype bridge is simply supported, when one or more end supports are skewed, vertical bending moments must develop in the girders at the skewed end support(s) in order to maintain static equilibrium with the net longitudinal components of the skewed end-support cross frame forces acting along each girder. Tables B4.31 through B4.33 give the end moments in each girder at the right support of the bridge from the 3D System analysis for Cases B, C and D, respectively (note: end moments do not develop in Case A, which has radial supports at both ends of the bridge).

GIRDER 1			GIRDER 2			GIRDER 3		
DL1	DL2	LL+I	DL1	DL2	LL+I	DL1	DL2	LL+I
177	57	-34	67	-33	-40	12	-19	-29

Table B4.31 – Girder End Moments (k-ft) at Right Support
Case B – Radial Support at Line 1L and 30° Skew at Right Support
(1 k-ft = 1.35582 kN-m)

GIRDER 1			GIRDER 2			GIRDER 3		
DL1	DL2	LL+I	DL1	DL2	LL+I	DL1	DL2	LL+I
12	-13	-84	15	-27	-60	13	-14	-27

Table B4.32 – Girder End Moments (k-ft) at Right Support
Case C – Case B w/ G1-G2 Cross Frame Removed at Line 2R
(1 k-ft = 1.35582 kN-m)

GIRDER 1			GIRDER 2			GIRDER 3		
DL1	**DL2**	**LL+I**	**DL1**	**DL2**	**LL+I**	**DL1**	**DL2**	**LL+I**
308	90	-30	125	5	-27	11	-15	-20

Table B4.33 – Girder End Moments (k-ft) at Right Support
Case D – Radial Support at Line 1L and 50° Skew at Right Support
(1 k-ft = 1.35582 kN-m)

For Case B, the DL1 end moment in Girder 1 is +177 k-ft (Table B4.31). The DL1 forces in the G1-G2 cross frame along the skewed support for Case B are as follows (Table B4.24):

Top Strut - A: - 45 kips
Diagonal - C: - 45 kips
Diagonal - E: +45 kips
Bot. Strut - B: +81 kips
Bot. Strut - D: +10 kips

The angle the diagonal makes with the top strut in the cross frame along the skewed support is approximately 38.7°. Therefore, the net force acting on Girder 1 at the top strut along the skew is –45 kips + -45 * cos(38.7°) = -80 kips ≅ +81 kips acting on Girder 1 at the bottom strut along the skew. The longitudinal components of these forces acting along Girder 1 at the end support are therefore approximately equal to ± 81 * sin(30.8°) = ± 41.5 kips, where 30.8° is the skew angle measured from the radial direction. The end moment acting on the approximately 49-inch-deep girder as a result of these forces can then be estimated as (41.5 * 49)/12 = +169.5 k-ft, which is approximately equal to the end moment of +177 k-ft computed from the analysis for this case. This moment computation is approximate since the girder is singly symmetric, but the computation does serve to illustrate how these end moments do in fact develop.

The net components of the skewed end-support cross frame forces *transverse* to the girders introduce a torque at the girder ends, which can result in significant twisting at the girder ends – in particular, when the cross-frame forces are large.

Bearing Orientation

This section summarizes the results of the analyses that were conducted to investigate the effects of bearing orientation (boundary conditions) on the behavior of the prototype bridge. Four separate cases were investigated as summarized below in Table B5.1 (refer to Figure B.1). Case A is the **BASE CASE**.

Case	Boundary Conditions						
	Girder	Stiffness at Line 1L			Stiffness at Line 1R		
		Tangential	Vertical	Radial	Tangential	Vertical	Radial
A	1	0	RIGID	0	0	RIGID	0
	2	RIGID	RIGID	RIGID	0	RIGID	RIGID
	3	0	RIGID	0	0	RIGID	0
B	1	0	RIGID	RIGID	0	RIGID	RIGID
	2	RIGID	RIGID	RIGID	0	RIGID	RIGID
	3	0	RIGID	RIGID	0	RIGID	RIGID
C	1	RIGID	RIGID	0	RIGID	RIGID	0
	2	RIGID	RIGID	RIGID	RIGID	RIGID	0
	3	RIGID	RIGID	0	RIGID	RIGID	0
D	1	RIGID	RIGID	RIGID	0	RIGID	RIGID
	2	RIGID	RIGID	RIGID	0	RIGID	RIGID
	3	RIGID	RIGID	RIGID	0	RIGID	RIGID

Table B5.1 – Case A through Case D – Assumed Boundary Conditions

In Table B5.1, ″RIGID″ means that the bearing at that support is assumed fully restrained in the indicated direction. A stiffness of ″0″ indicates that there is no support assumed in the indicated direction. The girders were free to rotate about their local X, Y and Z-axes at both Lines 1L and 1R. All restraints were applied in the element or local coordinate system. The bearing orientations are shown schematically in Figures B.15 through B.18 for Cases A through D, respectively. In each case, the framing plan shown in Figure B.1 and the cross-frame configuration shown in Figure B.2 were assumed. For these analyses, the bottom lateral bracing members shown in Figure B.1 were included at each end in the model. WT6 x 20 (WT155 x 30) structural tees were assumed for the lateral bracing members. Analyses were run for the non-composite dead load case only, i.e. for the self-weight of the steel and the weight of the concrete deck.

***Local Web Displacements*:** Tables B5.2 through B5.5 list the computed displacements from the BSDI 3D System in three orthogonal directions at the top and bottom of the web of Girders 1 through 3 for Cases A through D, respectively. The displacements are given at each cross-frame line due to the sum of the dead load of the structural steel and the dead load of the concrete deck. All displacements are indicated in the element or local coordinate system. Positive tangential and radial displacements are in the directions shown in Figures B.15 through B.18 (L = tangential and R = radial). Downward vertical displacements are negative. These results were obtained from a separate analysis of the bridge using the finite-element solver contained within the 3D System software.

CROSS-FRAME LINE	GIRDER 1					
	TOP OF WEB			BOTTOM OF WEB		
	TANGENTIAL	RADIAL	VERTICAL	TANGENTIAL	RADIAL	VERTICAL
1L	0.267	0.003	-0.002	0.073	-0.003	0.000
2L	0.256	0.328	-0.460	0.019	0.096	-0.460
3L	0.224	0.601	-0.853	0.007	0.133	-0.854
4L	0.178	0.795	-1.138	-0.002	0.156	-1.138
5L	0.124	0.896	-1.286	-0.011	0.168	-1.288
5R	0.067	0.896	-1.286	-0.017	0.171	-1.288
4R	0.012	0.796	-1.138	-0.020	0.167	-1.138
3R	-0.034	0.601	-0.853	-0.016	0.152	-0.854
2R	-0.064	0.328	-0.460	-0.002	0.132	-0.460
1R	-0.076	0.002	-0.002	0.119	-0.003	0.000

CROSS-FRAME LINE	GIRDER 2					
	TOP OF WEB			BOTTOM OF WEB		
	TANGENTIAL	RADIAL	VERTICAL	TANGENTIAL	RADIAL	VERTICAL
1L	0.412	0.003	-0.006	0.000	0.000	0.000
2L	0.391	0.329	-1.033	0.007	0.061	-1.033
3L	0.334	0.604	-1.926	0.025	0.103	-1.927
4L	0.252	0.800	-2.580	0.051	0.125	-2.583
5L	0.152	0.901	-2.926	0.082	0.136	-2.927
5R	0.048	0.901	-2.926	0.116	0.136	-2.927
4R	-0.052	0.800	-2.580	0.148	0.125	-2.583
3R	-0.135	0.603	-1.926	0.175	0.102	-1.927
2R	-0.191	0.329	-1.033	0.192	0.061	-1.033
1R	-0.212	0.002	-0.006	0.200	0.000	0.000

CROSS-FRAME LINE	GIRDER 3					
	TOP OF WEB			BOTTOM OF WEB		
	TANGENTIAL	RADIAL	VERTICAL	TANGENTIAL	RADIAL	VERTICAL
1L	0.578	0.003	0.009	-0.036	0.002	0.000
2L	0.548	0.334	-1.616	-0.027	0.058	-1.616
3L	0.462	0.612	-3.018	-0.003	0.096	-3.020
4L	0.336	0.809	-4.048	0.035	0.117	-4.052
5L	0.185	0.912	-4.593	0.081	0.128	-4.597
5R	0.024	0.912	-4.593	0.127	0.126	-4.597
4R	-0.128	0.809	-4.048	0.173	0.117	-4.052
3R	-0.254	0.612	-3.018	0.210	0.097	-3.020
2R	-0.339	0.334	-1.616	0.236	0.058	-1.616
1R	-0.369	0.003	-0.009	0.245	0.002	0.000

Table B5.2 – Case A -- BSDI 3D System Local Web Displacements (in.)
Due to Dead Load of Steel plus Concrete Deck
(1 in. = 25.4 mm)

CROSS-FRAME LINE	GIRDER 1					
	TOP OF WEB			BOTTOM OF WEB		
	TANGENTIAL	RADIAL	VERTICAL	TANGENTIAL	RADIAL	VERTICAL
1L	0.267	0.003	-0.002	0.073	0.003	0.000
2L	0.256	0.328	-0.461	0.019	0.096	-0.461
3L	0.223	0.601	-0.854	0.008	0.133	-0.854
4L	0.177	0.797	-1.139	-0.002	0.156	-1.139
5L	0.123	0.898	-1.288	-0.011	0.168	-1.288
5R	0.067	0.896	-1.288	-0.017	0.172	-1.288
4R	0.012	0.796	-1.139	-0.020	0.168	-1.139
3R	-0.035	0.601	-0.854	-0.017	0.154	-0.854
2R	-0.065	0.327	-0.461	-0.002	0.132	-0.461
1R	-0.078	0.002	-0.002	0.118	0.000	0.000

CROSS-FRAME LINE	GIRDER 2					
	TOP OF WEB			BOTTOM OF WEB		
	TANGENTIAL	RADIAL	VERTICAL	TANGENTIAL	RADIAL	VERTICAL
1L	0.412	0.003	-0.006	0.000	0.000	0.000
2L	0.391	0.329	-1.033	0.007	0.061	-1.033
3L	0.334	0.605	-1.926	0.025	0.103	1.927
4L	0.251	0.801	-2.580	0.050	0.126	-2.581
5L	0.152	0.902	-2.926	0.082	0.137	-2.927
5R	0.047	0.903	-2.926	0.116	0.137	-2.927
4R	-0.053	0.801	-2.580	0.148	0.127	-2.581
3R	-0.136	0.605	-1.926	0.174	0.102	-1.927
2R	-0.192	0.329	-1.033	0.191	0.061	-1.033
1R	-0.214	0.002	-0.006	0.199	0.000	0.000

CROSS-FRAME LINE	GIRDER 3					
	TOP OF WEB			BOTTOM OF WEB		
	TANGENTIAL	RADIAL	VERTICAL	TANGENTIAL	RADIAL	VERTICAL
1L	0.578	0.003	-0.009	-0.038	0.002	0.000
2L	0.547	0.334	-1.616	-0.028	0.059	-1.616
3L	0.461	0.613	-3.016	-0.003	0.097	-3.019
4L	0.336	0.810	-4.048	0.035	0.119	-4.049
5L	0.185	0.914	-4.592	0.079	0.129	-4.596
5R	0.024	0.913	-4.592	0.127	0.127	-4.596
4R	-0.128	0.810	-4.048	0.173	0.119	-4.049
3R	-0.254	0.612	-3.016	0.210	0.097	-3.019
2R	-0.339	0.334	-1.616	0.235	0.057	-1.616
1R	-0.369	0.003	-0.009	0.244	0.000	0.000

Table B5.3 – Case B -- BSDI 3D System Local Web Displacements (in.)
Due to Dead Load of Steel plus Concrete Deck
(1 in. = 25.4 mm)

CROSS-FRAME LINE	GIRDER 1					
	TOP OF WEB			BOTTOM OF WEB		
	TANGENTIAL	RADIAL	VERTICAL	TANGENTIAL	RADIAL	VERTICAL
1L	0.253	0.003	-0.003	0.000	0.002	0.000
2L	0.242	0.207	-0.577	0.001	0.024	-0.576
3L	0.216	0.477	-1.048	0.002	0.110	-1.047
4L	0.173	0.774	-1.381	-0.003	0.267	-1.381
5L	0.114	1.043	-1.553	-0.016	0.462	-1.553
5R	0.042	1.243	-1.553	-0.034	0.661	-1.553
4R	-0.035	1.352	-1.382	-0.052	0.840	-1.382
3R	-0.116	1.351	-1.050	-0.061	0.975	-1.048
2R	-0.190	1.243	-0.578	-0.060	1.046	-0.577
1R	-0.254	1.057	-0.003	-0.045	1.054	0.000

CROSS-FRAME LINE	GIRDER 2					
	TOP OF WEB			BOTTOM OF WEB		
	TANGENTIAL	RADIAL	VERTICAL	TANGENTIAL	RADIAL	VERTICAL
1L	0.395	0.003	-0.006	0.000	0.000	0.000
2L	0.376	0.209	-0.997	0.006	0.008	-0.995
3L	0.325	0.481	-1.857	0.026	0.099	-1.859
4L	0.244	0.779	-2.487	0.051	0.257	-2.489
5L	0.137	1.047	-2.819	0.073	0.453	-2.820
5R	0.020	1.250	-2.819	0.085	0.926	-2.820
4R	-0.106	1.357	-2.487	0.087	0.837	-2.487
3R	-0.224	1.355	-1.857	0.074	0.974	-1.858
2R	-0.324	1.246	-0.995	0.047	1.049	-0.995
1R	-0.394	1.055	-0.006	0.001	1.054	0.000

CROSS-FRAME LINE	GIRDER 3					
	TOP OF WEB			BOTTOM OF WEB		
	TANGENTIAL	RADIAL	VERTICAL	TANGENTIAL	RADIAL	VERTICAL
1L	0.538	0.002	-0.009	0.000	0.000	0.000
2L	0.512	0.214	-1.430	0.002	0.009	-1.430
3L	0.437	0.489	-2.684	0.021	0.095	-2.687
4L	0.316	0.788	-3.613	0.046	0.254	-3.617
5L	0.164	1.058	-4.105	0.070	0.448	-4.109
5R	-0.007	1.260	-4.105	0.088	0.651	-4.109
4R	-0.179	1.366	-3.612	0.092	0.832	-3.615
3R	-0.335	1.364	-2.683	0.081	0.972	-2.684
2R	-0.460	1.252	-1.428	0.050	1.046	-1.429
1R	-0.537	1.057	-0.009	0.000	1.054	0.000

Table B5.4 – Case C -- BSDI 3D System Local Web Displacements (in.)
Due to Dead Load of Steel plus Concrete Deck
(1 in. = 25.4 mm)

CROSS-FRAME LINE	GIRDER 1					
	TOP OF WEB			BOTTOM OF WEB		
	TANGENTIAL	RADIAL	VERTICAL	TANGENTIAL	RADIAL	VERTICAL
1L	0.197	0.003	-0.002	0.000	0.000	0.000
2L	0.186	0.266	-0.463	0.000	0.006	-0.463
3L	0.159	0.517	-0.859	-0.002	0.030	-0.859
4L	0.117	0.725	-1.145	-0.007	0.069	-1.145
5L	0.066	0.862	-1.295	-0.015	0.116	-1.295
5R	0.010	0.907	-1.295	-0.026	0.161	-1.295
4R	-0.046	0.845	-1.146	-0.034	0.188	-1.146
3R	-0.095	0.670	-0.860	-0.035	0.184	-0.861
2R	-0.130	0.381	-0.466	-0.023	0.132	-0.465
1R	-0.142	0.003	-0.002	0.055	0.001	0.000

CROSS-FRAME LINE	GIRDER 2					
	TOP OF WEB			BOTTOM OF WEB		
	TANGENTIAL	RADIAL	VERTICAL	TANGENTIAL	RADIAL	VERTICAL
1L	0.408	0.003	-0.006	0.000	0.000	0.000
2L	0.390	0.268	-1.030	0.006	0.001	-1.030
3L	0.336	0.520	-1.923	0.026	0.022	-1.924
4L	0.256	0.731	-2.577	0.055	0.059	-2.578
5L	0.159	0.868	-2.922	0.090	0.107	-2.924
5R	0.054	0.913	-2.922	0.123	0.151	-2.924
4R	-0.048	0.850	-2.578	0.152	0.179	-2.579
3R	-0.135	0.674	-1.924	0.174	0.176	-1.924
2R	-0.194	0.384	-1.031	0.187	0.119	-1.031
1R	-0.218	0.003	-0.006	0.195	0.000	0.000

CROSS-FRAME LINE	GIRDER 3					
	TOP OF WEB			BOTTOM OF WEB		
	TANGENTIAL	RADIAL	VERTICAL	TANGENTIAL	RADIAL	VERTICAL
1L	0.613	0.003	-0.009	0.000	0.000	0.000
2L	0.584	0.272	-1.609	0.011	-0.003	-1.610
3L	0.503	0.529	-3.006	0.041	0.016	-3.008
4L	0.382	0.740	-4.035	0.081	0.052	-4.037
5L	0.233	0.879	-4.579	0.128	0.098	-4.581
5R	0.073	0.924	-4.577	0.178	0.143	-4.581
4R	-0.081	0.860	-4.035	0.220	0.174	-4.037
3R	-0.209	0.681	-3.006	0.253	0.169	-3.008
2R	-0.296	0.387	-1.609	0.277	0.113	-1.609
1R	-0.328	0.002	-0.009	0.284	0.000	0.000

Table B5.5 – Case D -- BSDI 3D System Local Web Displacements (in.)
Due to Dead Load of Steel plus Concrete Deck
(1 in. = 25.4 mm)

All displacements in Cases A and B are approximately the same. In Case C, the tangential displacements at the top of the web are slightly less than the tangential displacements in Cases A and B near the left end of the bridge and are significantly larger near the right end of the bridge. The tangential displacements at the bottom of the web in Case C are significantly less along the entire span due to the tangential restraint at the bearing at Line 1R. The radial displacements at the top and bottom of the web in Case C are smaller than for Cases A and B near the left end of the bridge but become significantly larger toward the right end of the bridge due to the lack of radial restraint at Line 1R. The vertical displacements in Case C are smaller than the vertical displacements in Cases A and B in G2 and G3 but are larger in G1. In Case D, the vertical displacements are approximately the same as the vertical displacements in Cases A and B. The radial displacements at the top of the web in Case D are slightly less than the radial displacements in Cases A and B near the left end of the bridge and are slightly larger near the right end of the bridge. The tangential displacements at the top and bottom of the web in Case D are slightly less than the tangential displacements in Cases A and B in G1, are about the same as the tangential displacements in

G2 and are slightly larger than the tangential displacements in G3.

***End Reactions*:** Table B5.6 lists the computed end reactions for each case due to the sum of the steel and concrete deck weight from the BSDI 3D System analysis at Lines 1L and 1R (Figure B.1). Referring to Figures B.15 through B.18, a positive tangential reaction is in the direction of positive ″L″ and a positive radial reaction is in the direction of negative ″R″. An upward vertical reaction is negative.

Case	Non-Composite Dead Load Reactions						
	Girder	Reaction at Line 1L			Reaction at Line 1R		
		Tangential	Vertical	Radial	Tangential	Vertical	Radial
A	1	0	-15.6	0	0	-15.6	0
	2	0	-50.2	0	0	-50.2	0
	3	0	-80.2	0	0	-80.2	0
B	1	0	-16.0	5.2	0	-16.0	5.2
	2	0	-49.3	-0.9	0	-49.3	-0.9
	3	0	-80.8	-4.3	0	-80.8	-4.3
C	1	106.5	-14.7	0	-100.3	-14.5	0
	2	-22.8	-51.9	-2.3	23.2	-52.1	0
	3	-88.6	-79.4	0	82.5	-79.3	0
D	1	16.5	-15.4	-3.3	0	-15.6	10.0
	2	-26.0	-50.5	-0.8	0	-49.9	-1.7
	3	9.9	-80.1	3.5	0	-80.4	-7.6

Table B5.6 – Case A through Case D – End Reactions at Lines 1L and 1R (kips)
Due to Dead Load of Steel plus Concrete Deck
(1 kip = 4.4482 kN)

Note in Case A that G2 is fixed radially at both ends; however, a radial reaction is not generated at either end since G1 and G3 are free to float in any direction. In Case B, where G1 and G3 are also fixed radially at both ends, radial reactions are generated at both ends of all three girders. Fixing all three girders at the left end against translation in both the radial and tangential directions (Case D) significantly increased the radial reactions at Line 1R. As expected, large tangential reactions are generated at both ends in Case C because of the tangential restraint at both ends of each girder. These reactions are reduced in Case D by fixing only the left end of all three girders. When only G2 is fixed tangentially at the left end, no tangential reactions are generated (Cases A and B). With the increased end fixity in Cases C and D, there is a slight decrease in the vertical reactions at the ends of G1 and G3 and a slight increase in the vertical reactions at the ends of G2.

***Lateral-Bracing Forces*:** Table B5.7 lists the computed axial forces in the bottom flange lateral bracing members for each case due to the sum of the steel and concrete deck weight from the BSDI 3D System analysis at each end of the bridge (Figure B.1).

Lateral Bracing Forces (kips)				
Case	Bracing Member			
	G1-1L to G2-2L	G2-2L to G3-1L	G2-2R to G1-1R	G2-2R to G3-1R
A	-7.41	-5.22	-7.41	-5.21
B	-8.37	-6.18	-8.37	-6.18
C	+10.02	-0.27	+1.76	+7.87
D	+5.65	+3.76	-15.99	-9.51

Table B5.7 – Case A through Case D – Bottom Lateral Bracing Forces (kips)
Due to Dead Load of Steel plus Concrete Deck
(1 kip = 4.4482 kN)

The compressive forces in the lateral bracing members increase approximately 13 to 18 percent between Cases A and B. In Case B, tangentially guided bearings are used at the ends of G1 and G3 restricting the outward movement of these girders and increasing the compressive forces in the diagonal members. Fixing G1 and G3 tangentially (at both ends in Case C and at the left end in Case D) induces tension in the bracing members as the members elongate while attempting to displace with G2. The brace between G1 and G2 experiences a larger tensile force because G2 displaces further relative to G1 than G3. In Case D at Line 1R, the girders are guided tangentially, which again restricts outward movement and induces compressive forces in the bracing members at that end.

Summary

Detailed elastic analyses were carried out on the horizontally curved simple-span I-girder prototype bridge that was originally proposed for testing as part of this project. As discussed in Appendix A, these analyses were conducted using the BSDI 3D System, GTSTRUDL, the MDX grid-analysis program, and the V-load analysis method. After the analyses of the base model of the prototype bridge were completed, selected modifications were made to the BSDI 3D System base model of the prototype bridge and the bridge was re-analyzed. Specifically, variations were made to study the effects of cross-frame type, cross-frame spacing, radius, skew and bearing orientation (boundary conditions). The results of these analyses are described herein. For this relatively small simple-span bridge with a simple framing plan, drastic differences in the results were not necessarily evident as the modifications were made. However, the results were still instructive to illustrate basic behavior and to indicate significant trends that will only be magnified in much larger horizontally curved I-girder bridges.

Acknowledgments

The plan for these analyses was developed by John M. Yadlosky, P.E. of the Pittsburgh, PA office of HDR Engineering, Inc. and executed by James D. Carnahan P.E. of the Pittsburgh, PA office of HDR Engineering, Inc. A. Richard Lawin of Bridge Software Development International, Ltd. in Coopersburg, PA performed the 3D System analyses.

References

1. BRIDGE-SYSTEM, 3D System User Manual, Bridge Software Development International, Ltd., Coopersburg, PA.

2. GTSTRUDL User Manual, Georgia Institute of Technology, Atlanta, GA.

3. MDX User Manual, MDX, Columbia, MO.

4. VANCK User Manual, available from M.A. Grubb & Associates, LLC, Wexford, PA.

5. U.S. Steel Highway Structures Design Handbook (1965). Vol. I Chapter 12, "Horizontally Curved Girder", chapter available from M.A. Grubb & Associates, LLC, Wexford, PA.

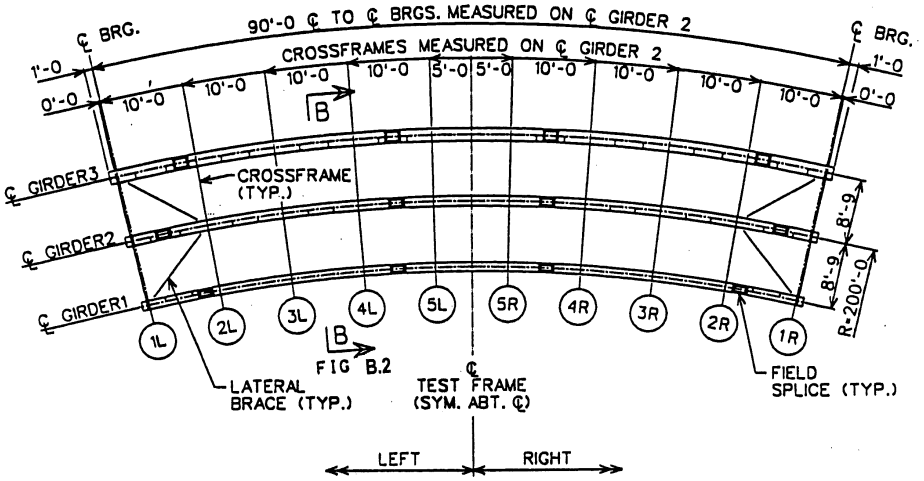

PROTOTYPE PLAN

1 ft. = 0.3048 m
1 in. = 25.4 mm

Figure B.1

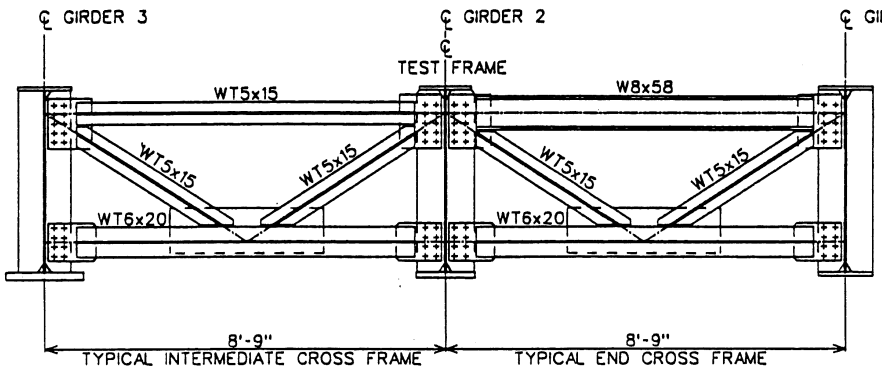

TYPICAL SECTION B-B
PROTOTYPE

1 ft = 0.3048 m
1 in. = 25.4 mm
1 lb/ft = 1.4882 kg/m

Figure B.2

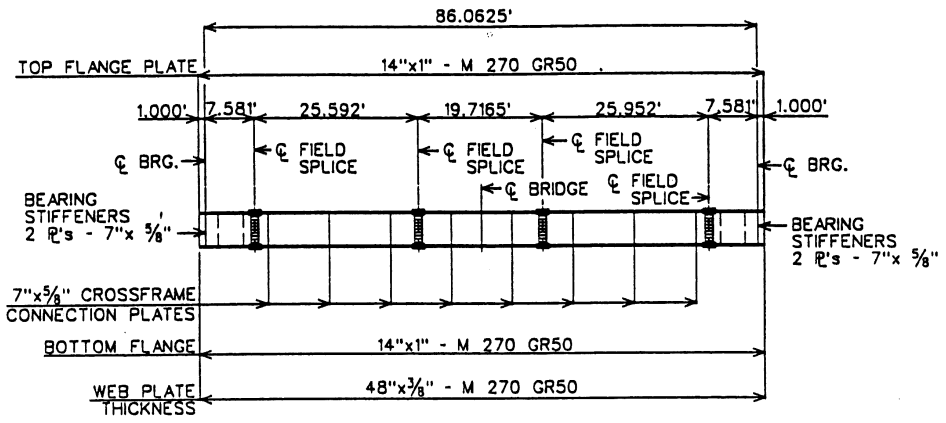

ELEVATION - GIRDER G1
PROTOTYPE

1 ft = 0.3048 m
1 in. = 25.4 mm
1 ksi = 6.8948 MPa

Figure B.3

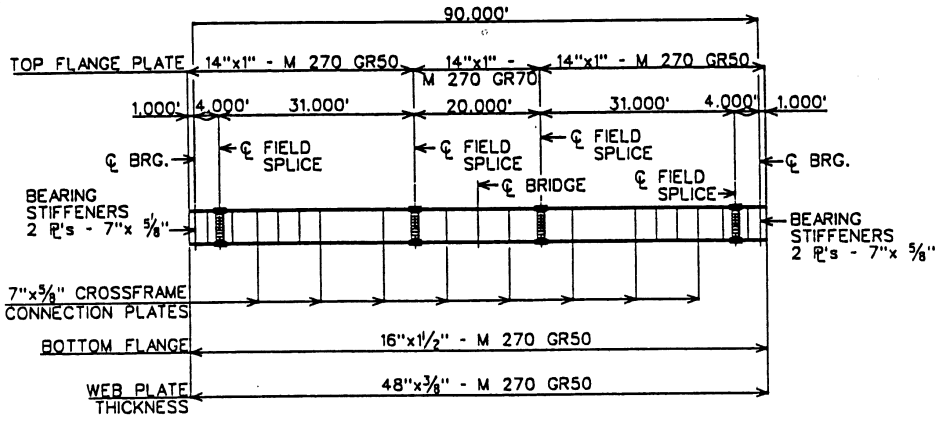

ELEVATION - GIRDER G2
PROTOTYPE

1 ft = 0.3048 m
1 in. = 25.4 mm
1 ksi = 6.8948 MPa

Figure B.4

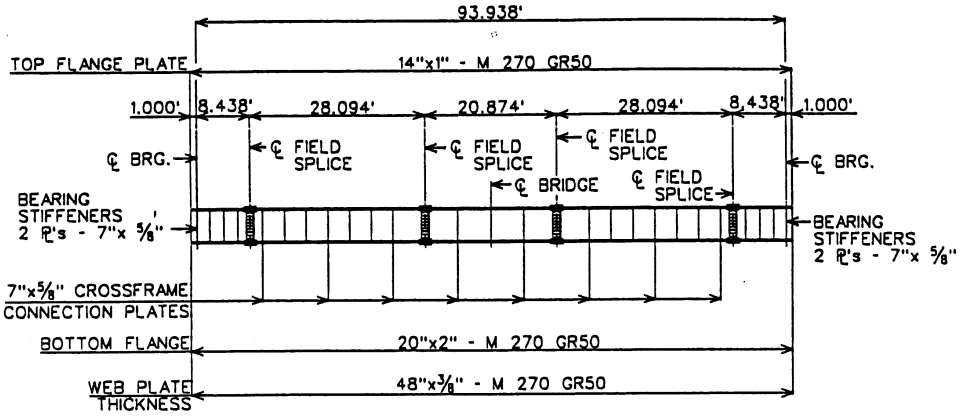

ELEVATION - GIRDER G3
PROTOTYPE

1 ft = 0.3048 m
1 in. = 25.4 mm
1 ksi = 6.8948 MPa

Figure B.5

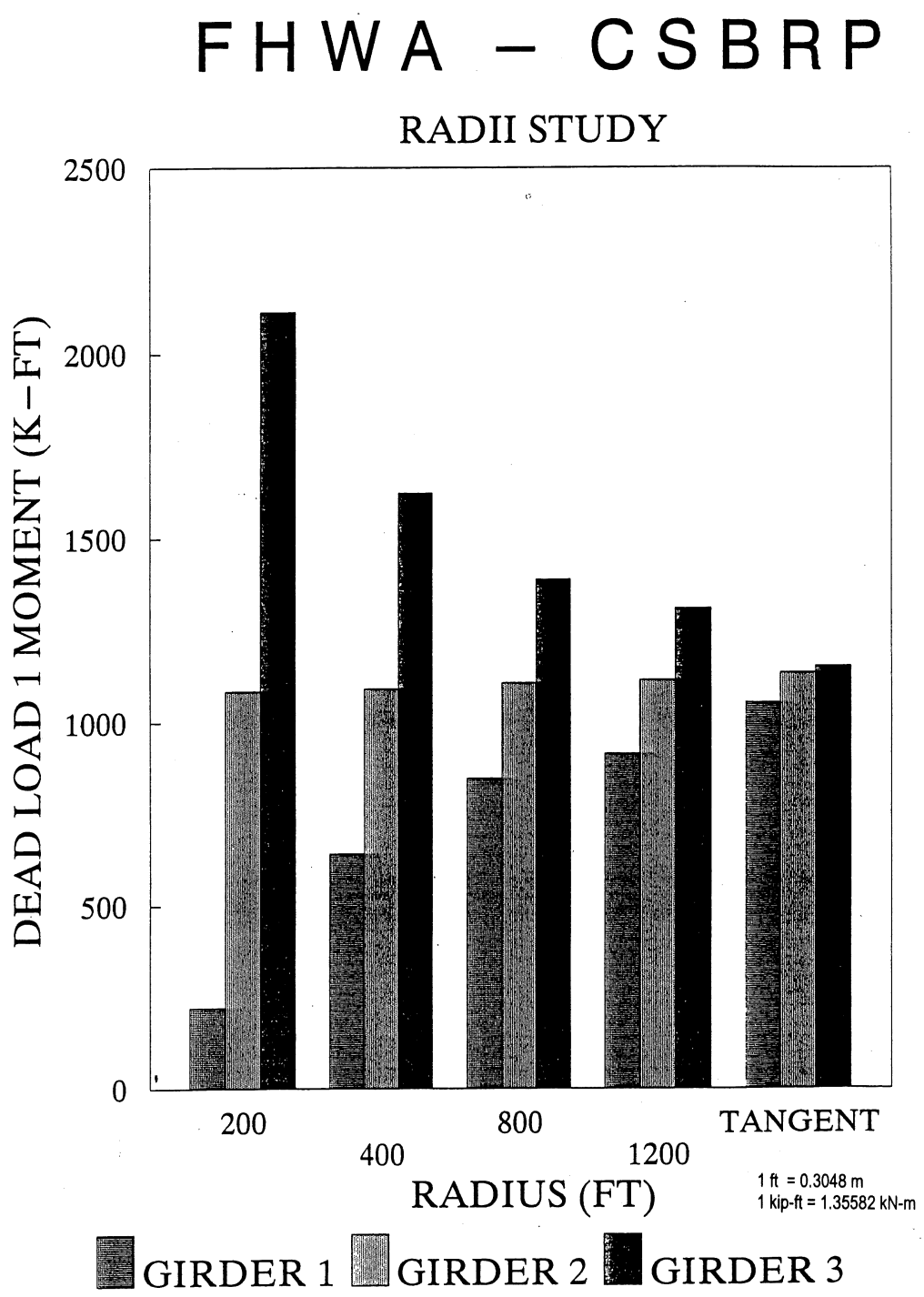
FHWA – CSBRP
RADII STUDY
DEAD LOAD 1 MOMENT (K–FT)
2500
2000
1500
1000
500
0
200
400
800
1200
TANGENT
RADIUS (FT)
1 ft = 0.3048 m
1 kip-ft = 1.35582 kN-m
GIRDER 1
GIRDER 2
GIRDER 3

Figure B.6

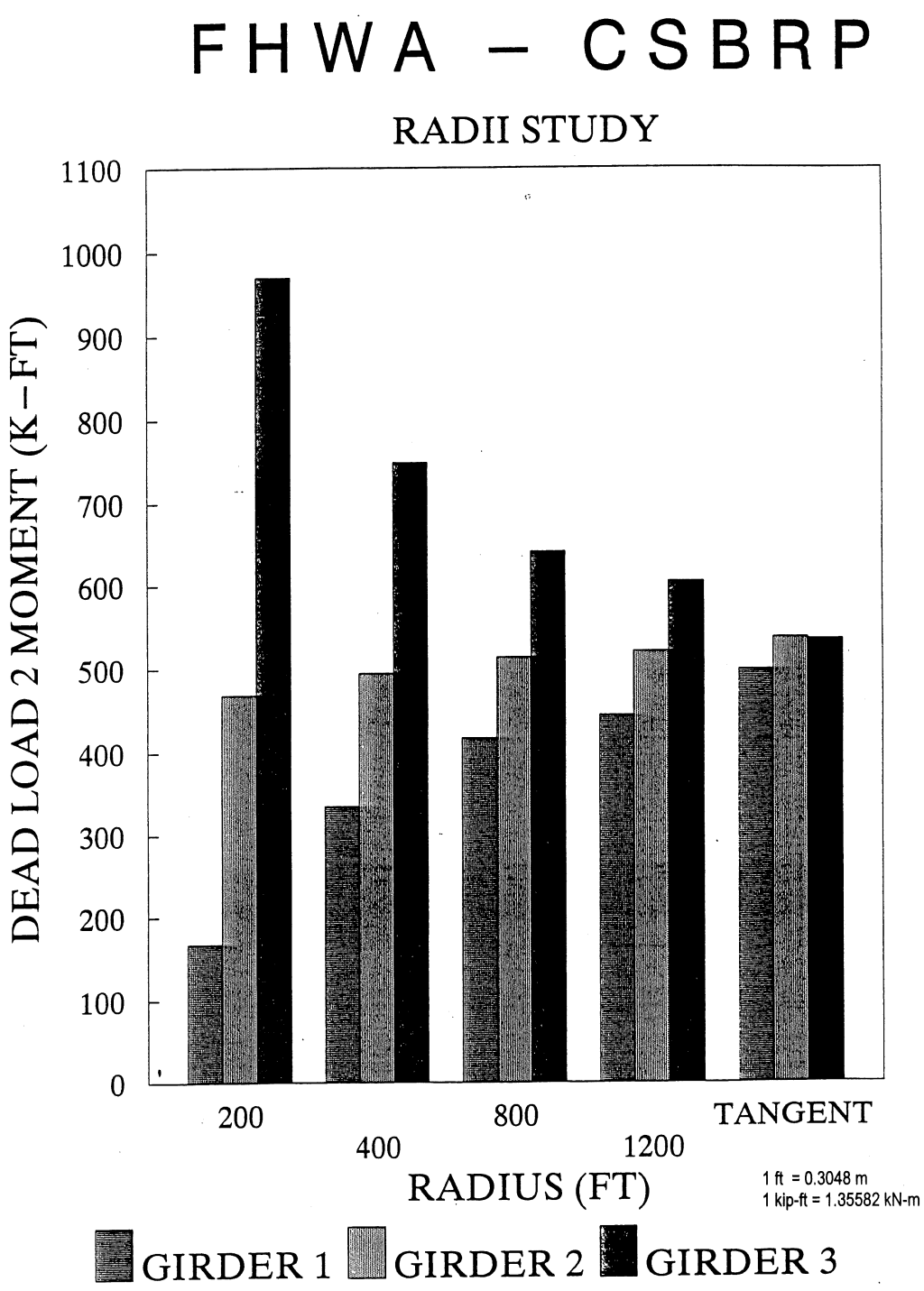
FHWA – CSBRP
RADII STUDY
DEAD LOAD 2 MOMENT (K–FT)
1100
1000
900
800
700
600
500
400
300
200
100
0
200
400
800
1200
TANGENT
RADIUS (FT)
1 ft = 0.3048 m
1 kip-ft = 1.35582 kN-m
GIRDER 1
GIRDER 2
GIRDER 3

Figure B.7

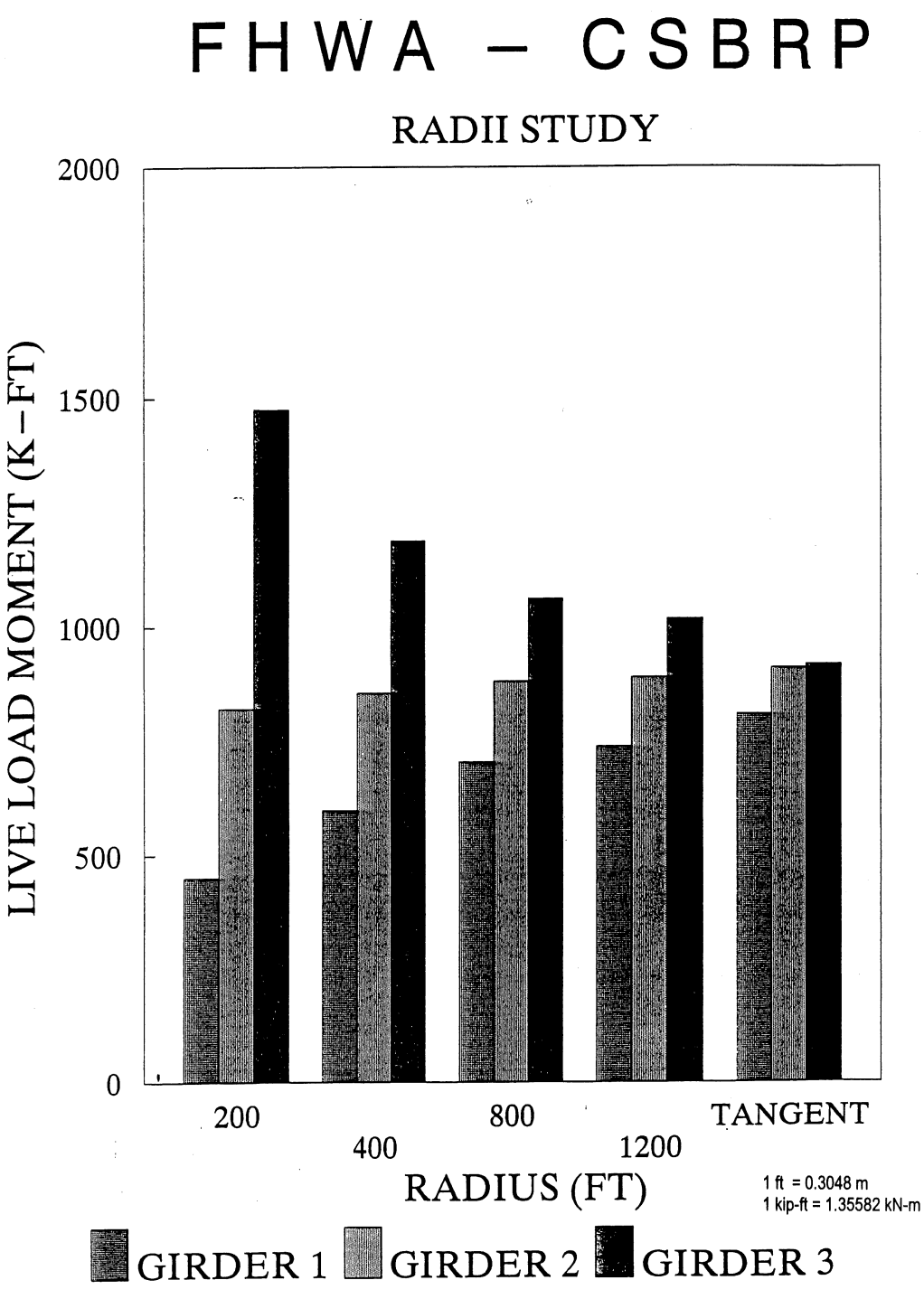
FHWA – CSBRP
RADII STUDY
LIVE LOAD MOMENT (K–FT)
2000
1500
1000
500
0
200
400
800
1200
TANGENT
RADIUS (FT)
1 ft = 0.3048 m
1 kip-ft = 1.35582 kN-m
GIRDER 1
GIRDER 2
GIRDER 3

Figure B.8

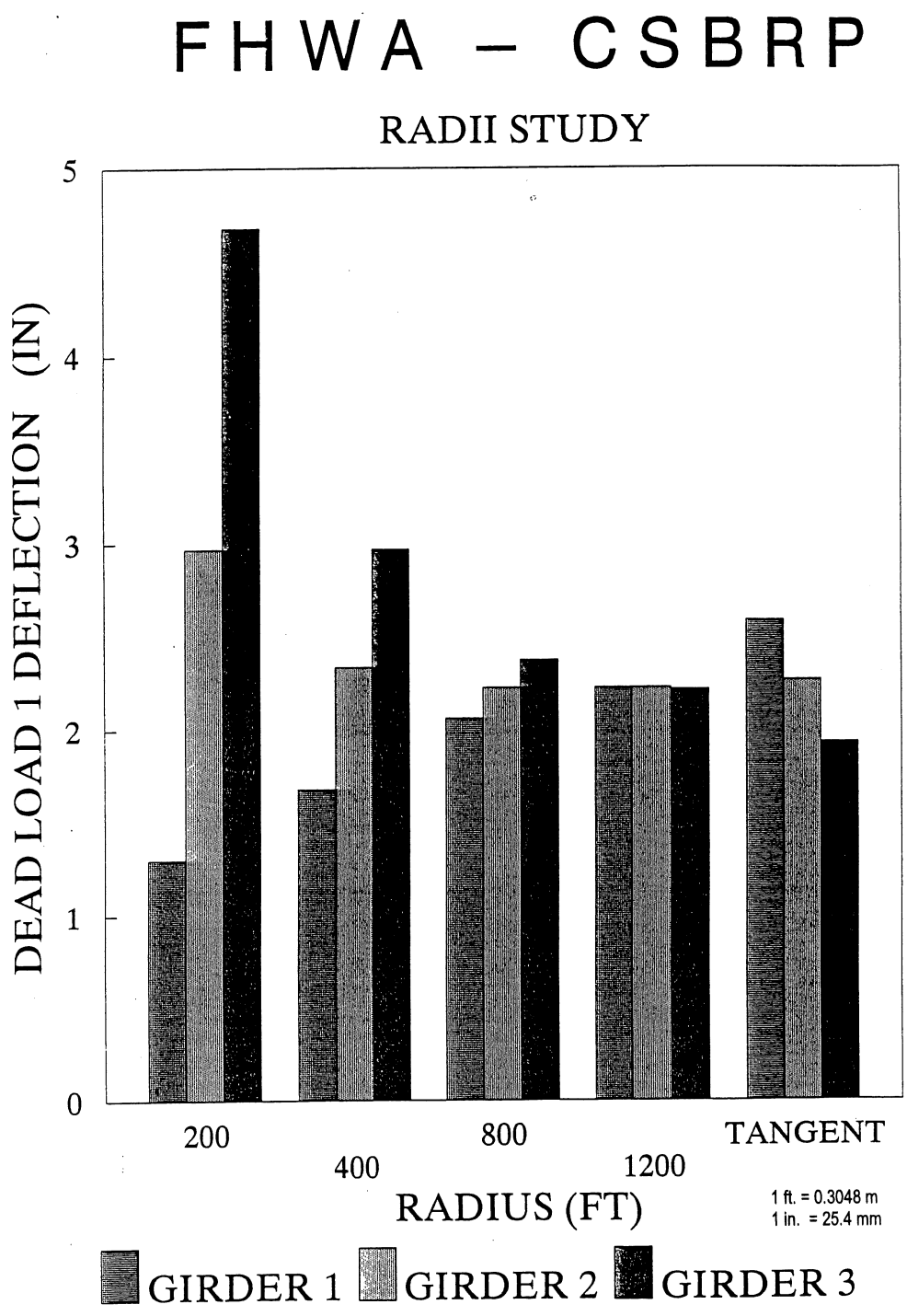
FHWA – CSBRP
RADII STUDY
DEAD LOAD 1 DEFLECTION (IN)
0
1
2
3
4
5
200
400
800
1200
TANGENT
RADIUS (FT)
1 ft. = 0.3048 m
1 in. = 25.4 mm
GIRDER 1
GIRDER 2
GIRDER 3

Figure B.9

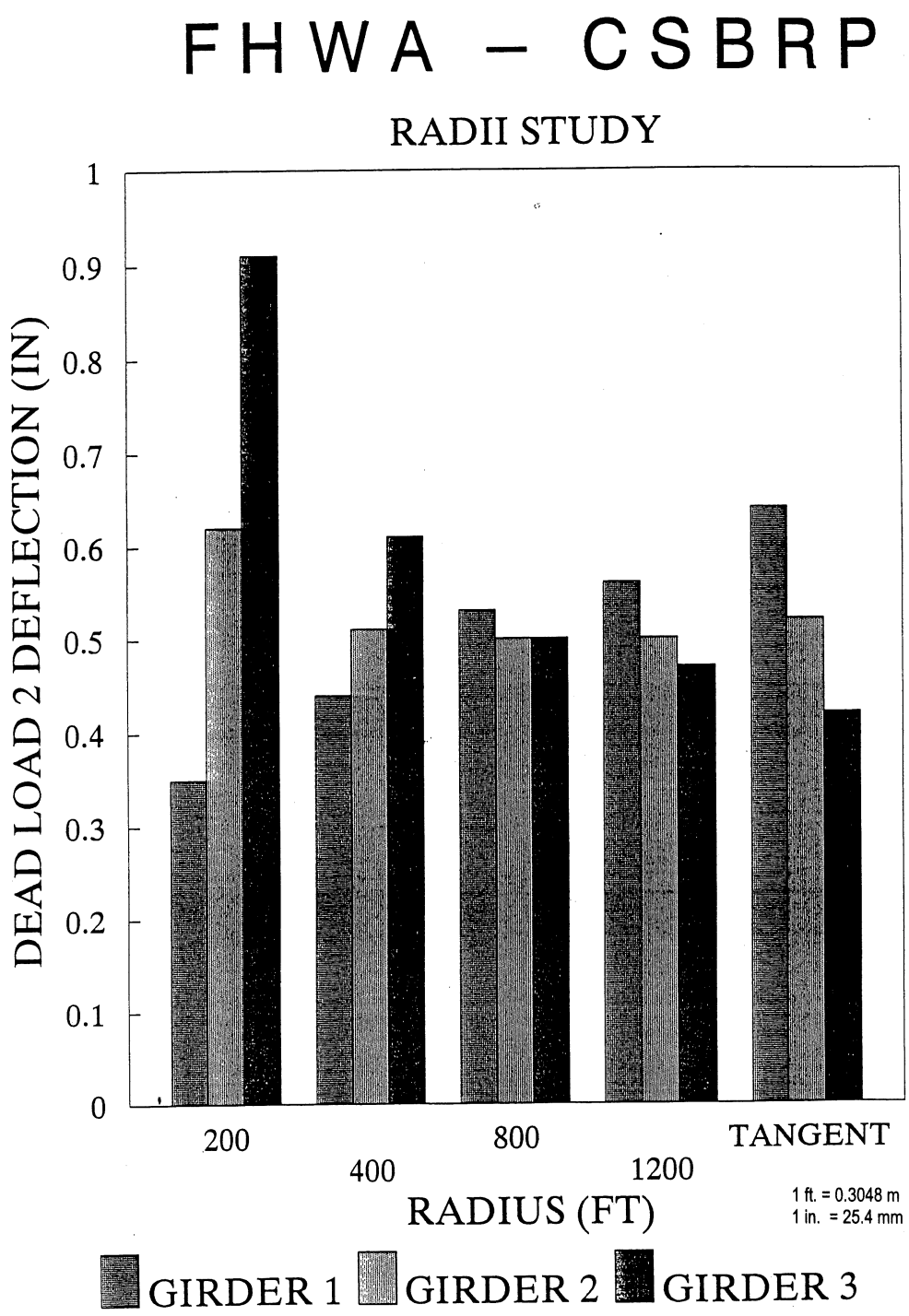
FHWA – CSBRP
RADII STUDY
DEAD LOAD 2 DEFLECTION (IN)
1
0.9
0.8
0.7
0.6
0.5
0.4
0.3
0.2
0.1
0
200
400
800
1200
TANGENT
RADIUS (FT)
1 ft. = 0.3048 m
1 in. = 25.4 mm
GIRDER 1
GIRDER 2
GIRDER 3

Figure B.10

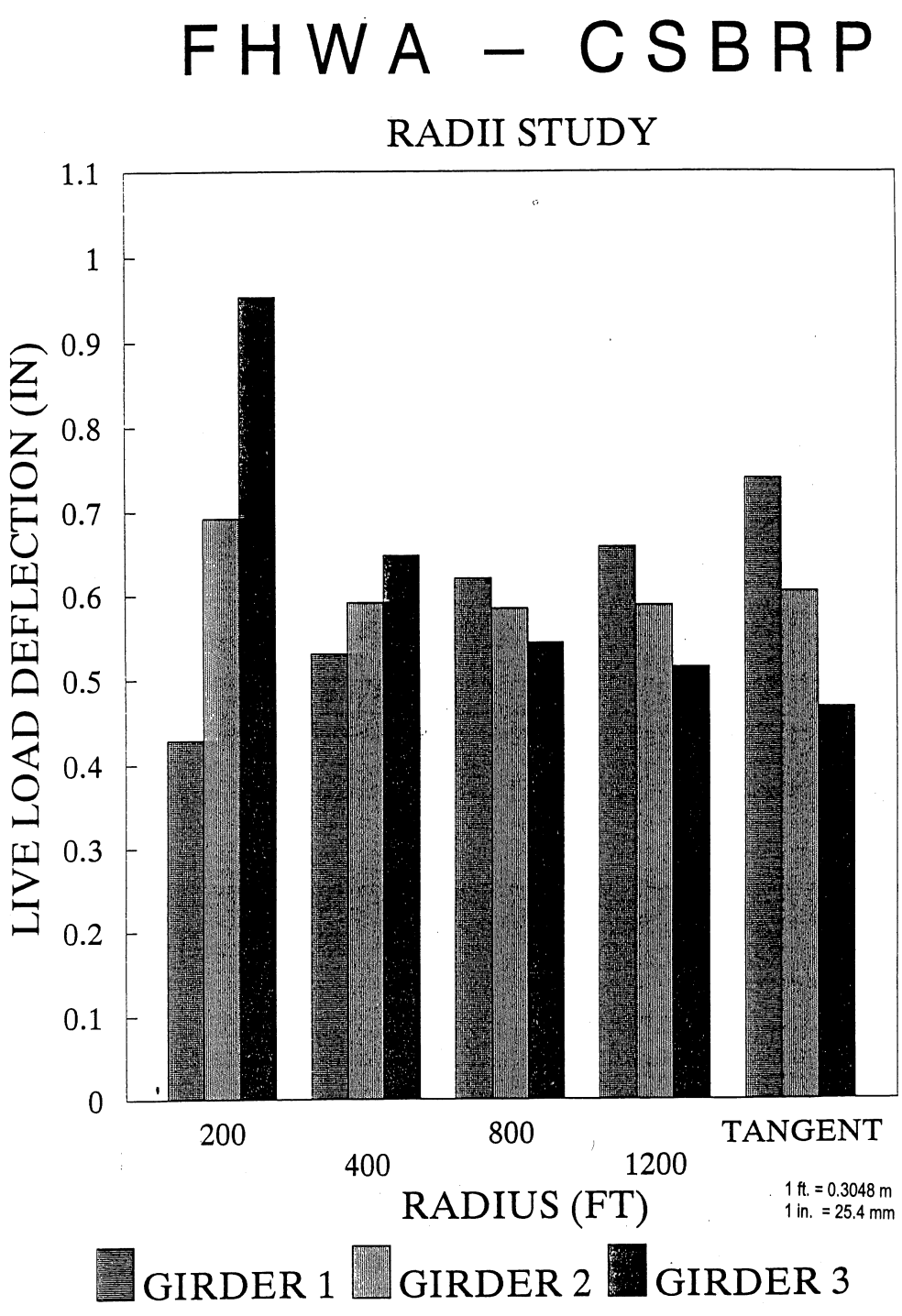
FHWA – CSBRP
RADII STUDY
LIVE LOAD DEFLECTION (IN)
1.1
1
0.9
0.8
0.7
0.6
0.5
0.4
0.3
0.2
0.1
0
200
400
800
1200
TANGENT
RADIUS (FT)
1 ft. = 0.3048 m
1 in. = 25.4 mm
GIRDER 1
GIRDER 2
GIRDER 3

Figure B.11

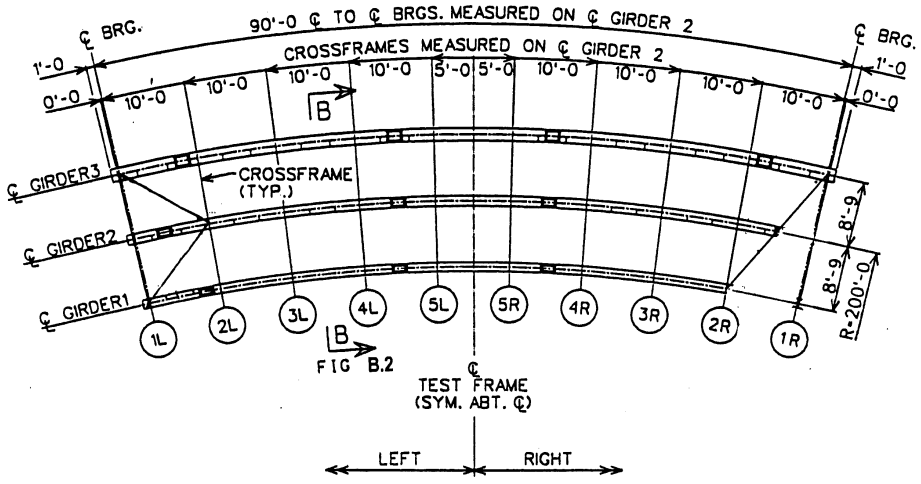

PROTOTYPE PLAN

SKEW CASE B

1 ft. = 0.3048 m
1 in. = 25.4 mm

Figure B.12

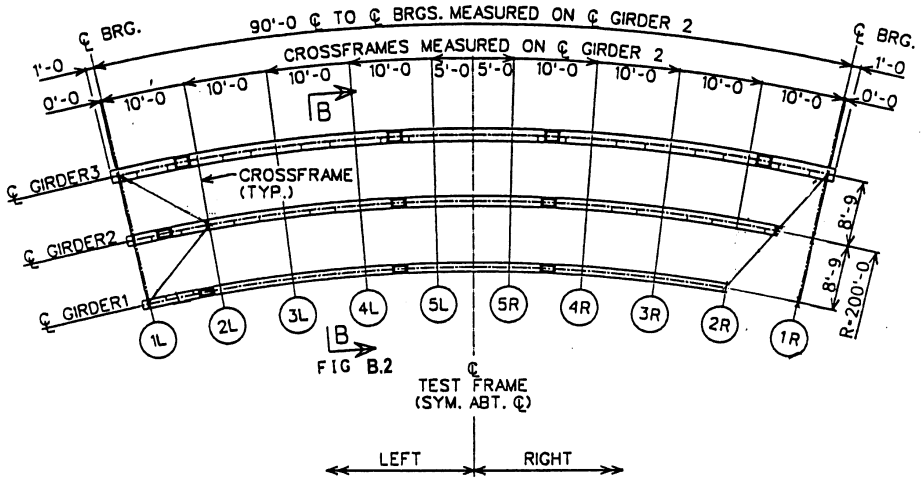

PROTOTYPE PLAN

SKEW CASE C

1 ft. = 0.3048 m
1 in. = 25.4 mm

Figure B.13

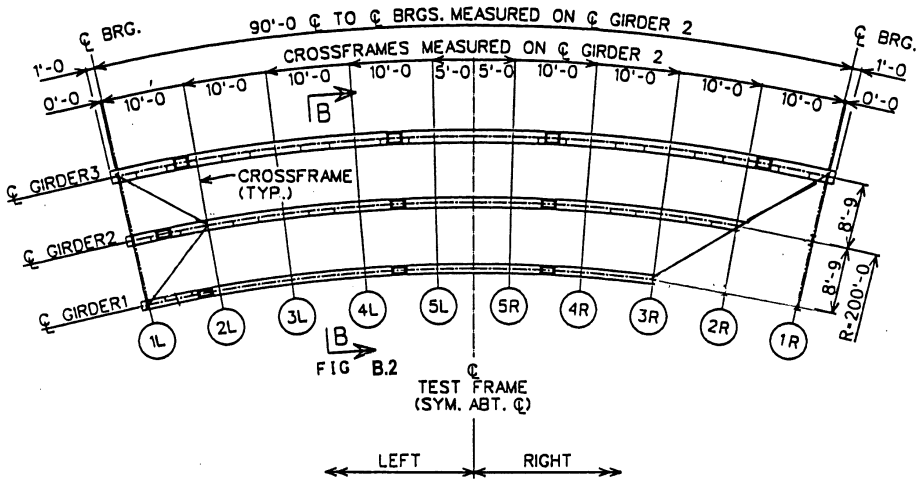

PROTOTYPE PLAN

SKEW CASE D

1 ft. = 0.3048 m
1 in. = 25.4 mm

Figure B.14

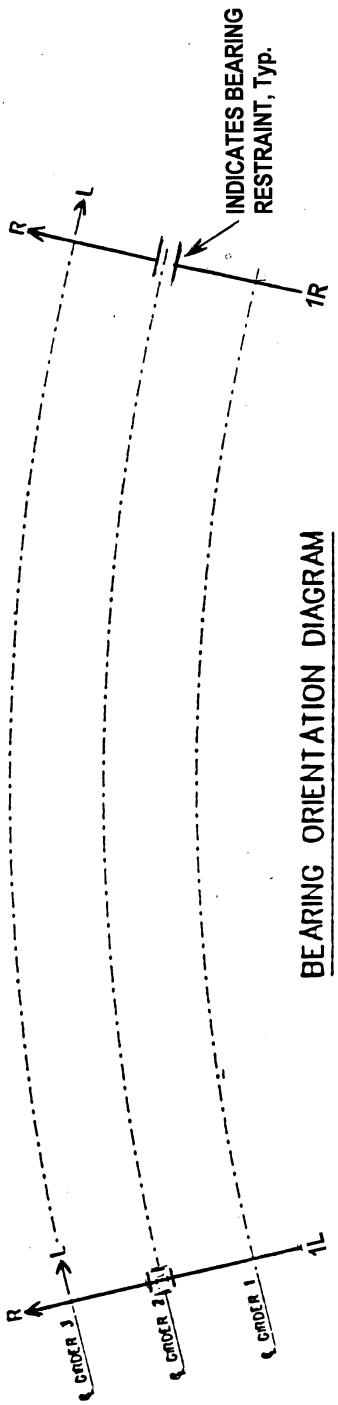

BEARING ORIENTATION DIAGRAM

CASE A

G2 Fixed at Line 1L and Guided Tangentially at Line 1R
G1 and G3 Non-Guided at Lines 1L and 1R

Figure B.15

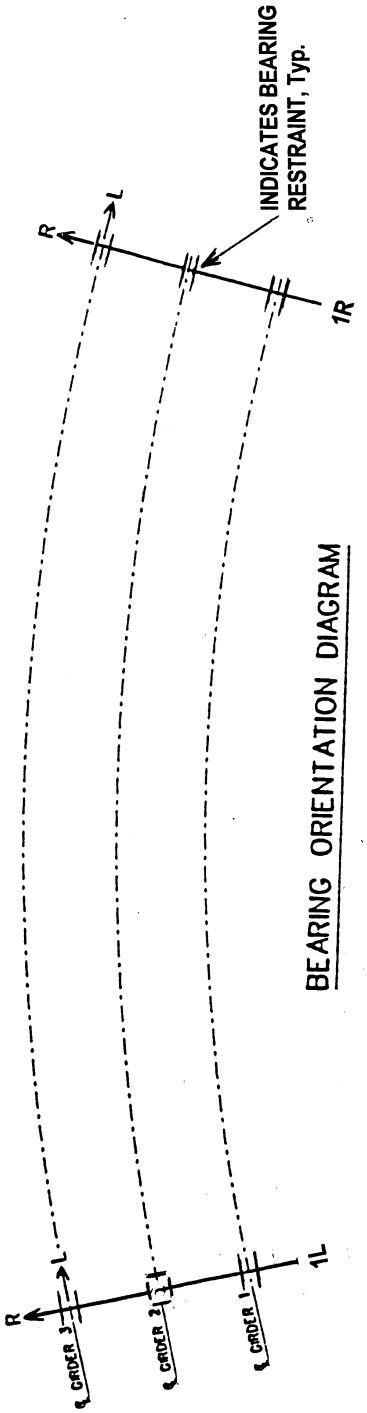
INDICATES BEARING
RESTRAINT, Typ.
R
L
1R
BEARING ORIENTATION DIAGRAM
CASE B
G2 Fixed at Line 1L and Guided Tangentially at Line 1R
G1 and G3 Guided Tangentially at Lines 1L and 1R
R
L
1L
GIRDER 3
GIRDER 2
GIRDER 1

Figure B.16

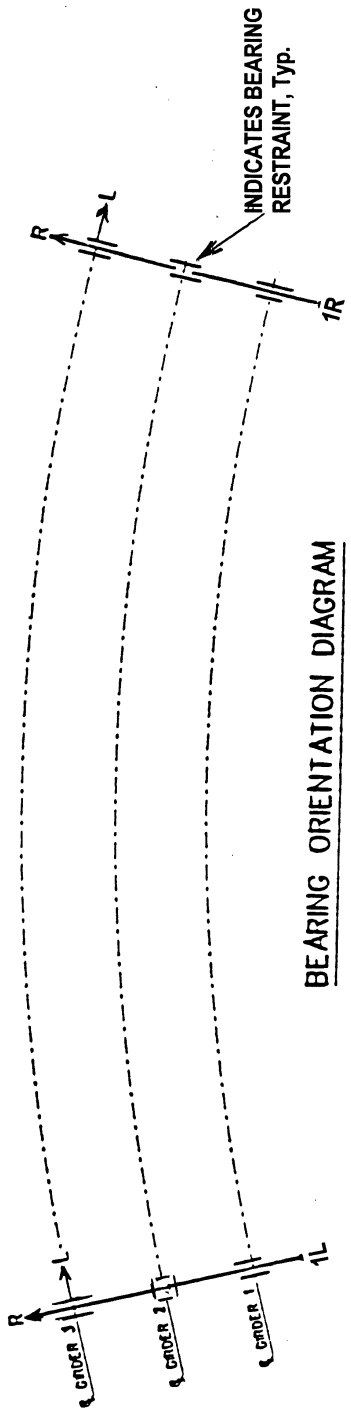

BEARING ORIENTATION DIAGRAM

CASE C

G2 Fixed at Line 1L and Guided Radially at Line 1R
G1 and G3 Guided Radially at Lines 1L and 1R

Figure B.17

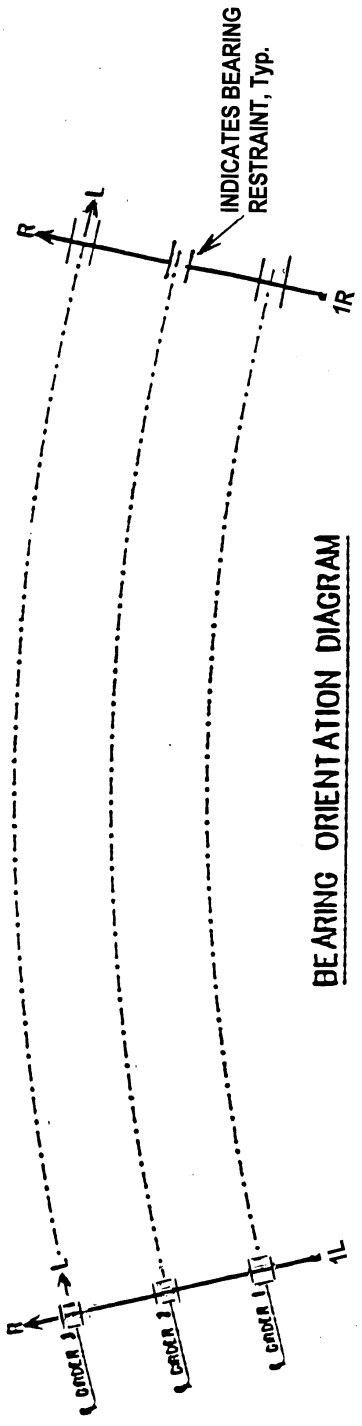

CASE D

G1, G2 and G3 Fixed at Line 1L and Guided Tangentially at Line 1R

Figure B.18